Mechanisms of dendritic peptide release

Olivia F. de S. Monteiro

Ph.D.

The University of Edinburgh

2009

Declaration

I declare that this thesis has been composed by the candidate, Olivia Monteiro and the work is that of my own. The work has not been submitted for any other degree or professional qualification except as specified.

Olivia Monteiro

Dec 2009

Acknowledgement

This thesis would not have been possible without the supervision of my supervisors Mike Ludwig, Gareth Leng and Rolly Wiegand. Mike and Rolly had contributed to the design of experiments and the analysis of results throughout the project. Moreover, they have introduced me to all the techniques used and helped with troubleshooting. Gareth had provided valuable insights to interpretation and analysis of results as well as the background to the project. They have guided me with stimulating discussions about my work and given me helpful feedback in the last three years. Most of all, they have always been inviting whenever I needed help and advice. I would like to thank them here for their friendship and support throughout.

It is a pleasure for me to thank all my friends in office 166 who have stood by me throughout the good times and the challenging times I have had, and everyone in the NCS who have given me so much encouragement throughout. I would especially like to mention Vicky Tobin who has helped me with endless discussions on the background and technical aspects of the project. All my friends in the NCS have made this PhD project and the working environment very enjoyable.

I am grateful to Simone Meddle and Valerie Bishop for managing the transgenic rat colonies used in this project. I would also like to acknowledge the staff in the animal facility in Hugh Robson Building who has been helpful throughout. In addition, I am grateful to everyone in the IMPACT imaging facility, especially Trudi Gillespie, for their help with the microscopy techniques used in this thesis.

I also owe my gratitude to Daniel Baptista-Hon, who has encouraged and inspired me time after time during my project and my thesis write-up.

Lastly, I would like to dedicate this thesis to my parents. Without their love, encouragement, and support, this project would not have been impossible. They have made the hard times a lot easier to face and have carried me through difficulties. I am forever indebted to their unconditional love and support.

Abstract

Magnocellular neurones (MCNs) are capable of secreting vasopressin and oxytocin from the somato-dendritic compartment, which can occur independently to secretion from nerve terminals. One hypothesis of the mechanism that regulates this differential release is that dendrites utilise different vesicle pools compared to those found in terminals.

Little is known for the function of neuronal dendrites, especially the mechanism for peptide release. One theory is that vesicles stored in dendrites are non-released vesicles ready for recycling or degradation. Immunofluorescent labelling was performed on hypothalamic slices of the transgenic rat where enhanced green fluorescent protein (eGFP) was tagged to vasopressin. Lysosomes were detected by the lysosome-associated membrane protein LAMP1. Correlation analysis of LAMP1 labelling and VP-eGFP had shown that localisation of lysosomes in dendrites is positively correlated to loci of high vasopressin expression. This suggests active degradation of vesicles in dendrites.

It is not known whether preferential release of peptides occurs along the profile of dendrites. Experiments were carried out using a temperature block to block exit of vesicles from the Golgi apparatus. Release of the temperature block triggered release of a wave of newly synthesised vesicles from the Golgi apparatus. Measurement of the fluorescent intensity of VP-eGFP showed that preferential release of peptides does not occur along the profile of dendrites.

I have also utilised confocal live cell imaging to study the dynamics of dendritic vasopressin release using VP-eGFP slice explants. Experiments using high potassium stimulation showed significant increase in the release of vasopressin after priming with thapsigargin (intracellular calcium mobiliser), in accordance to in vitro release and microdialysis studies. These results demonstrate that live cell imaging can be achieved in magnocellular neurons, providing a robust model system in the study of dendritic peptide release.

Large dense core vesicles (LDCVs) in other cell types such as bovine adrenal chromaffin cells were shown to segregate according to vesicle age, suggesting that vesicle age is an important factor in the regulation of peptide release. Whether vesicles of different age groups exist in magnocellular dendrites is not known. Thus, biolistic transfection with exogenous fluorescent proteins for expression under temporal control was carried out. However, low transfection rate in magnocellular neurones and the high background fluorescence caused by scattered gold particles used as bullets for transfection deemed this method inappropriate for the purpose of imaging vesicles. Hence, development of an adenoviral transduction system was employed. By using an inducible adenovirus gene construct coupled with a fluorescent reporter gene, it is possible to visualise vesicle pool segregation under different experimental conditions. Subcloning of a red fluorescent construct tagged to ppANF was tested on PC12 cells to show targeting of fluorescence expression to LDCVs. Successful production of an inducible adenoviral DNA with the red fluorescent construct insert was confirmed by PCR and DNA sequencing. Whilst the generation of viral particles is still to be achieved, successful production of the virus will be an invaluable system for inducible gene expression in neurones.

Contents

Declaration

Acknowledgement

Abstract

Contents

List of abbreviations

List of figures

List of tables

Chapter 1 Introduction 1

1.1 The Vasopressin and Oxytocin Systems 3

1.1.1 Architecture of the Vasopressin and Oxytocin Systems 3

1.1.2 Actions of Vasopressin and Oxytocin 4

1.1.3 Evidence of Dendritic Peptide Release 7

1.1.4 Regulation of Dendritic Vasopressin and Oxytocin Release 8

1.2 Physiological Significance of Dendritic Peptide Release 10

1.2.1 Morphological Plasticity 10

1.2.2 Parturition and the Milk-Ejection Reflex 11

1.2.3 Autonomic Control 12

1.2.4 Stress and Other Effects 16

1.3 Mechanisms of Dendritic Peptide Secretion 17

1.3.1 The Importance of Intracellular Calcium 18

1.3.2 Autoregulation 20

1.3.3 Facilitation of dendritic release via vesicle recruitment – priming 24

1.4 Exocytosis in Magnocellular Dendrites 26

1.4.1 Vesicle pools 29

1.4.2 Regulation of LDCV pools 32

1.5 Hypothesis 37

1.5.1 Objectives 40

Chapter 2 Degradation sites in magnocellular dendrites 52

2.1 Introduction 52

2.2 Material and Methods 56

2.2.1 Fixation by Transcardial Perfusion 56

2.2.2 Indirect Immunofluorescence Labelling for Free-floating Sections 57

2.2.3 Microscopic Image Acquisition 58

2.2.4 Image Processing 59

2.3 Results 60

2.3.1 Localisations of Lysosomes in Correlation with VP-eGFP in Dendrites 60

2.4 Discussion 62

Chapter 3 Vesicle trafficking along dendritic profiles 75

3.1 Introduction 75

3.2 Material and Methods 76

3.2.1 Block of peptide release from the GA 77

3.2.2 Indirect Immunofluorescence Labelling for Fresh Brain Sections – Double Label Immunofluorescence 78

3.2.2.1 Primary Antibodies **78**

3.2.2.2 Secondary Antibodies **80**

3.2.3 Microscopic Image Acquisition **80**

3.2.4 Image Processing **81**

3.3 Results **81**

3.3.1 Trafficking of Newly Synthesised Vesicles along Dendritic Profiles **81**

3.4 Discussion **84**

Chapter 4 Live cell imaging of dendritic peptide release **96**

4.1 Introduction **96**

4.2 Material and Methods **99**

4.2.1 Osmotic challenge in P7 rats **99**

4.2.1.1 Three-step ABC method for labelling of Fos protein **100**

4.2.2 Organotypic slice culture **102**

4.2.3 Live cell imaging **103**

4.2.3.1 Timeline for image acquisition **104**

4.2.3.2 Microscopic image acquisition **104**

4.2.3.3 Fluorescent image processing **105**

4.3 Results **106**

4.3.1 Osmotic challenge in P7 rats **106**

4.3.2 Live cell imaging **107**

4.4 Discussion **109**

Chapter 5 Biolistic transfection 125

5.1 Introduction **125**

5.2 Materials and Methods **128**

5.2.1 Organotypic slice explants **128**

5.2.2 Biolistic transfection **128**

5.2.3 Immunohistochemistry – double label immunofluorescence **129**

5.2.3.1 Primary Antibodies **130**

5.2.3.2 Secondary Antibodies **132**

5.2.4 Image acquisition **133**

5.2.4.1 Widefield fluorescence image acquisition **133**

5.2.4.2 Confocal image acquisition **134**

5.3 Results **134**

5.3.1 Organotypic slice culture – P7 vs. P14 **134**

5.3.2 Transfection efficiency – optimisation of transfection pressure **135**

5.3.3 Transfection of neurons, magnocellular neurons, and non-neuronal cells **137**

5.4 Discussion **138**

Chapter 6 Fluorescent protein expression in LDCVs and viral transduction **150**

6.1 Introduction **150**

6.2 Materials and Methods **155**

6.2.1 Construction of inducible ppANF-eGFP, ppANF-tdTomato and ppANF-Timer **156**

6.2.2 Amplification of DNA fragment by PCR **159**

6.2.3 Separation and purification of DNA fragments by **160**

electrophoresis and gel extraction

6.2.4 Ligation of vector DNA and insert 161

6.2.5 Amplification of plasmid DNA by *E. coli* 162

6.2.5.1 Preparation of competent cells **163**

6.2.5.2 Transformation of competent cells **164**

6.2.6 Miniprep plasmid DNA purification protocol 165

6.2.7 Sequence confirmation 165

6.2.8 Maxiprep plasmid amplification protocol 166

6.2.9 N2a and PC12 cell culture and transfection of recombinant 167

constructs

6.2.9.1 N2a culture **167**

6.2.9.2 Expanding N2a culture **168**

6.2.9.3 Cell freezing **168**

6.2.9.4 Transfection of single cells **169**

2.6.9.5 Double immunofluorescence labelling for adhering **169**

single cell cultures

6.2.10 Construction of recombinant adenoviral vectors 170

6.2.10.1 Construction of recombinant adenoviral DNA for **171**

Tet-on expression system

6.2.10.2 Construction of recombinant adenoviral DNA for Tet-off expression system **173**

6.2.10.3 Miniscale preparation of recombinant Adeno-X DNA **175**

6.2.11 HEK 293 cell culture **176**

6.2.11.1 Transfecting HEK 293 cells with recombinant Adeno-X DNA **176**

6.2.11.2 Amplifying recombinant adenovirus **178**

6.2.11.3 Determining viral titre with end-point dilution assay **178**

6.3 Results **179**

6.3.1 Exogenous fluorescent protein expression in LDCVs **179**

6.3.2 Expression of ppANF-Timer and pTRE-ppANF-Timer **180**

6.3.3 Expression of pTRE-ppANF-eGFP and pTRE-ppANF-tdTomato **183**

6.3.4 Generation of pAdeno-X constructs **185**

6.3.5 Expression of pDNR-ppANF-eGFP and pDNR-ppANF-tdTomato **188**

6.3.6 Generation of pLP-Adeno-X-TRE constructs **189**

6.4 Discussion 189

Chapter 7 Discussion 220

7.1 Vesicle pools and routing 220

7.2 New tools for studying dendritic peptide release 223

7.3 Future directions 228

7.4 Conclusion 231

References 233

Appendix I – Recipes i

Appendix II – Manuscript: Hot spots for degradation in dendrites of magnocellular neurones x

ABBREVIATIONS

3V	Third ventricle
αSNAP	α-soluble-NSF-attachment protein
Ab	Antibody
AC	Adenylate cyclase
aCSF	Artificial cerebrospinal fluid
ACTH	Adrenocorticotropic hormone
Ad5	Adenovirus type5
ANF	Atrial natriuretic factor
Ang II	Angiotensin II
ANOVA	Analysis of variance
ATP	Adenosine triphosphate
ATPase	Adenosine triphosphatase
AUC	Area under curve
BP	Band pass
BSA	Bovine serum albumin
cGMP	Cyclic guanosine monophosphate
CNQX	6-cyano-7-nitroquinoxaline-2,3-dione
CNTF	Ciliary neurotrophic factor
CRH	Corticotrophin-releasing hormone
CSF	Cerebrospinal fluid
DAG	Diacylglycerol
DBB	Diagonal band of Broca
DIV	Days *in vitro*
DNA	Deoxyribonucleic acid
Dox	Doxycycline
E1	Early region 1 of adenovirus genome

E3	Early region 3 of adenovirus genome
EDTA	Ethylenediaminetetraacetic acid
eGFP	Enhanced green fluorescent protein
EGTA	Ethylene glycol tetraacetic acid
ER	Endoplasmic reticulum
FNDI	Familial neurohypophysial diabetes insipidus
GA	Golgi apparatus
GABA	γ- Aminobutyric acid
GFAP	Glial fibrillary acidic protein
Glut	Glutamate
G-protein	Guanine nucleotide-binding proteins
HEK cells	Human embryonic kidney cells
HeNe	Helium-Neon
Hep	Heparin
HNS	Hypothamo-Neurohypophysial System
Icv	Intra-cerebroventricular
Ig	Immunoglobulin
i.p.	Intraperitoneal
IP_3	Inositol triphosphate
IP_3R	Inositol triphosphate receptor
LAMP1	Lysosomal-associated membrane protein 1
LC	Locus coeruleus
LDCV	Large dense core vesicle
LP	Long pass
MAP2	Microtubule-associated protein 2
MnPO	Median preoptic nucleus
(m)RNA	(messenger) Ribonucleic acid
N2a cells	Neuroblastoma 2a cells

NA	Noradrenaline / Numerical apperture
NMDA	N-methyl-D-aspartic acid
NO	Nitric oxide
NOS	Nitric oxide synthase
NSF	N-ethylmaleimide-sensitive factor
NTS	Nucleus tractus solaris
OB	Olfactory bulbs
OC	Optic chiasm
OTR	Oxytocin receptor
OVLT	Organum vasculosum of the lamina terminalis
P(n)	Postnatal day n
PB	Phosphate buffer
PBS	Phosphate buffer saline
PBT	Phosphate buffer (with triton-X100)
PC12 cells	Pheochromocytoma cells
PFA	Paraformaldehyde
$PI(4,5)P_2$	Phosphatidylinositol-4,5-bisphosphate
PKA	Protein kinase A
PKC	Protein kinase C
PLC	Phospholipase C
P_{minCMV}	Minimal immediate early promoter of cytomegalovirus
PMT	Photomultiplier tube
PNZ	Perinuclear zone
ppANF	Pre-pro-atrial natriuretic factor
PVN	Paraventricular nucleus
RGB	Red green blue
RP	Reserve pool
RRP	Readily releasable pool

rtTA	Reverse tetracycline-controlled transactivator
SCN	Suprachiasmatic nucleus
SFO	Subfornical organ
siRNA	Small interfering RNA
SNAP-25	Synaptosome-associated protein of 25,000 daltons
SNARE	Soluble NSF attachment protein receptors
SON	Supraoptic nucleus
Tc	Tetracycline
tdTomato	Tandem-tomato
TetR	Tetracycline repressor protein
Tg	Thapsigargin
TMN	Tuberomammilary nuclei
TRE	Tetracycline response element
TRH	Thyrotropin-releasing hormone
t-SNARE	target-_Soluble NSF attachment protein receptors
tTA	Tetracycline-controlled transactivator
V_{1a}	Vasopressin receptor 1a
V_{1b}	Vasopressin receptor 1b
VLM	Ventrolateral medulla
VGCC	Voltage-gated calcium channel
VP	Vasopressin
VP-eGFP	vasopressin-enhanced green fluorescent protein
v-SNARE	vesicle-_Soluble NSF attachment protein receptors

List of Figures

Figure 1-1. Coronal section of the hypothalamus showing the supraoptic and paraventricular nuclei (SON and PVN).

Figure 1-2. Coronal section of the hypothalamus showing the SON.

Figure 1-3. Downstream signalling pathways of VP and OT receptors.

Figure 1-4. Afferent inputs to the vasopressin and oxytocin magnocellular neurons of the HNS.

Figure 1-5. Figure showing the different functional aspects of dendritic peptide release.

Figure 1-6. Electron micrographs showing dendritic distributions of dense core vesicles.

Figure 1-7. Simplified figure of the regulated secretory pathway.

Figure 1-8. Images from bovine adrenal chromaffin cells transfected with a fluorescent time-stamp.

Figure 1-9. Possible mechanism of priming of dendritic release.

Figure 1-10. Structure of the VP-eGFP transgene.

Figure 2-1. Simplified pathways to delivery to lysosomes.

Figure 2-2. Beam path configuration for 2-channel imaging with the confocal laser scanning system.

Figure 2-3. Measurement of VP-eGFP intensity relative to locations of LAMP1 immunofluorescence.

Figure 2-4. Correlation of LAMP1 labelling with VP-eGFP intensity in the dendrite.

Figure 2-5. LAMP1 immunofluorescence in vasopressinergic dendrite.

Figure 3-1. Schematic diagram showing hypothetic outcome of temperature block on vesicle exit from the Golgi apparatus**.**

Figure 3-2. Beam path configuration for 3-channel imaging with the confocal laser scanning system.

Figure 3-3. Measurement of fluorescent intensity along the profile of a typical dendrite.

Figure 3-4. Mean total fluorescent intensity of dendrites measured.

Figure 3-5. Graph showing % fluorescence along the profile of dendrites.

Figure 4-1. Perfusion chamber components.

Figure 4-2. Perfusion set up for live cell imaging experiments.

Figure 4-3. Image acquisition timeline for live imaging.

Figure 4-4. Fos expression in the hypothalamus.

Figure 4-5. Effect of osmotic challenge on Fos expression in the SON on post-natal day 7 (P7) Sprague Dawley rats.

Figure 4-6. Measurement of VP-eGFP fluorescent intensity.

Figure 4-7. Live cell imaging of VP-eGFP dendrites in the SON.

Figure 4-8A. Changes of fluorescent intensity in dendrites after stimulation.

Figure 4-8B. Changes of fluorescent intensity in dendrites after stimulation.

Figure 4-8C. Rate of fluorescence decay in image backgrounds.

Figure 5-1. Schematic diagram of biolistic transfection of organotypic slice culture with the Helios Gene Gun.

Figure 5-2. Organotypic slice cultures P7 vs. P14. (A) P7 culture and (B) P14 culture stained for vasopressin by indirect double immunofluorescence labelling. (C) Transcardial perfused section of the hypothalamus from adult (200 – 300g) VP-eGFP rat.

Figure 5-3. Optimisation of transfection efficiency by changing helium pressure used for transfection.

Figure 5-4. Biolistic transfection of hypothalamic organotypic slice culture.

Figure 5-5. Typical SON after transfection.

Figure 5-6. Biolistic transfection of a magnocellular neuron in a hypothalamic organotypic slice culture.

Figure 5-7. Transfection of non-neuronal cells.

Figure 6-1. Adeno-x Tet-Off and Tet-on system.

Figure 6-2. Overview of recombinant adenovirus construction and infection.

Figure 6-3. Overview of the generation of inducible ppANF-tagged constructs to the generation of viral particles using the Adeno-X^{TM} Expression System 1 (Clontech).

Figure6-4. Plasmid maps of ppANF tagged fluorescent constructs and inducible constructs showing the promoters, proteins expressed, restriction sites used for subcloning, antibiotic resistant markers, and the sizes of the constructs.

Figure 6-5. PCR amplification and introduction of restriction sites.

Figure 6-6. Plasmid maps of pAdeno-X and pLP-Adeno-X.

Figure 6-7. Confirmation of recombinant pAdeno-x-ppANF-DsRed1-E5 ligation and transformation by PCR screening.

Figure 6-8. Determining viral titre with the end-point dilution assay.

Figure 6-9. ppANF-eGFP transfection of PC12 cells.

Figure 6-10. Gel images from electrophoresis of PCR amplification products of ppANF, ppANF-Timer and pTimer and restriction digest of ppANF-Timer, pTRE-ppANF-Timer and pTRE-Timer.

Figure 6-11. Transfection of N2a cells with pTRE-ppANF-Timer.

Figure 6-12. pTRE-Timer transfection of a N2a cell.

Figure 6-13. Gel images from electrophoresis of PCR amplification products of ppANF-eGFP and tdTomato and restriction digest of pTRE-ppANF-eGFP, pTRE-ppANF-tdTomato.

Figure 6-14A. Transfection of PC12 cells with pTRE-ppANF-eGFP and pTRE-ppANF-tdTomato.

Figure 6-14B. Colocalisation between ppANF-tdTomato and chromogranin A.

Figure 6-15. pTRE-ppANF-tdTomato expression in the GA, cell centre and cell periphery in transfected PC12 cells.

Figure 6-16. Analysis of pAdeno-X-TRE-ppANF-eGFP and pAdeno-X-TRE-ppANF-tdTomato.

Figure 6-17. A) Restriction analysis of pTRE-ppANF-eGFP and pTRE-ppANF-tdTomato with I-CeuI and PI-SceI.

Figure 6-18. Analysis of pDNR-ppANF-eGFP and pDNR-ppANF-tdTomato.

Figure 6-19. Transfection of N2a cells with pDNR-ppANF-eGFP and pDNR-ppANF-tdTomato.

Figure 6-20. Analysis of pLP-Adeno-X-TRE-ppANF-eGFP and pAdeno-X-LPTRE-ppANF-tdTomato.

Appendix I – Figure 1. Fluorescence spectra of fluorophores used (Alexa Fluor 488, 568 and 633 antibody conjugates and green fluorescent protein).

List of Tables

Table 3-1. Number of sections measured for every 6 µm segment in each treatment group.

Table 6-1. Typical reaction mix for PCR.

Table 6-2. PCR Cycles for the amplification of DNA fragment.

Table 6-3. Primers used in PCR amplification of DNA fragments for subcloning.

Table 6-4. Conditions for a typical restriction digest.

Table 6-5. Conditions for a typical ligation reaction.

Table 6-6. PCR Cycles for the screening of recombinant pAdeno-X and pLP-Adeno-X.

Appendix I - Table 1. Excitation and emission maxima of secondary antibodies used for indirect immunofluorescence labelling.

Chapter 1
Introduction

1. INTRODUCTION

Neurons transmit information via the release of neurotransmitters and neuromodulators. Neurons also communicate with each other via synapses. Classical synapses connect axons from one neuron to dendrites of another, where information is passed on through neurotransmission. In classical neurotransmission, dendrites have always been regarded as the "receiving" end of neurons in that they receive information from axonal afferent terminals and relay the information to the cell body. Ramon Cajal (Cajal 1891) proposed that information flows in a unidirectional manner from dendrites towards the soma and then along the axons. This concept still applies to most of the information processing in neurons, but there is strong evidence that electrical signals not only travel from dendrites towards the cell body, but can be generated in dendrites and propagate from the soma into the dendrite (Stuart *et al.* 1997). There is also evidence that dendrites can release neuro-active substances like those found in the nerve terminals. Studies on the dendrites of dopaminergic neurons in the substantia nigra (Cheramy *et al.* 1981; Conde 1992; Pucak & Grace 1994) demonstrated that their dendrites release dopamine, and the main functions of dendritic dopamine release is auto-regulation, modulation of neurotransmitter release from afferent terminals and modulation of activity in adjacent cells (Cheramy *et al.* 1981; Conde 1992; Pucak & Grace 1994).

Dendritic peptide release from magnocellular neurons is amongst the most extensively studied. Magnocellular neurons can be described as vasopressinergic or

oxytocinergic, depending on which of either of the two hormones they synthesise and release. Both hormones are released into the peripheral circulation via the posterior pituitary. Vasopressin is best known for its antidiuretic properties (Bankir 2001) whilst oxytocin is crucial in lactation and believed to play a role in parturition (Luckman *et al.* 1993; Lee *et al.* 2008). Oxytocin also acts on OT receptors in the kidneys and induce natriuresis (Verbalis & Dohanics 1991). Early studies using in vitro preparations of the supraoptic nucleus (SON) and the paraventricular nucleus (PVN) of the hypothalamus have shown vasopressin and oxytocin release from these hypothalamic nuclei (Moos *et al.* 1984). Further studies found in vivo oxytocin release in the SON during the milk ejection reflex (Moos *et al.* 1989). Vasopressin release in the SON and the PVN has also been measured in vivo in response to osmotic stimulation (Landgraf & Ludwig 1991). The SON is made up of vasopressin- and oxytocin-expressing magnocellular neurons and axons of these neurons all project to the posterior pituitary, leaving the soma and dendrites in the nucleus. This anatomical arrangement suggested that vasopressin and oxytocin release in the SON came from release from either the soma or the dendrites, or both, of magnocellular neurons. The PVN contains vasopressin- and oxytocin-releasing magnocellular neurons as well as parvocellular neurons, which secrete other neuro-active peptides such as corticotrophin-releasing hormone (CRH), thyrotropin-releasing hormone (TRH) and vasopressin. Moreover, the PVN receives vasopressinergic inputs from the suprachiasmatic nucleus (SCN) (Kalsbeek *et al.* 1993). This makes it difficult to study dendritic vasopressin release in the PVN. Hence, the SON is often used as a model system to study the mechanisms of dendritic release. This chapter aims to introduce the vasopressin and oxytocin

systems, focussing on the regulation, physiological significance, and mechanisms of dendritic peptide release of magnocellular neurons.

1.1 The Vasopressin and Oxytocin Systems

1.1.1 Architecture of the Vasopressin and Oxytocin Systems

Vasopressin-expressing magnocellular neurons are located in the ventral part of the SON and more medial part of the PVN and oxytocin-expressing neurons are located in the dorsal part of the SON and lateral part of the PVN (see **Figure 1-1** for immunohistochemical staining of vasopressin and oxytocin in the hypothalamus). Magnocellular neurons have large cell bodies (20 – 40 μm in diameter) which contain one to three dendrites (Armstrong *et al.* 1982; Dyball & Kemplay 1982). Vasopressin and oxytocin producing neurons in the SON generally have a single axon that projects to the posterior pituitary terminating on capillaries where peptides are released into the blood stream (Fisher *et al.* 1979). The magnocellular neurons in the PVN have the same morphology but their dendrites project to the parvocellular part of the PVN, towards the third ventricle (Armstrong *et al.* 1980). Axons of magnocellular neurons in the PVN also terminate in the neural lobe (Alonso & Assenmacher 1981). The parvocellular neurons in the PVN project to the median eminence (Vandesande *et al.* 1977), nucleus tractus solitaries (NTS), brain stem and spinal cord (Swanson & Sawchenko 1983), and limbic area (Buijs & Swaab 1979).

For the purpose of this thesis, the introduction is going to focus on vasopressin- and oxytocin-expressing magnocellular neurons in the SON.

Magnocellular neurons have very simple dendritic morphology and dendrites generally contain few dendritic spines (Armstrong 1995). Branching in dendrites was also found to be rare. Vasopressin and oxytocin dendrites have the same morphological properties in the SON and in the PVN. Dendrites of SON neurons extend ventrally and run adjacent to the ventral glial lamina for hundreds of micrometers providing extensive coverage of the brain surface and contact to cerebrospinal fluid (CSF) (Morris 2005). Along the profile of dendrites, large dilations were found to be filled with secretory vesicles (Sofroniew & Glasmann 1981) although vesicles are also contained in undilated parts. **Figure 1-2** shows the morphology of vasopressin-expressing magnocellular neurons in the SON.

1.1.2 Actions of Vasopressin and Oxytocin

Peripheral actions of vasopressin mainly include osmoregulation (Bankir 2001; Inoue *et al.* 2001; Bourque 1998) and blood pressure regulation (Aisenbrey *et al.* 1981). Osmoregulation is mediated through activation of Vasopressin-2 (V_2) receptors found in the distal convoluted tubules and collecting ducts in the kidneys (Bankir 2001). Activation of Vasopressin-1_a (V_{1a}) receptors mediates vasoconstriction (Aisenbrey *et al.* 1981). Oxytocin is important in parturition (Luckman *et al.* 1993) and lactation (Lee *et al.* 2008)). **Figure 1-3** shows the downstream signalling

pathways of the VP and OT receptors. Actions of oxytocin are mediated through activation of oxytocin receptors found in the myometrium and mammary smooth muscles (Gimpl & Fahrenholz 2001). In the brain, vasopressin affects the regulation of aggression in male and female rats (Caldwell *et al.* 2008b; Nephew & Bridges 2008), facilitation of pair bonding in prairie voles (Cho *et al.* 1999; Insel *et al.* 1994), regulation of the stress axis via control of adrenocorticotropic hormone (ACTH) release (Aguilera & Rabadan-Diehl 2000), and regulation of circadian rhythm (Buijs *et al.* 2003). The V_{1a} receptor is the most abundant vasopressin receptor found in the brain (Zingg 1996). V_{1b} receptors are mainly found in the adenohypophysis and its main function is to stimulate secretion of ACTH from the anterior pituitary (Volpi *et al.* 2004). Oxytocin acting on oxytocin receptors in the brain is involved in the regulation of maternal behaviour (Fahrbach *et al.* 1985; Pedersen & Prange, Jr. 1979), sexual behaviour (Caldwell & Moe 1999; Melis *et al.* 2007), pair bonding (Insel & Hulihan 1995) and aggression (Bosch *et al.* 2005; DeVries *et al.* 1997; Winslow *et al.* 2000) in both male and female rats, facilitation of social memory in mice and humans (Lee *et al.* 2008; Rimmele *et al.* 2009), and regulation of stress and anxiety (Ring *et al.* 2006; Windle *et al.* 1997). Since vasopressin and oxytocin released from the posterior pituitary enter the blood stream and do not cross the blood-brain barrier (Ermisch *et al.* 1993), the peptides found in CSF are a result of central release in the brain. Sources of central release are the parvocellular vasopressin and oxytocin neurons of the PVN, vasopressin neurons in the SCN, and magnocellular soma and dendrites of the PVN and SON. Concentrations of both peptides have been found to be high in CSF, indicating possible functions of peptides in the brain (reviewed in (Leng & Ludwig 2008). Also, both vasopressin and

oxytocin receptors are expressed throughout the brain (Caldwell *et al.* 2008a; Gimpl & Fahrenholz 2001). Vasopressin released from the parvocellular neurons stimulates ACTH release from the anterior pituitary by acting on V_{1b} receptors (for review see (Antoni 1993) and acts as an important regulator of stress (Aguilera & Rabadan-Diehl 2000). The suprachiasmatic vasopressin neuron also projects centrally to the PVN and releases vasopressin in a diurnal rhythm (Kalsbeek *et al.* 1993; Kalsbeek *et al.* 1995). Parvocellular oxytocin neurons mainly project to the brain stem and spinal cord and there, they are involved in the regulation of behaviours such as penile erection and yawning (Kita *et al.* 2006; Gimpl & Fahrenholz 2001) as well as modulation of nociception (Gerardo *et al.* 2010) via actions on oxytocin receptors. However, these are the main sites of parvocellular neuronal projection and innervations of other sites in the brain where vasopressin and oxytocin receptors are expressed are sparse. Vasopressin and oxytocin release from magnocellular neurones in the PVN is particularly important in the modulation of stress and anxiety-related behavioural response and also maternal behaviour in pregnant rats (Neumann *et al.* 2000; Neumann 2007). Magnocellular neurons contain a large resource of vasopressin and oxytocin, where most of their peptides are stored in the soma and in dendrites (Morris & Pow 1988; Leng & Ludwig 2008); suggesting that somato-dendritic release could be a main source of vasopressin and oxytocin in the brain. Vasopressin and oxytocin are cleared in the brain by aminopeptidases and have half-lives of 26 and 19 min in the CSF respectively (Mens *et al.* 1983). Since both oxytocin and vasopressin have long half-lives in the CSF, it is possible for both peptides to act on distant sites in the brain, which are not innervated by the respective neurons, via diffusion (Ludwig & Leng 2006). As

discussed above, dendrites of SON neurons extend for hundreds of micrometers providing coverage of a large portion of the brain surface (Morris 2005). The extensive coverage of the brain surface by magnocellular dendrites, and the fact that these dendrites are in close contact with CSF, offer an anatomical advantage to dendritically released peptides to act on distant sites.

1.1.3 Evidence of Dendritic Peptide Release

Several neuropeptides had been shown to be released from somato-dendritic compartments of different cell types. Galanin, which was found to co-exist with vasopressin in magnocellular neurons (Melander *et al.* 1986), is thought to be preferentially targeted to dendritic compartments and is believed to exert autocrine/paracrine control on membrane hyperpolarisation (Landry *et al.* 2005). Dynorphin, the peptide opiate, is synthesised in granule cells of the dentate gyrus and the majority of the peptide was found to be located in dendrites where its release negatively regulates afferent inputs (Drake *et al.* 1994). First evidence of dendritic peptide release from magnocellular neurons came from electron-microscopic studies with tannic acid fixation of dense core vesicles (Buma *et al.* 1984) applied to slices of the hypothalamus capturing exocytosis of vesicle cargo from dendrites (Pow & Morris 1989). Studies using dendrosomes of magnocellular neurons, which are portions of dendrites isolated to form membrane-bounded structures, showed release of vasopressin and oxytocin by hyperpolarising stimulus via exocytosis (Pow *et al.* 1990). Measurement of vasopressin and oxytocin levels by *in vivo* microsampling also showed high concentrations of the peptides in the extracellular fluid of the SON

(Landgraf & Ludwig 1991). In addition, secretion of vasopressin and oxytocin in the SON had been shown in vitro using high K^+ to depolarise cells in slices (Mason *et al.* 1986). Since the SON has no afferent inputs of vasopressin or oxytocin, contain very few axon collaterals, and as mentioned above, vasopressin and oxytocin released into the blood do not cross the blood brain barrier, it is clear that the peptides measured in the SON in these experiments were released from the somata and dendrites of magnocellular neurons.

1.1.4 Regulation of Dendritic Vasopressin and Oxytocin Release

The SON receives inputs from the subfornical organ, the organum vasculosum of the lamina terminalis, the brain stem, the nucleus of the solitary tract, and the ventrolateral medulla (see reviews (Leng *et al.* 1999; Swanson & Sawchenko 1983). Aside from inputs from these areas, the SON also receives inputs from neurons just outside the nucleus in the perinuclear zone. **Figure 1-4** summarises the afferent inputs to the HNS (Burbach *et al.* 2001). Glutamate and γ-Aminobutyric acid – GABA are the major excitatory and inhitory neurotransmitter input respectively. Other inputs include noradrenaline, serotonin, and dopamine. Noradrenergic inputs are mainly derived from the medulla oblongata and induce an increase in the firing rate of both VP-ergic and OT-ergic neurones (Randle *et al.* 1984). Serotonin input originates from the brain stem and was found to increase expression of OT but not VP in the SON (Vacher *et al.* 2002). Dopaminergic input from the brain stem increases peripheral release of both VP and OT (Buijs *et al.* 1984). In addition to peptidergic inputs from the brain stem, peripheral release of VP and OT are also

stimulated by angiotensin II (Ang II) which is important in salt and water homeostasis (Phillips 1987). Intravenous and intracerebral injection of Ang II both stimulates increase in neuronal activity in the SON (Rowland *et al.* 1994b; Rowland *et al.* 1994a). Moreover, direct application of Ang II to SON slice preparations increased the firing rate of magnocellular neurons (Okuya *et al.* 1987), indicating that magnocellular neuronal activity is also regulated by peripheral peptides.

Many studies have been done on the regulation of dendritic vasopressin and oxytocin release, testing both physiological and pharmacological agents. Ludwig 1998 reviewed a list of physiological and pharmacological stimuli to dendritic vasopressin and oxytocin release. Osmotic challenge (Landgraf & Ludwig 1991; Ludwig *et al.* 1996b; Ludwig & Landgraf 1992), dehydration (vasopressin) (Ludwig *et al.* 1996b), and suckling during lactation (oxytocin) (Moos *et al.* 1989; Neumann *et al.* 1993b) all had effects on dendritic vasopressin and oxytocin release, suggesting a physiological role for dendritic release. Agonist and antagonist treatment in the SON had also been demonstrated to affect dendritic peptide release, suggesting that these peptides act on vasopressin/oxytocin receptors in the SON to elicit their functions (Moos *et al.* 1984; Wotjak *et al.* 1994). In a review article, Landgraf and Neumann (Landgraf & Neumann 2004) added a series of behavioural stimuli to this list such as social behaviour, maternal behaviour and a range of stress stimuli. Sabatier *et al.* (Sabatier *et al.* 2003) found that α-melanocyte-stimulating hormone activates dendritic oxytocin release. All these findings indicate that the vasopressin and oxytocin system is regulated by a range of stimuli, which affects dendritic

vasopressin and oxytocin release to differing degrees. The physiological significance of dendritic peptide release during various physiological states including parturition, lactation, and dehydration is discussed below.

1.2 Physiological Significance of Dendritic Peptide Release

1.2.1 Morphological Plasticity

Interesting morphological changes occur after the onset of parturition and during lactation. At the end of pregnancy and in lactation, the dendrites of oxytocin neurons become bundled together without intervening glia (Theodosis & Poulain 2001), allowing synaptic boutons to contact more than one dendrite or cell body (Theodosis *et al.* 1998). An increase in the general numbers of synaptic terminals were found and these terminals were found to be of GABA-ergic, glutamatergic and noradrenergic synapses (Theodosis *et al.* 1998). Glial retraction promotes juxtapositioning of dendrites and somata, which could facilitate synchronisation of neuronal electrical activity (Theodosis *et al.* 2008). These kinds of synaptic plasticity regress after lactation, depend on dendritic oxytocin release (Theodosis 2002) and can be mimicked in *in vitro* slice culture of the rat hypothalamus using *in vitro* administration of oxytocin and the effect was blocked by oxytocin receptor antagonist (Langle *et al.* 2003). These effects of oxytocin on synaptic plasticity are facilitated by female sex steroids (Montagnese *et al.* 1990). Oxytocin gene expression had been shown to be increased by activation by sex steroids in the rat

(Crowley & Amico 1993) and oestrogen was shown to selectively induce vasopressin and oxytocin release from cell bodies and dendrites but not from axonal terminals (Wang *et al.* 1995). This kind of neuronal modelling does not only occur during pregnancy and lactation, but also under acute osmotic stimulation where there is an increase in oxytocin synthesis and release (Beagley & Hatton 1992; Perlmutter *et al.* 1985; Tweedle & Hatton 1984). Vasopressin's role in structural remodelling is unclear since osmotically induced morphological changes occur in Brattleboro rats, which lack vasopressin (Chapman *et al.* 1986). Synaptic plasticity and neuronal remodelling promote communication between afferent and efferent neurons and also between bundled oxytocin neurons. This can facilitate synchronisation of electrical activity (Theodosis & Poulain 1992), however, it is not essential for synchronised burst activity of oxytocin neurons since burst firing was observed before neuronal remodelling, reviewed in (Russell *et al.* 2003), and that absence of neuronal remodelling, prevented by removal of the sialylated isoform of the neural cell adhesion molecule, shown to be a prerequisite to neuronal remodelling, did not inhibit burst firing of oxytocin neurons during parturition and lactation (Catheline *et al.* 2006). Nevertheless, glial retraction and dendritic bundling encourage communication between oxytocin neurons and formation of glutamate and GABA synapses as a result is important in the fine tuning of oxytocin electrical activity.

1.2.2 Parturition and the Milk-Ejection Reflex

The role of centrally released oxytocin is important in parturition but not essential, as oxytocin gene knockout mice give birth normally (Young, III *et al.* 1996). It had

been proposed that vasopressin could have compensated for the effects of oxytocin deficiency; supported by the fact that vasopressin can act on oxytocin receptors (Barberis *et al.* 1998). Nevertheless, oxytocin release from the SON and PVN was found to be increased by 254% and 300% respectively during parturition (Neumann *et al.* 1993b), suggesting a role for central oxytocin release. Moreover, oxytocin antagonist treatment after the onset of labour was shown to slow down the process of pup-delivery (Neumann *et al.* 1996). At parturition, increase in local glutamate release stimulates dendritic release of oxytocin (Herbison *et al.* 1997), which acts on oxytocin receptors on oxytocin neurons to stimulate a positive feedback release of oxytocin in the SON (Moos *et al.* 1984). Moreover, oxytocin cells inhibit neighbouring cells via the release of endocannabinoids (Hirasawa *et al.* 2004), which are also released centrally by oxytocin neurons. This coupling of oxytocin neurons facilitates burst firing by enabling coupled neurons to be stimulated by a surge of glutamatergic activity (reviewed in (Brunton & Russell 2008). Synchronised firing of oxytocin neurons mediated by dendritic oxytocin release can then facilitate bursts of oxytocin release from the posterior pituitary at parturition.

In the rat, prolactin release is stimulated by oxytocin (Murai & Ben Jonathan 1987) and surges before parturition to prepare the mammary gland for the production of milk (Andrews 2005). This trigger of lactation, together with oxytocin neuron burst firing results in milk ejection when stimulated by suckling. The physiological aspect of dendritic oxytocin release was first shown in the milk-ejection reflex (Moos *et al.* 1989). It was shown that oxytocin antagonist administered to the SON disrupts the

milk ejection reflex by reducing burst amplitude and frequency of oxytocin neurons (Lambert *et al.* 1993), demonstrating the importance of centrally released oxytocin in the bursting behaviour of oxytocin neurons. In lactating rats, oxytocin injection into the SON or PVN stimulated bursting activity in oxytocin cells (Moos & Richard 1989). Injection of oxytocin in one SON or PVN resulted in firing of oxytocin neurons in the contralateral nucleus and this effect is specific to the magnocellular nuclei since injection of oxytocin away from the SON and PVN did not result in synchronised burst activity (Moos & Richard 1989). Direct evidence of central oxytocin release during the milk-ejection reflex came from *in vivo* push pull experiments where increase in oxytocin release was measured in the SON just before milk ejection (Freund-Mercier *et al.* 1988). These evidences suggested a positive feedback mechanism where oxytocin facilitates its own release. Moreover, this effect is specific to oxytocin since intra-cerebroventricular (icv) administration of vasopressin did not induce burst firing of oxytocin cells or milk let-down (Freund-Mercier & Richard 1981). Oxytocin facilitates oxytocin burst firing in the magnocellular nuclei and once the reflex is started, more oxytocin is released from the somata and dendrites to sustain the pulsatile release from the axon terminals in the posterior pituitary needed for foetus expulsion and milk let-down.

1.2.3 Autonomic Control

Vasopressin neurons respond to changes in plasma osmolality and peripheral vasopressin secretion results in high osmolality, leading to reabsorption of water in the kidney collecting tubules. Systemic administration of hyperosmotic stimuli such

as hypertonic saline results in both vasopressin and oxytocin secretion from the posterior pituitary and also from the SON (Ludwig *et al.* 1994a). Magnocellular neurons, being osmosensitive, respond to plasma osmolality changes not only by activation of cell surface osmoreceptors but by afferent inputs from circumventricular organs (for review see (McKinley *et al.* 2001). Lesion of the anterior and ventral region of the third ventricle abolished intranuclear release in response to systemic hyperosmotic stimulation (Ludwig *et al.* 1996a). Also, administration of tetrodotoxin, which blocks voltage-gated sodium channels and hence the generation of action potentials, diminished release of vasopressin and oxytocin in the SON in response to systemic hyperosmotic stimulation (Ludwig *et al.* 1995), indicating the importance of afferent inputs in the regulation of dendritic peptide release in the SON. Recently, nitric oxide (NO) has been implicated in dendritic vasopressin release in the SON in response to osmotic stimulus (Gillard *et al.* 2007). Water deprivation (Ueta *et al.* 1995) and salt loading (Villar *et al.* 1994) increased nitric oxide synthase activity in magnocellular neurons. Gillard *et al.* found that NO stimulated increased dendritic vasopressin release after systemic osmotic stimulation and this increase of dendritic vasopressin release was due to increase in glutamatergic signalling. Hence, NO released from magnocellular dendrites enhance presynaptic glutamatergic input to vasopressin neurons, increasing dendritic vasopressin release and actions on V_{1a} receptor activation (Gillard *et al.* 2007).

It was found that different osmotic stimuli result in differential regulation of dendritic vasopressin release. For example, water deprivation, but not salt loading, triggers vasopressin release in the SON after acute osmotic challenge, while release from posterior pituitary was unaffected (Ludwig *et al.* 1996b). Salt loading depletes somato-dendritic stores of vasopressin and has a major impact on plasma sodium concentration while water deprivation has an impact on plasma volume. The consequent dendritic vasopressin release after water deprivation is then due to activation of baroreceptors-mediated pathways. Vasopressin is important in the regulation of cardiovascular function, and central vasopressin release from the SON was found to be important in blood pressure regulation (Toba *et al.* 1994). The baroceptor pathway provides tonic inhibition of magnocellular neurons in the SON via activation of afferents in the NTS and GABA release from the perinuclear zone (Grindstaff & Cunningham 2001). Angiotensin administration through icv increases vasopressin release from both the dendrites of the SON and PVN and the posterior pituitary (Moriguchi *et al.* 1994), in accordance to vasopressin's role in blood volume regulation. There is evidence that intranuclear vasopressin release is regulated by interactions between baroreceptor inhibition and chemoreceptor activation in the aortic arch and carotid body. Denervation of baroreceptors was found to increase release of vasopressin and oxytocin from the posterior pituitary and in the SON after hyperosmotic stimulation (Callahan *et al.* 1997; Morris & Alexander 1989). Hyperosmolar stimulation of the SON was also found to stimulate release of vasopressin from both the SON and neural lobe and this stimulus was found to increase mean arterial blood pressure (Ludwig *et al.* 1994b). Application of a V_1 receptor antagonist intravenously was found to have no effect on mean arterial

pressure, indicating that central activation of vasopressin release is important in regulation of blood pressure.

1.2.5 Stress and Other Effects

Vasopressin and oxytocin had been implicated in behavioural regulation where physical and emotional stress is implied, for example in forced swimming, it was shown that there was an increase in vasopressin and oxytocin release in the SON and PVN (Wotjak *et al.* 1998). Interestingly, vasopressin release from the posterior pituitary, unlike oxytocin release, was not increased in parallel to release in the SON and PVN in forced swimming. A more recent study using the morris watermaze as a swim stress paradigm showed that vasopressin release in the PVN, and oxytocin release in the SON, was increased during the swim stress (Engelmann *et al*. 2006). These increases in intrahypothalamic release also coincided with an increase in the plasma stress hormone (ACTH) levels. Involvement of dendritic vasopressin and oxytocin release has been shown in other stress paradigms. Microdialysis studies have shown that dendritic oxytocin release is involved in the male social defeat paradigm (Engelmann *et al.* 1999). Moreover, oxytocin release in the PVN was found to be elevated in lactating female rats defending their litter (maternal defence) in highly aggressive rats (Bosch *et al.* 2005). Meanwhile, oxytocin infusion to the PVN was found to reduce anxiety-related behaviour in male rats (Blume *et al.* 2008).

1.3 Mechanisms of Dendritic Peptide Secretion

As discussed so far, dendritic release of vasopressin and oxytocin does not always match release from the neural lobe. Stimulated secretion of vasopressin by dehydration or intravenous/intraperitoneal bolus hypertonic saline administration showed that vasopressin released in the SON is delayed compared to peripheral release, and occurs over a much longer duration (Ludwig *et al.* 1994a; Ludwig *et al.* 1994b). The spatial and temporal differences in peripheral and central release indicate differences in secretory mechanisms in the different cellular compartments. Immunocytochemical and electron-microscopic studies revealed peptide-containing dense core vesicles in the dendrites of magnocellular neurons (Pow & Morris 1989). These peptides, i.e. vasopressin and oxytocin, were found to be quite distal from the cell body and were contained in the classical 160 nm dense core secretory vesicles. However, little is known about the differential regulation of transport mechanisms of vesicles in dendrites compared to axon terminals. It had been proposed that neurosecretory vesicles are transported to the dendrites in the same way they are transported down axonal microtubules (Pow & Morris 1989).

Unlike release from axon terminals, dendritic peptide release from magnocellular neurons was not blocked by the sodium channel blocker tetrodotoxin (Scala-Guenot *et al.* 1987), suggesting that dendritic release is not potentiated by action potentials. However, voltage-gated Ca^{2+} channels have been reported on somata and these Ca^{2+} channel subtypes were found to be different to those in axon terminals (Fisher & Bourque 1995; Fisher & Bourque 1996). Moreover, like stimulated release from

axon terminals, Ca^{2+} was found to be important in dendritic release of magnocellular neurons (Mason *et al.* 1986; Neumann *et al.* 1993b; Wang *et al.* 1995). Hence, extracellular Ca^{2+} entry is important in triggering dendritic peptide release, but as discussed in more details below, it is not the only Ca^{2+} requirement for release.

1.3.1 The Importance of Intracellular Calcium

Under normal conditions, dendritic release of peptides does not occur from electrical stimulus. However, dendritic vasopressin and oxytocin release was found to be stimulated by high K^+ levels and is dependent on Ca^{2+} concentrations and central release of oxytocin induced by suckling in lactating rats was shown to be diminished by microdialysis with Ca^{2+}-free solution (Neumann *et al.* 1993b). Similarly, addition of K^+ to hypothalamic slices stimulates vasopressin and oxytocin release and this release is blocked in Ca^{2+}-free medium (Mason *et al.* 1986; Wang *et al.* 1995).

The inhibition of vasopressin and oxytocin release in the absence of Ca^{2+} indicates that release is triggered by influx of Ca^{2+} through Ca^{2+} channels in the dendritic plasma membrane. However, application of 100 nM oxytocin in a low Ca^{2+}-EGTA buffer can induce oxytocin release by triggering Ca^{2+} release from intracellular stores (Dayanithi *et al.* 2000) meaning that calcium entry through the plasma membrane is important in the initiation of stimulus-triggered dendritic release but intracellular Ca^{2+} mobilisation is important in the maintenance of dendritic release. These stores were found to be thapsigargin-sensitive stores of the endoplasmic reticulum –

thapsigargin inhibits the Ca^{2+}ATPase found on endoplasmic membrane and hence inhibits endoplasmic re-uptake of Ca^{2+} (Lytton *et al.* 1991). Oxytocin is thought to induce calcium release from thapsigargin sensitive calcium stores since application of oxytocin to isolated oxytocin cells after thapsigargin treatment did not induce further rise in intracellular calcium (Lambert *et al.* 1994) and oxytocin failed to elicit $[Ca^{2+}]_i$ increase after prolonged exposure to thapsigargin (Dayanithi *et al.* 2000). Oxytocin can mobilise Ca^{2+} from intracellular Ca^{2+} stores via G-protein coupled oxytocin receptors on dendritic membrane or on the soma (Chevaleyre *et al.* 2000; Lambert *et al.* 1994; Moos *et al.* 1989). Binding of oxytocin to its receptor activates PLC coupled to G-protein, which leads to conversion of phosphatidylinositol-4,5-bisphosphate ($PI(4,5)P_2$) to inositol triphosphate (IP_3). IP_3 binds to IP_3-sensitive receptors on the endoplasmic reticulum membrane facilitating release of calcium into the cytoplasm (Molnar & Hertelendy 1990) (**Figure 1-3**). Thus, oxytocin released from dendrites could trigger sufficient intracellular Ca^{2+} release to sustain its own release, and this release could be long-lasting.

Application of vasopressin to magnocellular neurons in the SON was also found to induce an increase in $[Ca^{2+}]_i$ but this increase is not only due to the release from intracellular stores but activation of voltage-gated calcium channels on the cell membrane (Dayanithi *et al.* 2000). Removal of extracellular Ca^{2+} completely abolished the effects of vasopressin and continuous application of vasopressin was found to desensitise the calcium response. Similar to oxytocin neurons, vasopressin neurons contain thapsigargin-sensitive calcium stores (Dayanithi *et al.* 2000).

Thapsigargin was also found to stimulate vasopressin release from isolated SON preparation by inducing a rise in intracellular [Ca^{2+}] (Ludwig *et al.* 2005). Application of thapsigargin to vasopressin neurons in Ca^{2+}-EDTA buffer elicited an increase in $[Ca^{2+}]_i$, demonstrating that intracellular calcium release can contribute to vasopressin induced increase in $[Ca^{2+}]_i$ (Dayanithi *et al.* 2000). However, prolonged stimulation by thapsigargin did not abolish the vasopressin induced rise in Ca^{2+}, unlike in oxytocin neurons, further confirming the importance of extracellular Ca^{2+} influx in vasopressin neurons. Dendritically released vasopressin can act on V_1 receptors to facilitate further vasopressin release through coupling to different second messenger systems. V_{1a} receptor was found to be coupled to PLC and also activates adenylate cyclase (AC) (Sabatier *et al.* 1998). Inhibition of protein kinase C (PKC) and protein kinase A (PKA) attenuated intracellular calcium release (Sabatier *et al.* 2004) (**Figure 1-3**) pointing to a role in calcium channel phosphorylation. There have been contrasting reports on whether V_{1b} receptors were expressed in the SON (Hernando *et al.* 2001; Hurbin *et al.* 1998; Hurbin *et al.* 2002; Vaccari *et al.* 1998). V_{1b} agonist was found to have no effect on intracellular calcium release (Sabatier *et al.* 2004) although V_{1b} receptors are coupled to PLC via $G_{\beta\lambda}$-protein (Jard *et al.* 1987; Michell *et al.* 1979). Hence, it is difficult to conclude whether V_{1b} receptors play a physiological role in somato-dendritic release.

1.3.2 Autoregulation

One of the major functions of dendritic release is autoregulation. Vasopressin and oxytocin are packaged with various neuro-active substances such as the endogenous

opioid dynorphin and the κ-receptor which dynorphin acts on (Shuster *et al.* 1999; Watson *et al.* 1982), providing an inhibitory effect on neuronal activity. Endocannabinoids, anandamide and 2-arachidonoyl glycerol, were found to be released from magnocellular neurons in an activity dependent manner to negatively regulate vasopressin and oxytocin neuronal activity by modulating presynaptic glutamate release (Di *et al.* 2005). Nitric oxide synthase (NOS), the enzyme that synthesises NO, is found to be upregulated in the SON by a range of osmotic stimuli (Ueta *et al.* 2002). NO can activate guanylyl cyclase in magnocellular neurons (Stern & Zhang 2005) which results in inhibition of calcium entry into the cell, leading to decrease in intracellular calcium concentration (Ignarro 1990). NOS is expressed in both vasopressin and oxytocin neurons (Hokfelt *et al.* 1994) and seems to have a dual regulatory effect on vasopressin and oxytocin neurons in that NO tonically inhibits vasopressin and oxytocin neuronal activity but enhances dendritic vasopressin release during osmotic stimulation (Gillard *et al.* 2007). **Figure 1-5** summarises the autocrine and paracrine actions of dendritic peptide release.

Of interest is that vasopressin and oxytocin themselves can modulate neuronal activity by acting on different subtypes of receptors. Early *in vitro* studies indicated that dendritic secretion of vasopressin and oxytocin act as autocrine and/or paracrine signals to modulate activities of vasopressin and oxytocin neurons (Gouzenes *et al.* 1998; Richard *et al.* 1991). This action of the magnocellular peptides is further demonstrated by the fact that vasopressin and oxytocin neurons express vasopressin and oxytocin receptors respectively (Hurbin *et al.* 2002; Freund-Mercier *et al.* 1994).

Furthermore, vasopressin receptors co-localise with vasopressin in the same secretory vesicles (Hurbin *et al.* 2002), indicating that vasopressin could act on its own receptors, which are delivered to the plasma membrane at the same time as the exocytosis of vasopressin.

In parturition and lactation, dendritic oxytocin release was shown to facilitate axonal oxytocin release and dendritic oxytocin release has also been shown to enhance activity of oxytocin neurons during hyperosmolarity (Morris *et al.* 1993; Richard *et al.* 1991). Oxytocin receptors are coupled to phospholipase C (PLC) (Gimpl *et al.* 2008) which activates mobilisation of Ca^{2+} from intracellular stores. This increase in $[Ca^{2+}]_i$ activates exocytosis of large dense core vesicles (LDCVs) from oxytocinergic dendrites. Unlike oxytocin, vasopressin's modulation of vasopressin neurons is less straight forward. Central application of vasopressin in the SON via microdialysis was shown to induce, and V_1 receptor antagonist reduced, vasopressin release in the SON (Wotjak *et al.* 1994). Since vasopressin acts on V_{1a}/V_{1b} receptors coupled to PLC to induce intracellular increase in Ca^{2+}, it is not surprising that vasopressin acts on vasopressin receptors to increase dendritic release. On the other hand, vasopressin was shown to inhibit phasic firing of vasopressin neurons via activation of V_1 receptors (Ludwig & Leng 1997). Icv administration of vasopressin was found to decrease plasma vasopressin concentration (Wang *et al.* 1982), suggesting an inhibitory role of dendritic vasopressin release on the activity of vasopressinergic neurons. It was proposed that vasopressin's activation of voltage-gated calcium channels induces rapid hyperpolarisation of vasopressin neurons leading to inhibition

of firing rate. Moreover, it had been shown that vasopressin facilitates pre-synaptic GABA release by increasing GABA-ergic neuronal activity (Hermes *et al.* 2000), indicating that the inhibitory effects of dendritically released vasopressin could be mediated through modulation of inhibitory inputs. Vasopressin has also been shown to reduce excitatory post-synaptic current acting on V_1 receptors (Kombian *et al.* 2000). Dendritic vasopressin release was found to be temporally different from vasopressin release in the posterior pituitary under systemic hyperosmotic challenge or intranuclear osmotic stimulation via microdialysis (Ludwig *et al.* 1994a; Ludwig *et al.* 1994b). Since dendritic release is delayed and outlasts release into the plasma, it was proposed that dendritic release of vasopressin stimulates further dendritic release until intranuclear vasopressin concentration reached a threshold that is able to trigger hyperpolarisation or increased GABA activity (Ludwig & Leng 1997; Ludwig 1998). This function of dendritic vasopressin is proposed to sustain the phasic firing of vasopressin neurons where continuous stimulation does not induce maximal vasopressin release and phasic firing induce maximal vasopressin secretion (Ludwig & Leng 2006). Moreover, there have been reports that both V_{1a} and V_{1b} receptors were found in the brain (Hurbin *et al.* 1998; Hurbin *et al.* 2002), leading to the speculation that the dual property of vasopressin's effect on the firing rate of vasopressinergic neurons, is exerted via the activation of the two subtypes of receptors (Gillard *et al.* 2007; Gouzenes *et al.* 1998; Ludwig & Leng 2006).

1.3.3 Facilitation of dendritic release via vesicle recruitment - priming

As mentioned above administration of thapsigargin to the SON was able to potentiate dendritic oxytocin release subsequent to an activating stimulus (Ludwig *et al.* 2002). In the same study, it was shown that application of an oxytocin agonist was able to generate the same effect. The action of oxytocin inducing dendritic oxytocin release is important because basal spike activity or antidromic stimulation of oxytocin neurons do not stimulate dendritic oxytocin release (Ludwig *et al.* 2002). However, after administration of thapsigargin or oxytocin to the SON, high-K^+ stimulation causes a remarkable increase in dendritic oxytocin release (Ludwig *et al.* 2002). The authors called this phenomenon the self-priming of dendritic oxytocin release where oxytocin acts on oxytocin autoreceptors to prepare oxytocin-expressing neurons for further activity-dependent release. This potentiation of oxytocin release was shown to be long-lasting (increased oxytocin release 30, 60 and 90 min after thapsigargin or oxytocin pre-treatment). Thus, oxytocin serves an important role in priming dendritic stores to enable activity-dependent dendritic oxytocin release for a prolonged period. On the contrary, even though vasopressin could induce dendritic vasopressin release, it does not induce priming. Priming of dendritic vasopressin release only occurs after thapsigargin pre-treatment (Ludwig *et al.* 2005), indicating the importance of intracellular Ca^{2+} mobilisation. The priming action of oxytocin is also thought to be dependent on the release of calcium from endoplasmic stores since the oxytocin receptor is coupled to PLC (Gimpl *et al.* 2008), which can activate release of endoplasmic stores of Ca^{2+} via conversion of $I(4,5)P_2$ to IP_3. A study based on quantifying the number of vesicles at 500 nm proximity to the plasma membrane showed that thapsigargin priming involves the recruitment of vesicles closer to the plasma membrane, making vesicles more readily releasable (Tobin *et al.*

2004) (see **Figure 1-6**). In bovine adrenal chromaffin cells, it was found that dense core vesicle translocation to the plasma membrane during activity-dependent potentiation (ADP), a phenomenon similar to vesicle priming in dendrites where LDCVs were translocated to the plasma membrane, is dependent on F-actin disassembly and MAP kinase activity (Park *et al.* 2006). The level of activated MAP kinase was found to be correlated to the level of calcium influx and inhibition of MAP kinase was found to inhibit F-actin disassembly, leading to decreased ADP. It is possible that the thapsigargin-induced rise in intracellular calcium concentration could activate similar mechanisms leading to LDCV translocation and exocytosis, however, this is yet unknown. Similarly, actin remodelling was found to be important in the self-priming of gonadotrophin-releasing hormone (GnRH) on gonadotrophs, where exposure of gonadotrophs to oestrogen and subsequently GnRH, produced an enhanced secretory response from the gonadotrophs in later GnRH stimulation (Aiyer *et al.* 1974). Inhibition of actin polymerisation by cytochalasin B was found to abolish the self-priming effect of GnRH (Lewis *et al.* 1985). Remodelling of the actin cytoskeleton was also found to be important in dendritic peptide release since active depolymerisation of F-actin by latrunculin was found to significantly increase high K^+ induced dendritic peptide release and polymerisation of actin by jasplakinolide inhibited release *in vitro* (Tobin & Ludwig 2007b). Axonal release was found to be unaffected by the two drugs mentioned. In the same study, thapsigargin-primed dendritic release of peptides was blocked by both the actin polymerising and depolymerising agents, suggesting that priming of vesicle release is affected by actin remodelling. Further studies using the transcription inhibitor antinomycin D and the translation inhibitor cycloheximide

showed that priming in oxytocin dendrites was not prevented by these two drugs, indicating that priming of vesicles by thapsigargin is not dependant on *de novo* synthesis of vesicles (Tobin & Ludwig 2007a).

So far, I have discussed that dendritic vasopressin and oxytocin release have important physiological effects and that release from dendrites is temporally and functionally separated from release in the neural lobe. To understand the mechanism regulating release from magnocellular dendrites, it is important to understand the molecular machinery governing release itself. The section below will concentrate on the regulation of exocytosis in reference to dendritic vasopressin and oxytocin release with comparison to axonal release.

1.4 Exocytosis in Magnocellular Dendrites

Ever since tannic acid fixation of dense core cargo in magnocellular dendrites (Pow & Morris 1989), it had been accepted that the magnocellular peptides are located in LDCVs and release of these peptides is via regulated secretion. Vasopressin and oxytocin are both synthesised as preprohormones (the nonapeptide oxytocin or vasopressin are synthesised with their respective neurophysin and a glycopeptide in the case of vasopressin). The function of neurophysin was found to be critical in sorting the prohormone into the regulated secretory pathway (Zhang *et al.* 2005). Abolishment of hormone-neurophysin association by point mutation in the

vasopressin domain was found to cause the prohormone to be trapped in the endoplasmic reticulum of neuroblastoma (N2a) cells (de Bree *et al.* 2003). The processed prohormone (neurophysin and vasopressin/oxytocin) then enters the Golgi apparatus for further glycosylation and packaging into LDCVs (for review see (Brownstein 1983). The hormones are then cleaved by enzymes that are packaged in the secretory granules along with secretory proteins such as chromogranin to mature (Loh 1987). The secretory granule enters the regulated secretory pathway and releases its contents upon stimulus (Huttner *et al.* 1995). **Figure 1-7** summarises the regulated secretory pathway of neuroendocrine cells. Upon activating stimuli, the plasma membrane depolarises, leading to calcium entry into the cell through voltage gated calcium channels, triggering fusion of vesicle membrane with plasma membrane, which results in release of the peptides, a process known as exocytosis. This regulated secretory pathway is different from the constitutive secretory pathway that is present in all cell types. Constitutive secretion also involves vesicles packaged in the Golgi apparatus and release of vesicle cargo is also via exocytosis. However, in constitutive secretion, an external stimulus, like an action potential or plasma membrane receptor activation is not required (Kelly 1985).

In axonal terminals, exocytosis of LDCVs is regulated by a plethora of proteins. The Soluble NSF (N-ethylmaleimide-sensitive factor) Attachment protein Receptors (SNARE) proteins were found to be critical (Jurgutis *et al.* 1996). There are many different important members of the SNARE family which participate at different stages of exocytosis. The regulated secretory pathway requires vesicles to be

transported from the cytoplasm to the plasma membrane, where they become docked and release their cargo when the correct stimulus arrives. Molecular evidence of exocytosis in dendrites came from the findings that important parts of the exocytotic machinery are also found in magnocellular dendrites (de Kock *et al.* 2003; Schwab *et al.* 2001). Many of these proteins have been identified in axon terminals, and proteins crucial for forming the SNARE complex, in which SNARE proteins anchored at the plasma membrane (t-SNAREs) and those that are found on vesicular membrane (v-SNAREs), have also been identified in dendrites of magnocellular neurons. Synaptotagmin (Ca^{2+} sensor found on vesicular membrane), SNAP-25 and syntaxin (both t-SNAREs) were found in dendrites of neonatal hypothalamic neurons (Schwab *et al.* 2001). Synaptobrevin (v-SNARE) has also been implicated in dendritic oxytocin release where membrane capacitance change was decreased in the presence of tetanus toxin which cleaves synaptobrevin in hypothalamic slice preparation (de Kock *et al.* 2003). α-soluble-NSF-attachment protein (αSNAP) which has an important role in detaching the SNARE complex after exocytosis has also been reported in magnocellular dendrites (Morris *et al.* 2000). In synaptic terminals, exocytosis involves recruitment of vesicles close to the plasma membrane. Three different pools of vesicles with different release properties and mobilisation kinetics have been found (Kuromi & Kidokoro 1998; Richards *et al.* 2003; Schneggenburger *et al.* 1999). As discussed above, priming of vesicle release in magnocellular dendrites was shown to recruit vesicles to closer proximity to the plasma membrane and this recruitment did not require protein synthesis (Tobin *et al.* 2004; Tobin & Ludwig 2007b). This points to the possibility of the existence of differentially regulated vesicle pools in magnocellular dendrites, similar to those

found in axon terminals (Hsu & Jackson 1996). The regulation of vesicle pools is further discussed below.

1.4.1 Vesicle pools

Much of our understanding of vesicle pools came from studies of synaptic vesicles (SVs). Most synaptic terminals rely on three vesicle pools for neurotransmission: the readily releasable pool (RRP), the reserve pool (RP) and a recycling pool of vesicles (Rizzoli & Betz 2005). Studies in synaptic terminals revealed that neurotransmitter release from vesicles displayed differences in kinetics within the same terminal (Kuromi & Kidokoro 1998; Richards *et al.* 2003; Schneggenburger *et al.* 1999). One store of transmitters releases readily upon electrical stimulation (RRP) and another that releases upon intense or prolonged stimulation (RP). The RRP is made up of a small number of vesicles immobilised (docked) at the plasma membrane (Heuser *et al.* 1979) and the release of the RRP can be exhausted with high frequency electrical stimulation. Since these vesicles are docked at the plasma membrane, they are available for instantaneous release upon stimulation. Moreover, these vesicles are gathered at "active zones" where there is a concentration of Ca^{2+} channels (Neher 1998)and hence, upon activating stimulus, influx of Ca^{2+} through voltage dependent Ca^{2+} channels trigger exocytosis of the vesicles docked at these sites (Murthy & De Camilli 2003). This concentration of Ca^{2+} channels means that a high level of Ca^{2+} does not have to be reached in the whole cell but only at active zones. The proximity of vesicle pools and Ca^{2+} channels also mean that activation of exocytosis is a quick process. However, as opposed to SVs release, LDCV release in magnocellular nerve

terminal and in magnocellular dendrites does not seem to be associated with active zones since release is possible at all areas of the dendritic plasma membrane (Pow & Morris 1989). The non-association of vesicle release and active release sites is probably one of the reasons why latency to release after stimulation is longer in peptide-secreting neurons. Moreover, in axonal terminals, recycling SVs also facilitate quick exocytosis via rapid endocytosis which enables endocytosed vesicles to be re-released by joining a recycling vesicle pool (Harata *et al.* 2001). The recycling pool of vesicles is an intermediary pool found between the RRP and RP. It contains more vesicles than the RRP but less than the RP and is released under more prolonged stimulation than required for RRP release, but less than required for RP release (Harata *et al.* 2001; Kuromi & Kidokoro 2003). There is a possibility that the recycling pool of vesicles is made up of vesicles that has gone through 'kiss-and-run' exocytosis, where vesicles fuse with the plasma membrane, release part of their cargo content, and are quickly retrieved, whereby then they join the recycling vesicle pool which can be mobilised when the RRP is depleted (Aravanis *et al.* 2003). 'Kiss-and-run' exocytosis has recently been demonstrated in LDCV secretion from the soma and neurites of cultured hippocampal neurons (Xia *et al.* 2009). Vesicles which have partially released their contents were also shown to re-participate in release within a short period of time, suggesting that a recycling vesicle pool might be present in the LDCV secretory pathway. This has also been shown in mouse chromaffin cells where endocytosed LDCVs can be re-recruited for release (Bay *et al.* 2007). However, a recycling vesicle pool has yet to be demonstrated in magnocellular dendrites. The third vesicle pool, the RP, is the largest pool and is released only after the depletion of the RRP and the recycling pool. The

physiological function of the RP is unclear since physiological stimulation does not mobilise this pool. However, release of RP vesicles under prolonged stimulation suggests that this vesicle pool act as a reserve of vesicles which can be released under high physiological demand (Kuromi & Kidokoro 1998).

Given that the neural lobe contains ~1.48 x 10^{10} vasopressin and around the same number of oxytocin vesicles (Leng & Ludwig 2008), there seems to be an excessive amount of peptides stored in the neural lobe. In the magnocellular oxytocin system, the milk-ejection reflex releases about 0.5 pg of oxytocin per burst fired (~5 vesicles from all the oxytocin terminals in the neural lobe) (Leng & Ludwig 2008), leaving a large pool of vesicles unreleased. It was also found that each dendrite and soma contains ~15000 oxytocin vesicles and ~60000 for vasopressin (Leng & Ludwig 2008). Since the biggest pool of vesicle comes from the RP, it is intriguing as to why the magnocellular cells contain such a vast amount of vesicles that do not release under normal physiological stimulation. However, unlike SVs that are replenished by endocytic recycling of neurotransmitters near the plasma membrane (Morris & Schmid 1995), LDCVs have to be synthesised and packaged in cell bodies. Since sites of release are often far away from the somata, it is probable that the abundance of vesicles stored in the RP in axonal terminals in the magnocellular neurosecretory system could serve a purpose in maintaining a constant supply of peptides in the event of prolonged shortage of water where vasopressin release has to be maintained until water is found, or in the case of oxytocin, an increased demand of milk from the young might require release from the RP and this may also apply to

dendritic release. Magnocellular axonal terminals also contain a non-releasable pool of vesicles found in specialised swellings known as Herring Bodies (Heap *et al.* 1975; Krsulovic *et al.* 2005). It is not known whether dendrites also contain a non-releasable vesicle pool. This is further discussed in the next section.

1.4.2 Regulation of LDCV pools

Tobin & Ludwig postulated that cortical actin microtubules are involved in regulating vesicle pools in magnocellular dendrites (Tobin & Ludwig 2007a). The involvement of F-actin in vesicle pool regulation has also been found to be key in bovine adrenal chromaffin cells (Vitale *et al.* 1995; Trifaro *et al.* 2000). It was shown that magnocellular dendritic peptide release requires the depolymerisation of the filamentous or F-actin cytoskeleton beneath the plasma membrane (Tobin & Ludwig 2007a) since the actin polymerising agent jasplakinolide inhibited and latrunculin (actin depolymerising) enhanced high K^+ -induced peptide release. However, this is specific to dendritic peptide release since jasplakinolide did not block high K^+-induced peptide release from axon terminals. Latrunculin facilitated peptide release from the neural lobe but did not potentiate further release by high K^+ depolarisation (Tobin & Ludwig 2007b; Tobin & Ludwig 2007a). Potentiation of peptide release in dendrites by K^+ after latrunculin also indicates that actin depolymerisation can access a pool of vesicles inaccessible by K^+ depolarisation. Involvement of F-actin in the regulation of exocytosis has been shown in other neuroendocrine cell types such as pancreatic β-cells (Wilson *et al.* 2001), isolated rat islet cells (Thurmond *et al.* 2003), bovine adrenal chromaffin cells (Vitale *et al.*

1995), and pheochromocytoma (PC12) cells (Matter *et al.* 1989). Jasplakinolide was shown to inhibit high K^+-induced insulin release in pancreatic β-cells and latrunculin was shown to potentiate high K^+-induced release (Thurmond *et al.* 2003; Wilson *et al.* 2001), much similar to the events in magnocellular dendritic peptide release. In bovine adrenal chromaffin cells, disruption of F-actin increased the number of vesicles at subplasmalemal level indicating that F-actin is important in the regulation of movement of vesicles from the RP to the RRP (Vitale *et al.* 1995). The two vesicle pools have been proposed to be linked by cytoskeletal elements, one of which is actin (Hirokawa *et al.* 1989). Actin filaments has been implicated in the movement of vesicles and also translocation of RP vesicles to RRP (Doussau & Augustine 2000; Kuromi & Kidokoro 2003). As discussed above, priming of oxytocin release involves translocation of vesicles to the plasma membrane, making them more readily releasable. If priming does not involve *de* novo synthesis of vesicles and if actin is involved in the recruitment of vesicles during priming, then it is very possible that vesicles from a RP are recruited to the plasma membrane in dendrites during priming. **Figure 1-8** summarises the possible mechanism for oxytocin priming in magnocellular dendrites. Hence, it is possible that regulation of dendritic peptide release is more similar to the regulation of LDCV release from endocrine cells than release from the neural lobe. In bovine adrenal chromaffin cells, it had been shown that newly synthesised LDCVs become 'docked' at the plasma membrane soon after their biogenesis and join the RRP (**Figure 1-9**). These newly synthesised vesicles were found to be docked at the plasma membrane and could be released by nicotine stimulation. Matured LDCVs was found to make up the RP. These matured LDCVs were found to occupy the cell centre and were not

immediately released by nicotinic stimulation. The same study showed that different sets of stimuli could stimulate the release of different vesicle pools independently (Duncan *et al.* 2003; Wiegand *et al.* 2003). Hence, it was hypothesised that newly synthesised vesicles were docked at the plasma membrane for a short period of time and when exocytosis does not occur, they undock and translocate to the functionally different RP. The underlying mechanism for this age-dependency on vesicle sorting is, however, unknown. It is currently unknown whether dendrites also contain these functionally distinct pools of vesicles.

Routing of LDCVs into dendrites can occur via several pathways. LDCVs can be synthesised directly in dendrites, transported from the soma to dendrites, or transported retrogradely from axonal terminals. One study found that deletion of a single nucleotide could prevent the targeting of vasopressin mRNA to the axons but not to the dendrites (Mohr *et al.* 1995). This nucleotide deletion resulted in a disruption in the stop codon for mRNA translation. Hence, it was proposed that peptide transport to the axon terminal occur after translation and since transport to dendrites was not disrupted, mRNA translocation to dendrites must occur before translation. Magnocellular dendrites were found to contain ribosomes and rough endoplasmic reticulum, hence, mRNA may be translocated to dendrites for translation (Trembleau *et al.* 1994). However, although Golgi elements were found in the proximal parts of dendrites (Ma & Morris 2002), polyribosomes were found to extend to distal locations of dendrites, making it unclear whether protein biosynthesis actually occur in dendrites. It is unclear why mRNA is transported to the dendrite if

translation doesn not occur in dendrites. Moreover, since elements of the GA, which is essential for vesicle packaging and is the last stage of vesicle synthesis before trafficking into the cytoplasm, were mostly found in the proximal parts of dendrites, close to the soma, translocation of vesicles still mainly occurs from the soma to dendrites It had been proposed that neurosecretory vesicles are transported to the dendrites in the same way they are transported down axonal microtubules (Morris & Ludwig 2004). In magnocellular neurons, another peptide, galanin, was found to be specifically routed to dendrites (Landry *et al.* 2003). Galanin which was co-expressed in the same LDCV as vasopressin was found to be targeted to the axon terminals whereas dendritically located galanin was mostly not found to be co-expressed with vasopressin. The mechanism of this routing, however, is not clear. Unlike the routing of galanin, specific targeting of vasopressin and oxytocin to dendrites has not been shown. If vesicle pools can be regulated by age, would vesicle age affect the preference of translocation along the length of dendrites? Another interesting question is whether routing of LDCVs could be dependent or independent on vesicle age. It is also possible that dendrites do not contain different pools of vesicles segregated by age, but instead, vesicles that are not released from the axon terminal may translocate in a retrograde fashion (Alonso & Assenmacher 1983) to the dendrite, making up the dendritic pool of vesicles. If dendritic vesicles were made up of retrogradely transported vesicles from the neuronal terminal, dendrites may also be important compartments for degradation since matured vesicles would eventually enter the degradation pathway (Broadwell *et al.* 1980; Krsulovic *et al.* 2005; Heap *et al.* 1975). Since normal physiological conditions do not release all vesicles in magnocellular neurons, a vast amount of vesicles remain

unreleased. In the magnocellular neuronal terminals, RRP vesicles enter endings of magnocellular terminals where stimulation triggers peptide release. Unreleased vesicles join the RP in swellings where they could be re-recruited for release (Heap *et al.* 1975; Krsulovic *et al.* 2005). However, a separate pool of vesicles was found in the specialised swellings, the Herring Bodies (Heap *et al.* 1975; Krsulovic *et al.* 2005), which contain an abundance of lysosomes. It is believed that unreleased vesicles are translocated to these specialised compartments for degradation. Moreover, it was found that vesicles which have entered these Herring Bodies could not be re-recruited for secretion, making up a non-releasable pool of vesicles. It is uncertain whether magnocellular dendrites also contain a non-releasable pool of vesicles and whether magnocellular dendrites contain specialised compartments for degradation. Although dilations were found in parts of dendrites (Sofroniew & Glasmann 1981), these dilations were not found to be different in properties from the rest of the dendrite. Electron microscopy and immunohistochemistry have revealed the presence of lysosomes in magnocellular dendrites (Ma & Morris 2002), although the physiological significance of these lysosomes has not yet been verified. If dendrites are important destinations for aged vesicles ready for degradation, then thapsigargin priming represents a unique way of recruitment of aged vesicles in magnocellular dendrites which does not occur in magnocellular axon terminals. On the other hand, like their axonal counterparts, dendrites can contain specialised compartments for degradation, which will lead to the speculation of the presence of both newly synthesised and aged LDCVs. Nevertheless, evidence of the existence of different vesicle pools in magnocellular dendrites is still lacking and questions about whether these vesicle pools, if they exist, can be differentially regulated, would be

essential to understanding the mechanisms of vesicle priming and vesicle release in magnocellular dendrites.

1.5 Hypothesis

The dynamics of dendritic release of vasopressin and oxytocin has been extensively studied. However, the mechanisms that govern dendritic release of peptides are still unknown. Meanwhile, dendritic peptide release had been shown to be temporally segregated from axon terminal release (Ludwig *et al.* 1994a) indicating that mechanisms governing release at the two ends of a neuron can be different. Evidence of vesicle priming in magnocellular dendrites (Ludwig *et al.* 2002) and study inducing actin (de)polymerisation (Tobin & Ludwig 2007b) suggested the existence of differentially regulated vesicle pools. It had been shown that priming did not require synthesis of new proteins (Tobin & Ludwig 2007a), pointing to the existence of a reserve pool of vesicles in magnocellular dendrites that are made up of aged vesicles and can be recruited. It is likely that vesicle pools exist in dendrites and these vesicle pools are differentially regulated to those found in axon terminals. The hypothesis of this thesis is that vesicle pools exist in magnocellular dendrites and these vesicle pools may be differentially regulated. The aim of this study is to find out the mechanisms of vasopressin release in dendrites by addressing the question of how LDCVs are organised in and released from dendrites of magnocellular neurons.

With the production of a transgenic rat line where endogenous vasopressin is tagged to enhanced green fluorescent protein (VP-eGFP) (Ueta *et al.* 2005), it is now possible to visualise vasopressin-containing cells under fluorescence without pre-treatment. The transgene used to produce VP-eGFP transgenic rats consists of the eGFP coding sequence inserted in exon III of the VP structural gene (**Figure 1-10**). VP-eGFP mRNA and eGFP fluorescence in the SON and PVN was shown to be increased after dehydration for 2 days, in accordance with normal physiological response of endogenous vasopressin (Ueta *et al.* 2005). Further electrophysiological recordings by the authors confirmed that eGFP-expressing cells have membrane properties characteristic of vasopressin cells. Because the SON only contain magnocellular cell bodies and dendrites, with very few vasopressinergic axonal collaterals, it is feasible to dissect out the SON and study specifically the dendrites. Previous studies expressing a similar VP-eGFP chimera in PC12 cells has found that the VP-eGFP transgene enters the regulated secretory pathway (Zhang *et al.* 2005). Hence, eGFP targeted to LDCVs is an ideal tool to study the dynamics of vesicle pools in magnocellular dendrites. Since vasopressin is endogenously tagged to eGFP, identification of vasopressin and vasopressin-expressing neurons does not require immunohistochemical labelling of vasopressin. This helps avoid the disadvantages of immunohistochemical labelling where the level of peptide detection hugely depends upon the method of tissue fixation. Correlation studies of endogenous VP-eGFP with lysosomes in magnocellular dendrites can be carried out to investigate whether dendrites are important destinations for aged vesicles and also whether dendrites contain compartments for degradation by analysing the amount of endogenous VP-eGFP where lysosome staining is seen. Endogenous tagging of VP-

eGFP also allows for the tracing of vesicles along dendritic profiles according to age by using a timed release protocol following a block in vesicle exit from the Golgi apparatus (GA). LDCV release from the GA is inhibited at 20°C (Saraste *et al.* 1986). By inhibiting LDCV release from the GA and releasing this exit block by increasing incubation temperature of *in vitro* hypothalamic slices, it is possible to trace LDCVs that are newly packaged and released from the GA. This investigation allows one to study whether newly synthesised LDCVs are translocated to dendrites and also, whether these vesicles are preferentially targeted along the profiles of dendrites. In addition to the in vitro visualisation of eGFP-tagged vasopressin LDCVs in magnocellular dendrites, one of the most interesting aspects that is afforded by the use of endogenous VP-eGFP tagging is the possibility for live cell imaging. Using organotypic slice explants of the hypothalamus, the soma and dendrites of magnocellular neurons are retained and can be cultured for up to weeks (Stoppini *et al.* 1991; Wellmann *et al.* 1999). Live cell imaging of VP-eGFP-expressing magnocellular dendrites in organotypic slice cultures coupled with differential stimulation offers a possibility to analyse release of LDCVs in terms of fluorescent intensities in living magnocellular neurons. It is also possible to express a time stamp in these cells using either fluorescent compounds that change their fluorescent properties during maturation (Duncan *et al.* 2003; Terskikh *et al.* 2000) or an inducible fluorescent construct can be expressed where a pulse-chase time lapse protocol can be used to study regulation of newly synthesised and older vesicles in magnocellular dendrites to establish the existence of vesicle pools. This study also allows for the use of different pharmacological interventions to study the functional significance in terms of vesicle release of the different vesicle pools

found. The aim of this thesis is to establish the existence of vesicle pools in dendrites, and to study the regulation of these vesicle pools.

1.5.1 Objectives

It is not known whether vesicle pools in magnocellular dendrites are segregated by vesicle age and whether LDCVs destined for magnocellular dendrites are specifically targeted. As discussed above, parts of the protein synthesis machinery are found in magnocellular dendrites (Ma & Morris 2002) but the non-association of the biosynthetic pathway makes the theory that LDCVs are synthesised directly in dendrites unlikely. Retrograde transport from neuronal terminals to dendrites occurs in magnocellular neurons (Alonso & Assenmacher 1983) and hence, it is possible that the dendritic vesicle pool could be made up of retrogradely transported LDCVs. As unreleased LDCVs mature, they undergo degradation. Hence, if the dendritic vesicle pool was made up of retrogradely transported vesicles, a high incidence of lysosomes will be expected in dendrites. The first objective of this project is to establish whether magnocellular dendrites are important sites for vesicle degradation through labelling of lysosomes and correlation of lysosomal locations, and hence the importance of dendrites as a compartment for degradation, with density of VP-eGFP in those locations. On the other hand, the dendritic vesicle pool may exist separately from the axonal pool. The second objective of this project is to find out whether newly synthesised LDCVs translocate from the soma to the dendrites. By blocking

vesicle exit from the GA, newly packaged VP-eGFP vesicles can be traced. Tracing of the change in fluorescent intensity along dendritic profiles will provide an idea of whether newly synthesised vesicles translocate to dendrites, and also whether there are any preferential sites for translocation of newly synthesised vesicles. The third objective is to study LDCV release from magnocellular dendrites via live cell imaging of cultured hypothalamic slices of the VP-eGFP transgenic rat. This study will also look at the effects of thapsigargin priming in live magnocellular neurons. In addition, to establish whether dendrites contain vesicle pools of different age and whether these vesicle pools were segregated by age, transfection studies will be carried out to express reporter proteins targeted to LDCV. A fluorescent time stamp which changes colour as it matures over time can be used to image LDCVs of different age. Another way to segregate vesicles by their age is by the expression of an inducible reporter protein via neuronal transfection where the induction of protein expression can be controlled. By fixing or imaging magnocellular neurons at specific time points after induction of protein expression, LDCVs of different age can be visualised. The final objective of this project is to establish a system whereby difficult to transfect magnocellular neurons can be transfected to express reporter time stamps for LDCV age visualisation.

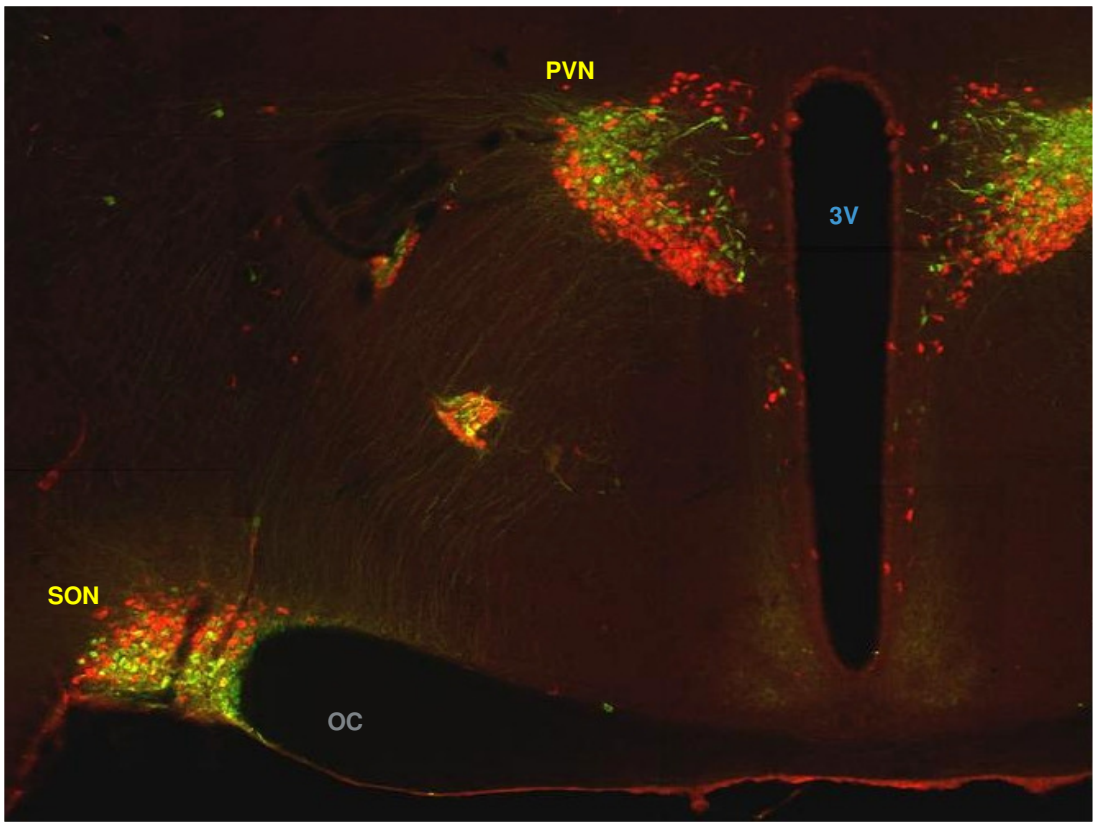

Figure 1-1. Coronal section of the hypothalamus showing the supraoptic and paraventricular nuclei (SON and PVN). Immunofluorescent labelling shows vasopressin cells (green) are located in the ventral part of the SON and medial part of the PVN and oxytocin cells (red) are located in the dorsal part of the SON and lateral part of the PVN. 3V = third ventricle and OC = optic chiasm. (Taken from Ludwig and Leng 2006).

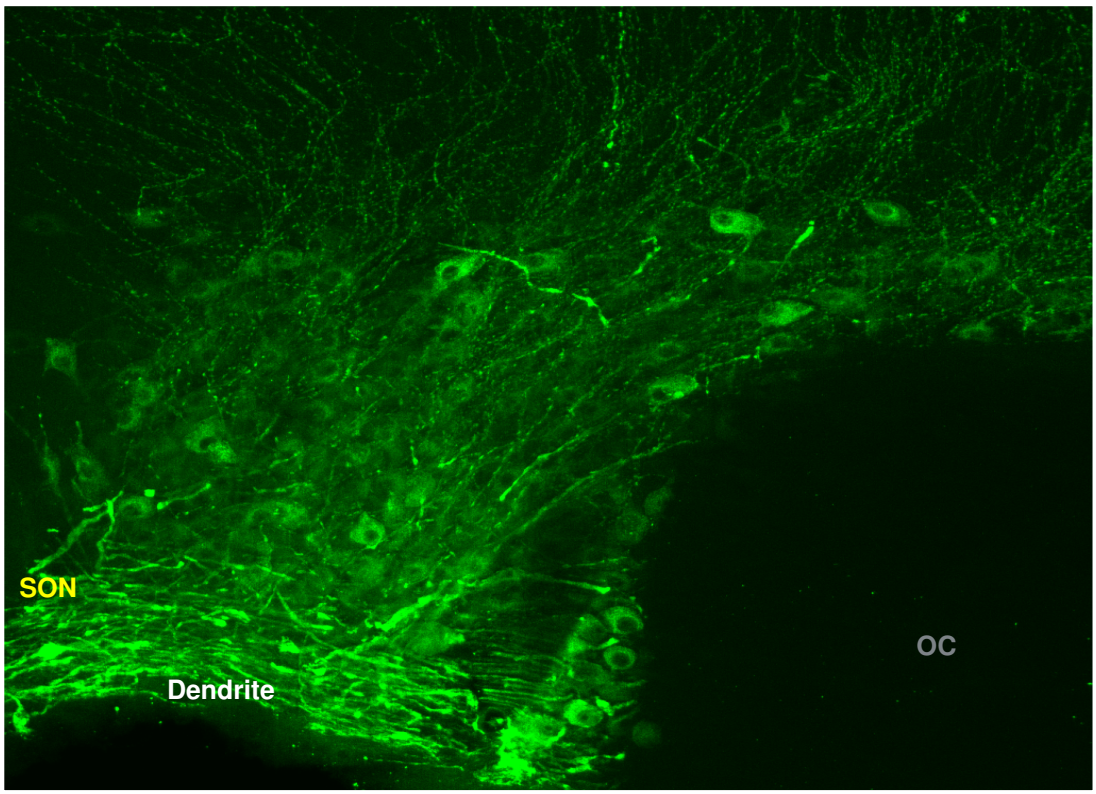

Figure 1-2. Coronal section of the hypothalamus showing the SON. Cell bodies and dendrites of vasopressin expressing neurons (green) can clearly be identified. OC = optic chiasm. (Taken from Ludwig and Leng 2006).

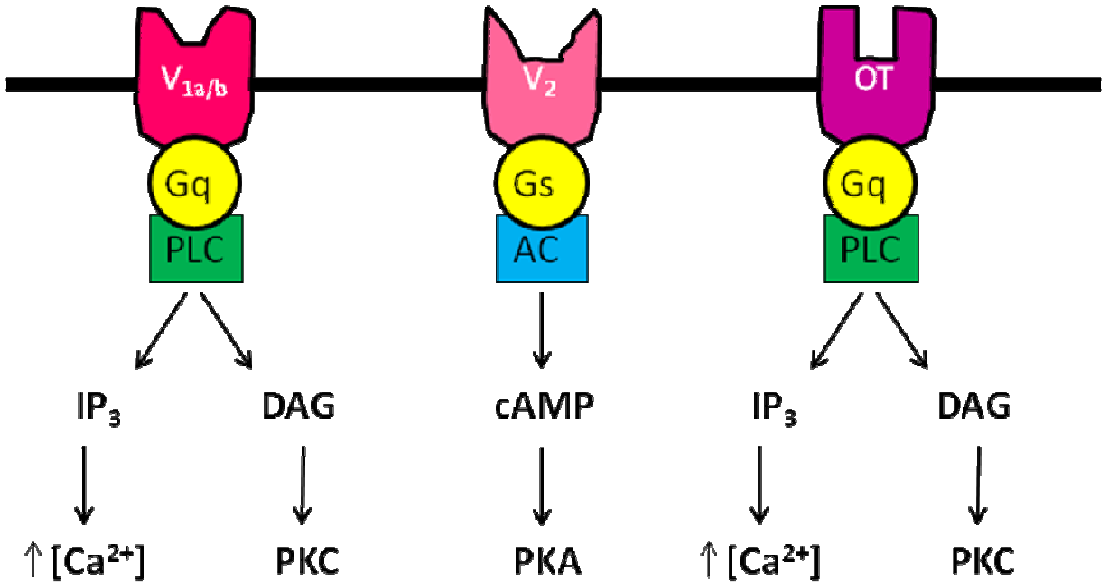

Figure 1-3. Downstream signalling pathways of VP and OT receptors. V_{1a}, V_{1b} and OT receptors are coupled to PLC via Gq protein. Activation of PLC leads to conversion of PIP_2 to IP_3 and DAG. IP_3 binds to IP_3 receptors on membranes of the ER to activate Ca^{2+} release into the cytoplasm. DAG activates PKC. V_2 receptors are coupled to AC via Gs protein. Activation of AC via Gs protein to induce cAMP production which activates PKA. Figure adapted from (Dayanithi *et al.* 2000).

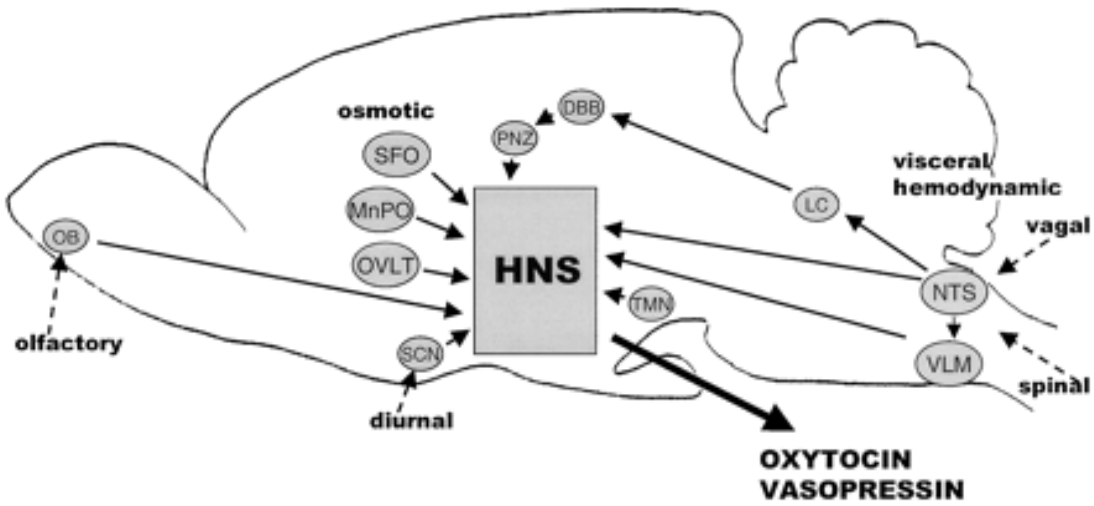

Figure 1-4. Afferent inputs to the vasopressin and oxytocin magnocellular neurons of the HNS. DBB = diagonal band of Broca; LC = locus coeruleus; MnPO = median preoptic nucleus; NTS = nucleus of the tractus solitarius; OB = main and accessory olfactory bulbs; OVLT = organum vasculosum of the lamina terminalis; PNZ = perinuclear zones adjacent to the supraoptic and tuberomammillary nuclei; SFO = subfornical organ; SCN = suprachiasmatic nucleus; TMN = tuberomammillary nuclei; VLM = ventrolateral medulla. Figure obtained from (Burbach *et al.* 2001).

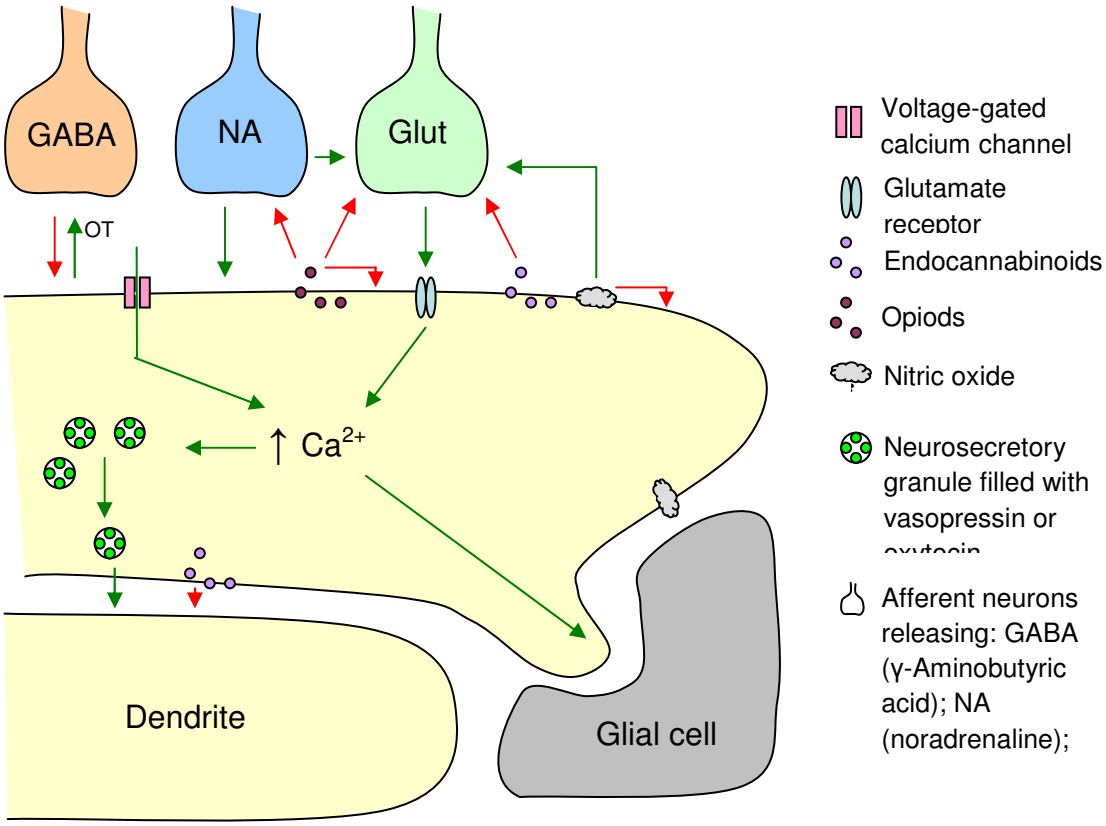

Figure 1-5. Figure showing the different functional aspects of dendritic peptide release. Dendritic peptide release is involved in the modulation of pre-synaptic transmission (red arrows = inhibition and green arrows = facilitation). Autoregulation of dendritic release occurs via modulation by dendritically released peptides and co-released substances such as opiods (enkaphalin and dynorphin), endocannabinoids, and nitric oxide. In the case of oxytocin dendrites, oxytocin acts on paracrine oxytocin receptors to stimulate further oxytocin release. Both vasopressin and oxytocin can act on dendritic autoreceptors to regulate neuronal activity (Ludwig & Leng 2006). At the onset of parturition, during lactation, and during acute osmotic challenges, dendrites become morphologically plastic and bundling of dendrites occur due to glial retraction (Theodosis *et al.* 2008). Nitric oxide tonically inhibits dendritic release but induced glutamatergic activation of dendritic release during stimulation (Gillard *et al.* 2007). Endocannabinoids released from magnocellular neurons contributing to retrograde signalling and inhibition of paracrine dendritic release (Hirasawa *et al.* 2004) which plays a role in synchronisation of dendritic oxytocin release during burst firing. (Figure adapted from Ludwig & Pittman 2003).

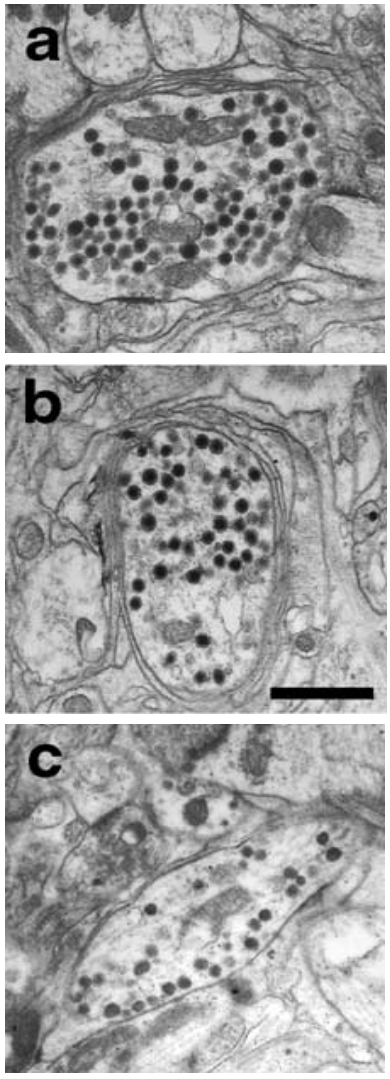

Figure 1-6. Electron micrographs showing dendritic distributions of dense core vesicles from (a) a control, (b) a salt-loaded control, and (c) a salt-loaded thapsigargin-treated rat. Scale bar = 1 µm. Dense core vesicles were found to have translocated to close proximity of the plasma membrane after thapsigargin treatment, making them more readily releasable. (Figures taken from (Tobin *et al.* 2004)

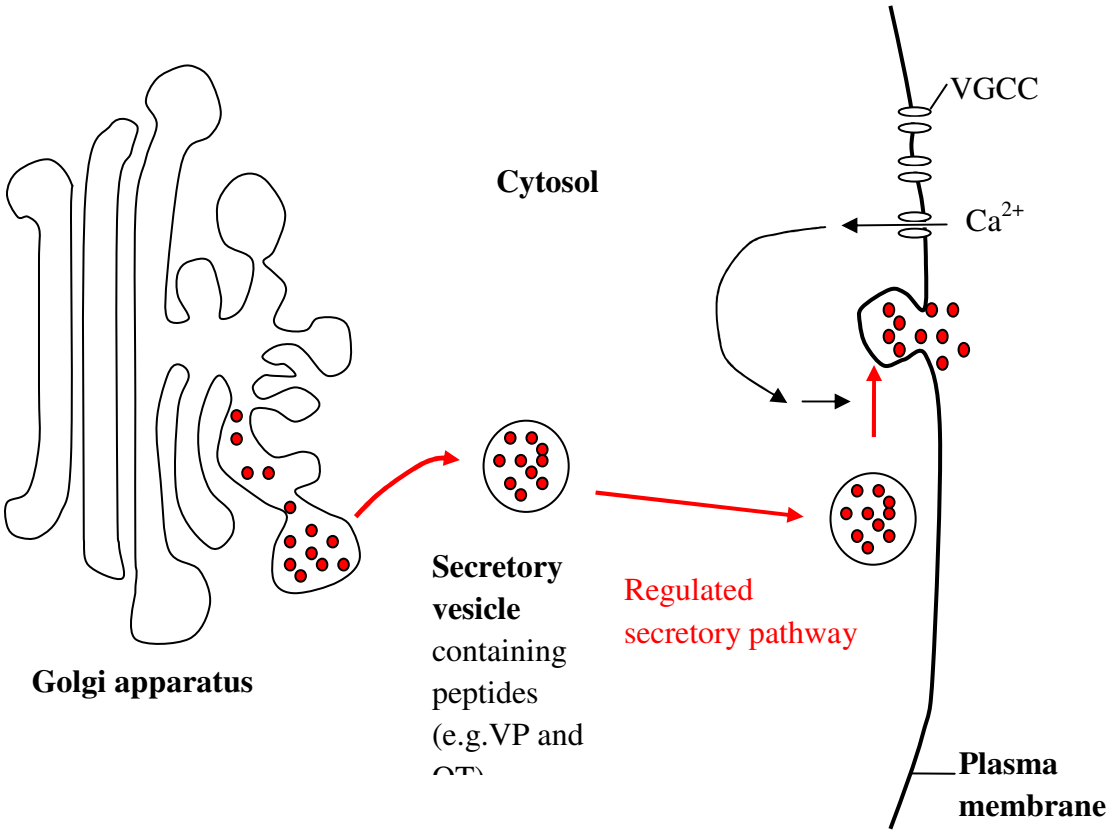

Figure 1-7. Simplified figure of the regulated secretory pathway. Vasopressin and oxytocin are packaged with their respective neurophysins, and glycopeptide in the case of vasopressin, into secretory vesicles in the Golgi apparatus and enter the regulated secretory pathway. Peptides concentrate in secretory vesicles and form dense core vesicles which translocate to the plasma membrane where they are docked and ready for release. Upon stimulation, calcium enters through voltage gated calcium channels (VGCCs) which triggers fusion of vesicle and plasma membrane, resulting in release of vesicular cargo (exocytosis). (Adapted from(Alberts *et al.* 1994)).

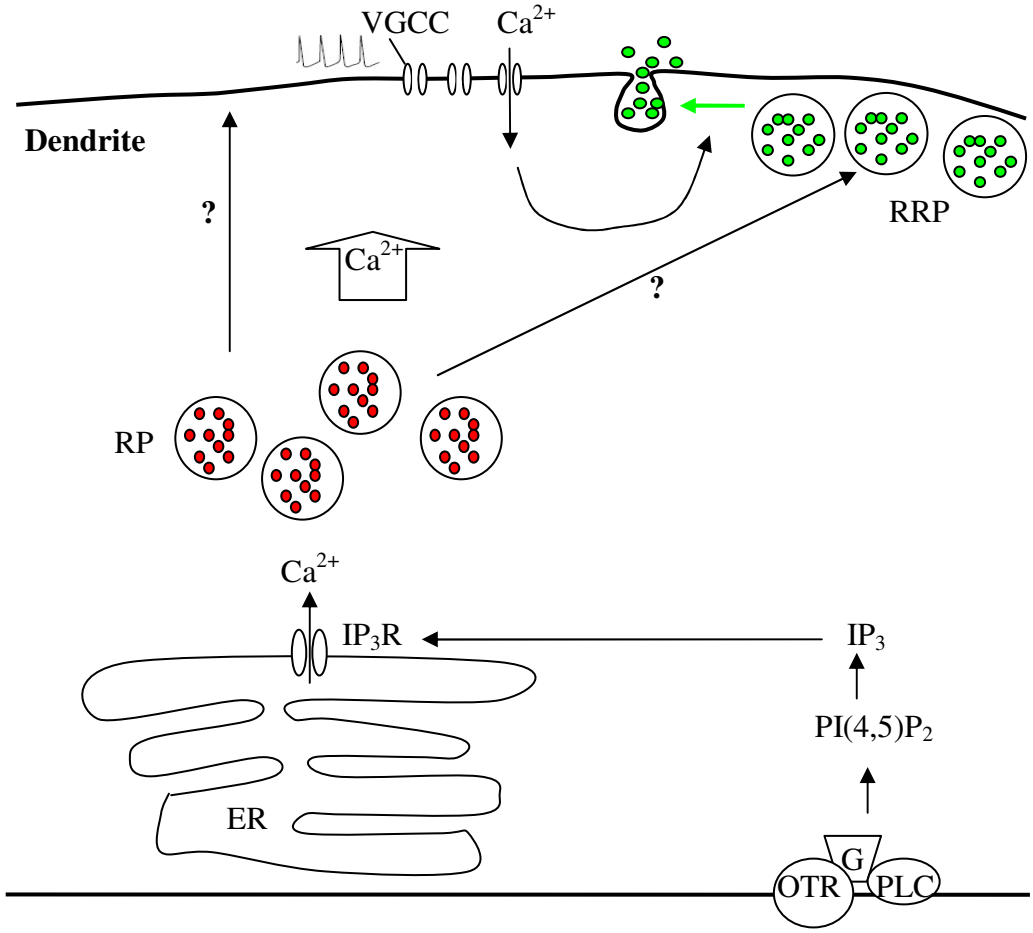

Figure 1-8. Possible mechanism of priming of dendritic release. Oxytocin binds to G-protein (G) coupled oxytocin receptor (OTR) which activates phospholipase C to convert phosphatidylinositol-4,5-bisphosphate ($PI(4,5)P_2$) to inositol triphosphate (IP_3). IP_3 activates IP_3 receptors (IP_3R) on the endoplasmic reticulum (ER) to release Ca^{2+} into the cytoplasm. Increase in intracellular Ca^{2+} could cause vesicles in the reserve pool (RP, red) to join the readily releasable pool (RRP, green) docked at the plasma membrane (priming). (Figure adapted from Ludwig & Leng 2006).

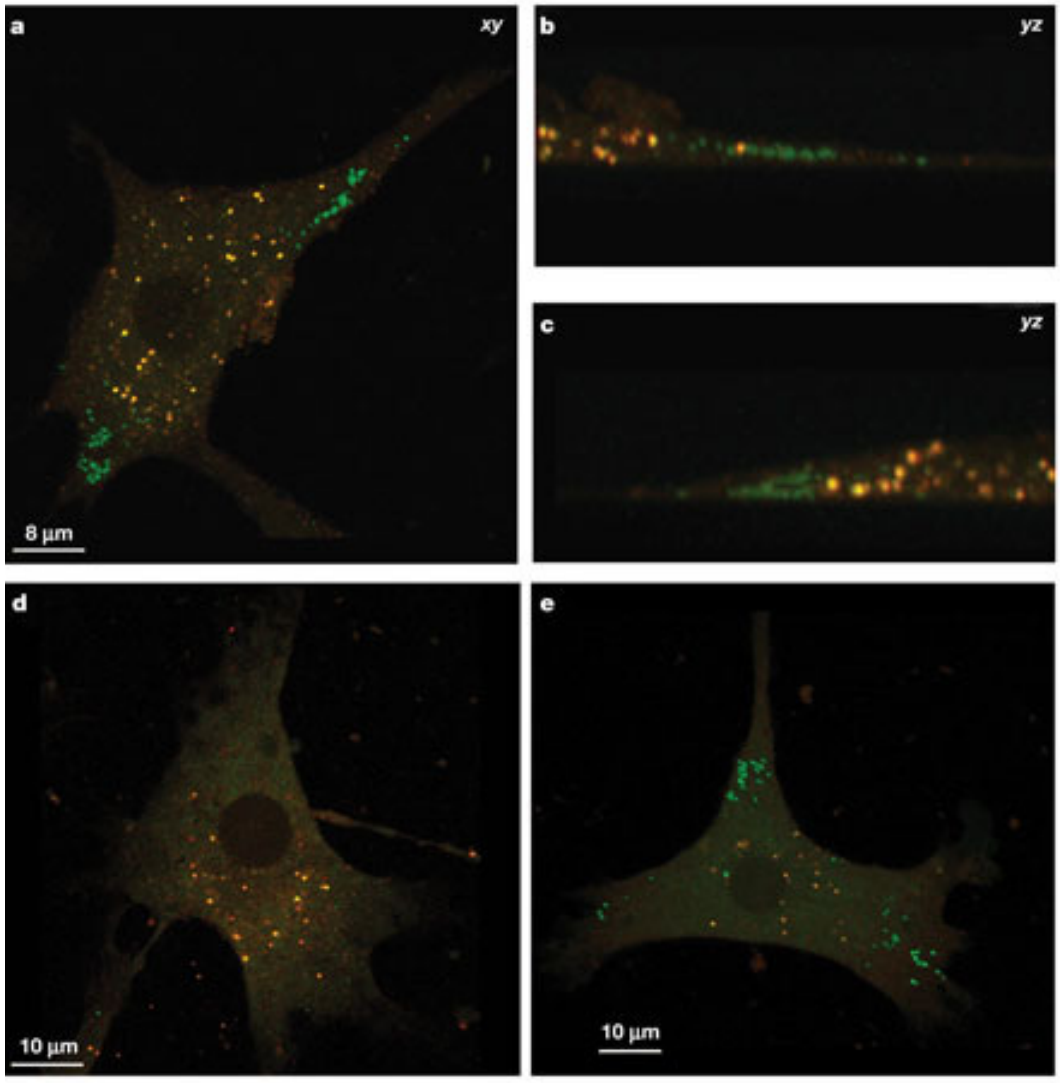

Figure 1-9. Images from bovine adrenal chromaffin cells transfected with a fluorescent time-stamp that changes colour from green to red as the fluorescent protein matures within 16 hr showing that newly synthesised LDCVs (green) were docked at the plasma membrane while older vesicles (yellow and red) resided further inside the cells. (Images taken from Duncan *et al.* 2003).

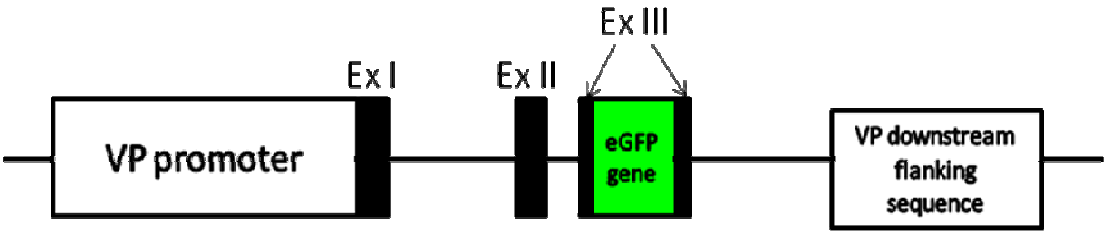

Figure 1-10. Structure of the VP-eGFP transgene used to generate VP-eGFP rats. The eGFP coding sequence was inserted between exon III in frame with the VP structural gene, downstream of the VP promoter, and exons I and II of the VP gene and upstream of 3kbp downstream flanking sequence. Figure adapted from (Ueta *et al.* 2005).

Chapter 2

Degradation sites in magnocellular dendrites

2. DEGRADATION SITES IN MAGNOCELLULAR DENDRITES

2.1 Introduction

The neural lobe contains a large amount of vasopressin and oxytocin (~$1.48x10^{10}$ vesicles of each peptide hormone) (Leng & Ludwig 2008). This large store of vesicles is not all released under physiological stimuli. High intensity i*n vivo* acute electrical stimulation was shown to release approximately 10% of vasopressin from the neural lobe (Leng *et al.* 1994) (also reviewed in (Leng & Ludwig 2008). Acute electrical stimulation in *in vitro* neural lobe preparations showed a similar percentage of release of both vasopressin and oxytocin (Bicknell & Leng 1981). Chronic osmotic stimulation by salt loading released ~85% of vasopressin vesicles from the neural lobe, leaving ~15% unreleased (Ehrhart-Bornstein *et al.* 1990). Hence, there seems to be three pools of vesicles in the magnocellular axon terminal: ~10 % of vesicles are readily released under stimulation, ~ 75% of vesicles released under prolonged stimulation, and a non-releasable pool. The neurosecretory axons in the neural lobe are made up of different compartments consisting of undilated segments, endings and swellings (Heap *et al.* 1975). Vesicles were proposed to arrive at the endings through the undilated segments, and become stored in the swellings if they were not released (Heap *et al.* 1975; Krsulovic *et al.* 2005). A specialised compartment, known as the Herring body, was found to be filled with lysosomes (Dellmann & Rodriguez 1970) and was found to be the site of degradation for aged, non-released vesicles (Krsulovic *et al.* 2005). Hence, the three different pools of vesicles found in the magnocellular neuronal terminals are stored in different

compartments. In comparison, magnocellular dendrites typically contain ~60000 vesicles of vasopressin per soma or dendrite and ~15000 vesicles of oxytocin (Morris & Pow 1991) (reviewed in (Leng & Ludwig 2008) and it is not known whether distinct vesicle pools exist and whether specialised compartments exist for degradation. Regarding somato-dendritic release, high potassium depolarisation applied to the SON for 10 -15 min released ~2.5% of oxytocin vesicles (Ludwig *et al.* 2002), and 30 min microdialysis in the SON of suckling rats released ~10% of oxytocin vesicles from the somato-dendritic compartment (Neumann *et al.* 1993b; Neumann *et al.* 1993a). Hence, it is possible that there are non-releasable vesicle pools residing in dendrites. Moreover, magnocellular dendrites could be important sites for the storage and degradation of aged vesicles. However, morphological studies of magnocellular neurons in the SON (Morris & Dyball 1974) have not found specialised compartments for degradation.

There are three pathways in which substrates destined for degradation can be delivered to lysosomes: endocytosis, phagocytosis and autophagy (Luzio *et al.* 2007). The various lysosomal pathways are summarised in **Figure 2-1**. Substrates such as ligand-receptor complexes from the plasma membrane enter the endocytic pathway where they are delivered to endosomes en-route to lysosomes. There are several theories regarding the delivery of endosomal materials to lysosomes including maturation of endosomes into lysosomes, budding of vesicles from endosomes to fuse with lysosomes, a “kiss and run” vesicular fusion, and a hybrid formation model where endosomes and lysosomes fuse to form a hybrid organelle. Each of these

models have been studied and reviewed and are not thought to be mutually exclusive of one another (Bright *et al.* 2005; Gu & Gruenberg 1999; Luzio *et al.* 2007; Murphy 1991; Pillay *et al.* 2002; Storrie & Desjardins 1996). Phagocytosis occurs in specialised cells and serves to engulf foreign materials like bacteria and other pathogens and also apoptotic cells to form phagosomes which fuse with lysosomes (Jahraus *et al.* 1998) and will not be discussed in this chapter. Autophagy is the process in which spent and/or damaged organelles become degraded (Levine & Klionsky 2004). Autophagy is thought to play a crucial role in the regulation of intracellular homeostasis and disruption in the autophagic pathway can lead to the development and progression of several neurodegenerative diseases (Boland & Nixon 2006; Gorman 2008; Jellinger & Stadelmann 2000). Aged, non-released vesicles, like aged organelles, undergo degradation via the autophagic pathway. Ultrastructural studies of lysosomes in the magnocellular neurosecretory terminals had found that non-released neurosecretory vesicles were engulfed *in toto* in autophagosomes which were positively labelled for acid phosphatase, an acid hydrolase found in lysosomes (Whitaker & LaBella 1972). Acid hydrolases are enzymes important for the hydrolysis lysosomal contents. One acid hydrolase, Cathepsin D which is a protease, had been shown to increase in expression when a mutant transgene expressed in vasopressinergic neurons resulted in increased protein degradation by autophagy (Davies & Murphy 2002). This, and other studies demonstrated that lysosomes are plastic organelles which increase in number and activity when the demand for degradation is high. For example, when there is an increase in misfolded proteins which do not enter the secretory pathway (Davies & Murphy 2002); or when a dehydration protocol was exercised to stimulate release of

vasopressin where an increased amount of vesicular membranes retrieved after vasopressin release were sequestered for degradation (Whitaker & LaBella 1972; Kobayashi *et al.* 1962).

In neurons, endocytosis had been shown to occur throughout the length of hippocampal dendrites and endocytosed material was found to be transported to the cell bodies where the lysosomes were found for degradation (Parton *et al.* 1992). However, evidence of lysosome staining had been seen in magnocellular dendrites (Morris & Dyball 1974). Since dendrites can extend to hundreds of micrometers, endocytosed materials will have to travel for long distances if degradation only occurs in cell bodies. There is evidence of autophagosomes, a double membrane structure which sequesters spent/damaged organelles and fuses with or mature to form lysosomes for degradation (Klionsky 2005; Levine & Klionsky 2004) in the dendrites of cerebral cortical neurons (Koike *et al.* 2005). Even though there is no direct evidence of autophagososomes, lysosomes had been visualised in magnocellular dendrites (Ma & Morris 2002). Moreover, as discussed above, dendrites may contain aged, non-released secretory vesicles. Hence, it is possible that magnocellular dendrites are important sites for degradation, similar to the functions of Herring bodies for local proteolysis. To investigate the significance of lysosomes and the regulation for lysosome expression in magnocellular dendrites, this chapter discusses lysosomal localisations in magnocellular dendrites by identification of lysosomes locations in correlation to peptide vesicle density.

2.2 Material and Methods

2.2.1 Fixation by Transcardial Perfusion

Four adult male transgenic VP-eGFP rats (200 – 300 g), were anaesthetised with 1 ml sodium pentobarbitone and laid on their backs until response to toe pinching ceased. A horizontal incision to the skin under the diaphragm was made and the chest was opened up by cutting through the rib cage on either side. Whilst the heart was still beating, a blunted 21-gauge needle connected to heparin-saline (hep-saline) solution (appendix I) was inserted through the left ventricle into the aorta. When the needle was in place, a small cut was made to the left atrium of the heart so that blood and perfusion solution could flow out. The perfusion pump was then started and Hep-saline solution was perfused through the heart until the liver turned pale (100 – 200 ml). When most of the blood was cleared out by hep-saline solution, the perfusion solution was changed to 4% (w/v) PFA (appendix I). Perfusion with 4% (w/v) PFA was performed until the animal was completely fixed (300 – 400ml). The brain was removed and the hypothalamus was dissected into a block and stored in post-fix solution (15% sucrose w/v in 4% PFA (w/v)) at 4^{o}C until the tissue block sank to the bottom of the container. The tissue block was stored in cryoprotective solution (30% (w/v) sucrose in 0.1M PB) at 4^{o}C overnight, and snap-frozen on dry ice. The hypothalamus was subsequently sectioned using a freezing microtome. 52 µm sections were collected in 0.1 M PB and stored in cryoprotectant (appendix I) at 20^{o}C until use.

2.2.3 Indirect Immunofluorescence Labelling for Free-floating Sections

Sections were washed three times for 10 min in 0.1 M PBS (appendix I) if they were stored in cryoprotectant. An orbital rotation platform was used at all the incubation steps described here. The sections were first incubated in 50 mM NH_4Cl for 10 min and then washed three times in 0.1 M PBS. If sections were to be used immediately after cutting, the first three washes were not carried out. After washing in 0.1 M PBS, sections were incubated in a blocking solution which contained 0.1 M PBS, 0.3% (v/v) Triton X100, and 10% (v/v) pre-immune goat serum for 30 min at room temperature. The primary antibody used to label lysosomes is the mouse monoclonal IgG raised against lysosomal associated membrane protein 1 (LAMP-1, LY1C6, Santa Cruz Biotechnology, Inc.) and recognises a single band at 120 kDa in Western blot of fibroblasts whole cell lysates (manufacturer's specification). LAMP-1 was found to be important in the regulation of cathepsin D distribution in the brain (Andrejewski *et al.* 1999) and together with LAMP-2, is required for the recruitment of the small GTPase Rab7 to autophagic vacuoles (pre-lysosomal bodies), impairing fusion with or formation of mature lysosomes (Eskelinen *et al.* 2004; Eskelinen 2006). Primary anti-LAMP1 antibody was added to the blocking solution at 1:50 dilution (4 µg/ml) and sections were incubated in the primary antibody cocktail at 4^oC overnight. Negative controls were carried out by replacing primary antibody incubation with pre-immune serum incubation. The next day, the primary antibody was washed off three times in 0.1 M PBS for 10 min. Then, a secondary antibody cocktail of 1:500 dilution of AlexaFluor 568 (Invitrogen) was made up in blocking

solution. Slices were incubated in the secondary antibody cocktail at 4°C overnight. The secondary antibody cocktail was then washed off with 0.1 M PBS for three times 10 min. The sections were mounted onto gelatinised slides (appendix I), air dried and mounted with mowiol (appendix I, medium refractive index 1.4) mounting medium and coverslipped. The mounting medium was left to cure overnight protected from light and sections were imaged once the medium was dry.

2.2.3 Microscopic Image Acquisition

The Zeiss LSM510 inverted microscope was used for all imaging. The 488 nm line of the Argon laser was used to excite eGFP which has an excitation maximum of 488 nm and an emission maximum of 509 nm. A dichroic beam splitter, HFT 488, was in place and the excitation laser passed through two mirrors before the emitted light was collected by a band pass 500 – 550 filter. The helium-neon 1 (HeNe1) laser line (excitation wavelength 543 nm) was used to excite the AlexaFluor 568 staining (excitation maximum 578 nm, emission maximum 603 nm). The photomultiplier tube (PMT) settings and laser powers were kept exactly the same for all samples. The pinhole was adjusted to 1 Airy unit for confocal image acquisition. **Figure 2-2** shows the excitation and emission filter settings used. Images were acquired by sequential scanning to avoid bleed through of emitted light from either channel. An x63 oil immersion objective (NA1.4) was used. Images were acquired close to double Nyquist sampling rate to avoid under sampling (Nyquist calculator available at www.svi.nl). 3-dimensional images were obtained by scanning the x, y –planes at 60 nm, achieved by line scanning 1024 x 1024 pixels with an optical zoom of 2.4,

and intervals of 170 nm along the z-axis. 8 bit pixel depth, line averaging of 1 (no averaging) and maximum scan speed were chosen for image acquisition to avoid photobleaching.

2.2.4 Image Processing

The acquired stack of images was deconvolved to remove aberrations caused by the intrinsic physical properties of the microscope. Deconvolution of images was achieved by use of the Huygens Essential software (Scientific Volume Imaging, NL, www.svi.nl) available in the IMPACT imaging facility in our centre. The Huygens deconvolution software restores convolution in images taken by removing blurring caused by diffraction of light and noise introduced by the microscope photomultiplier tube. Image restoration is based on the iterative application of a maximum likelihood estimate algorithm where the point spread function – the smallest fluorescent single point object that can be resolved in 3 dimensions by the microscopic parameters used, is used to calculate and reassign out-of focus light signals to the point of origin (Shaw PJ & Rawlins DJ 1991).

The microscopic parameters used for deconvolution was set according to the parameters used for imaging: microscope type – confocal; numerical aperture – 1.4; lens immersion and medium refractive indices – 1.51 and 1.4; x and y sample sizes – 60 nm; z sample size – 170 nm; excitation wavelengths – 488 nm, 543 nm; emission wavelength – 509 nm, 603 nm; excitation photon count – 1; pinhole = 1 Airy unit.

These parameters help the deconvolution software to calculate a theoretical point spread function used. A signal to noise ratio is used in the software to control the sharpness of the restoration result of the image and can be calculated as the square root of the brightest intensity in the image divided by the average intensity of a single photon hit caused by photon noise. Generally, the lowest signal to noise ratio, 3, was employed, assuming a very noisy image, so that no background noise would be enhanced by deconvolution. Because of the calculations involved in deconvolution, 8 bit unsigned images, where pixel intensities were described by 256 shades of grey, were converted to 32 bit float images where shades of grey can be described by 1.17549435^{e-38} to 3.40282347^{e+38} values.

2.3 Results

2.3.1 Localisations of Lysosomes in Correlation with VP-eGFP in Dendrites

26 dendrites from 4 rats were imaged according to the protocol described above. Images were selected with long profiles of dendrites where no overlapping with other dendrites could be seen clearly. Lysosomes were located by going through optical sections in the z direction to ensure that stained lysosomes analysed were not from presynaptic terminals but occurred within the dendrites. Images were separated into the green (eGFP signal) and red (LAMP-1 staining) channels using ImageJ (http://rsb.info.nih.gov/ij/). The scale of the image was calibrated using ImageJ. The two channels were merged into RGB colour images and locations where lysosome

staining was observed, an area of interest of 1 µm in diameter was drawn around it. This area of interest was saved and the same was carried out for the whole dendrite. Correlation analysis, but not colocalisation analysis, was carried out because lytic activity in the lysosome could change eGFP excitation and/or emission or simply deform the eGFP fluorophore. Emission of green fluorescent protein is also highly pH sensitive (Tsien 1998). Hence, the low pH, pH 4.5, found in lysosomes will greatly reduce the fluorescent intensity of eGFP. Moreover, correlation analysis will give an idea of whether lysosomes are located where there is a high density of vasopressin eGFP vesicles. After all the areas of interest were obtained, the red channel was switched off and the original 32-bit image of the green channel was used for a "SUM" projection of the image where pixel intensities were summed up in each column of pixels in the z-stack using ImageJ to take into account the whole dendrite in 3 dimension. The saved areas of interest were then superimposed onto the green channel where mean VP-eGFP intensity measurements (density/area) were calculated for each area (spot intensity). Areas of interest were also made for whole dendrites and mean VP-eGFP intensity measurements recorded. Please refer to **Figure 2-3** for a diagrammatic representation of the image analysis and an example of areas of interest drawn on a representative dendrite.

To compare whether lysosomal locations are preferentially situated where there is a high density of vasopressin-containing vesicles, the difference between the mean spots VP-eGFP fluorescent intensity and the whole dendrite VP-eGFP fluorescent intensity was obtained and compared using the Chi-square test where positive

intensity = location of lysosome correlated to high VP-eGFP density, zero = no difference and negative intensity = location of lysosome correlated to low VP-eGFP density (all measurements are relative to whole dendrite VP-eGFP intensity). **Figure 2-4** shows the Chi-square plot (mean spot intensity – mean whole dendrite intensity for each dendrite measured). Chi-square test showed that the spot intensities were significantly different from zero ($p<0.001$) suggesting a positive correlation of lysosome locations and areas with high vasopressin vesicle density. **Figure 2-5** shows optical sections of a portion of a representative dendrite in the z-direction where lysosome labelling is in red and VP-eGFP is in green. It is clearly shown in these images that lysosomes were preferentially located at areas where there was high vasopressin density, suggesting that dendrites are important compartments for degradation.

2.4 Discussion

The Herring bodies in magnocellular terminals are filled with lysosomes and are the final destination for aged vesicles (Krsulovic *et al.* 2005) providing a local capacity for degradation where aged vesicles do not need to be transported back to the cell body. It is not known whether dendrites, like neuhypophyseal terminals contain specialised compartments for degradation. Magnocellular dendrites have been shown to contain lysosomes (Morris & Dyball 1974), however, their functional significance in dendrites is not known. In hippocampal neurons, lysosomes were

found only in cell bodies and very proximal segments of dendrites, and endocytosed materials were found to be retrogradely transported to cell bodies, where lysosomes were found (Parton *et al.* 1992). Having identified lysosomes in dendrites of magnocellular neurons in the present study, it is certain that local degradation occurs in this compartment. Since magnocellular dendrites contain a large reserve of vesicles, it is possible that "centres" for degradation occur in the dendritic compartment. In the present study, it was found that instead of clustering of lysosomes found in one special part of the dendrite, lysosomes were found to be located at areas where there was high density of vasopressin vesicles. These hot spots for degradation were found throughout the dendrites. Since magnocellular dendrites were not found to contain accumulations of lysosome clusters, it is unlikely that dendrites are the destination of all aged and non-released vesicles. However, lysosomes were found where vasopressin-eGFP vesicles cluster suggesting that non-released vesicles gather as a pool around these lysosomes or lysosomes were preferentially transported to these non-released pools of vesicles. Dendritic lysosomal content is known to be variable where the number of lysosomes increases during high cellular activity, e.g. dehydration, and decreases during low activity, e.g. rehydration (Morris & Dyball 1974). Similarly, in axon terminals, lysosomes-containing Herring bodies were found to be abolished during rehydration (Krsulovic *et al.* 2005) suggesting that Herring bodies are plastic structures that disappeared when old vesicles were spent and newly synthesised vesicles do not enter the lysosomal pathway. Hence, it is likely that lysosomes are targeted to loci where there is a high demand for degradation; i.e. where pools of non-released secretory vesicles reside. In the magnocellular neuronal terminal, the smooth endoplasmic

reticulum (SER) was found to contribute to the formation of lysosomes (Whitaker & LaBella 1972). Elements of the rough endoplasmic reticulum (RER) had been shown in magnocellular dendrites (Ma & Morris 2002), however, elements of the SER had not been studied. Hence, there could be two ways in which lysosomes are targeted to dendrites: 1) translocation from the soma to sites of aged, non-released vesicle pools in dendrites; and/or 2) local synthesis of lysosomes in dendrites. However, the capability of dendrites to synthesise lysosomes require further studies.

In many different cell types, lysosomal degradation is a plastic process which increases in activity according to the demand of the cell. Early studies in rat anterior pituitary cells showed that lysosomes have important functions in the regulation of prolactin secretion (Smith & Farquhar 1966). When suckling pups were separated from lactating mothers, production of prolactin continued until there was an increase in the number of lysosomes and lysosomal enzyme activity. In secretion deficient β-pancreatic islet cells, increased autophagic activity was shown to control hormone content in the cells under stimulation for insulin production (Marsh *et al.* 2007). Autophagy was proposed to have roles in cell death and cell survival. Inhibition of autophagy was shown to increase cell death in neuroblastom cells expressing a mutant VP transgene, indicating that autophagy acted as a cell protective mechanism (Castino *et al.* 2005a). However, in the same model, autophagy-triggered apoptotic cell death was found in cells exposed to oxidative stress (Castino *et al.* 2005b). In cortical neurons, inhibition of autophagosome activity or fusion with lysosomes resulted in an accumulation of autophagic vacuoles, similar to that seen in

Alzheimer's disease (Boland *et al.* 2008). Disruption of the autophagic pathway in dopaminergic neurons was found to play a similar role in Parkinson's disease (Cuervo *et al.* 2004). In magnocellular neurons, autophagy has been shown to be linked to a specific form of diabetes insipidus (familial neurohypophysial diabetes insipidus, FNDI) (Davies & Murphy 2002). Autophagy was found to be responsible for the degradation of mutated vasopressin gene product and also normal vasopressin gene product associated with the mutated form, leading to increased degradation of vasopressin and decreased secretion. In magnocellular neurons of FNDI transgenic rats, increased lysosome staining was found in SON tissue preparations using western blotting (Davies & Murphy 2002). Since the transgene used caused truncation of vasopressin gene product and did not affect the lysosomal pathway, it indicates that lysosomal activity increased in the somato-dendritic compartment when the demand for degradation increased and hence, controlled somato-dendritic hormone content.

In addition to autophagy, dendrites participate in endocytosis and recycling of substrates. In the magnocellular neuronal terminal, it was found that dehydration, which stimulates an increase in vasopressin release into the circulation, led to an increase in lysosomal activity (Whitaker & LaBella 1972). In the same study, it was found that during dehydration, lysosomes contained microvesicles which were electron-translucent. These electron-translucent microvesicles represent recycled membranes from endocytosis. In control conditions, non-released neurosecretory granules were seen to be engulfed by autosomes. This suggests that lysosomes are

not only important for degradation of non-released secretory vesicles but also important for membrane recycling after exocytosis. Endocytosis in the magnocellular somato-dendritic compartment had been shown in isolated SON neurons from virgin and lactating rats and that the amplitude of endocytosis is directly proportional to the rate of exocytosis (de Kock *et al.* 2003). This indicates a local regulation of plasma membrane content in the soma and dendrites. Aside from local degradation, it has been found that materials endocytosed at the neurohypophyseal terminals undergo retrograde transport to enter the lysosomal pathway in the cell bodies and dendrites (Theodosis 1982). Moreover, it was found that these endocytosed materials were sequestered in pre-existing lysosomes (Broadwell *et al.* 1980; Theodosis 1982) indicating that dendrites are involved in endolysosomal degradation of retrograde transported materials. Endocytosis is an important pathway to lysosomal degradation and recycling of substrates (Maxfield & McGraw 2004). Endocytosed substrates can either be delivered to lysosomes for degradation or be sorted for recycling in endosomes. These substrates, including plasma membrane receptors, can be directly transported back to the plasma membrane for re-use or delivered to the Golgi apparatus where they are further sorted for degradation or recycling. Since there is no evidence that magnocellular dendrites contain the Golgi apparatus, it is likely that substrates destined for sorting in the Golgi will be transported back to the cell body. Further experiments will have to be carried out to find out whether endosomal sorting occurs in magnocellular dendrites. In hippocampal neurons, functional differences in endocytic pathways were found between axonal and somato-dendritic compartments where brefeldin A changed protein distribution in the endocytic pathway of dendrites but not in axon

terminals (Mundigl *et al.* 1993). This kind of functional difference has not been found in magnocellular dendrites.

In the present study, it was also found that lysosomes are located in the centre of dendrites (observation, **Figure 2-5**). As discussed in the previous chapter, in bovine adrenal chromaffin cells newly synthesised vesicles are preferentially targeted to the cell membrane and aged vesicles reside in the centre of the cell (Duncan *et al.* 2003). Since aged vesicles were shown to be associated with lysosomal degradation, (Krsulovic *et al.* 2005), this suggests that aged, non-released vesicles reside in the centre of dendrites allowing newly synthesised vesicles to be primed close to the plasma membrane in accordance with the findings in bovine adrenal chromaffin cells.

In conclusion, the present study suggests that dendrites are not centres for degradation and recycling but contain hot spots of lysosomes where local degradation and regulation of peptide and membrane content occurs. In contrast to magnocellular neuronal terminals, ultrastructural studies of the perikarya in the SON had shown that the number of lysosome bodies found after dehydration was unchanged (Morris & Dyball 1974), suggesting that release of neurosecretory vesicles, which subsequently leads to plasma membrane retrieval, from the cell soma is less significant than release from the neural lobe. Interestingly, Morris & Dyball found an increase in the number of lysosome bodies in the perikarya after a

dehydration-rehydration regime. The authors concluded that lysosomes found in the perikarya are important sites for the disposal (autophagy) of the biosynthetic machinery involved in the increased peptide synthesis during dehydration. Whether the plasticity in lysosomal degradation in dendrites resembles that in the soma or in the neuronal terminal is unknown. However, water deprivation and salt loading had been found to stimulate release of vasopressin from the SON (Ludwig *et al.* 1996b) and from magnocellular dendrites (Tobin *et al.* 2004). Hence, it is possible that regulation of lysosomes in dendrites will be similar to that found in magnocellular neuronal terminal. Nevertheless, this study showed that lysosomes are targeted to loci of high vasopressin expression indicating that lysosomes found in dendrites are important for the disposal of non-released LDCVs. Whether lysosomal contents in dendrites change similarly to that found in neuronal terminals during chronic stimulation by salt loading or dehydration remains to be studied. In neuronal terminals, lysosomes were found to contain recycled membranes after chronic stimulation (Whitaker & LaBella 1972). Recycling of endocytosed substrates has been demonstrated in dendrites of other neuronal systems but not magnocellular neurons (Xia *et al.* 2009). Further experiments involving dehydration and rehydration will be needed to find out whether dendritic content of lysosomes changes during these stimuli and whether endocytic sorting occurs in magnocellular dendrites, providing a local recycling pathway for plasma membrane components. The present study suggested that old, non-released vesicles are situated in the centre of dendrites indicating that regulation of vesicle pools might be similar to that found in bovine adrenal chromaffin cells (Duncan *et al.* 2003) where aged LDCVs reside in the centre of the cell. Moreover, the shortage of lysosomal accumulations suggested

that, unlike Herring Bodies, dendrites are not specialised compartments for degradation but disposal of unreleased secretory vesicles occur at hot spots. This further suggests that pools of aged vesicles are concentrated at these hot spots, making it likely that dendrites do not only contain aged, non-released vesicles, but may also contain a mixture of newly synthesised vesicles for release.

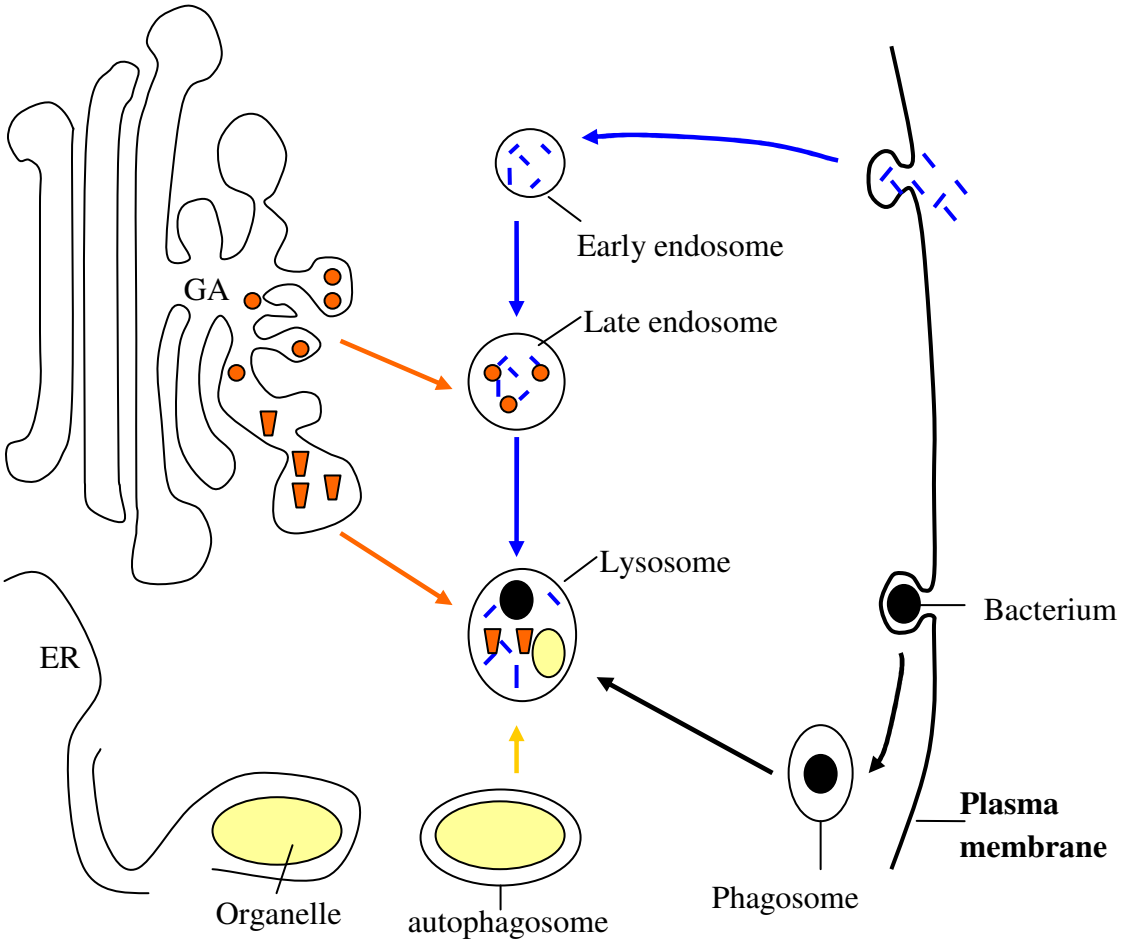

Figure 2-1. Simplified pathways to delivery to lysosomes. Endocytosed materials, such as ligand-bound receptors from the plasma membrane (blue), form early endosomes which can sort receptors and ligands for recycling or degradation. Early endosomes either mature to late endosomes or fuse to join pre-existing late endosomes. Late endosomes contain hydrolytic enzymes (orange circles) which are responsible for protein degradation. Late endosomes then mature to or fuse to join lysosomes which contain a pool of hydrolytic enzymes (orange trapezoids). Lysosomes are also responsible for autophagy of cell organelles and destruction of foreign material (e.g. bacteria phagocytosis in neutrophils and macrophages). (Figure adapted from Alberts *et al.* 1994).

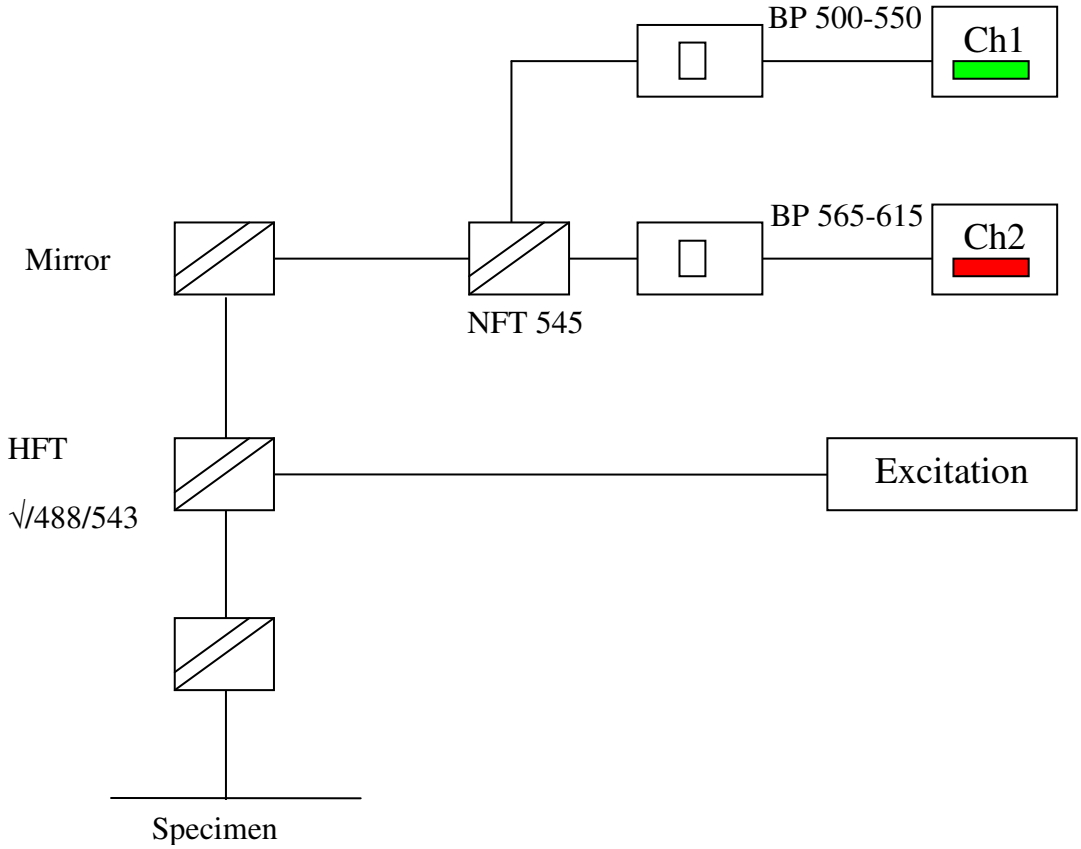

Figure 2-2. Beam path configuration for 2-channel imaging with the confocal laser scanning system. BP 500 – 550 and BP 565 – 615 filters collect emissions between 500 – 550 nm and 564 -615 nm wavelengths and direct the emission light through to detection channel 1 (Ch1) and detection channel 2 (Ch2) respectively. HFT √/488/543 is the main dichroic beam splitter which passes all the specified excitation wavelengths (488 and 543 nm) to the sample. The mirror reflects all the light to the NFT 545. The NFT 545 is the secondary dichroic beam splitter which allows excitation wavelengths above 545 nm to pass straight through to Ch2 and reflect wavelengths below 545 nm 90^{o} through to Ch1. Emission signals are detected through photo multiplier tubes (PMT) and the detector gain and amplifier offset can be set for different detection channels.

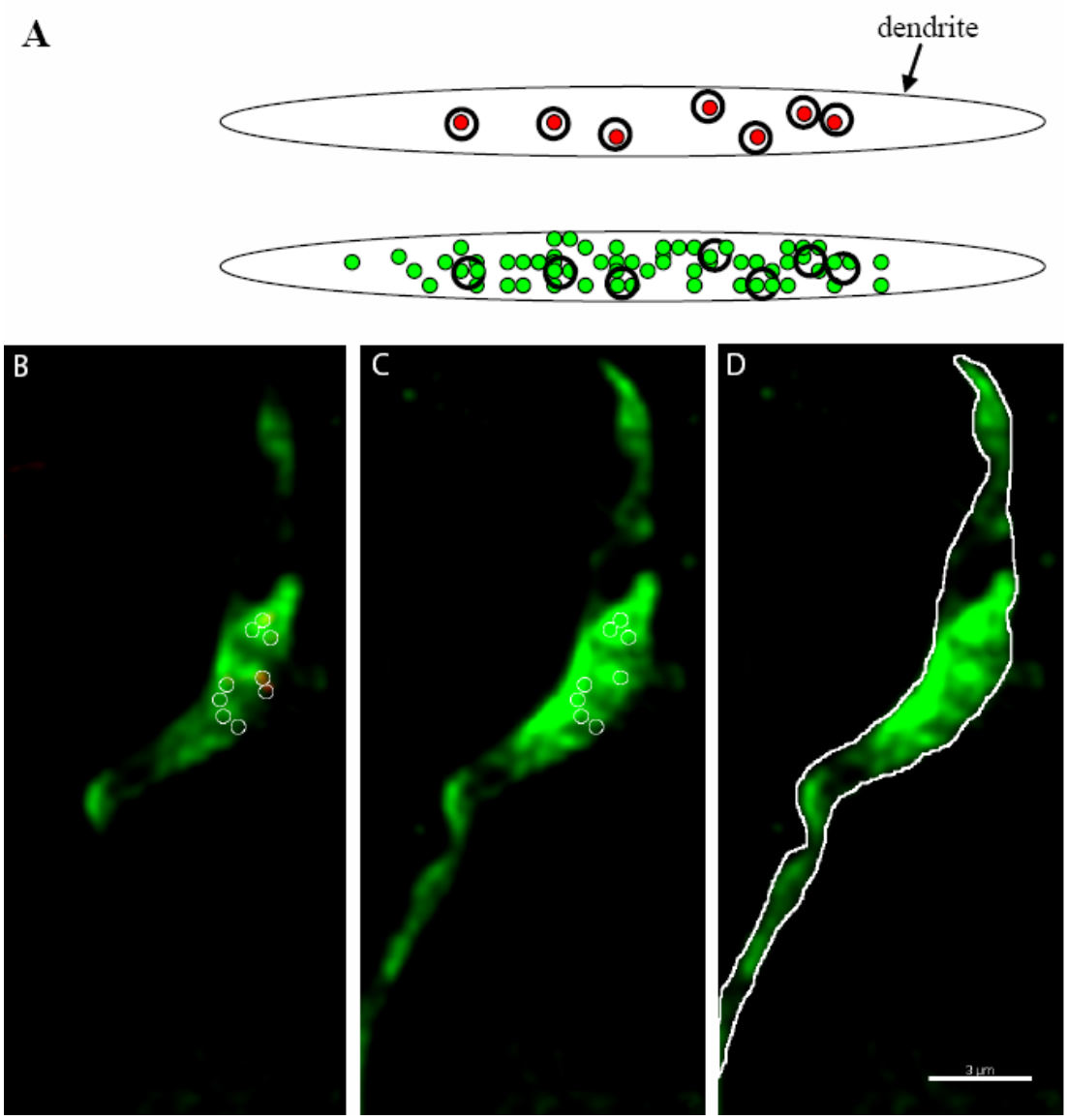

Figure 2-3. Measurement of VP-eGFP intensity relative to locations of LAMP1 immunofluorescence. (A) Schematic diagram of VP-eGFP intensity measurement. Red circles in the top panel = LAMP1 labelling of lysosomes; green circles in bottom panel = VP-eGFP. Masks of 1 µm diameter (bold circles) were drawn on images with the green VP-eGFP channel switched off to identify locations of LAMP1 labelling. These masks were then imported onto the green channel of the same image and the intensity of VP-eGFP at these locations was measured as spots (mean intensity/area). The whole dendrite in 3-D was taken into account by taking a sum of the image stack. The intensity of the whole dendrite was then measured for comparison (B) Determination of areas of interest as discussed above; one optical section is shown. (C) 3-D image stack converted to 2-D by the sum slices function in ImageJ where the sum of the pixels from the stack of images were displayed from 32-bit optical slices. Areas of interest described in (A) were then imported onto this image to measure VP-eGFP intensity. (D) VP-eGFP intensity of the whole dendrite was then obtained by measuring sum slices image of the whole dendrite. Scale bar = 3 µm.

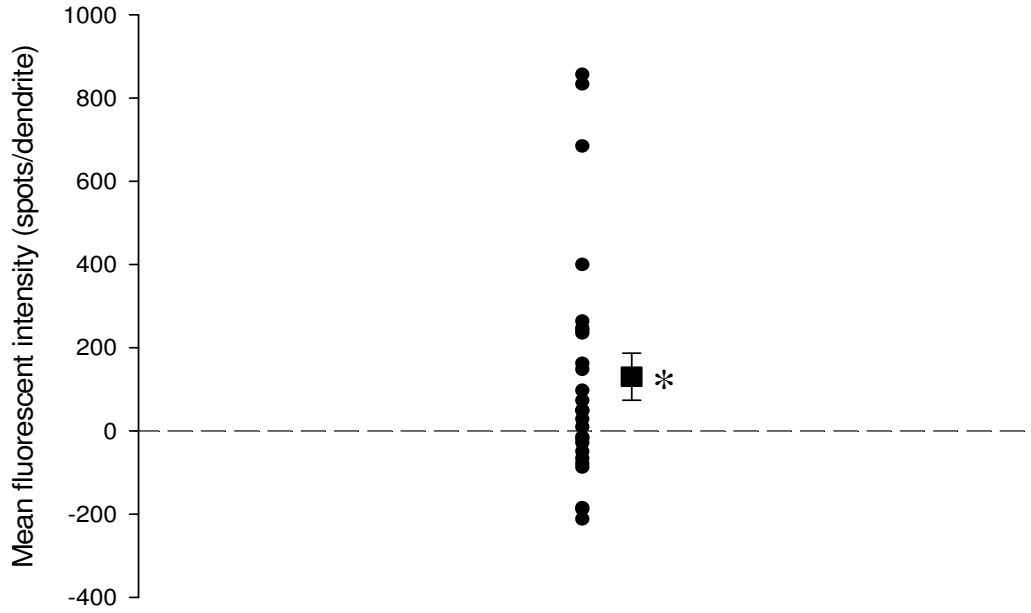

Figure 2-4. Correlation of LAMP1 labelling with VP-eGFP intensity in the dendrite. Full circles represent mean spot intensity – mean dendrite intensity for dendrites measured. Filled box represent the mean of all the data points (error bar = ±SEM). Chi-squared test showed that there is a significant difference between the mean intensity of spots and the mean intensity of whole dendrites ($p<0.001$; $n = 26$). This suggests that lysosomes were predominantly located in areas with high density of vasopressin vesicles.

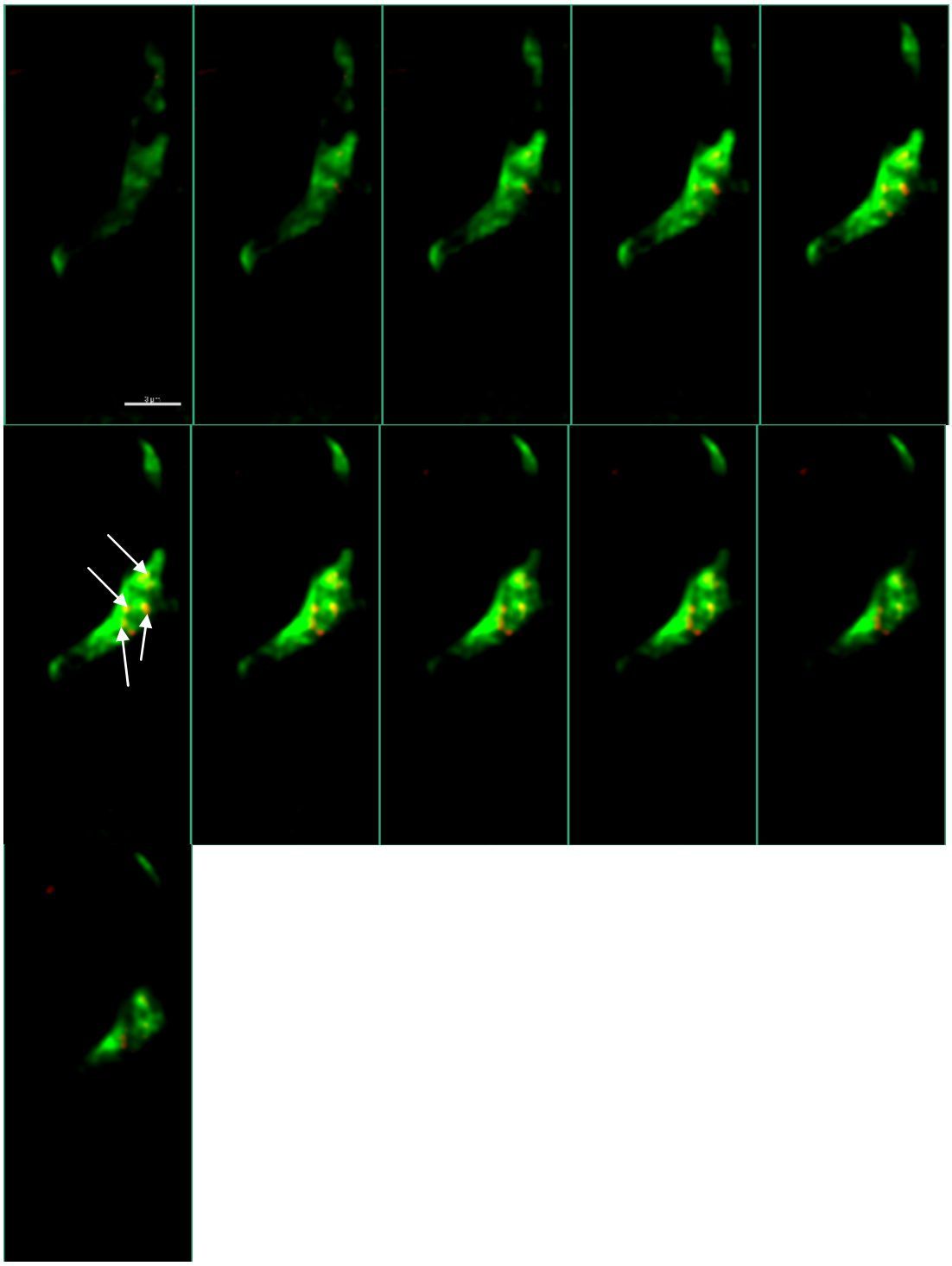

Figure 2-5. LAMP1 immunofluorescence in vasopressinergic dendrite. Images are consecutive optical slices of 167 nm z-stepping. Red labelling is LAMP1 and green is VP-eGFP. Figure shows that LAMP1 staining of lysosomes was preferentially located where there was high vasopressin density (indicated by arrows). Scale bar = 3 μm.

Chapter 3

Vasopressin trafficking along dendritic profiles

3. VESICLE TRAFFICKING ALONG DENDRITIC PROFILES

3.1 Introduction

Magnocellular dendrites extend to ~200 micrometers long (Pow & Morris 1989) and peptides in dendrites are thought to be transported from the cell bodies where the Golgi apparatus (GA) is found (Morris 2005). As discussed in Chapter 1, vasopressin and oxytocin are processed in the endoplasmic reticulum and packaged into vesicles in the GA. Dendritic peptides are believed to travel along microtubules (Morris *et al.* 2000) in a similar fashion to peptide transport to axonal terminals. It is not known whether dendritic peptide release occurs at any preferential sites along the dendritic membrane. There is no evidence of active release zones in magnocellular dendrites and it has been found that all parts of the dendritic membranes were capable of exocytosis (Pow & Morris 1989). In bovine adrenal chromaffin cells, it was found that vesicular age is an important factor in vesicle pool segregation (Duncan *et al.* 2003). It is unknown whether newly synthesised vesicles are found in dendrites and whether there are preferential sites for storage of newly synthesised vesicles and for aged vesicles. As the results indicated in Chapter 2, it is likely that aged vesicles occupy the centre of the dendrite leaving the periphery to newly synthesised vesicles. However, it is not known whether there is a difference in storage along the profile of dendrites. Newly synthesised vesicles can either be transported to the distal portion of dendrites, leaving aged vesicles at the proximal portion, or vice versa. It is also possible for there to be no differential location for storage of newly synthesised and aged vesicles; i.e. it might be that vesicle storage

and release is homogenous along dendritic profiles with no relation to age of vesicles. To test this hypothesis, fresh hypothalamic sections containing the SON were incubated at 20°C to block exit of proteins from the GA (Griffiths & Simons 1986). It was found in exocrine pancreatic cells that transport of secretory proteins through the GA is temperature-sensitive (Saraste *et al.* 1986). In the same study, incubation of pancreatic cells at 20°C resulted in the trapping of secretory peptides in the GA. Using microsomal fractions, it was also found that at 20°C, secretory proteins remained trapped in the endoplasmic reticulum and the GA. Another study found that this blockage of exit is due to the degradation of proteins found in the *trans*-Golgi compartment (Ladinsky *et al.* 2002), leading to an inhibition of vesicle movement through the GA. Sorting through the trans-Golgi network (TGN) is known to be important for peptides like vasopressin, and proteins destined for the regulated secretory pathway. Temperature inhibition is reversible by incubation at increased temperatures (Saraste *et al.* 1986; Griffiths *et al.* 1985), making this a useful tool to study the dynamics of newly synthesised vesicles. The release of GA exit block will generate a wave of newly packaged vesicles trafficking down dendritic profiles and hence, enable tracing of these newly synthesised vesicles along dendritic profiles. **Figure 3-1** summarises the possible outcomes of GA exit block and subsequent release. In this study, hypothalamic slices of the VP-eGFP rat were used to study trafficking of newly synthesised vesicles.

3.2 Material and Methods

3.2.1 Block of peptide release from the GA

Sections of the hypothalamus were collected from post-natal day 7 VP-eGFP rats (n=8). Neonatal rat brains were used because slice sections obtained from adult brains require constant oxygenation (Aitken *et al.* 1995), making the later incubation process required for GA exit block unfeasible since slices were submerged in media. Rats were anaesthetised with halothane or isofluorane and decapitated and their brains quickly removed. Hypothalamic tissue blocks were cut by sectioning the brains with a vibratome in aCSF-sucrose-KOH solution (Appendix I). The osmolarity of the solution was 300 mOsm/L. The solution was gassed with oxygen throughout slicing. 350 µm thick coronal sections containing the SON were obtained from each brain. Sections were kept in ice cold Gey's Balanced Salt Solution (Sigma-Aldrich, UK) enriched with 0.5% (w/v) glucose (Sigma-Aldrich, UK). 20 selected sections were kept in petri dishes with Gey's solution at 4^{o}C for 30 min. Slice sections were then transferred to pre-warmed serum-containing medium (Appendix I) and were either incubated at 37^{o}C for 90 min (8 sections, control), incubated at 20^{o}C for 60 min (6 sections, GA exit block), or incubated at 20^{o}C for 60 min and 37^{o}C for 30 min (6 sections, release of GA exit block). A 30 min incubation at 37^{o}C was found to be efficient for transport of secretory proteins to the site of exocytosis in the presence of a secretagogue (Saraste *et al.* 1986). Serum-containing medium was supplemented with 25 mM K^{+} which acted as stimulus for secretion in these experiments. Sections were then transferred to ice cold 4% (w/v) PFA (Appendix I) for up to 1 hr fixation.

3.2.2 Indirect Immunofluorescence Labelling for Fresh Brain Sections – Double Label Immunofluorescence

The fixative was removed and the tissue was washed three times for 15 min in 0.1 M PB (Appendix I) with 0.3% (v/v) Triton X100 (PBT). Triton X100, a detergent, was used to permeabilise cell membranes for easy access for antibodies to intracellular antigens. The fixed sections were then incubated in 50 mM NH_4Cl in 0.1 M PB for 10 min after which they were washed three times in 0.1 M PBT for 15 min before incubating in a blocking solution (10% (v/v) normal goat serum in 0.1 M PBT) for 30 min to block non-specific binding of primary antibody to antigens in the tissue. Tissue sections were incubated in a primary antibody cocktail (1^oAb + 10% (v/v) serum in 0.1 M PBT) for 2 nights at 4^oC, gently rocking. Negative controls were carried out for each group by leaving out the primary antibodies, and incubating the samples in pre-immune serum (control: 7 sections + 1 negative control; GA exit block: 5 sections + 1 negative control; release of GA exit block: 5 sections + 1 negative control).

3.2.2.1 Primary Antibodies

Neuronal marker – MAP2

MAP2 (microtubule associated protein found in neurons) was used as a neuronal marker. The polyclonal chicken IgY (Abcam) used detects all three isoforms of MAP2: MAP2c is present in the newborn rat brain until postnatal day 10 – 20, and is replaced by MAP2a which is present from postnatal day 10 onwards, MAP2b is

present throughout life. MAP2a and MAP2b are both expressed in cell bodies and dendrites of neurons (Goedert *et al.* 1991), making it ideal to be used as a general marker for neurons. The pre-immune IgY was used to test for MAP2 antibody specificity and was not found to produce any signal, while in contrast the immune IgY produced strong, clear staining of dendrites and perikarya of neurons (information provided by Abcam). MAP2 antibody was used in 1:1000 dilution in this experiment.

GA marker – GM130

GM130 (BD Transduction Laboratories™) is the monoclonal mouse anti *cis*-Golgi matrix protein of 130 kDa, raised against rats and used a GA marker. Western blot analysis of GM130 on rat brain lysate had shown detection at 130kDa (information provided by BD Transduction Laboratories™). The antibody was used at 1:500 dilution.

After incubation with the primary antibodies, and pre-immune serum incubation for negative controls, sections were washed three times in 0.1 M PBT for 30 min to ensure that most of the unbound primary antibody was washed away. A second blocking step with 0.2% (w/v) BSA in 0.1 M PBT for 1 hr ensures that any remaining non-specific binding sites were blocked. Sections were then incubated in fluorophore-conjugated secondary antibody solution (2^{o}Ab + 0.2% (w/v) BSA in

PBT + 0.3% (v/v) Triton) at 4°C overnight. From this step onwards, the samples were protected from light.

3.2.2.2 Secondary Antibodies

All secondary antibodies used were from Molecular Probes, Invitrogen: AlexaFluor ® 568 goat anti-mouse (λ_{Ex} = 579 nm, λ_{Em} = 603 nm) and Alexa Fluor ® 633 goat anti-chicken (λ_{Ex} = 632 nm, λ_{Em} = 647 nm). The excitation and emission wavelengths are summarised in **Table 1 Appendix I.**

After secondary antibody incubation, the secondary antibody solution was removed and sections were washed three times for 15 min in 0.1 M PB. Sections were then mounted on microscope slides and coverslipped (coverslip thickness #1, VWR). Mowiol (Calbiochem) supplemented with DABCO (Sigma) was used as the mounting medium with a refractive index of 1.41. Sections were left to cure at 4°C in darkness until the mounting medium had set.

3.2.3 Microscopic Image Acquisition

The Zeiss LSM510 inverted microscope was used for all imaging. Laser excitation and emission filters were described in **Section 2.2.3, Chapter 2**. In addition to the 488 nm Argon and the 543 nm HeNe1 excitation lasers, a HeNe2 excitation laser λ_{Ex} 633 nm was used to excite the far red secondary antibody. All settings for image

acquisition were as described in Chapter 2 except that a HFT √/488/543/633 was used as the main dichroic beam splitter which passes all the specified excitation wavelengths (488, 543, and 633 nm) to the sample. Another HFT 633 mirror was in place to reflect all the excitation light above 633 nm to a long pass 650 filter to collect emission of over 650 nm in a third channel. **Figure 3-2** shows the settings used for imaging in this experiment. All other parameters were the same as described in Chapter 2.

3.2.4 Image Processing

The acquired stack of images was deconvolved to as described in Chapter 2. The microscopic parameters used for deconvolution were as described except that the excitation and emission wavelengths of the third fluorescent protein was included.

Briefly described, the microscope type – confocal; numerical aperture – 1.4; lens immersion and medium refractive indices – 1.51 and 1.4; x and y sample sizes – 60 nm; z sample size – 170 nm; excitation wavelengths – 488 nm, 543 nm, 633 nm; emission wavelength – 509 nm, 603 nm, 647 nm; excitation photon count – 1; pinhole = 1 Airy unit; a theoretical point spread function was used.

3.3 Results

3.3.1 Trafficking of Newly Synthesised Vesicles along Dendritic Profiles

Images were selected where long profiles of dendrites with no overlapping could be seen clearly. Images were separated into the green (VP-eGFP), red (GM130 staining) and blue (MAP2 staining) channels using ImageJ (http://rsb.info.nih.gov/ij/). The scale of the image was calibrated using ImageJ. The three channels were merged into RGB colour images and a segmented line (360 nm wide, diameter of approximately 2 LDCVs) was drawn from the edge of the stained GA down individual optical slice of dendrites where vasopressin staining was observed and the line selection was saved. Measurements of individual optical slices were used to ensure that there were no overlapping dendritic projections included in the measurements. After all the line selections were obtained, the red and blue channels were switched off and the original 32-bit image of the green channel was used. The saved line selections were then superimposed onto the green channel where fluorescent intensity measurements of VP-eGFP were made for each line. Fluorescent intensity was recorded for every pixel at 60 nm interval along each line selection, to ensure that as much information was recorded as possible. These measurements were saved and the area under curve (AUC; intensity x distance) was calculated for each segment of 6 µm of each line to compare fluorescent intensity along the dendrite. **Figure 3-3** shows a diagrammatic representation of the image analysis and an example of line selection drawn on a representative dendrite. Moreover, VP-eGFP fluorescence was measured at the GA by outlining the immunolabelled GA and superimposing this region of interest onto the VP-eGFP channel, where the sum intensity of VP-eGFP of the whole cell was measured.

To study whether newly synthesised vesicles translocate to dendrites and whether there is preferential translocation of newly synthesised vasopressin vesicles along the profile of dendrites, 125 dendrites were analysed using the methods described above. Varying lengths of dendritic profiles were analysed and dendritic profiles of as long as 54 µm were measured. AUC measurements were divided into 6 µm segments. **Table 3-1** shows the number of dendrites measured for each distance in each treatment group. The AUC was used to calculate the mean intensity of each 6 µm segment. All measurements comparing the effects of treatment to the distances measured were normalised to the total fluorescence intensity of each dendrite. Since data was normalised to the total fluorescence intensity, only dendrites with the same distances measured were chosen for comparison. This reduces the number of dendrites measured in each group and hence, the three longest distances (42 µm, 48 µm and 54 µm) were analysed. AUC of each line measurements of the 6 µm segment was compared between the three treatment groups using two-way ANOVA comparing treatment at each segment. **Figure 3-4** shows the mean total fluorescent intensity of the three treatment groups. One-way ANOVA showed that there is no difference in mean total fluorescence intensity measured between groups. **Figure 3-5** shows the % fluorescence comparison between the different treatment groups of the three total distances measured. There is significantly less fluorescence at 6 µm in the GA exit block released compared to control and GA exit block (48 µm analysis) and between GA exit block released and GA exit block (54 µm analysis). This difference is not seen with the 42 µm analysis. At 24 µm there is a significantly higher % fluorescence in control compared to GA exit block. Comparing distances within groups, there is a significantly higher % fluorescence at 6 µm compared to the

rest of the dendrite in control and GA exit block, showing that the low temperature did not affect vesicles already in the dendrites at the time of GA exit block. There is, however, no significant difference in % fluorescence between any distance in the GA block released group in all three total distances analysed. This indicates that newly synthesised VP-eGFP vesicles released from the GA forces a redistribution of vesicles near the GA, represented by the % fluorescence at 6 µm.

3.4 Discussion

The findings in this study showed that newly synthesised vesicles translocate to magnocellular dendrites and that there is no difference in newly synthesised vasopressin vesicle location throughout the distances of the dendrites measured. As mentioned in the introduction of this chapter, dendrites can be up to 200 µm long and hence the furthest distance analysed, up to 54 µm, should be considered as the proximal/middle portions of dendrites. The purpose of this study is to find out whether there are progressively more/less newly synthesised vesicles located along the profile of dendrites. 20^{o}C temperature incubation blocks vesicles exit from the GA (Griffiths *et al.* 1985; Ladinsky *et al.* 2002) and hence, release of temperature block leads to release of newly packaged vesicles. In the present study, GA exit block at 20^{o}C incubation did not affect vesicle distribution along the profile of dendrites since no significant difference in immunolabelled vasopressin intensity compared to control was observed. There is a significantly higher percentage of

vesicles at 6 µm in both control and GA exit block compared to the rest of the dendrite. Portions of dendrites proximal to the cell bodies were observed to be wider compared to the more distal portions measured. The higher density of vasopressin in these dilatations may account for the higher immunolabelled vasopressin fluorescent intensity measured at proximal portions of dendrites since more peptides can be stored in these portions. Interestingly, this difference was not observed in dendrites where the GA exit block was released. Although there were significantly less vesicles at 6 µm in GA exit block released compared to control and GA exit block in the analysis where 48 µm and 54 µm of dendrites were taken into account, this difference was not observed in 42 µm analysis where more dendrites were analysed. Difference in % fluorescence between 6 µm and longer lengths of dendrites measured was not observed in GA exit block released experiments. This indicates that release of newly synthesised vesicles from the GA might induce a redistribution of vesicles at close proximity to the GA and these newly synthesised vesicles translocate to dendrites. The homogenous distribution of vesicles after GA exit block release also indicates that there are no preferential sites of storage for newly synthesised vesicles. However, a difference in % fluorescence was not observed between GA exit block released compared to control. This is probably due to that fact that the analysis method used was not sensitive enough to pick up all newly synthesised vesicles that translocated to the dendrite. This is further demonstrated by the fact that there is no difference in mean total fluorescent intensity between the three groups (**Figure 3-4**).

Another reason why there is no difference in % fluorescence between GA exit block release and control might be due to the fact that high K^+ was used in the incubation medium. It was found previously in pancreatic cells that release of GA exit block by re-incubation of sections at 37°C in the presence of a secretagogue triggered secretion of insulin (Saraste *et al.* 1986). In the present study, the incubation medium contains high K^+ which has been shown to promote neuronal survival in explants of the hypothalamus (Shahar *et al.* 2004) and to stimulate dendritic peptide release (Ludwig *et al.* 2002). Hence, one reason why no difference in vesicle distribution was observed along dendrites after release of the GA exit block is that vesicles were undergoing exocytosis during the 30 min incubation at 37°C. If newly synthesised vesicles were preferentially released (Duncan *et al.* 2003), then no effect of vesicle re-distribution after the release of GA exit block will be observed since newly synthesised vesicles released from the GA will be exocytosed. However, in pancreatic cells, it was found that there was a 20 - 30 min lag period of insulin release after cells were re-incubated at 37°C (Saraste *et al.* 1986). Therefore, it is unlikely that increased exocytosis can fully account for the fact that no difference was found in vesicle distribution after the release of GA exit block. is a homogenous distribution of vesicles throughout the profiles of dendrites.

One limitation to the present study is that because magnocellular dendrites contain a large amount of peptides, and in this case, vasopressin, it is difficult to quantify vasopressin content using any other method than fluorescent intensity. Salt loading animals before experiments can lower vesicle content in dendrites and make

quantification more reliable (Tobin *et al.* 2004). However, salt loading has been found to increase the number of newly synthesised, immature secretory granules (Morris & Dyball 1974). Moreover, salt loading has been found to change the average diameter of dendrites (Dyball & Garten 1988; Hatton 1990). As mentioned earlier, vesicle accumulation is preferential in dilatations of dendrites (Morris 2005) and hence, salt loading was not used in this study to minimise the vasopressin density for measurement.

As discussed in Chapter 1, it was found that there are no active sites for peptide release in dendrites and all parts of the dendritic plasma membrane are capable of exocytosis (Pow & Morris 1989). After exit from the GA, vesicles travel to their sites of secretion via microtubules (for review see (Park *et al.* 2009). Hence, microtubule distribution is an important factor regulating distribution of newly synthesised vesicles. *In vitro* secretion studies showed a decrease in peptide release from magnocellular dendrites after applying a depolarising stimuli subsequent to colchicine treatment which inhibits polymerisation of microtubules (Tobin & Ludwig 2007a) suggesting the importance of microtubules in the transport of peptide-containing vesicles in magnocellular dendrites. The same study reported immunoreactivity of β-tubulin, one of the polymers that make up microtubules, in dendrites. However, the distribution of β-tubulin in dendrites was not discussed. Studies using immunohistochemistry to stain for microtubule-associated protein, an important component of microtubule crossbridges, has found extensive staining in oxytocin labelled neurons in the dendritic zone in the SON (Matsunaga *et al.* 1999),

further suggesting the presence of microtubules in dendrites. Further experiments looking at the distribution of tubulin during GA exit block and release of GA exit block along magnocellular dendrites can be done to complement the present study.

Combining the findings in this chapter with results in Chapter 2, where lysosomes were identified, it is likely that both newly synthesised and aged peptide vesicles are found in magnocellular dendrites. However, it is still unknown whether there are specific mechanisms controlling peptide vesicle routing to magnocellular dendrites and whether the dynamics of vesicle transport and segregation of vesicle pools are regulated according to vesicle age. Vesicle age cannot be studied in fixed tissue sections unless it is possible to distinguish newly synthesised vesicles and aged vesicles. Since it is still unknown whether like newly synthesised vesicles in bovine adrenal chromaffin cells (Duncan *et al.* 2003), newly synthesised vesicles in magnocellular dendrites are preferentially released, it is important to identify vesicular age. One method to study newly synthesised vesicles in dendrites is to express inducible exogenous reporter proteins targeted to vesicles (Zhang *et al.* 2002; Taupenot 2007). If vesicle expression can be switched on/off as desired, then newly synthesised vesicles and aged vesicles can be identified using a "pulse-chase" protocol (Han *et al.* 1999). The expression of the exogenous reporter protein can switched on for certain periods before fixation to identify newly synthesised vesicles, or expression can be switched off to identify aged vesicles. Another way is to use a fluorescent time stamp that changes colour as it matures over time (Terskikh *et al.* 2000) to label both newly synthesised and aged vesicles like that used in bovine

adrenal chromaffin cells as discussed in Chapter 1 (Duncan *et al.* 2003). Both these methods will be discussed in later chapters but to carry out these experiments, first it is important to establish viable slice cultures of the hypothalamus (House *et al.* 1998) which is essential for pulse-chase experiments and second, because neurons are non-dividing cells, they are difficult to transfect, making it difficult to express exogenous proteins. Moreover, it is also important to establish a live cell imaging technique that can be used in the magnocellular system so that the dynamics of newly synthesised and aged vesicles and the segregation into different vesicle pools can be visualised in real time. Hence, the next chapters will look at the establishment of viable organotypic slice cultures of the hypothalamus, a live cell imaging technique suitable for use in the study of vesicle release in magnocellular dendrites, transfection techniques that have been tested on magnocellular neurons, and generation of a range of constructs targeted for expression in dense core vesicles.

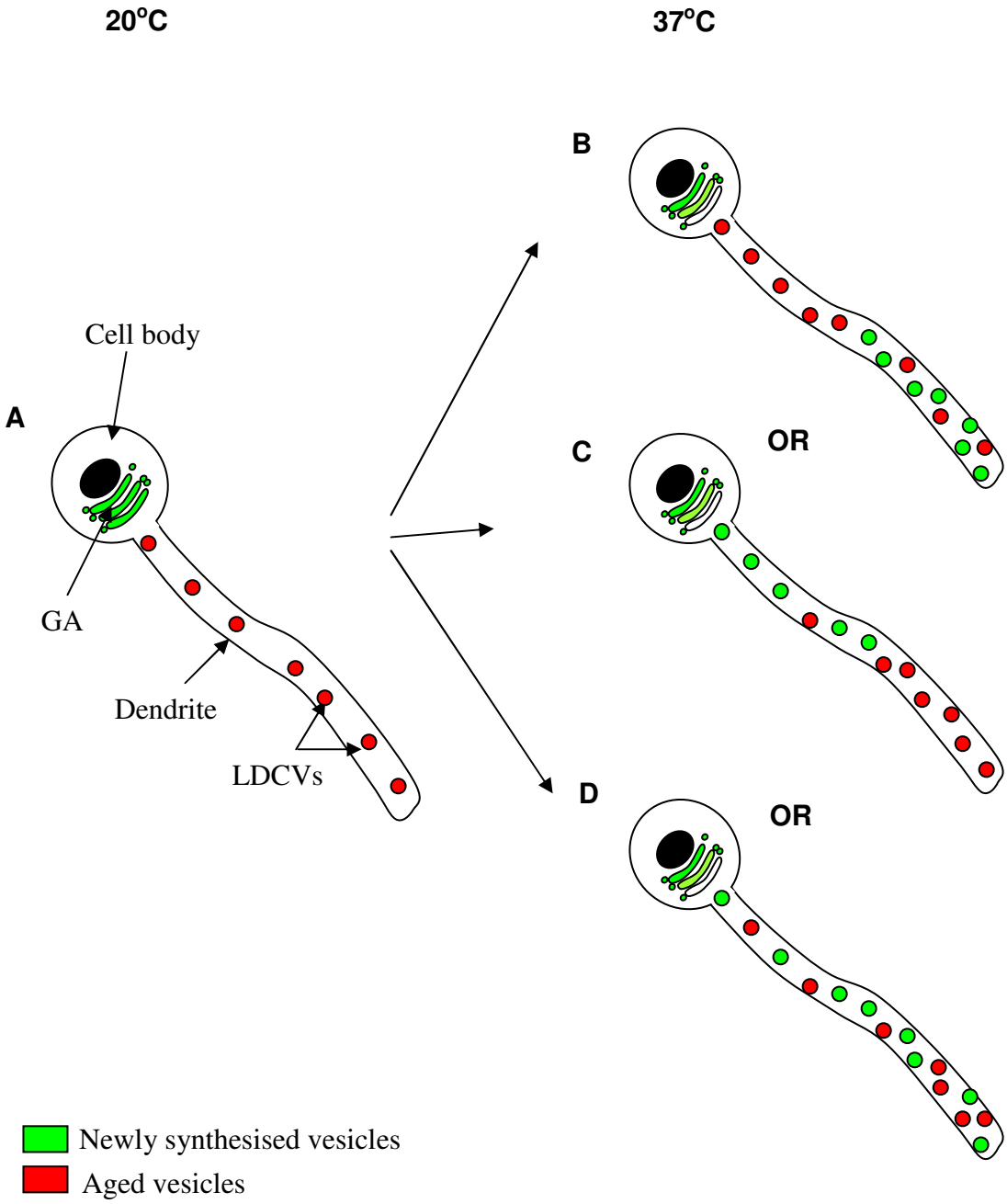

Figure 3-1. Schematic diagram showing hypothetic outcome of temperature block on vesicle exit from the Golgi apparatus**.** (A) Vesicle exit from GA blocked by low temperature (20°C). Re-incubation at 37°C lead to release of GA exit block and: (B) newly synthesised vesicles preferentially transported to distal dendrite; (C) Newly synthesised vesicles reside at proximal potion of dendrite; or (D) Homogenous storage of newly synthesised and aged vesicles along dendritic profiles with no relation to vesicular age.

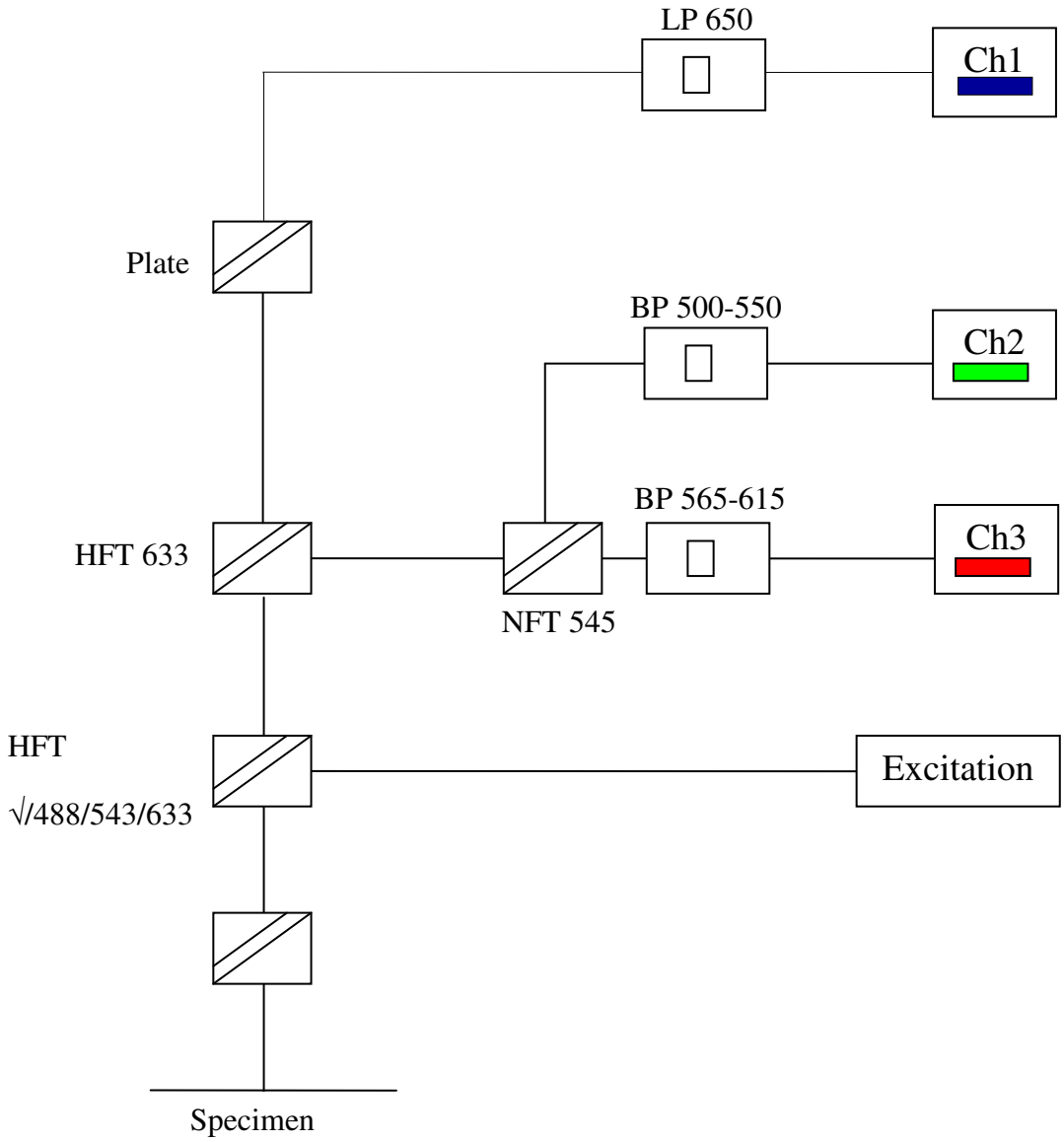

Figure 3-2. Beam path configuration for 3-channel imaging with the confocal laser scanning system. BP 500 – 550 and BP 565 – 615 as described before. HFT √/488/543/633 was used as the main dichroic beam splitter which passes all the specified excitation wavelengths (488, 543 and 633 nm) to the sample. The HFT 633 reflects all the excitation light above 633 nm to the long pass 650 filter and all the light under 633 nm to the NFT 545 filter. The NFT 545 is the secondary dichroic beam splitter.

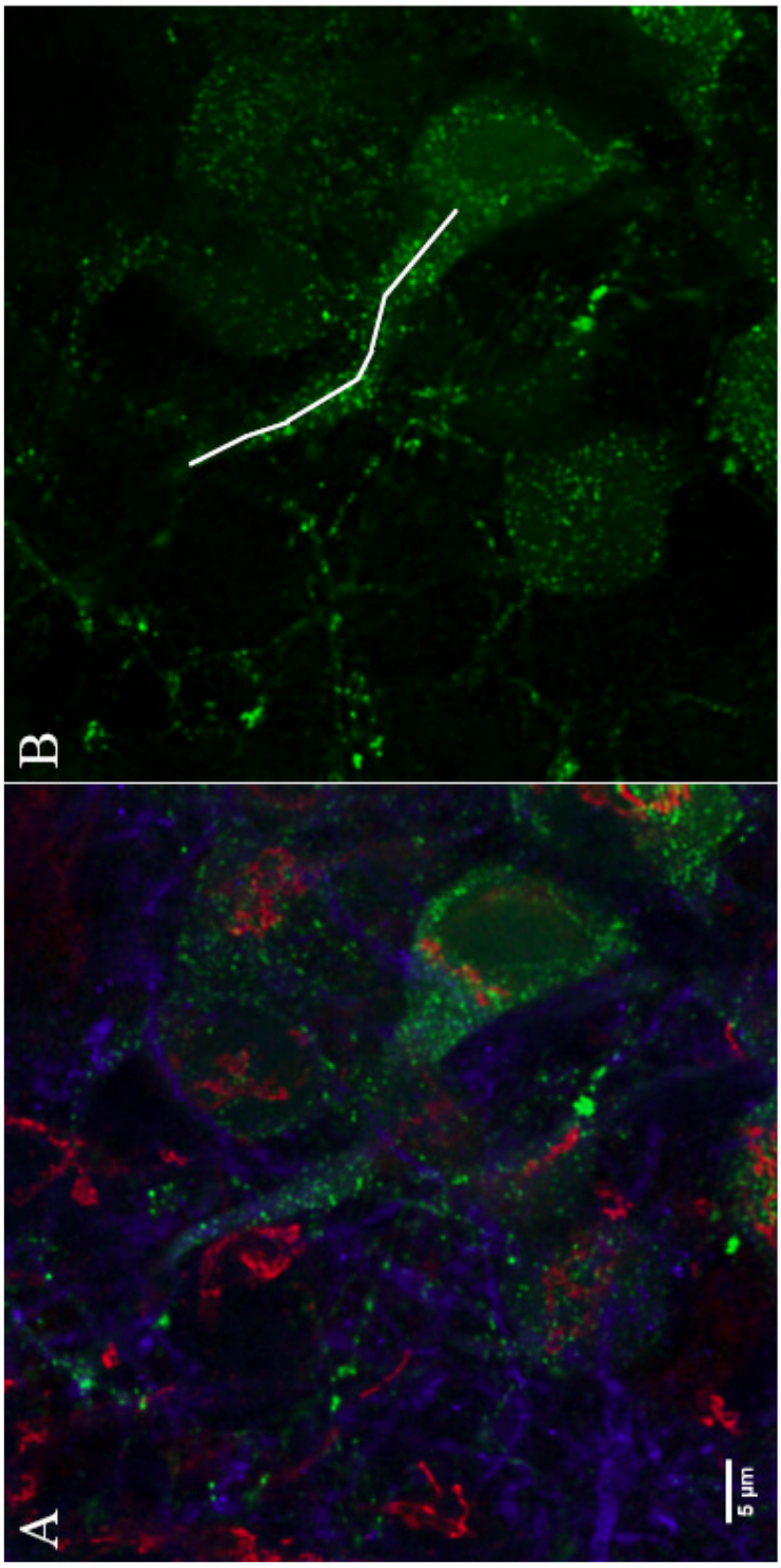

Figure 3-3. Measurement of fluorescent intensity along the profile of a typical dendrite. (A) Immunofluorescent labelling of the Golgi apparatus (red), MAP2 (blue) and VP-eGFP (green). (B) Line drawn along the profile of the dendrite to measure fluorescent of vasopressin (green). Lines were drawn down the centre of dendrites and line width is 357 nm thick. Measurements were made of individual optical slices to ensure the same dendrite was measured throughout the profile of the line. Scale bar = 5 µm.

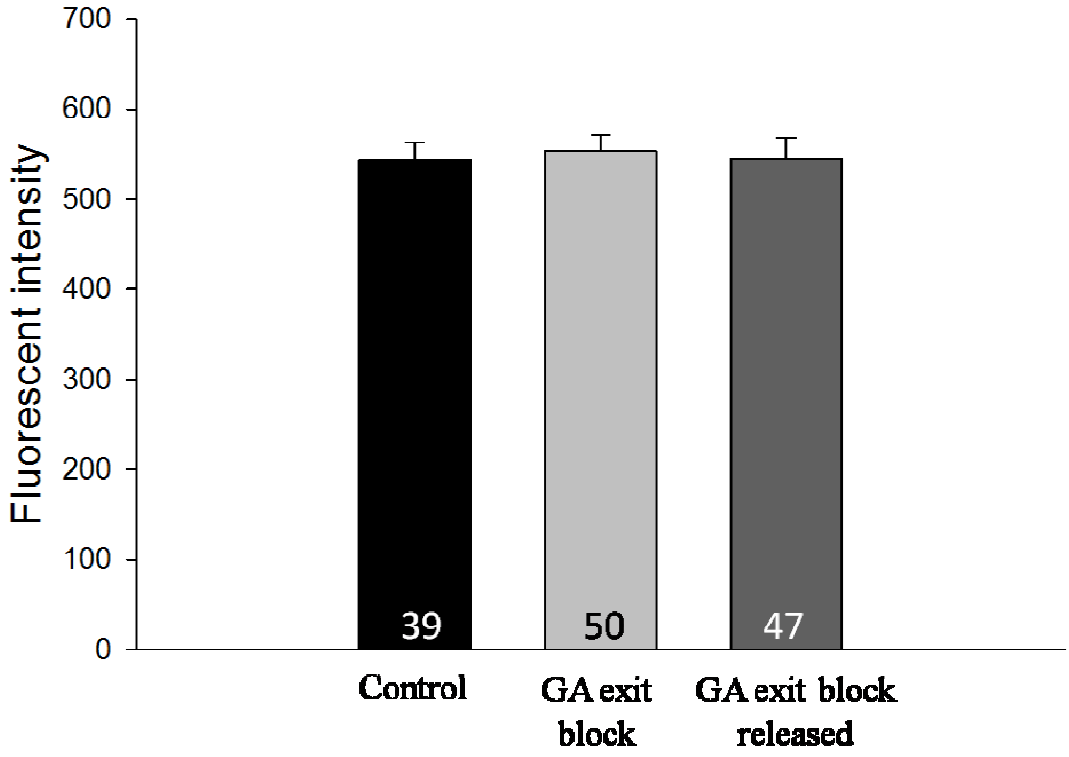

Figure 3-4. Mean total fluorescent intensity of dendrites measured. There is no difference between treatment groups (one-way ANOVA).

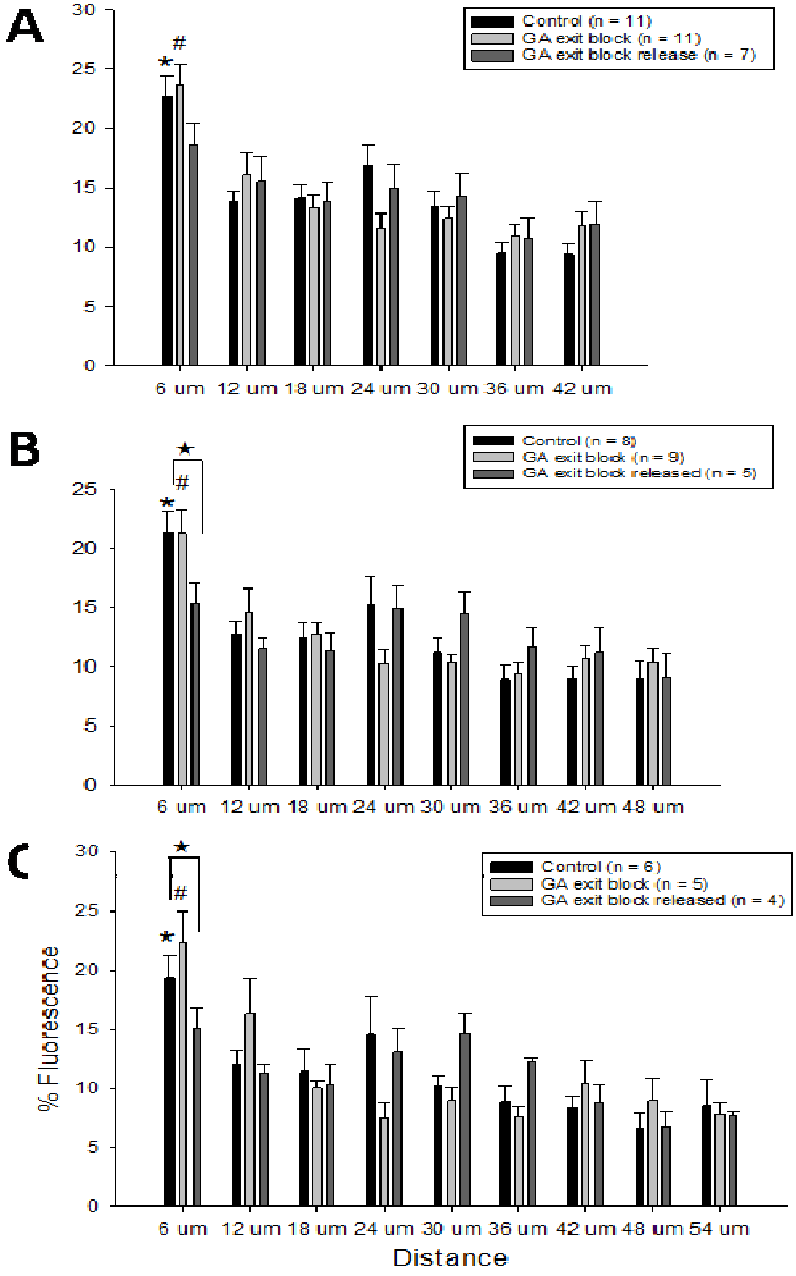

Figure 3-5. Graph showing % fluorescence along the profile of dendrites. % fluorescence is measured in 42 µm, 48 µm, and 54 µm of dendrites (A, B and C respectively). In all the three lengths measured, two-way ANOVA comparing treatment groups at each distance showed significant difference between 6 µm and the rest of the dendrite in control and GA exit block only ($p<0.05$). There is a significantly higher % fluorescence at 6 µm in control and GA exit block compared to GA exit block released ($p<0.05$) (B and C). However, this difference was not observed when only 42 µm of the dendrite was measured. Values are mean ± SEM, normalised to total fluorescent intensity.

Number of sections measured in each group			
Distance Measured	Control	GA exit block	GA exit block released
6 µm	39	50	47
12 µm	39	49	46
18 µm	35	39	39
24 µm	29	33	29
30 µm	22	27	19
36 µm	17	17	12
42 µm	11	11	7
48 µm	8	9	5
54 µm	6	5	4

Table 3-1. Number of sections measured for every 6 µm segment in each treatment group.

Chapter 4

Live cell imaging of dendritic peptide release

4. LIVE CELL IMAGING OF DENDRITIC PEPTIDE RELEASE

4.1 Introduction

The VP-eGFP transgenic rat has provided a valuable resource for identifying vasopressinergic neurons in different brain areas without prior staining procedures (Ueta *et al.* 2005). Moreover, it provides the opportunity for live cell imaging of vasopressinergic neurons without prior transfection or transduction. Live cell imaging is a technique that had been vastly used to study the exocytotic machinery of neuroendocrine cell lines. A range of different microscopic techniques have been used to offer deeper understanding in vesicle motility, segregation of vesicle pools, and dynamics of exocytosis. (Levitan 1998; Steyer *et al.* 1997; Straub *et al.* 2000). Although some of these techniques, for example, Total Internal Reflection Microscopy (TIRFM) which images events occurring at the plasma membrane, are used with great success to image exocytotic/endocytotic events in neuroendocrine cell lines (Merrifield *et al.* 2002; Nofal *et al.* 2007), they have limited use for imaging vesicle release from magnocellular neurons. TIRFM uses evanescent wave illumination and only illuminates within 100 nm of the specimen and hence, specimens imaged will have to be adhered to the cover glass that these cells were cultured on. Isolated cell preparation of magnocellular neurons is largely devoid of dendrites, so brain slices had to be used to image dendritic release of vasopressin in the form of VP-eGFP. Brain slices contain layers of different cell types and connective tissues hence, making them unsuitable for TIRFM imaging. On the other

hand, wide field microscopy offers a simple and fast way to image fluorescence. However, this technique has the drawback of collecting light that is in and also out of focus, making it impossible to determine peptide release from a single neuron. Therefore, it is important to determine the appropriate microscopy technique to be used for live cell imaging, meanwhile, taking into consideration the preparation of the specimen used for imaging. In contrast to wide field imaging, confocal imaging only samples from the plane of focus and hence, it is possible to identify single neurons.

An important aspect of live cell imaging is the choice of preparation of the cells imaged. As discussed above, brain slices are more appropriate for imaging dendritic peptide release in magnocellular neurons than isolated neurons. Acute brain slices are soft and thick, and flatten under their weight on cover slips over the time course of imaging. Due to these physical properties, cultured brain slices were more ideal for imaging purposes. Stationary organotypic slice culture provides a means of keeping slice tissues alive for up to several weeks (Stoppini *et al.* 1991; Gahwiler *et al.* 1997) and also, slice tissues flatten and adhere to the culture interface during culture, making it easier to handle and reduce flattening during imaging. The organotypic slice culture technique offers a way to study molecular mechanisms of magnocellular neurons where neurons maintain their synaptic connections as well as their physiological and morphological properties (House *et al.* 1998; Stoppini *et al.* 1991; Gahwiler *et al.* 1997; Cho *et al.* 2007). Although cultures of dissociated hypothalamic neurons are possible, these cultures survive best when the neurons

were obtained at the embryonic stage of the animal (Benda *et al.* 1975; Jirikowski *et al.* 1981), when these cells contain very little vasopressin and almost no oxytocin (Sinding *et al.* 1980b). The main advantage of organotypic slice culture technique is that brain tissues were obtained from neonatal animals, where the magnocellular neurons have fully differentiated. Moreover, neurons maintain their cytoarchitectural features, as well as their physiological phenotype. Slices typically thin down to 80 – 100 µm (House *et al.* 1998) which enable further manipulations like immunohistochemistry and live cell imaging. All these characteristics of slice cultures, coupled with the use of VP-eGFP rats, made live cell imaging of magnocellular cell bodies and dendrites possible.

While slice cultures prepared from neonatal rat brains are optimal for imaging, it is important to establish the physiological significance of using the SON of neonatal rats as a model system. In neonatal rats, osmotic challenge had been shown to induce vasopressin release into the plasma (Sinding *et al.* 1980a). This stimulus was found to deplete vasopressin content in the neurohypophysis by ~40%. Osmotic challenge is known to activate neurons in both the SON and the PVN (Penny *et al.* 2005). In adult rats, magnocellular neurons of both the SON and PVN respond to osmotic challenge by releasing vasopressin (reviewed in (Leng *et al.* 1999) into the circulation which then acts as a vasoconstrictor and anti-diuretic agent in response to increased osmolality. In the rat, oxytocin was also released after osmotic stimulation (Brimble *et al.* 1978). The magnocellular vasopressin system is responsive by the time of birth (Altman & Bayer 1986; Sinding *et al.* 1980a). However, direct

evidence for the activation of the neonatal SON in the rat in response to osmotic stimulation had not been shown. In this chapter, the activation of the neonatal SON under osmotic challenge, and live cell imaging of VP-eGFP neurons using organotypic slice explants of post natal day 7 (P7) rats will be discussed. Stimulated and primed vasopressin release from dendrites by thapsigargin was visualised using single photon laser scanning microscopy.

4.2 Material and Methods

4.2.1 Osmotic challenge in P7 rats

Twelve P7 rat pups, chosen from two separate litters were used in this experiment. Six P7 rats were injected with hypertonic saline solution, 1 ml/100 g of 1.5 M NaCl (i.p.) (Giovannelli *et al.* 1992), the other six were used as control without injections. Isotonic saline injection had been shown to have no effect on Fos expression in the SON, compared to animals not injected (Sharp *et al.* 1991); hence control animals received no injections. Three male and three female rats were used in each group. One adult rat was injected with hypertonic saline as a positive control for immunolabelling. Animals were killed by decapitation 1 hr after injection, since Fos production should be seen 30 – 90 min after induction of vasopressin neuronal activity (Kawasaki *et al.* 2005; Sharp *et al.* 1991). The hypothalami were then trimmed from the brain, fixed in 4% (w/v) PFA in 0.1 M PB (recipes of all solutions can be found in Appendix I), changed to 2% (v/v) PFA and 15% (w/v) sucrose in PB,

then to 30% (w/v) sucrose in 0.1 M PB (all overnight incubations at 4^{O}C). The fixed tissue was then snap-frozen on dry ice and cut on a freezing microtome to 52 µm sections. Only sections containing the SON were collected for immunohistochemical labelling of Fos protein. Fos protein is derived from c-Fos, an immediate early gene, which is transcribed upon activation of many cell types, including magnocellular neurons in the hypothalamus (Berciano *et al.* 2002; Luckman *et al.* 1994; Hoffman *et al.* 1993). The use of Fos immuno-staining as an indication of neuronal activation is well documented for magnocellular neurons under osmotic stimulation (Giovannelli *et al.* 1992; Hoffman *et al.* 1993; Sharp *et al.* 1991).

4.2.1.1 Three-step ABC method for labelling of Fos protein

Sections containing the SON were washed in 0.1 M PB + 0.2% (v/v) Triton X100 (PBT) four times for 10 min. To deactivate endogenous peroxidases, sections were then incubated in 20% (v/v) methanol and 1% (v/v) H_2O_2 in 0.1 M PB for 15 min. Sections were then washed in 0.1 M PBT twice for 10 min then in 0.1 M PB once for 5 min. To block non-specific binding of antibodies, sections were incubated in a cocktail of 1% (v/v) animal serum in 0.1 M PBT (blocking solution) at room temperature for 1 hr. A primary antibody solution, containing the antibody against Fos protein, rabbit polyclonal Ab-2 Fos (Oncogene Sciences), was made up with 1% (v/v) animal serum in 0.1 M PBT and Ab-2 Fos in a concentration of 1:1000. The primary antibody was left out in the negative control, where sections were only incubated in blocking solution. Sections were incubated in either primary antibody solution or blocking solution at 4^{o}C overnight.

The next day, sections were washed with 0.1 M PBT for three times for 5 min then twice for 10 min. During these washes, the avidin DH:biotinylated horseradish peroxidase complex was made up in PBT in the ratio of 1:1:3. This complex had to be made up half an hour prior to use. After washing, sections were incubated in biotinylated anti-rabbit immunoglobulin (Vector labs) and 30% (v/v) normal goat serum in 0.1 M PBT at room temperature for 1 hr. Sections were then washed in 0.1 M PBT three times for 5 min. After washing, sections were incubated in the Avidin DH complex at room temperature for 1 hr. Sections were then washed twice for 10 min and then rinsed in 0.1 M sodium acetate (pH6) for 5 min.

To visualise, Nickel II sulphate was dissolved in 0.2 M sodium acetate buffer (appendix I). Sections were incubated in this buffer until a colour change was observed and the reaction was terminated by the addition of 0.1 M sodium acetate. Sections were then mounted on 0.5% (v/v) gelatinised slides and air dried. Air dried sections were then washed in a series of ethanol solutions: 50% for 5 min, 70% for 5 min, 90% for 5 min, 95% for 5 min, 100% twice for 10 min each, and xylene twice for 10 min each. After dehydration, sections were coverslipped with DPX (VWR) and the mounting medium was left to cure overnight.

Sections containing the SON, identified by the anatomical location in the hypothalamus, were viewed by a light microscope. Ten sections containing the SON

were analysed per animal. Fos immunoreactive cells were counted manually and the mean ±SEM for Fos counts per animal was compared between osmotically challenged and control groups by one way ANOVA. All statistical tests were carried out using Sigma Stat.

4.2.2 Organotypic slice culture

Rat pups, 7 days old were anaesthetised with halothane or isofluorane and decapitated and their brains quickly removed. Hypothalamic tissue blocks were cut by sectioning the brains with a vibratome in aCSF-sucrose-KOH solution (appendix I). Osmolarity of solution was 300 mOsm/L. Solution was gassed with oxygen throughout slicing. Three to four 300 µm thick coronal slices containing the SON and part of the PVN were obtained from each brain. Slices were kept in ice cold Gey's Balanced Salt Solution (Sigma-Aldrich, UK) enriched with 5 mg/ml glucose (Sigma-Aldrich, UK). Selected sections were kept in a petri dish with Gey's solution at 4^{o}C for 1-2 hours. Explants were then placed on Millicell-CM filter inserts (Millipore, pore size 0.4 µm, diameter 30 mm) in 6-well culture dishes with 1.1 ml of culture medium (Stoppini *et al.* 1991). Explants were incubated at 37^{o}C in 5% CO_2 in a stationary manner. Culture medium was replaced three times a week (House *et al.* 1998). Explants were maintained for up to 14 days *in vitro* (DIV).

Culture Media: Serum-containing medium

Serum-containing growth medium was shown to help the slices to thin down to a few cell layers so that procedures such as live cell imaging could be done on the slices as whole mounts (House *et al.* 1998). The serum-containing medium was composed of 50% (v/v) Eagles basal medium (BME, Sigma-Aldrich, UK), 25% (v/v) heat-inactivated horse serum (Harlan, UK), and 25% (v/v) Hanks balanced salt solution (Gibco). The osmolarity of the medium was 320-325 mOsm/L. Medium was supplemented by 0.5% (w/v) glucose, 2 mM glutamine, 25 µg/ml penicillin/streptomycin (House *et al.* 1998), 20 ng/ml ciliary neurotrophic factor (CNTF) (all from Sigma-Aldrich, UK), and 25 mM KCl. It has been suggested that a higher KCl content increased the exocytotic capabilities of rat cerebellar granule neurons (Yamagishi *et al.* 2000). CNTF was found to substantially increase the survival of both oxytocin and vasopressin magnocellular neurons in the SON in organotypic slice cultures by preventing programmed cell death (Rusnak *et al.* 2003).

4.2.3 Live cell imaging

Live cell imaging experiments were performed on organotypic slice cultures of the SON between 7 days in vitro (DIV7) to DIV14 when slices had adhered to membrane filters and flattened down. The slices were excised from the membrane filter and placed inverted on a 30 mm coverslip (thickness #1) and assembled in a POC open perfusion adaptor (LaCon, Germany) as shown in **Figure 4-1**. The perfusion chamber was then placed on a microscope stage heated to 37^{o}C and inside an environmental chamber gassed with humidified air and 5.5% CO_2. A 21-gauge

needle was used for the outflow instead of the original outlet of the chamber. The needle was connected to two outflow tubes being pumped at the same time to ensure constant rate of outflow. The tissue was continuously perfused with tyrode solution at a rate of 0.5 ml/min, with or without stimulus. All solutions were adjusted to pH 7.2 and 300mOsm. Tyrode's solutions were warmed to 37^{o}C throughout the experiment. Refer to appendix I for recipes. **Figure 4-2** shows a schematic diagram of the perfusion set up.

4.2.3.1 Timeline for image acquisition

Thapsigargin had been shown to potentiate release of oxytocin and vasopressin after 30 min of pre-treatment (Ludwig *et al.* 2002; Ludwig *et al.* 2005). Hence, experiments were carried out at 42 min sessions. Four groups of experiments were carried out: control (42 min Tyrode's solution), potassium stimulated (30 min Tyrode's + 10 min 50 mM K^+), thapsigargin treatment (42 min 200 nM Thapsigargin), and thapsigargin treated, potassium stimulated (30 min Thapsigargin + 10 min K^+). 2 min was allowed for change of solution. A schematic diagram showing the imaging timeline is presented in **Figure 4-3**.

4.2.3.2 Microscopic image acquisition

The Zeiss LSM510 inverted microscope was used for all imaging. The 488 nm line of the Argon laser was used to excite eGFP which has an excitation maximum of 488 nm and an emission maximum of 509 nm. A HFT 488 filter was in place and the

excitation laser passed through two mirrors before the emitted light was collected by a band pass 500 – 550 filter (please refer to **Figure 2-2**). The photomultiplier tube (PMT) settings were adjusted so that small projections from the neurons would be visible and were the same for all experiments. The pinhole was adjusted to maximum so that the maximal emission from the specimen could be collected. The laser excitation was set to 15% so that visualisation of eGFP was achievable whilst bleaching was kept at minimal. Images were acquired with an x63 water immersion objective (NA1.2). The lateral resolution was 216 nm for 509 nm emission wavelength and NA1.2. The Nyquist sampling rate, calculated by the Nyquist calculator on the Scientific Volume Imaging support website, was 106 nm, 106 nm and 341 nm for x, y, and z sampling respectively. Double nyquist sampling rate was employed to avoid under-sampling. 3-dimensional images were obtained by scanning the x, y –planes at 60 nm, achieved by line scanning 1024 x 1024 pixels with an optical zoom of 2.4, and intervals of 170 nm along the z-axis was acquired at the time points mentioned above. 8 bit pixel depth, line averaging of 1 (no averaging) and maximum scan speed were chosen for image acquisition to avoid photobleaching.

4.2.3.3 Fluorescent image processing

The acquired stack of images was deconvolved to remove aberrations caused by the intrinsic physical properties of the microscope. The microscopic parameters used for deconvolution was set according to the parameters used for imaging: microscope

type – confocal; numerical aperture – 1.2; lens immersion and medium refractive indices – 1.3; x and y sample sizes – 60 nm; z sample size – 170 nm; excitation wavelength – 488 nm; emission wavelength – 509 nm; excitation photon count – 1; backprojected pinhole – maximum. These parameters were used to calculate a theoretical point spread function. Please refer to Chapter 2, **section 2.2.4** for a more detailed account on image manipulation.

4.3 Results

4.3.1 Osmotic challenge in P7 rats

Figure 4-4 shows Fos expression in the SON of P7 control and osmotically challenged rats, and adult positive control. The SON was identified by its anatomical location. Landmark features like the 3rd ventricle and the optic chiasm are also shown in the images. **Figure 4-5** shows the mean number of Fos positive cells per SON ±SEM in control and osmotically challenged P7 rats. One way ANOVA followed by post-hoc Student's t-test showed that there was significant difference ($p<0.001$) in the number of Fos positive cells between the two groups. Marked increase in the number of Fos immunoreactive cells in the SON suggests activation of magnocellular neurons due to osmotic stimulation. This indicates that magnocellular neurons in P7 rats were responsive to the osmotic challenge.

4.3.2 Live cell imaging

Deconvolved images were viewed and analysed by the image analysis software, ImageJ (http://rsb.info.nih.gov/ij/). The 3-D image acquired at each time point was then represented as a 2-D image by adding the values of each pixel through the z stack and displays it as a sum value. Due to the decrease in fluorescent intensity as the imaging depth increased, 10 optical slices of dendrites from the centre of each stack were summed up for 2-D representation. Hence, 32-bit images were analysed so that accurate sums were retained. The 2-D images were created for image stacks collected for each time point and then aligned using the stacks shuffling plug-in (Thevenaz *et al.* 1998) to ensure that the same area was measured for each time point. This allowed for measurement of fluorescent intensities in regions of interest by the analyse and measure functions in the software. An example of region of interest measurement is shown in **Figure 4-6**. Measurements made for different time points were done separately to indicate the amount of eGFP fluorescent gained or lost throughout the experiment.

Figure 4-7 shows images of dendrites acquired in the live cell imaging experiments. One example of control, K^+ stimulated and thapsigargin pre-treated K^+ stimulated experiment is shown. **Figure 4-8A** shows the changes in fluorescent intensity in dendrites after stimulation. Fluorescent intensity data collected was normalised to data at 30 min, the time point imaged before stimulation. Mean fluorescent intensities ±SEM were calculated and compared between groups using two-way ANOVA on repeated measures to show changes in intensities between time points

and between groups. The control experiment, with no stimulation, recorded the extent of photobleaching and basal vesicle release. This accounts for ~ 25% loss of eGFP signal. Comparing 32 min to 42 min, there is a significant decrease in fluorescent intensity in dendrites in K^+ stimulated and thapsigargin pre-treated K^+ stimulated groups but not in control and thapsigargin treated groups (two-way ANOVA, post-hoc Student's t-test, $p<0.05$), showing release of VP-eGFP vesicles after stimulation. Fluorescent intensity in thapsigargin pre-treated K^+ stimulated group showed significant decrease compared to other groups at 42 min ($p<0.05$), suggesting that thapsigargin pre-treatment was able to potentiate further release of vesicles after K^+ stimulation (a further ~ 20% release compared to K^+ depolarisation alone, **Figure 4-8B**).

To ensure that fluorescent intensity changes were due to release of VP-eGFP, background fluorescence decay was obtained by measuring the fluorescent intensity of 10 x 2 μm squared areas in the background of each image. A single exponential decay function was fitted to the data. The mean exponential decay constants (**Figure 4-8C**) for each group were compared (two-way ANOVA) and showed no difference in rate of decay, suggesting that decrease in fluorescent intensity measured in dendrites were due to the release of VP-eGFP and not due to increase in fluorescent decay caused by treatment.

4.4 Discussion

Use of organotypic slice cultures provides several advantages to the efficacy in live cell imaging. However, since cultures had to be obtained from neonatal rats, it was necessary to establish the physiological responsiveness of magnocellular neurons at that age. Neonatal P7 rats had been shown to have a raised membrane capacitance and decreased membrane resistance compared to adult rats (Chevaleyre *et al.* 2001). These characteristics were correlated to an increase in dendritic ramifications. Despite these early differences, the membrane potential of magnocellular neurons at this age was shown to start to stabilise and display typical firing patterns of adult magnocellular neurons. The increase in number of dendritic ramifications could facilitate the formation of glutamatergic synapses, as found in the dendrites of hippocampal neurons (Tyzio *et al.* 1999). In magnocellular neurons, excitatory postsynaptic currents were found to be blocked by CNQX (NMDA receptor antagonist) around P7 – P8, suggesting glutamatergic activation (Chevaleyre *et al.* 2001). In the osmotic challenge experiments, the SON of P7 animals were shown to be responsive to hypertonic saline injections, suggesting activation of the magnocellular neurons by osmotic challenge. Although neurons were not labelled for VP or OT, it is likely that the activated cells in the SON represent magnocellular neurons.

In the present study, thapsigargin priming induced a ~ 20% potentiation of K^+ stimulated vasopressin release (**Figure 4-8B**). Compared to *in vitro* release

experiments, K^+ depolarisation induced a ~ 30% increase in vasopressin release after thapsigargin pre-treatment for 30 min compared to high K^+ treatment alone (Ludwig *et al.* 2005). It is worth noting that whilst the VP-eGFP gene was incorporated into vasopressin cells, endogenous vasopressin was still being produced. Hence, whilst measurement of VP-eGFP intensity only detected release of vasopressin tagged to eGFP, endogenous vasopressin release would not be accounted for using this method. LDCV release from the magnocellular dendrite is considered a rare event (Leng & Ludwig 2008). Intracellular Ca^{2+} mobilisation caused by thapsigargin treatment enhanced this rare release event by recruitment of LDCV to the RRP (Tobin *et al.* 2004). Thus, vesicle recruitment to the RRP can increase release by 20 – 30%. Interestingly, there were no differences in fluorescent intensity measured at 42 min comparing high K^+ depolarisation and control, even though there was a significant decrease in intensity at 42 min compared to 32 min with K^+ stimulation only (**Figure 4-8A**). This difference was contributed by an insignificant increase in fluorescent intensity in the K^+-treated group at 32 min compared to other groups. This suggests that K^+ depolarisation may cause quick vesicle mobilisation and vesicle pool replenishment, resulting in a higher VP-eGFP fluorescent intensity right after K^+ stimulation. Studies in the Calyx of Held synapse (Hosoi *et al.* 2007) and the synapses in the auditory brainstem (Wang & Kaczmarek 1998) found that strong depolarising potentials caused an influx of calcium which was essential to rapid vesicle recruitment to the presynaptic terminal. It is not known whether magnocellular neurons display rapid vesicle recruitment after depolarisation with K^+, however, vesicle recruitment in the magnocellular dendrite has previously been

shown using thapsigargin (Tobin *et al.* 2004). It is unlikely that vesicle pools mobilised by thapsigargin is the same vesicle pool mobilised by high potassium stimulation since potassium depolarisation was unable to mobilise the thapsigargin-sensitive vesicle pool in magnocellular dendrites (Ludwig *et al.* 2002). Nevertheless, an ability to recruit and mobilise vesicle pools in magnocellular dendrites may explain the small rise in VP-eGFP fluorescent intensity at 32 min in K^+-treated samples leading to a significant difference in fluorescent intensity compared to 42 min, although VP-eGFP fluorescent intensity at both time points was not different between K^+-treated and control groups.

Basal release of VP-eGFP and photobleaching accounted for ~ 25% loss of eGFP signal. It could be argued that usage of two-photon excitation would minimise loss of eGFP signal due to photobleaching since multiphoton excitation only occurs in one focal plane and hence, other focal planes of the cell would not be bleached during stack acquisition. Reduction in photo-excitation of cells in general also reduces phototoxicity, which is the result of free radicals generation by laser excitation. However, studies comparing cell viability between the use of one- and two-photon excitation in chondrocytes found that 84% of cells survived 30 min of continuous irradiation of 488 nm single-photon laser excitation (Bush *et al.* 2007). Moreover, photobleaching of GFP by two-photon excitation was found to be more enhanced compared to single-photon excitation (Chen *et al.* 2002) in live cell imaging of transfected HeLa cells. Single-photon confocal imaging of cultured brain slices has also been achieved in other brain areas and cell types, e.g. endothelial cells

in capillaries and noradrenalinergic neurons in brainstem slices, and pyramidal cells in the hippocampus (Teschemacher *et al.* 2005).

There are several problems associated with imaging live cells in slices. Firstly, instability and movements in both the microscope and the tissue are the major problems. A 1^{o}C change in temperature of the microscope set up could account for a 1 µm movement in the lateral or axial direction (Kasparov *et al.* 2002). Therefore, it was important to minimise these movements by the use of environmental chambers, heated microscope stage, heated solutions and by taking a stack of images in the Z direction to make sure that the whole cell is accounted for. Solution flow rate and change of solution can also affect displacement of the tissue. An environmental chamber had been used to keep the temperature on the microscope stage stable. Two outflow tubes had also been attached to the perfusion chamber to ensure steady flow of solutions. Aside from the inherent problems encountered from the microscope set up, scattering of light and difference in light absorbance throughout the thickness of the section affect the resulting image quality. These affect organotypic slice cultures to a lesser extent since cultures are made from neonatal animals which are optically optimal; and slice explants flatten to a few cell layers. Nevertheless, to image whole neuronal cell bodies along with their dendritic projections may require imaging depths of tens of micrometers. This depth of image is in itself a problem since fluorescence from the top of the image has less distance to travel compared to fluorescence from within the tissue; i.e. fluorescent intensity is stronger at the top of the image. This has to be taken into consideration when quantifying fluorescent

intensity and hence, 10 optical slices (~1.67 µm in total) in the centre of the stack were selected for image analysis.

Lastly, photobleaching and phototoxicity are the most important factors of concern in live cell imaging. The fluorophore used in the experiments in this chapter is eGFP, which is a mutated (S65T) version of wild-type green fluorescent protein, GFP. Photobleaching in eGFP had been reported to be relatively stable (Swaminathan *et al.* 1997; Tsien 1998) making it suitable as a reporter protein in live cell imaging experiments. Live cell imaging of VP-eGFP in organotypic slice cultures revealed significant loss of VP-eGFP within dendrites after depolarisation by 50 mM K^+ and further potentiated release by depolarisation after thapsigargin pre-treatment. This is in accordance with findings in *in vitro* experiments where isolated SON was stimulated and release measured with radioimmunoassays (Ludwig *et al.* 2002; Ludwig *et al.* 2005). Since vasopressin release was quantified by the loss of VP-eGFP fluorescence, it is important to establish that eGFP fluorescence was not affected by the treatments used. eGFP is a class2 GFP, where two point mutations led to enhanced photostability, increased fluorescence and stability at 37^{o}C. eGFP is also pH sensitive, decreasing in fluorescent intensity at slightly acidic pH (Patterson *et al.* 1997). To ensure that loss of eGFP fluorescence was due to vasopressin release, background fluorescent decay was measured. Background fluorescence was caused by eGFP cells not in focus and by noise. If the stimuli applied caused a decrease in eGFP emission, there would also be a significant decrease in background fluorescence compared to control. Analysis of the exponential decay constants

demonstrated that this was not the case; i.e. there was no change in background fluorescence in any group at any time point. Also, thapsigargin treatment without depolarisation did not cause a significant change in fluorescent intensity in dendrites, suggesting that thapsigargin was unable to induce a significant amount of release of VP-eGFP detectable by fluorescent intensity measurement and that thapsigargin treatment did not cause changes in properties of eGFP fluorescence.

Results from the live cell imaging experiments showed that live cell imaging of P7 organotypic slice cultures provided comparable findings as in *in vitro* release experiments. Results from the osmotic challenge experiments also showed that neonatal P7 rats were suitable for use in live cell imaging experiments. In addition, organotypic slice cultures are easy to handle and maintain, and could be transfected to induce expression of other fluorescent constructs of interest by use of biolistic transfection (discussed in next chapter) or viral transduction for live cell imaging (Teschemacher *et al.* 2005) providing a robust model system to study dendritic peptide release in magnocellular neurons.

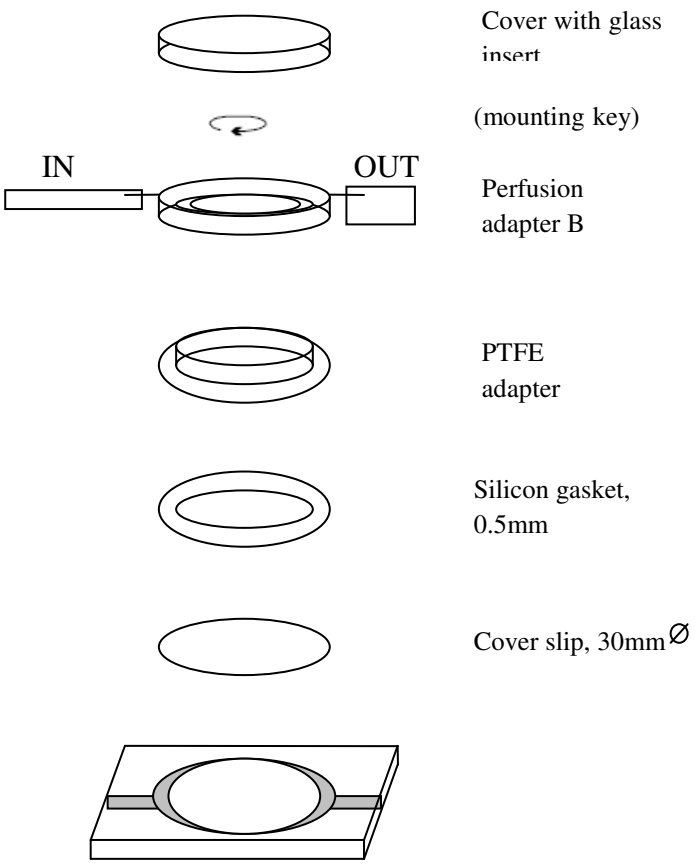

Figure 4-1. Perfusion chamber components. The POC mini chamber (LaCon, Germany) has an observation area of 17 – 22 mm. A slice explant was placed inverted on top of a 30 mm diameter cover slip (thickness #1). The perfusion adaptor allowed for an open perfusion system; influx was through the inlet attached to the perfusion adaptor and outflow was achieved by a 21-gauge needle attached to two outflow tubes.

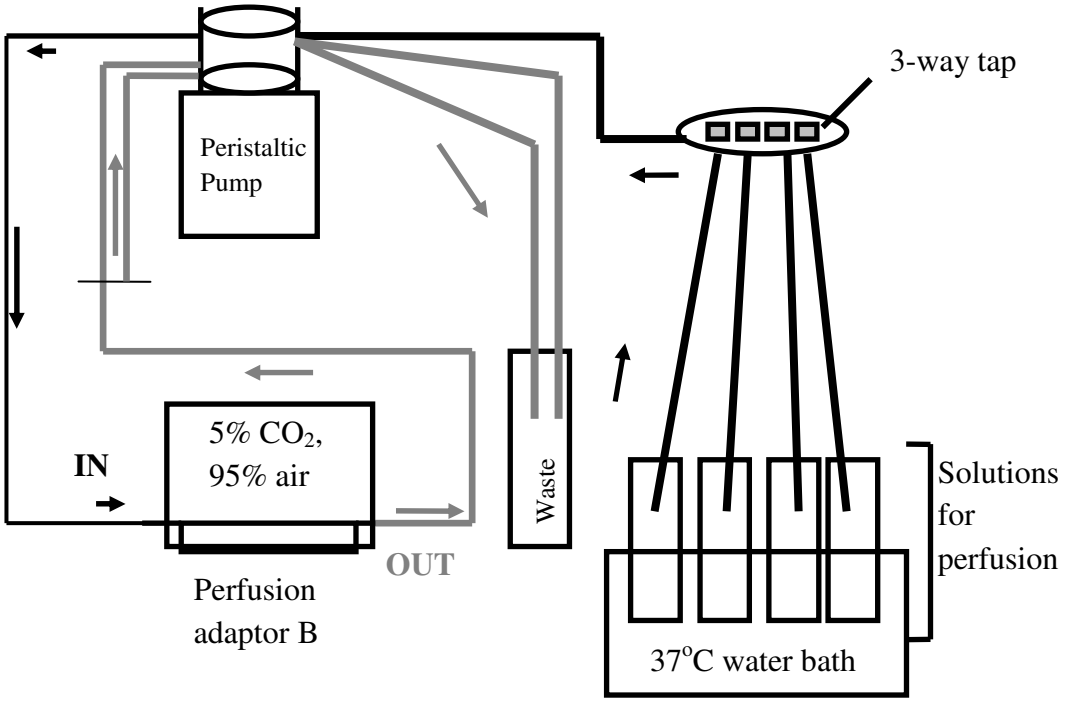

Figure 4-2. Perfusion set up for live cell imaging experiments. Solutions were heated up in a 37°C water bath and pumped in to the perfusion adaptor by a peristaltic pump (0.5 ml/min). Two outflow lines were used to keep the outflow stable. Solution change was achieved by a three-way tap. The perfusion adaptor was placed on a stage heated to 37°C. The heated stage was encased in an environmental chamber where 5% CO_2 and 95% humidified air was pumped in.

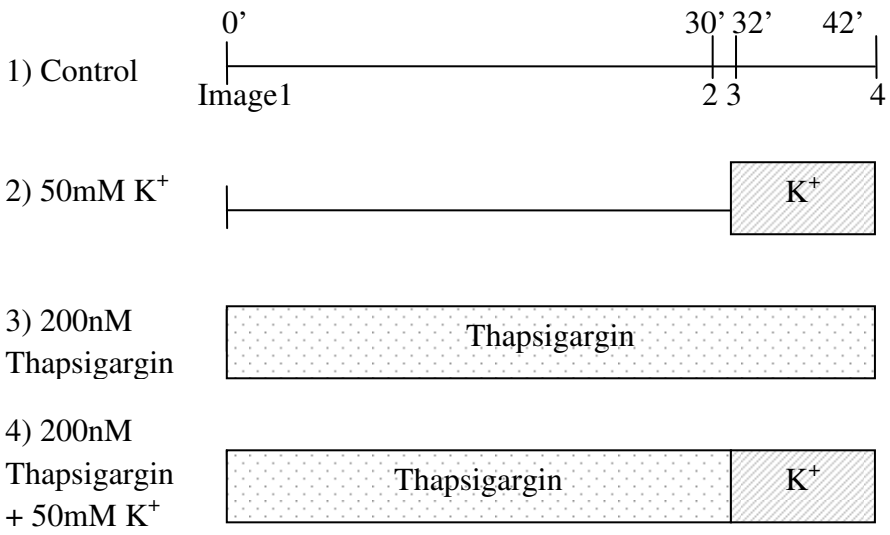

Figure 4-3. Image acquisition timeline for live imaging. A stack of images were taken at 0 min, 30 min, 32 min and 42 min. 1) Control: sections were perfused with Tyrode's solution throughout; 2) 30 min Tyrode's solution + Tyrode's solution containing 50 mM K^+ thereafter; 3) perfusion with Tyrode's solution containing 200 nM thapsigargin throughout; 4) perfusion with Tyrode's solution containing 200 nM thapsigargin for 30 min + Tyrode's solution containing 50 mM K^+ thereafter.

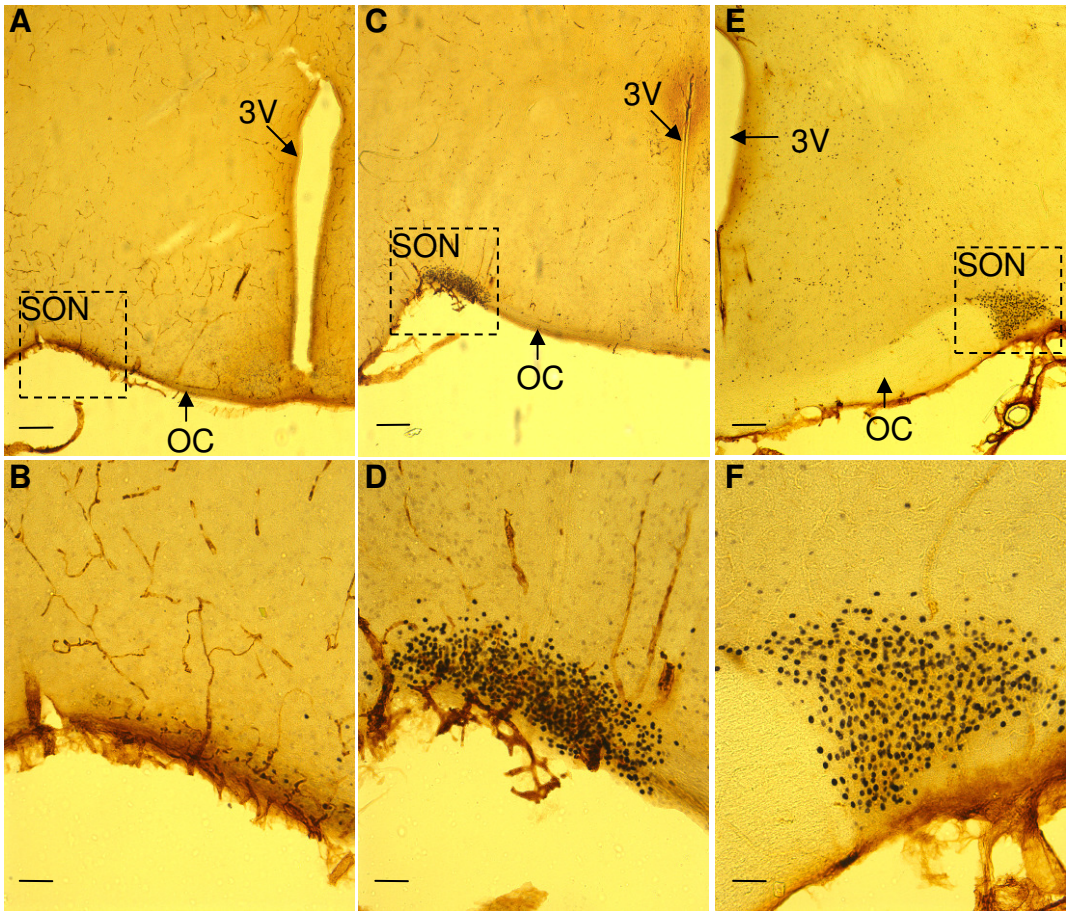

Figure 4-4. Fos expression in the hypothalamus. A-D: postnatal day 7 (P7) Sprague Dawley rats; E and F: adult positive control. B, D and F (scale bar = 50 µm) are magnified images of the SON from A, C and E (scale bar = 200 µm) respectively. A and B: control; C – F: osmotically challenged, i.p. 1ml/100g 1.5 M saline solution. 3V = 3rd ventricle; OC = optic chiasm; SON = supraoptic nucleus.

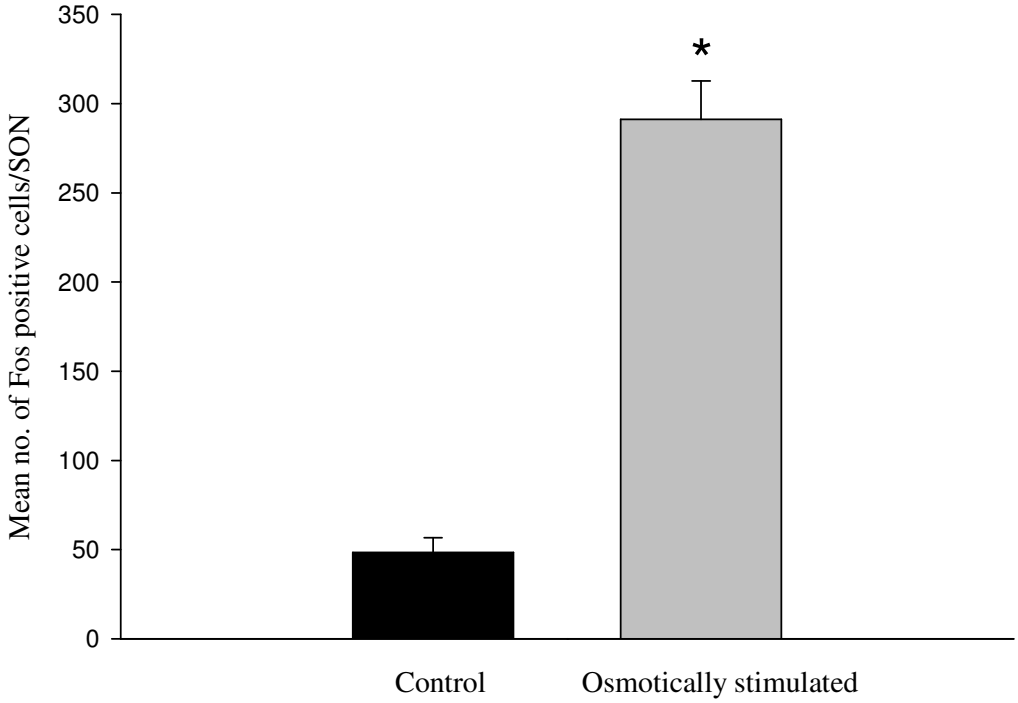

Figure 4-5. Effect of osmotic challenge on Fos expression in the SON on post-natal day 7 (P7) Sprague Dawley rats. Animals were divided into two groups: (1) osmotically challenged with 1ml/100g 1.5 M saline solution (i.p.) and (2) control. Values are group means ± SEM; 10 SON analysed per animal, n = 6 for each group. Student's t-test showed significant difference in the number of Fos immunoreactive cells between control and osmotically challenged groups ($p<0.001$), suggesting activation of the SON in P7 rats after osmotic challenge.

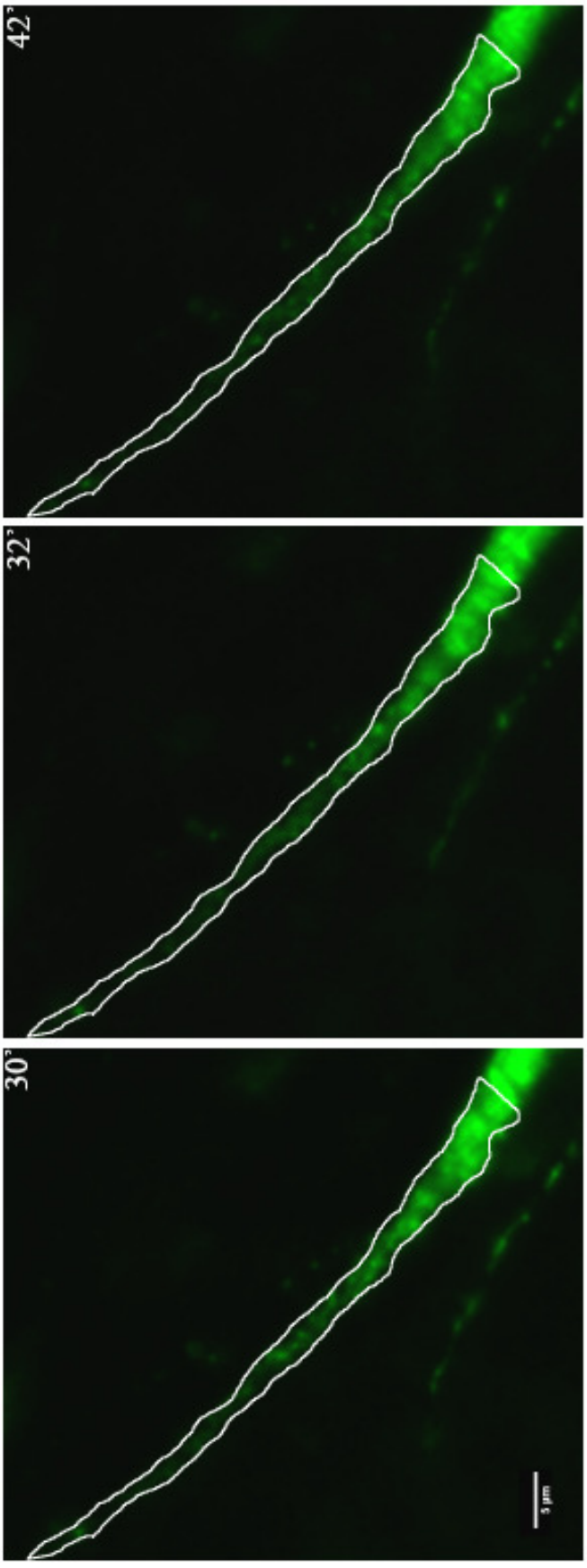

Figure 4-6. Measurement of VP-eGFP fluorescent intensity. Each image is a sum projection of 10 optical slices taken at time points 30', 32' and 42'. Image from each time point was aligned using ImageJ plugin: stacks - shuffling/align slices/rigid body (Thevenaz et al. 1998) to ensure that the same area of interest was measured throughout. The mean intensity (intensity/area) was recorded and analysed for each image.

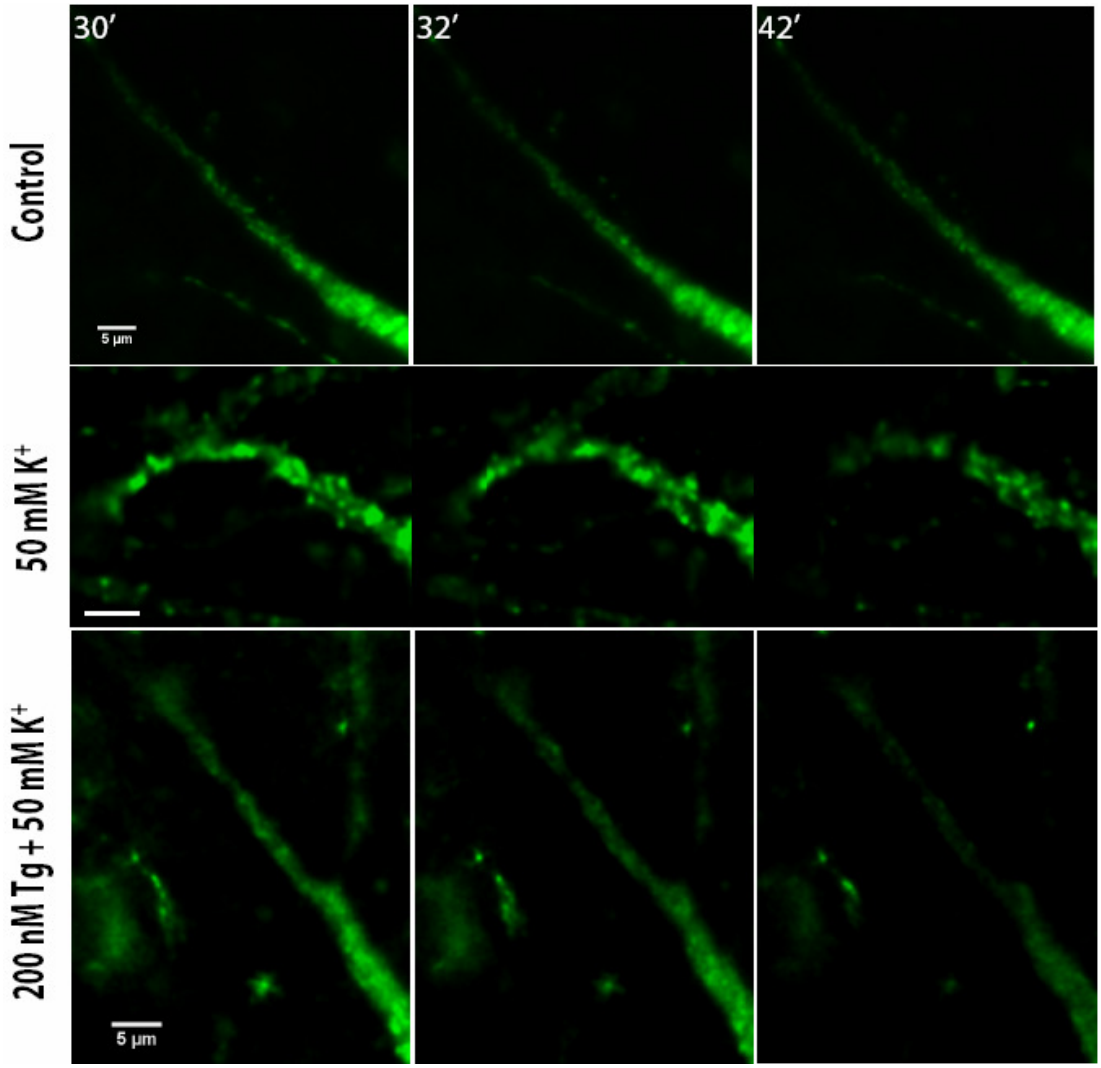

Figure 4-7. Live cell imaging of VP-eGFP dendrites in the SON. Images are examples of control, K^+ stimulated and Tg primed K^+ stimulated experiments. A change in fluorescent intensity indicate a change of VP-eGFP content in the dendrites. Images were acquired at 30', 32' and 42'. For K^+ stimulation only, control Tyrode's solution was applied for 30'. Thereafter, K^+ stimulation was applied. For Tg primed, K^+ stimulated experiments, control solution was replaced with Tyrode's solution containing 200 nM Tg. Scale bars = 5 µm.

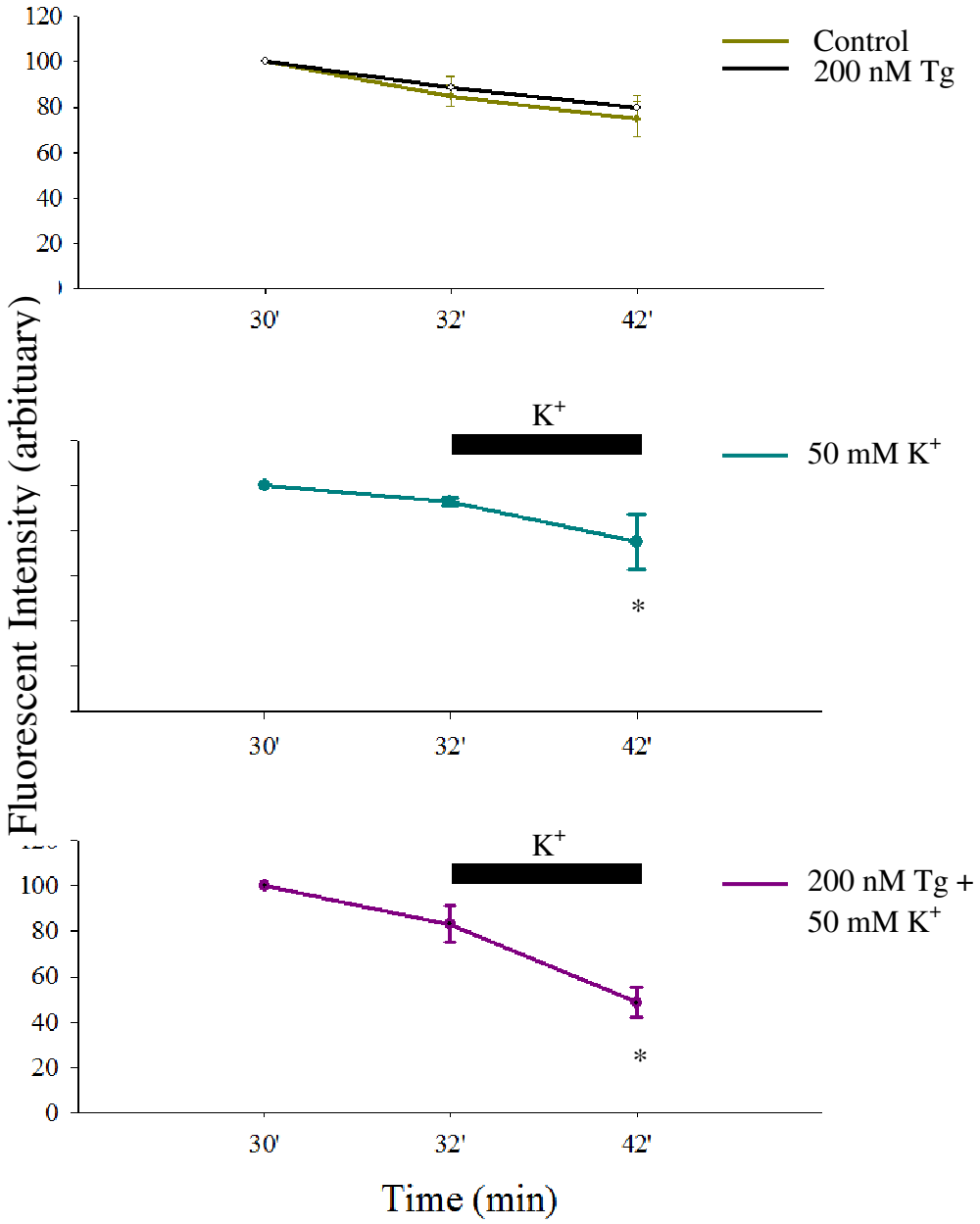

Figure 4-8A. Changes of fluorescent intensity in dendrites after stimulation. All data were normalised to 30 min. Intensity in the dendrite was obtained by measuring the mean (intensity/area) in 10 optical slices in the centre of a 3-D stack of images using ImageJ. Data analysis was performed with Sigma Stat using two-way ANOVA on repeated measures. A post-hoc Student's t-test showed significant decreases in intensity after K^+ stimulation and K^+ stimulation after thapsigargin (Tg) priming ($p=0.04$ and $p<0.001$, $n=4$ and 3 respectively; comparison was made between 32' and 42'). This shows release of vasopressin by high K^+ stimulation. There are no significant differences in intensity in control ($n=4$) and in 200 nM Tg priming ($n=4$) between 32' and 42'.

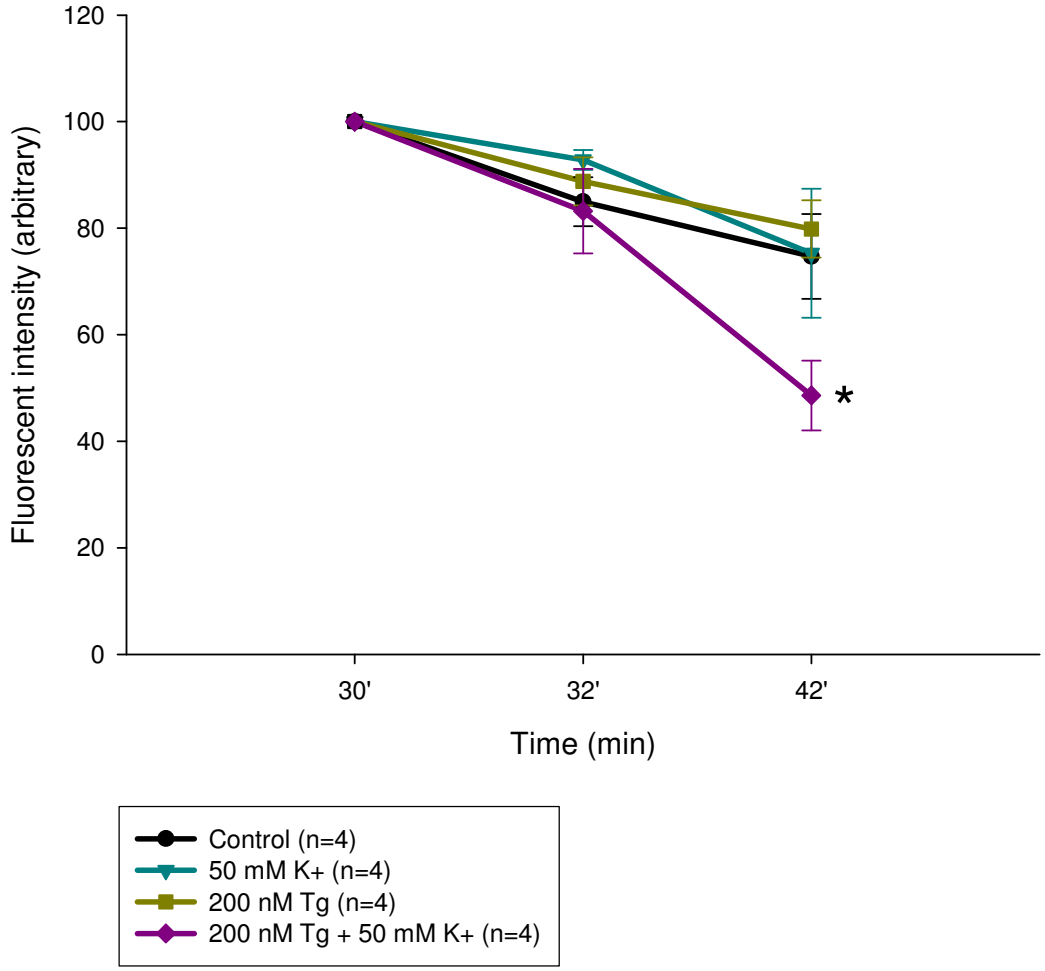

Figure 4-8B. Changes of fluorescent intensity in dendrites after stimulation. All data analysis as described in Figure 7A. Two-way ANOVA on repeated measures with post-hoc Student's t-test comparing intensity at 42' between different groups showed significant decrease in intensity in Tg + K^+ stimulated dendrites ($p<0.05$) showing that 30 min of Tg priming leads to increase release of vasopressin after 50 mM K^+ stimulation in dendrites.

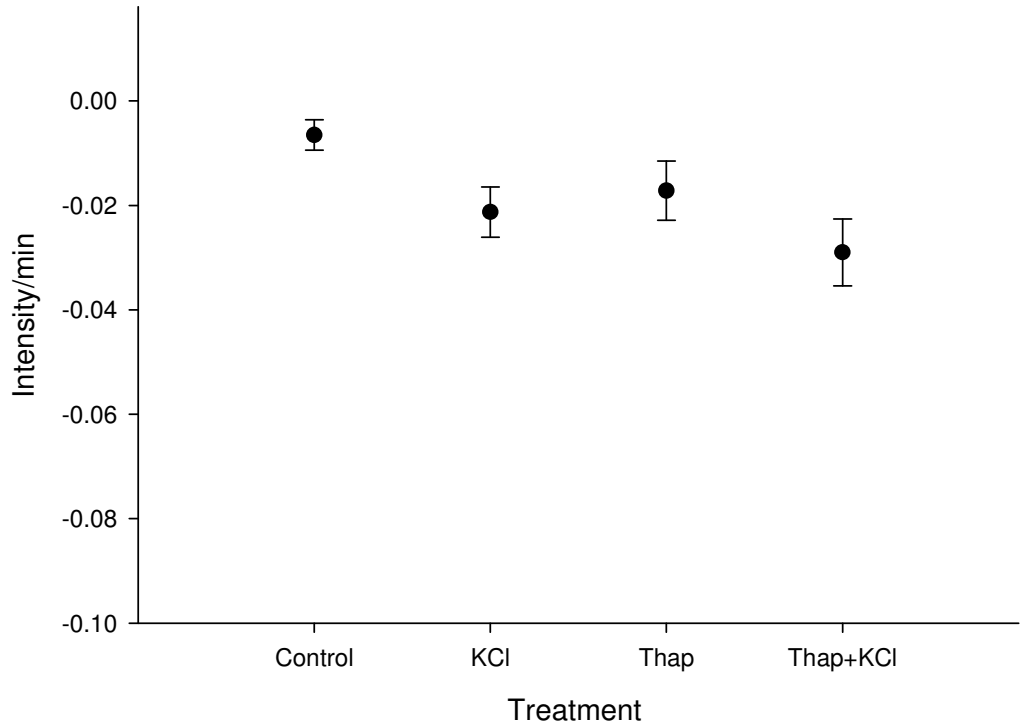

Figure 4-8C. Rate of fluorescence decay in image backgrounds. Background fluorescence decay was obtained by measuring the fluorescent intensity of 10 x 2 µm squared areas in the background of each image. Exponential decay curves were fitted using ImageJ. The mean decay constants of each group are shown here. Two-way ANOVA comparing the decay constants of each group showed no difference between background fluorescent decay in all groups, suggesting that decrease in fluorescent intensity shown in Figure 4-8B is due to increase in vasopressin release and not due to an increase in fluorescent decay caused by the treatment.

Chapter 5
Biolistic transfection

5. BIOLISTIC TRANSFECTION

5.1 Introduction

Chapter 4 described a live cell imaging model using organotypic slice explants of the hypothalamus of neonatal transgenic VP-eGFP rats. To study the dynamics of vesicle pools and vesicle pool segregation in magnocellular dendrites, it is essential to distinguish between different vesicle pools. Exogenous fluorescent proteins tagged to LDCV cargoes enable visualisation of vesicle pools of different age and hence, the regulation of these vesicle pools, by expression of a fluorescent time stamp (Duncan *et al.* 2003; Terskikh *et al.* 2000) or by inducible fluorescent expression (Han *et al.* 1999). Cellular transfection offers a way of introducing foreign material, for example, DNA, into eukaryotic cells. Methods available for cellular transfection include viral transduction (discussed in next chapter), calcium phosphate (Graham & van der Eb 1973) and lipid-mediated cell transfection (Felgner *et al.* 1987), electroporation (Shigekawa & Dower 1988), and biolistic transfection (Ye *et al.* 1990). With the exception of viral transduction, these methods provide a cost effective and non-laborious means of targeting exogenous DNA expression in cells. Of these methods, calcium phosphate co-precipitation and lipid-mediated transfection offer the simplest way for delivery of exogenous genetic material since neither of these methods require specialist equipments (Graham & van der Eb 1973; Felgner *et al.* 1987). However, these methods require delivery of the genetic material to the nucleus for transcription, and entry to the nucleus mostly occurs during cell division. Since neurons do not divide, calcium phosphate co-precipitation and lipid-

mediated transfection do not usually result in successful expression of exogenous DNA in neurons. Electroporation delivers DNA into a cell by perturbation of the cell membrane via electrical pulses generated through a micropipette. Biolistic transfection involves ejection of DNA-coated particles through high pressure, in another word, "shooting" DNA-coated "bullets" into cells. Comparing electroporation and biolistic transfection, it was found that biolistic transfection resulted in a higher number of transfected cells (Murphy & Messer 2001) using cerebellar organotypic slice cultures. Although both methods require fine tuning, strength and length of electrical pulse for electroporation and ejection pressure and DNA to particle ratio for biolistics; biolistic transfection had been successfully used to express exogenous genetic material in magnocellular neurons of hypothalamic organotypic slice cultures (Fields *et al.* 2003). Hence, this chapter focuses on the establishment of biolistic transfection as a model to target genetic material to magnocellular neurons to study vesicle pool dynamics in dendrites.

Biolistic transfection, also known as particle-mediated gene transfer and biological ballistics, is the transfer of DNA into cells by an apparatus called the gene gun (Biorad). Originally, biolistics is a technique designed for gene expression in plant cells (Ye *et al.* 1990), where tungsten particles were used as bullets and were coated with DNA of interest. These bullets were accelerated into plant cells by the use of gunpowder. The technique was then adapted to transfect animal cells and the use of gunpowder was replaced by a blast of helium gas and gold particles were used as bullets instead. Transfection of animal cells with the use of the gene gun was

achieved both *in vitro* (Gainer *et al.* 2001; Williams *et al.* 1991; Fields *et al.* 2003) and *in vivo* (Williams *et al.* 1991). Because gene transfer by biolistic transfection does not depend on the up-take of DNA during cell division, but the physical penetration of particles into cell membranes, it is a suitable technique to transfect neurons. Gene particles were made into bullets where supercoiled plasmid DNA was coated onto gold particles. One or more DNA constructs can be used in a single batch of bullets, allowing expression of more than one DNA construct per transfection. Biolistic transfection had been effectively combined with organotypic slice explants of brain tissues to express foreign DNA in neurons (Arnold *et al.* 1994; Horch *et al.* 1999; Lo *et al.* 1994), and especially in vasopressin-expressing neurons in the hypothalamus (Gainer *et al.* 2001; Fields *et al.* 2003).

In this chapter, biolistic transfection was applied to organotypic slice cultures of the hypothalamus. The aim was to introduce fluorescent reporter DNA to magnocellular neurons so that vesicle trafficking and segregation of vesicle pools can be visualised by targeting fluorescent protein expression to dense core vesicles. The age of rats most suitable for use for biolistic transfection was also investigated. peGFP-N1 (Clontech; plasmid map in Appendix II) with the immediate early promoter of cytomegalovirus ($P_{CMV\ ie}$) was used as the reporter gene initially to establish the efficiency of biolistic transfection because peGFP-N1 is expressed in the cytoplasm and is extremely bright, facilitating the visualisation of successful transfection.

5.2 Materials and Methods

5.2.1 Organotypic slice explants

Hypothalamic slices were collected from postnatal day 7 (P7) and postnatal day 14 (P14) wild type Sprague Dawley rat pups and cultured for 7 days. 300 µm coronal sections were collected with a vibratome in aCSF solution (Appendix I). The detailed culture protocol is described in Section 4.2.2, Chapter 4.

5.2.2 Biolistic transfection

The principle of Biolistic transfection involves the blasting of plasmid DNA coated gold particles into cultured tissue using a gene gun (Helios Gene Gun, Biorad). **Figure 5-1** shows a schematic diagram of biolistic transfection using the gene gun. Sections of the hypothalamus containing the SON were collected from neonatal wild type Sprague Dawley rats, and cultured as described in section 4.2.2, Chapter 4. Gold particles of 1.0 µm had been shown to effectively transfect neurons in hypothalamic slice explants (Fields *et al.* 2003; Gainer *et al.* 2001). DNA:gold ratio used was 2 µg:1 mg. All materials to be used were incubated in a desiccation chamber overnight. 100 µl of 0.05 M spermidine was added to the gold particles to help the precipitation of DNA. Immediately after mixing, 100 µl of 1 M $CaCl_2$ was added slowly onto the gold solution further aiding DNA precipitation onto the gold particles. Spermidine and $CaCl_2$ coating the gold particles are cationic and hence, attracts negatively charged DNA to the surface of the gold particles. After

incubation at room temperature for 10 min, the mixture was centrifuged at 400rpm for 20 sec. 1 ml of 100% ethanol was used to wash the DNA/gold pellet twice. The pellet was then re-submerged in 600 µl + 600 µl of ethanol and transferred to a 2 ml tube. The gold mixture was subsequently sucked into a dry silicon tube by a syringe and was allowed to precipitate for 15 min. Once the DNA/gold particles have precipitated onto the silicon tubing, the ethanol was pulled out, leaving the gold particles coating the tube. The gold particles were then dried by a nitrogen gas supply for 15 min. Individual Bullets were made by cutting the silicon tubing and were stored at 4^{o}C with desiccating agents for up to two weeks.

On the day of transfection, slice cultures were taken out from 37^{o}C incubation and placed on a 60 mm Petri dish. The gene gun was aimed onto the section, as described in Figure 5-1. A nylon mesh was used to minimise the impact of the helium blast on the section. The helium pressure used was determined by experiments described below. The sections were shot at individually and quickly brought back to 37^{o}C incubation. Transfected sections were cultured for another 24 hr before further immunohistochemistry was carried out.

5.2.3 Immunohistochemistry – double label immunofluorescence

Transfected organotypic slice explants were taken out of culture and the culture medium was removed. 1 ml of 4% (w/v) PFA in 0.1 M PB was added and the tissue

was incubated in the fixative for 1 hour. The fixative was then removed and the rest of the procedure is as described in section 3.2.2, Chapter 3. Primary antibodies were replaced by non-pre-immune serum to act as negative controls for immunolabelling. Non-transfected hypothalamic slices cultured under the same conditions as the transfected cultures were included for immunolabelling and act as positive controls for immunolabelling and negative controls for transfection.

5.2.3.1 Primary Antibodies

Vasopressin antibodies

The vasopressin primary antibody used was either the rabbit polyclonal vasopressin primary antibody (Calbiochem) used at a concentration of 1:500, or PS41, a mouse monoclonal antibody which was a gift from Professor Harold Gainer. The rabbit polyclonal vasopressin antibody had been tested by Calbiochem on rat PVN and SON and staining was completely eliminated by arginine vasopressin pre-treatment (10 µg/ml) (Calbiochem). Information on cross-reactivity between the antibody and oxytocin was also provided and tests by preabsorption of the antibody with 100 µg/ml oxytocin showed no effects on vasopressin staining. PS41 was produced against vasopressin-associated neurophysin in rats (Ben Barak *et al.* 1985). The specificity of PS41 against vasopressin-neurophysin is well described by Ben Barak et al. using liquid phase assays, immunoblot, and immunoprecipitation experiments. PS41 was pre-diluted 1:50, from the stock obtained from Prof Gainer, in 10% (v/v)

NGS and 0.01% (w/v) sodium azide in 0.1 M PB. The pre-diluted antibody was kept at 4^{o}C. The final concentration of the PS41 antibody used was 1:1000.

Oxytocin antibodies

In some experiments, oxytocin primary antibodies were used in addition to vasopressin primary antibody to identify all magnocellular neurons in the SON. The mouse monoclonal anti-oxytocin antibody, PS38, was a gift from Prof Harold Gainer. PS38 is directed against oxytocin-associated neurophysin and its specificity was also characterised by liquid phase assays, immunoblot, and immunoprecipitation (Ben Barak *et al.* 1985).

Neuronal marker – MAP2

MAP2 (microtubule associated protein found in neurons) was used as a neuronal marker. The polyclonal chicken IgY (Abcam) used detects all three isoforms of MAP2: MAP2c is present in the newborn rat brain until postnatal day 10 – 20, and is replaced by MAP2a which is present from postnatal day 10 onwards, MAP2b is present throughout life. MAP2a and MAP2b are both expressed in cell bodies and dendrites of neurons (Goedert *et al.* 1991), making it ideal to be used as a general marker for neurons. The pre-immune IgY was used to test for MAP2 antibody specificity and was not found to produce any signal, while in contrast the immune IgY produced strong, clear staining of dendrites and perikarya of neurons (information provided by Abcam).

Glial cells marker – anti-GFAP

Anti-glial fibrillary acidic protein (GFAP; Sigma) rabbit polyclonal antibody was used to identify glial cells in organotypic slice cultures. GFAP encodes for intermediate filament protein in astrocytes. Anti-GFAP antibody was used at 1:400 final concentration.

After incubation with the primary antibody, and pre-immune serum incubation for negative controls, sections were washed three times in 0.1 M PBT for 30 min to ensure that most of the unbound primary antibody was washed away. A second blocking step with 0.2% (w/v) BSA in 0.1 M PBT for 1 hour ensures that any remaining non-specific binding sites were blocked. Sections were then incubated in fluorophore-conjugated secondary antibody solution (2^{o}Ab + 0.2% (w/v) BSA in PBT + 0.3% (v/v) Triton) at 4^{o}C overnight. From this step onwards, the samples were protected from light.

5.2.3.2 Secondary Antibodies

All secondary antibodies used were from Molecular Probes, Invitrogen: Alexa Fluor ® 568 goat anti-mouse, Alexa Fluor ® 568 goat anti-rabbit, and Alexa Fluor ® 633 goat anti-chicken. The excitation and emission spectra, and the emission filters used for confocal imaging are shown in **Table 1 Appendix 1.**

After secondary antibody incubation, the secondary antibody solution was removed and sections were washed three times for 15 min in 0.1 M PB. Sections were then mounted on microscope slides and coverslipped (coverslip thickness #1, VWR). Mowiol (Calbiochem) supplemented with DABCO (Sigma) was used as the mounting medium with a refractive index of 1.41. Sections were left to cure at 4^{o}C in darkness until the mounting medium had set.

5.2.4 Image acquisition

5.2.4.1 Widefield fluorescence image acquisition

Widefield fluorescent images were acquired with the LeicaDMR upright light microscope using either the Hamamatsu ORCA HR digital camera, acquired by OpenLab (Improvision), or using the Leica DFC490 digital camera, acquired by the Leica Application Suite V2.7. Images acquired with the Hamamatsu camera were obtained with a band pass 450 – 490 nm excitation filter and a long pass 515 nm emission filter for visualisation of green fluorescence, and band pass 515 – 560 nm excitation and long pass 590 nm emission filters for visualisation of red fluorescence. Images acquired with the Leica DFC490 camera were obtained with Fitc 488 nm and Texas Red 568 nm excitation filters and band pass 516 – 556 nm and 604 – 644 nm emission filters to visualise green and red fluorescence respectively.

5.2.4.2 Confocal image acquisition

Confocal images were acquired using the Zeiss LSM510 inverted microscope. eGFP was excited with the 488 nm line of the Argon laser, emission collected through a band pass 500 – 550 nm filter. Alexa Fluor 568 staining was excited with the 543 nm HeNe1 laser and emission collected through a band pass 565 – 615 nm filter. Alexa Fluor 633 staining was excited with the 633 nm HeNe2 laser and emission collected with a long pass 650 nm filter. Filter settings are summarised in **Figure 3-2, Chapter 3**. The pinhole was adjusted to 1 Airy unit for all channels for confocal imaging. Images were acquired with an x63 oil immersion objective (NA1.4). 3-dimensional images were obtained by scanning the x, y –planes at 60 nm, achieved by line scanning 1024 x 1024 pixels with an optical zoom of 2.4, and intervals of 170 nm along the z-axis was acquired to avoid under sampling. 8 bit pixel depth, line averaging of 1 (no averaging) and maximum scan speed were chosen for image acquisition to avoid photobleaching. All 3-D images were deconvolved to remove background noise (Huygens Deconvolution Software, SVI). Please refer to section 2.2.4 of Chapter 2 for parameters used for deconvolution.

5.3 Results

5.3.1 Organotypic slice culture – P7 vs. P14

Empirical experiments were carried out to determine the age of neonatal rats suitable to be used in organotypic slice culture for biolistic transfection studies. **Figure 5-2**

(A) and **(B)** show two organotypic slice explants both cultured for 7 days, one obtained from a P7 rat pup and the other obtained from a P14 rat pup. The sections were stained for vasopressin and visualised using by the Alexa Fluor 568 antibody as described above. **Figure 5-2 C** shows a transcardially perfused section of the hypothalamus from an adult (200 – 300 g) VP-eGFP transgenic rat (transcardial perfusion was described in Chapter 2). Green signals were from vasopressin eGFP cells in the SON. Comparing the morphology of the SON between the three ages, the SON in P14 rats closely resembled that of an adult rat. Vasopressinergic neurons in the P14 slice culture are more spread out in the SON (**Figure 5-2 B**), similar to the anatomy of the SON of an adult rat (**Figure 5-2 C**). Vasopressinergic neurons in the P14 slice culture have also migrated towards either side of the optic chiasm (not shown in figure) resembling the location of the SON in adult rats. Therefore, P14 rats were chosen for biolistic transfection experiments.

5.3.2 Transfection efficiency – optimisation of transfection pressure

Using eGFP as the reporter gene, optimisation of helium pressure used was carried out on P14 organotypic slice cultures of non-VP-eGFP rats. The peGFP-N1 plasmid localises in the nucleus and produces an enhanced green fluorescent protein. This allowed easy identification of cells that had been transfected with peGFP-N1.

Slice explants were shot at 120 psi (827.4 kPa), 160 psi (1103.2 kPa), 180 psi (1241.2 kPa) and 200 psi (1379 kPa) (n=4 slices per pressure) to determine the best

pressure of helium gas to use for transfection of magnocellular neurons. In a separate experiment, slice explants were shot at 50 psi (344.75 kPa) and 60 psi (413.7 kPa) (n=3 slices per pressure). Two slices from each experiment were not transfected and were used as positive controls for immunohistochemistry. Slices were fixed >20 hr after transfection in 4% (w/v) PFA and immunolabelled for vasopressin and oxytocin (PS41 and PS38, both raised in mouse) and MAP2 (raised in chicken) for identification of neurons, and in particular magnocellular neurons. Secondary antibodies used were Alexa Fluor 588 goat anti-mouse and Alexa Fluor 633 goat anti-chicken.

10 x63 images were taken of slices from each transfection pressure used using the confocal microscope. The transfection efficiency, i.e. the number of cells transfected per section, of the different transfection pressures used is shown in **Figure 5-3B**. One way ANOVA comparing the number of transfected cells showed that there were significantly more cells transfected at 160 psi compared to all other pressures used except to 180 psi ($p<0.05$, Student's t-test). The transfection efficiency for the number of neurons, i.e. transfected cells expressing green fluorescent and labelled with MAP2, was also counted (**Figure 5-3C**). There was no significant difference in the number of neurons transfected between the different pressures used (one-way ANOVA). 160 psi was chosen as the transfection pressure in further experiments. An example of a transfected neuron labelled with MAP2 is shown in **Figure 5-4**. The transfection efficiency of neurons was calculated to be 7% of the total number of cells transfected. Immunofluorescence labelling of VP and OT was carried out on

the same sections and no magnocellular neurons were found to be transfected. Hence, further experiments were carried out where sections were either labelled with MAP2, VP/OT or GFAP antibodies to investigate the cell types transfected (Section 5.3.3).

5.3.3 Transfection of neurons, magnocellular neurons, and non-neuronal cells

15 hypothalamic sections from four P14 pups were collected and cultured for 1 day *in vitro* (DIV) before transfection. Sections were fixed <20 hr after transfection and were immunolabelled for VP/OT (PS41 and PS38) and MAP2 or GFAP. **Figure 5-5** shows a representative example of the SON after transfection (red = VP/OT; blue = MAP2). Mixing of PS41 and PS38 antibodies allows visualisation all transfected magnocellular neurons alongside staining with MAP2. **Figure 5-6** shows a transfected magnocellular neuron, stained for vasopressin/oxytocin (red) and MAP2 (blue), transfected with the peGFP-N1 plasmid (green). This shows that the biolistic technique was successful in transfecting magnocellular neurons (transfection efficiency = 1.8% of the total number of cells transfected). There are also other non-neuronal cell types not stained for MAP2 which were also transfected with the biolistic technique. **Figure 5-7** shows eGFP expression (green) in sections stained for GFAP (red) an astrocyte marker. Although no astrocytes were found to express the peGFP-N1 plasmid, other cell types such as fibroblasts-like cells and oligodendrocytes were found to be transfected. **Figure 5-7 (A)** and **(B)** show putative fibroblasts and **Figure 5-7 (C)** shows a putative oligodendrocyte expressing the peGFP-N1 plasmid. Although optimisation of the biolistic transfection technique

did result in the transfection of magnocellular neurons, the number of neurons transfected was still found to be low and random.

5.4 Discussion

Stationary organotypic slice culture is an ideal system to study magnocellular neurons due to the conservation of the topography of the hypothalamus in these cultures. Using organotypic slice cultures from the hypothalamus of neonatal rats, magnocellular neurons can be easily identified through immunohistochemical labelling with vasopressin and oxytocin antibodies. *In vitro* slice cultures also allow for post-culture transfection of cells of interest without the use of *in vivo* viral transduction or transgenic models. Brain cultures had been prepared from foetal (Jiao *et al.* 1993) to mature rats (Xiang *et al.* 2000). To determine the age which is most suitable for organotypic slice culture from the hypothalamus, P7 and P14 rats were used. Slices were obtained from the hypothalamus and cultured under the same conditions for seven days. At the end of culture, slice tissues were fixed and labelled for vasopressin staining. Comparing cultured slices labelled for vasopressin and slices obtained from an adult VP-eGFP rat (**Figure 5-2**), the SON from P14 animals showed a closer morphological resemblance to that of the adult rat than P7 animals. Hence, P14 rats were chosen for further transfection experiments.

Biolistic transfection had been used as an approach to transfect hard-to-transfect, or non-dividing cells (e.g. neurons) as an alternative to viral transduction to express foreign DNA in these cell types (Fields *et al.* 2003; Lo *et al.* 1994). A range of different helium pressures used for transfection on cultured neuronal cells had been reported: 100 psi for cultured hippocampal and cerebellar neurons (Wellmann *et al.* 1999); 175 psi for dorsal root ganglion explants (O'Brien *et al.* 2001); 180 psi for hypothalamic slice cultures (Fields *et al.* 2003). It is evident that the higher the transfection pressure used, the deeper the penetration of particles into the brain slices, but also, the lower the survival rate of cells (O'Brien *et al.* 2001). Hence, it was essential to determine the optimal helium pressure to be used in experiment. All pressures used were successful in transfection, and 160 – 180 psi was found to transfect with the highest efficiency, although there was no significant difference in the number of neurons transfected with the pressures used.

The transfection efficiency of neurons was found to be 7% of the total number of cells transfected using 160 psi transfection pressure, transfection efficiency in magnocellular neurons was much lower at ~ 1.8%. Several measures could be taken to improve transfection efficiency, for example, by adjusting the diameter of gold particle used, and by adjusting the DNA:gold ratio. However, gold particle diameter of 1 μm and DNA:gold ratio of 2 μg:1 mg had been successfully used to transfect magnocellular neurons in hypothalamic slice cultures before (Fields *et al.* 2003). Another aspect which could improve transfection efficiency is the use of younger animals for culture. Fields et al. (Fields *et al.* 2003) had successfully transfected

magnocellular neurons using slices from postnatal day 6-8 rats cultured for up to 15 days in vitro. In fact, several studies have used early postnatal rat pups for biolistic transfection in different brain areas with success (Lo *et al.* 1994; Wellmann *et al.* 1999; Thomas *et al.* 1998). However, other studies had successfully transfected cortical neurons in slice culture prepared using P12 – P14 rats (Tao *et al.* 1998; Arnold & Clapham 1999), suggesting that age is not the factor that determines transfection efficiency. Whilst survival of cells after transfection is an important factor in transfection efficiency, and it is known that cultures prepared from younger rats survive better, it was demonstrated (**Figure 5-6**) that cultures prepared from P14 rats survived biolistic procedure, even though transfection efficiency was low. Nevertheless, cell death after particle bombardment is an important limiting factor to transfection efficiency in neurons. It had been shown that localised cell death occurs as soon as after the biolistic transfection process (Raju *et al.* 2006; Young, III *et al.* 1999). Another factor that strongly affected the transfection efficiency is the length of culture. Organotypic slice cultures were found to contain a dense layer of glial cells over the surface of the slice tissue (personal observation), hence favouring transfection of glial cells on the surface of the explant as demonstrated in **Figure 5-7**. The development of a glial cell layer over the surface of cultured organotypic slices had been shown in cultured slices from other brain areas (Coltman & Ide 1996) and can be prevented by the omission of animal serum in the culture media (Czapiga & Colton 1999). On the other hand, it is possible to target gene expression to specifically to neurons. In hypothalamic slice culture, the nerve-specific enolase promoter had been shown to target gene expression to neurons and the vasopressin

promoter had been shown to target expression specifically to vasopressinergic neurons (Gainer *et al.* 2001).

Although it is possible to target gene expression specifically to specific neuronal phenotypes, and despite the fact that the biolistic technique was successful in transfecting neurons and magnocellular neurons, the low and random transfection efficiency achieved with biolistic transfection means that a very high number of samples would be required to achieve the initial aim of this experiment to label vesicles and look at the behaviour vesicle pools under different stimuli. Another major concern deeming this transfection technique unsuitable for the studying of vesicle behaviour is the scattering of gold particles which reflected laser excitation across the tissues transfected. It was realised that the scattered gold particles closely resembled large dense core vesicles and because gold particles were excited by all the excitation lasers used, emission was collected from all three emission channels, rendering it impossible to differentiate between large dense core vesicles and gold particles. Since the aim of this project is to study the distribution of dense core vesicles in magnocellular dendrites, it is unfeasible to progress with biolistic transfection to label these vesicles.

Other methods available for transfection of neurons as discussed at the beginning of this chapter include calcium phosphate and lipid-mediated cell transfection, electroporation, and viral transduction. All of these methods, except for viral

transduction, would not be suitable for the use with organotypic slice cultures due to low transfection efficiency and the growth of a dense glial cell layer on the surface of slice tissues, preventing access of transfection agent to the neurons underneath. Viral transduction, on the other hand, has several advantages including high transfection efficiency in all cell types including neurons. Hence, the next chapter of this thesis will discuss the development of a suitable viral transduction system for the use in hypothalamic slice culture.

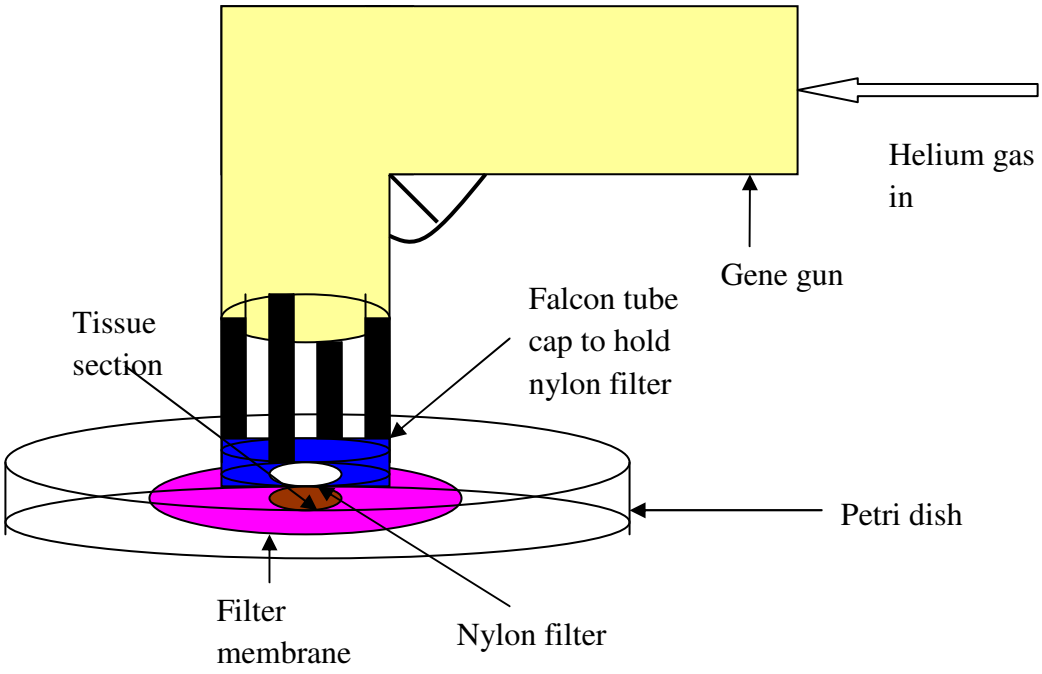

Figure 5-1. Schematic diagram of biolistic transfection of organotypic slice culture with the Helios Gene Gun.

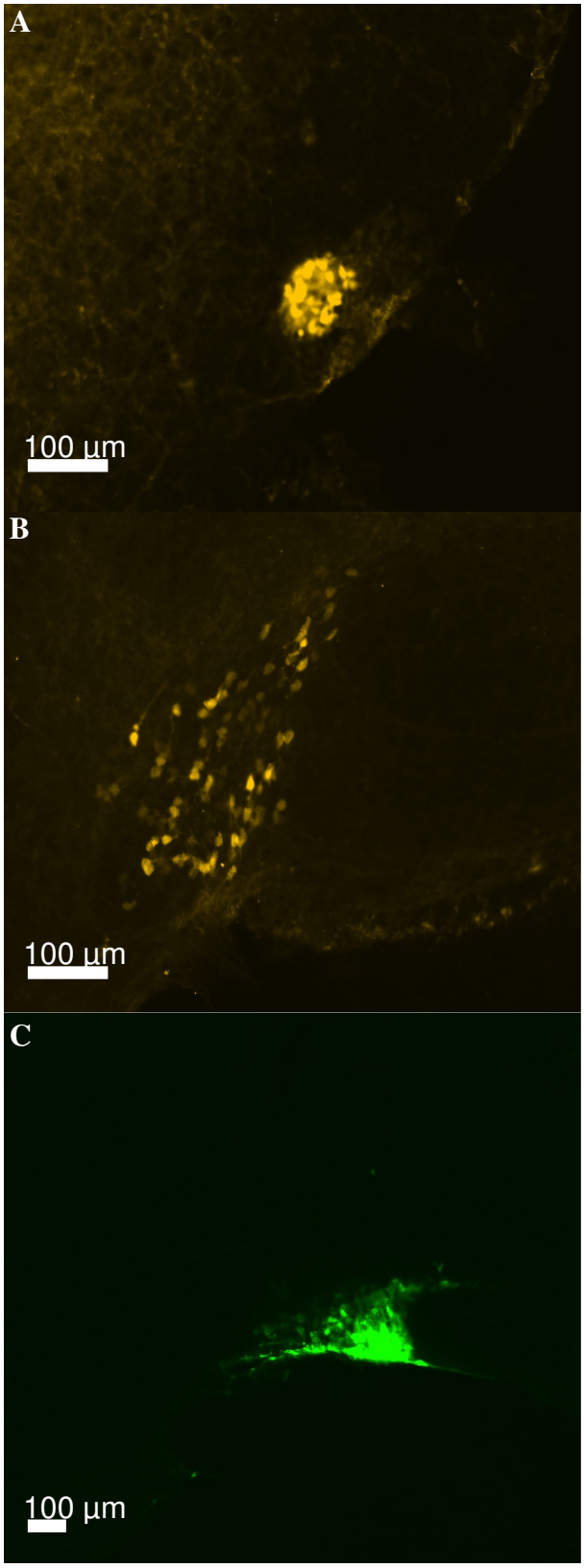

Figure 5-2. Organotypic slice cultures P7 vs. P14. (A) P7 culture and (B) P14 culture stained for vasopressin by indirect double immunofluorescence labelling. The yellow staining in these images shows vasopressin cells present in the SON. (C) Transcardial perfused section of the hypothalamus from adult (200 – 300g) VP-eGFP rat. Green signal represents vasopressin in the SON. Images were acquired with the Hamamatsu camera (excitation band pass 450 – 490 nm filter and a long pass 515 nm emission filter for (C), and band pass 515 – 560 nm excitation and long pass 590 nm emission filters for (A) and (B). The morphology of the SON in the P14 slice culture (B) closely resembles that of the adult SON (C).

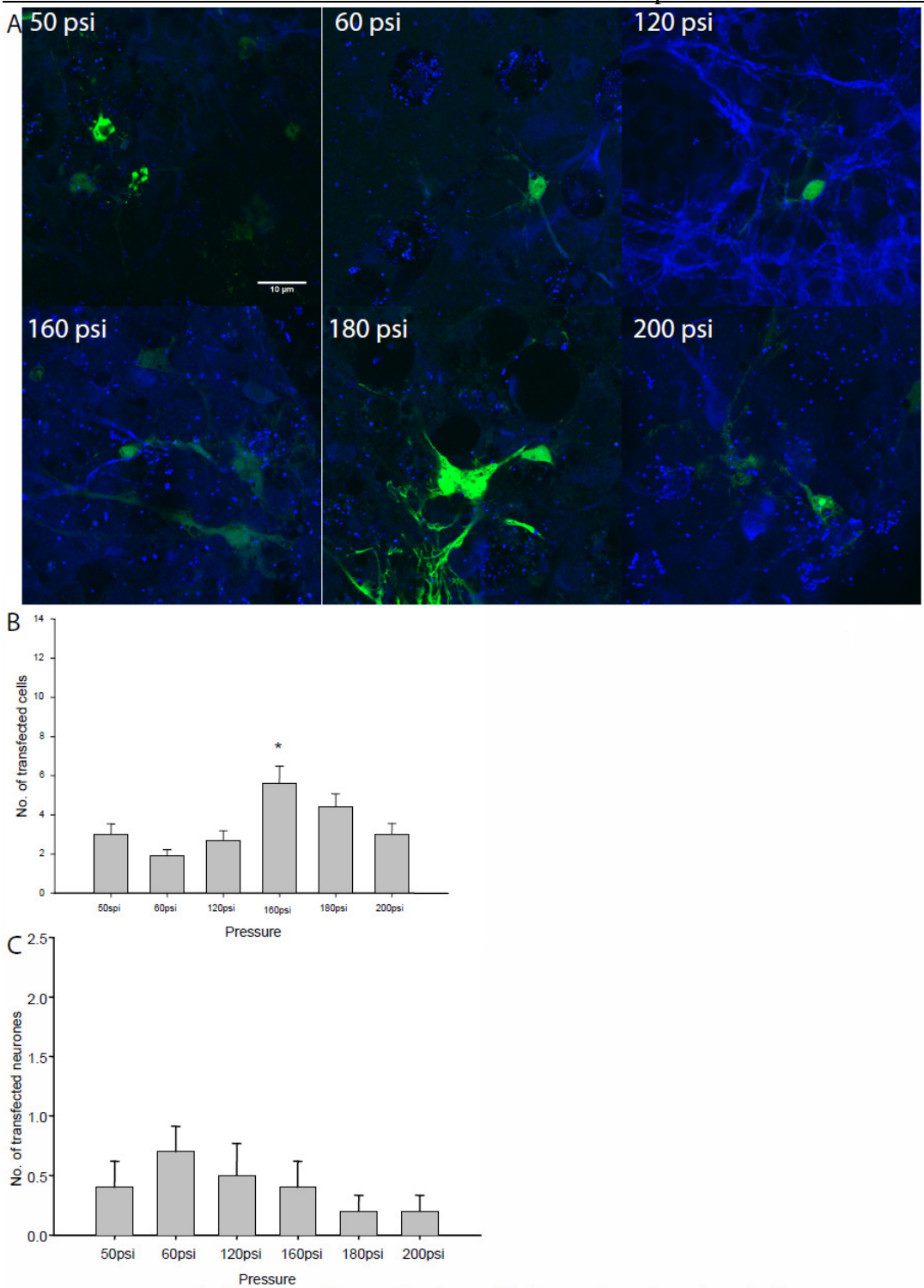

Figure 5-3. Optimisation of transfection efficiency by changing helium pressure used for transfection. A) Representative images of transfected cells (green) and MAP2 immunofluorescence (blue). Scale bar = 10 µm. The total number of cells (B) and total number of neurons (C) transfected was counted in 10 x63 fields of images acquired on the Zeiss LSM510 (n≥3 slice culture per pressure used). There are significantly more cells transfected using 160 psi pressure compared to all other pressures used ($p<0.05$; one way ANOVA; Student's t-test), except for 180psi. There is no difference in the number of neurons transfected using different helium pressures.

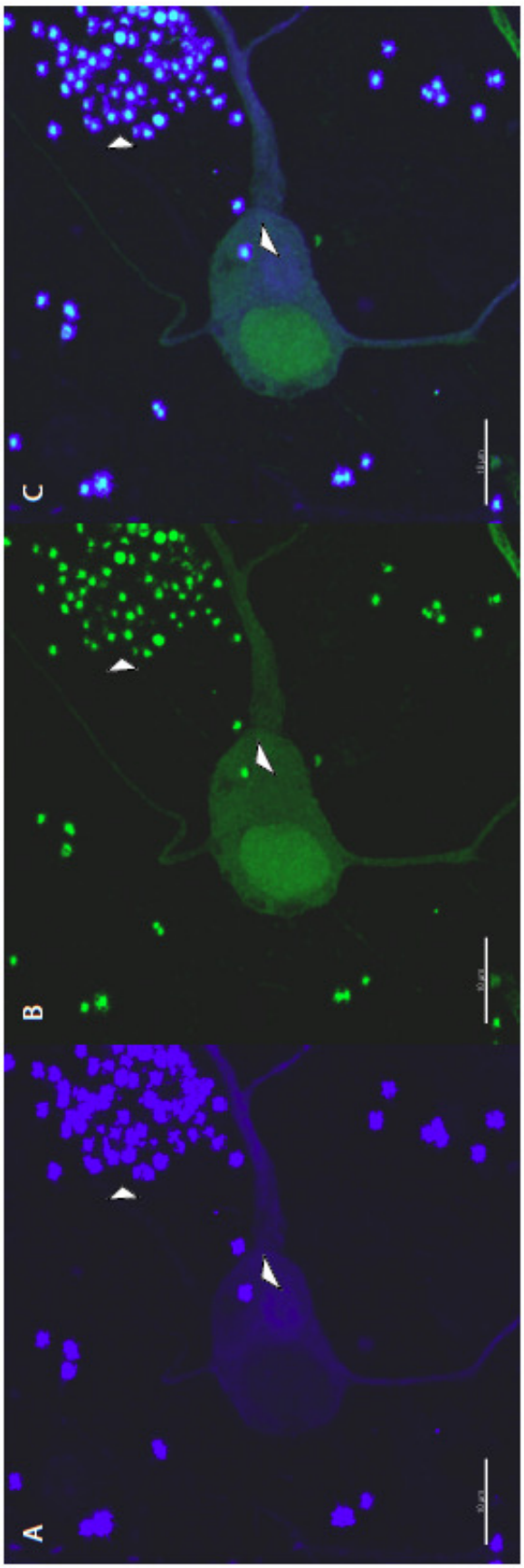

Figure 5-4. Biolistic transfection of hypothalamic organotypic slice culture. (A) Immunofluorescence showing labelling of a neuron by the neuronal marker MAP2. (B) Transfection of the same cell shown in (A) by the eGFP-N1 plasmid (green). (C) Merged image of (A) and (B) showing that the biolistic technique is efficient in neuronal transfection. Helium pressure used was 60 psi. Scale bar = 10 µm. Block arrows show reflected gold particles.

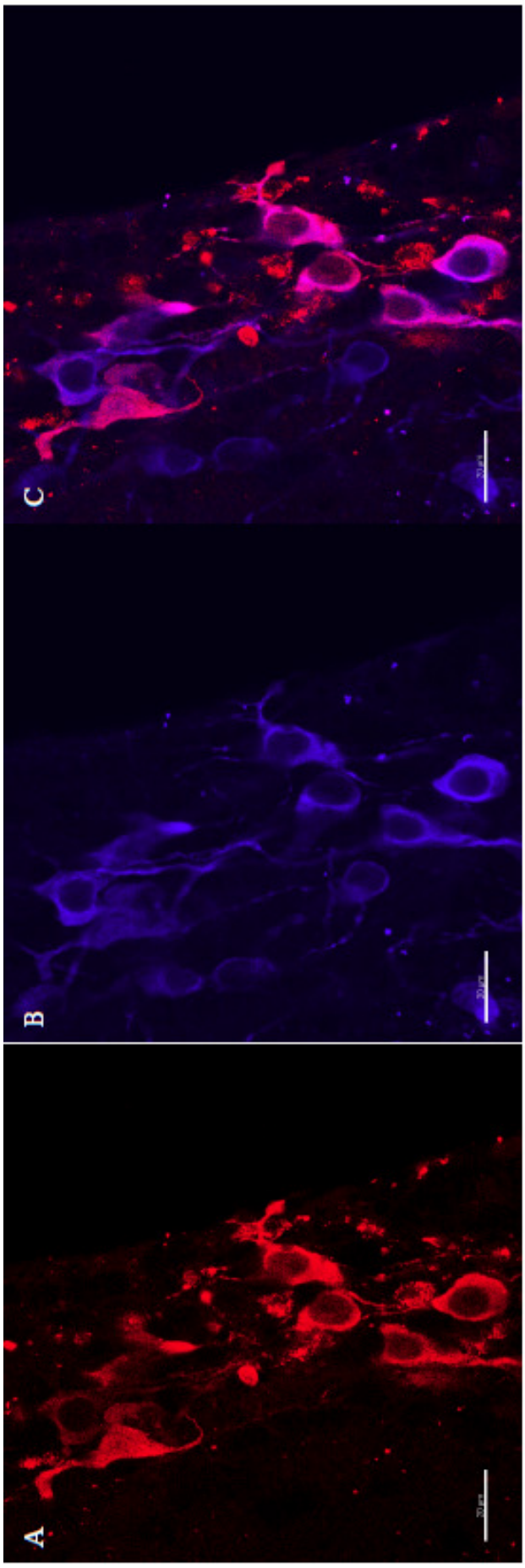

Figure 5-5. Typical SON after transfection. Images show co-labelling of magnocellular neurones with MAP2 in a transfected organotypic slice culture showing presence of magnocellular neurones. (A) Vasopressin/oxytocin labelling with PS41 and PS38; (B) labelling of neurones with MAP2; (C) Merged image of (A) and (B). Scale bar = 20 µm.

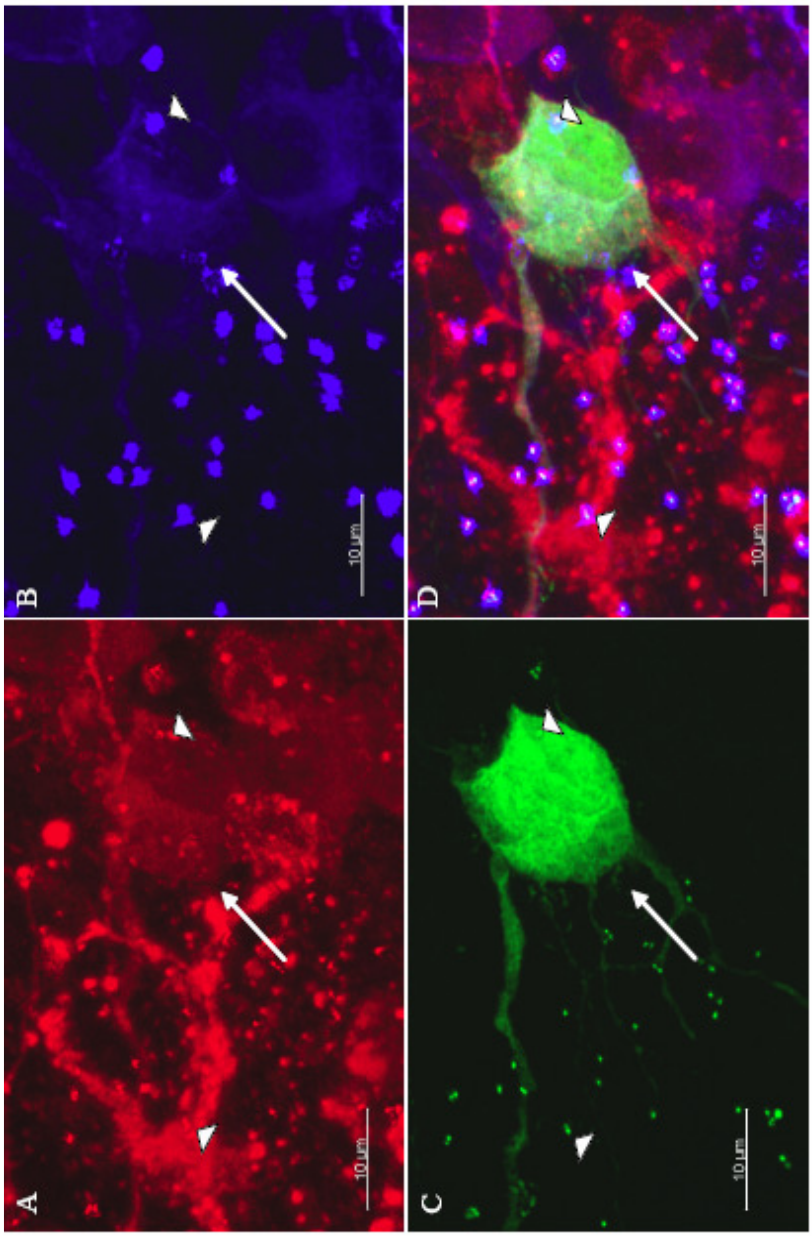

Figure 5-6. Biolistic transfection of hypothalamic organotypic slice culture. (A) Immunofluorescence labelling of a magnocellular neuron with vasopressin/oxytocin antibodies (PS41/PS38 mouse monoclonal; gift from Prof Hal Gainer, NIH). (B) Neuronal marker, MAP2, labelling of neuron. (C) Expressin of eGFP-N1 plasmid via biolistic transfection. (D) Merged image showing biolistic transfection of magnocellular neuron. Helium pressure used was 160 psi. Scale bar = 10 µm. Block arrows show reflected gold particles.

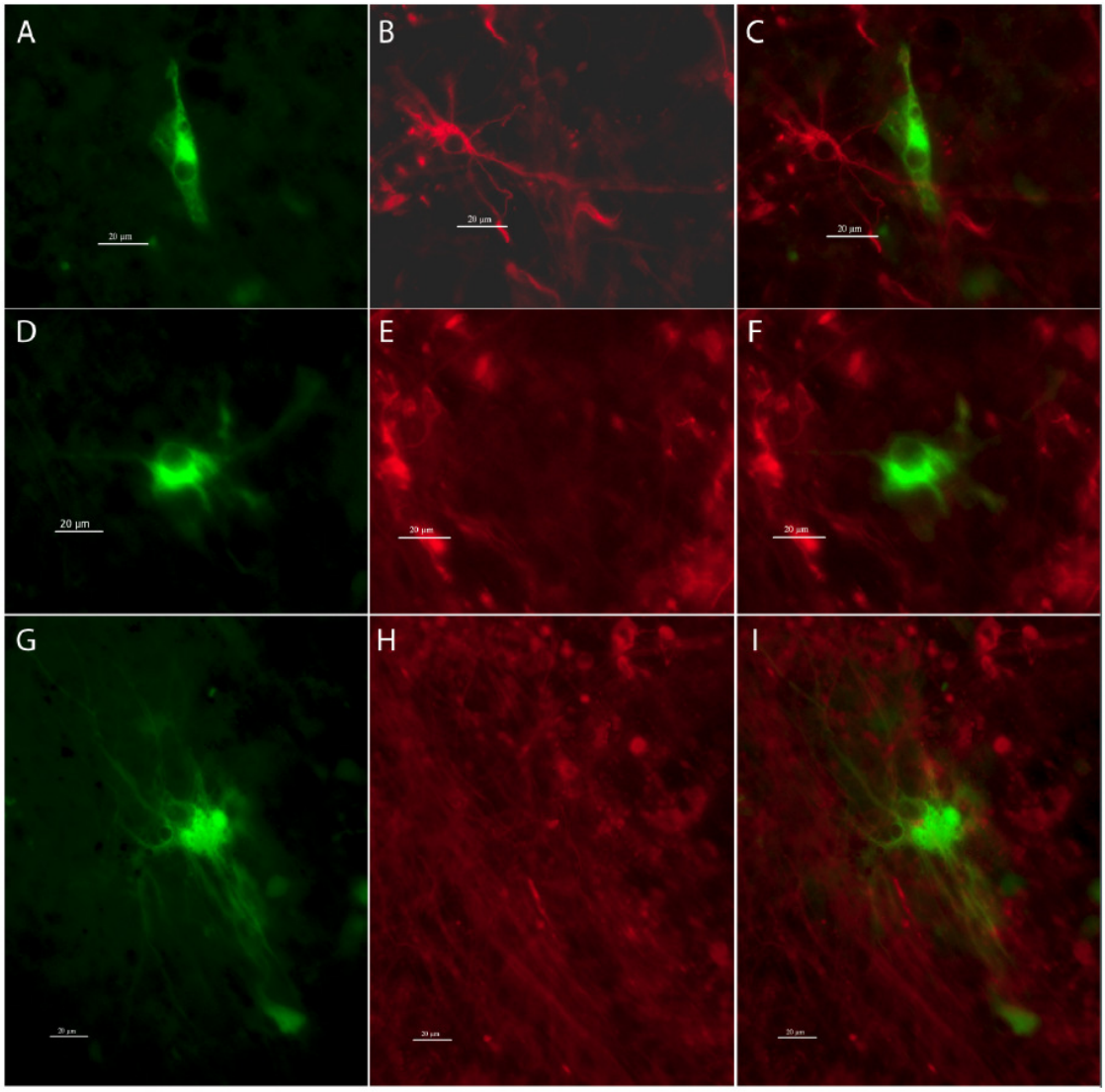

Figure 5-7. Transfection of non-neuronal cells. (A - D) Putative fibroblasts transfected with peGFP-N1; (G) putative transfected oligodendrocyte;. (A, D and G) Expression of eGFP; (B, E and H) GFAP immunofluorescence labelling; (C, F and I) overlay images. All scale bars = 20 µm. Images acquired with the Leica DMR upright widefield microscope (Leica DFC 490 camera) fitted with Fitc 488 nm and Texas Red 568 nm excitation filters, coupled with 516 - 556 nm and 604 - 644 nm emission filters.

Chapter 6
Fluorescent protein expression in LDCVs and viral transduction

6. FLUORESCENT PROTEIN EXPRESSION IN LDCVs AND VIRAL TRANSDUCTION

6.1 Introduction

Viral transduction is well known for its use to target gene expression in hard to transfect cells and its high transfection efficiency (Slack & Miller 1996; Washbourne & McAllister 2002). Gene targeting using viral transduction techniques has improved dramatically by reducing cytotoxicity and the cost in production. Non-viral transfection techniques offer much lower production cost and can transfer genetic material of almost any size to the target cell. However, as seen in Chapter 5, in non-dividing cells like neurons, non-viral transfection techniques offer disappointing transfection efficiency. Viral transduction had been successfully used to express genes of interest in different neuronal cell types (Ehrengruber *et al.* 2001; Keir *et al.* 1999; Ridoux *et al.* 1995; Vasquez *et al.* 1998). Another important factor to consider is that expression of virally transduced genes typically occurs 1-7 days after transduction, depending on the type of cells targeted and the type of virus used (Ridoux *et al.* 1995). Successful transduction of magnocellular neurons in organotypic slice cultures of the hypothalamus (Keir *et al.* 1999) and *in vivo* transduction of magnocellular neurons (Vasquez *et al.* 2001) using adenoviral gene transfer has been previously reported .

Several different types of recombinant viral vectors are currently used for gene delivery in research each possessing different levels of cytotoxicity, transduction efficiency, maximal size of insert, onset of protein expression, etc (reviewed in (Washbourne & McAllister 2002). Hence, there is not one virus that is suitable for use in every system. Most recently, the success of adenovirus and adeno-associated virus-mediated gene transfer in magnocellular neurons had been demonstrated (Vasquez *et al.* 2001; Keir *et al.* 1999; Cho *et al.* 2007). The virus chosen for expression of exogenous proteins in magnocellular neurons in this study is the replication-incompetent adenovirus with human adenoviral type5 (Ad5) genome (Adeno-X^{TM} Expression Systems, Clontech). The adenovirus is modified for recombination and used to target exogenous protein expression since large portions of the Early Regions 1 (E1) and 3 (E3) of the viral genome had been deleted to enable accommodation of larger DNA insert (up to 8kb) and also, making it unable to replicate itself unless grown in cell lines which expressed the Ad5 Early Regions (i.e. HEK 293 cells that stably express the Ad5 E1 genes are used for propagation of viral particles after recombination). Adenovirus particles infect cells by interaction of the adenovirus fibre antigen with proteins found on cell membranes (Lonberg-Holm & Philipson 1969). Adenoviruses are endocytosed by host cell membranes and this endocytosis is clathrin-dependent (Meier & Greber 2003). After successful entry into the cell, the adenoviral particles dissociate from endosomes. Soon after dissociation from endosomes, the capsids, along with other viral structures, disassemble and release the recombinant DNA, in addition to the viral genome, to the infected cell cytoplasm and these gain entry to the nucleus through nuclear pores for replication (Greber *et al.* 1993).

To target fluorescent protein expression in LDCVs, the pre-pro-atrial natriuretic factor (ppANF) was chosen to be tagged to the fluorescent reporter protein. ppANF has been found to target reporter proteins to LDCVs (Duncan *et al.* 2003; Wiegand *et al.* 2003; Burke *et al.* 1997). Moreover, release of co-packaged peptides was not found to be affected by ppANF expression (Shields *et al.* 1990). The three reporter constructs chosen are: the ppANF-Timer (to be used as a fluorescent time-stamp), and ppANF-tdTomato and ppANF-eGFP (see Appendix II for plasmid maps and sequences). All three constructs will be used for inducible fluorescent protein expression as described below. tdTomato (Shaner *et al.* 2004) is a dimeric mutant of DsRed (Campbell *et al.* 2002), a red fluorescent protein derived from the coral of the *Discosoma* genus, which is an obligate tetramer. The tetramerisation of DsRed often results in the aggregation of the fluorescent protein in cellular compartments (Lauf *et al.* 2001). This aggregation is overcome in the tdTomato protein which forms dimers. tdTomato is also 160% as bright as DsRed and the half time for the protein to mature is 1 hr as opposed to ~10 hr for DsRed (Shaner *et al.* 2004). This increased brightness offers an opportunity for live cell imaging, where increased laser excitation to illuminate dim fluorescence often leads to cell death. Moreover, at the early maturation of the DsRed protein, the fluorophore emits in the green spectrum and slowly matures to emit in the red. The slow maturation time of DsRed meant that traces of green fluorescence could be detected long after transfection or transduction. The much shorter maturation time of tdTomato made it superior as a red fluorescent protein. On the other hand, the slow maturation of DsRed gave rise

to another mutant, the fluorescent Timer DsRed-E5, which will be known as Timer from now on. The fluorescent Timer was first described by Terskikh *et al.* (Terskikh *et al.* 2000). The slow maturation of the fluorescent timer protein is characterised by the time that is required for the protein to fold and tetramerise requiring > 16 hr – acting as a time stamp. It has been used in bovine adrenal chromaffin cells to study segregation of vesicle pools according to age (Duncan *et al.* 2003; Wiegand *et al.* 2003). Hence, this study will use the Timer protein as a time-stamp on LDCVs, investigating the segregation of vesicle pools according to age. In addition to the fluorescent time-stamp, utilisation of an inducible expression system targeting fluorescent reporter proteins to LDCVs will allow "pulse-chase" experiments to be carried out where fluorescent protein production is induced or stopped at different time points (Han *et al.* 1999). The tetracycline/doxycycline inducible system had been chosen for this study. In the tet-on system, binding of tetracycline/doxycycline to the reverse tetracycline repressor protein downstream of the silent minimal immediate early promoter of cytomegalovirus (P_{minCMV}) induces transcription of reporter proteins. In the tet-off system, binding of tetracycline/doxycycline to the tetracycline repressor protein switches off transcription of the gene of interest downstream. When target cells, in this case magnocellular neurons are infected with constructs containing the TRE and a (reverse) tetracycline repressor protein, transcription of the reporter gene is turned on (tet-on system) or off (tet-off system) by the addition of tetracycline or doxycycline. This system also ensures that all cells which received doxycycline switch transcription on/off at the same time. The tetracycline repressor protein (TetR) works by negatively regulating the genes of interest in the absence of tetracycline. In the Adeno-X^{TM} Expression System 1

(Clontech), TetR is fused with an activation domain found in the Herpes simplex virus (VP16 protein) (Triezenberg *et al.* 1988). Fusion of VP16 to TetR converts the repressor element of TetR to an activator in the absence of tetracycline/doxycycline, the resulting fusion gene is called the tetracycline-controlled transactivator (tTA) (Gossen & Bujard 1992) found in the Tet-off system (**Figure 6-1**). In the Tet-on system, the regulatory protein is a reverse TetR fused to VP16 making the reverse tetracycline-controlled transactivator (rtTA) (Gossen & Bujard 1995), resulting in activation of transcription in the presence of tetracycline/doxycycline (**Figure 6-1**). The P_{CMVie} promoter does not enhance transcription unless tTA or rtTA binds the TRE upstream of the promoter. Hence, for successful expression of the gene of interest, the regulatory and response virus has to be co-infected. **Figure 6-2** shows an overview of recombinant virus construction and subsequent infection of target cells, using the Tet-on virus as an example.

In addition to the time-stamp labelling LDCVs, either by the fluorescent Timer or the inducible fluorescent proteins, expression of LDCV targeted fluorescent constructs can be used in conjunction with live cell imaging, where ppANF-tdTomato can be imaged together with VP-eGFP expressing magnocellular neurons in organotypic slice cultures of the hypothalamus. Dendrites of VP-eGFP magnocellular neurons are easily identified by green fluorescence (Chapter 4) and vesicles expressing the ppANF-tdTomato protein after viral transduction can be identified as red fluorescence. Using the inducible construct, ppANF-tdTomato can be expressed for different lengths of time before imaging to visualise the dynamics of vesicles of

different age. On the other hand, transduced magnocellular neurons can be fixed before imaging, allowing the use of immunohistochemical labelling and the expression of ppANF–Timer or ppANF-eGFP constructs to study segregation of vesicle pools. As discussed above, the targeting of fluorescent reporter proteins to LDCVs requires tagging of the fluorescent construct to ppANF. Generation of ppANF-tagged fluorescent constructs enables direct visualisation of LDCVs. Previous studies in LDCV dynamics and vesicle pool segregation, mostly carried out in clonal cell lines, provided insights of LDCV dynamics in endocrine neurons. Hence, clonal cells (PC12 and N2a) were transfected with ppANF-tagged fluorescent construct to examine fluorescent protein targeting. Expression of a fluorescent time stamp, via a fluorescent protein that changes its emission over time or an inducible expression system, in magnocellular neurons provides an important tool to study vesicle pool segregation in magnocellular dendrites.

6.2 Materials and Methods

Generation of viral particles containing the desired constructs regulated by an inducible promoter required several steps of subcloning: 1) To generate ppANF-tagged reporter constructs, 2) To insert the ppANF-tagged construct into a shuttle vector that contains recombination sites for transferring into the viral vector, 3) To produce recombinant virus with the inducible ppANF-tagged construct, 4) To produce viral particles utilising HEK293 cell culture. **Figure 6-3** shows an overview

of the whole procedure from the generation of ppANF-tagged constructs to the generation of viral particles. To generate a Tet-on expression system, ppANF-tagged constructs were inserted into a shuttle vector containing the Tet-responsive promoter – pTRE-shuttle2 vector (Clontech). This shuttle vector also contains unique recombination sites which are compatible with two unique recombination sites in the viral vector. To generate a Tet-off expression system, ppANF-tagged constructs were inserted into the pDNR-CMV donor vector (Clontech) which contains two loxP sites that are recognised by a specific recombination enzyme, Cre recombinase. Cre recombinase catalyses the cleavage of loxP sites and the subsequent recombination of these sites. Thus, cre-loxP recombination enables genes inserted between the loxP sites to be transferred to a special Adeno-X acceptor virus, also containing loxP sites and a Tet-responsive promoter. The ppANF-eGFP plasmid was a gift from Dr. Rolly Wiegand, University of Edinburgh (Wiegand *et al.* 2003) and ptdTomato (Shaner *et al.* 2004) was a gift from Dr. Colin Rickman, University of Edinburgh. The pTRE-shuttle2, pDNR-CMV donor vector, and pTimer constructs were available from Clontech.

6.2.1 Construction of inducible ppANF-eGFP, ppANF-tdTomato and ppANF-Timer

Subcloning was carried out by PCR amplification of a cDNA fragment encoding the rat ppANF (Seidman *et al.* 1984), ligation of insert DNA to vector DNA, purification and amplification, and finally ligation to the viral vector DNA. All these procedures are described in detail in the sections below. This section describes the insert DNA

fragments amplified, the vectors used and the restriction sites used for subcloning of each plasmid. The selected restriction sites used for each construct ensured that the insert DNA was in the same reading frame as the vector DNA.

ppANF-Timer

PCR was used to introduce two unique restriction sites, HindIII and AgeI, to the ppANF fragment of ppANF-eGFP. ppANF-Timer was produced by subcloning the ppANF (insert, 466 bp) fragment from ppANF-eGFP into the pTimer vector (Clontech) which contains unique HindIII and AgeI restriction sites. **Figure 6-4A** shows a plasmid map for ppANF-eGFP and **Figure 6-4B** shows a plasmid map for ppANF-Timer. Restriction sites for subcloning were also shown.

pTRE-ppANF-eGFP

The pTRE-shuttle2 (Clontech) vector contains the tetracycline response element coupled to the P_{CMVie} promoter and a multiple cloning site where the DNA of interest can be inserted. NheI and EagI are unique restriction sites in the pTRE-shuttle2 vector and were used for subcloning the ppANF-eGFP insert. NheI and EagI sites were introduced to the 5' and 3' end of ppANF-eGFP (1.2 kb) via PCR amplification. **Figure 6-4C** shows a plasmid map for pTRE-shuttle2 and **Figure 6-4D** shows the plasmid map for pTRE-ppANF-eGFP and the restriction sites used.

pTRE-ppANF-tdTomato

pTRE-ppANF-tdTomato was produced by replacing the eGFP sequence from pTRE-ppANF-eGFP with a tdTomato sequence. A tdTomato fragment (1.4 kb) was amplified by PCR and AgeI and EagI restriction sites were introduced. AgeI and EagI are unique restriction sites found in pTRE-ppANF-eGFP and were used for insertion of tdTomato. **Figure 6-4E** shows a plasmid map for pTRE-ppANF-tdTomato and the restriction sites used.

pTRE-ppANF-Timer

The ppANF-Timer fragment (1.15 kb) of the ppANF-Timer construct was amplified by PCR and subcloned into the pTRE-shuttle2 vector via the unique NheI and EagI restriction sites. **Figure 6-4F** shows the plasmid map for pTRE-ppANF-Timer and the restriction sites used.

pTRE-Timer

pTimer (687 bp) was amplified via PCR where a NheI restriction site was introduced to the 5' end of the Timer DNA and the EagI site at the 3' end was included in the amplification. The amplified Timer fragment was subcloned via the NheI and EagI sites of the pTRE-shuttle2 vector. **Figure 6-4G** shows the plasmid map for pTRE-Timer and the restriction sites used.

pDNR- ppANF-eGFP

ppANF-eGFP (1.2 kb), containing unique HindIII and XbaI sites on the 5' and 3' ends of the insert DNA fragment respectively, was inserted into pDNR-CMV donor vector, also containing the same unique restriction sites. **Figures 6-4 H** and **I** show the plasmid maps of pDNR-CMV donor vector and pDNR-ppANF-eGFP respectively.

pDNR-ppANF-tdTomato

pTRE-ppANF-tdTomato was used as a template for PCR amplification of ppANF-tdTomato (1.9 kb) where HindIII and XbaI sites were introduced to the 5' and 3' ends of the ppANF-tdTomato fragment respectively. The amplified ppANF-tdTomato was then inserted into the pDNR-CMV donor vector. **Figure 6-4 J** shows the plasmid map of pDNR-ppANF-tdTomato.

6.2.2 Amplification of DNA fragment by PCR

Before a DNA fragment was subcloned into a vector, the DNA fragment was amplified by polymerase chain reaction (PCR). Typical conditions used for PCR are summarised in **Tables 6-1** and **6-2**. PCR is a technique that uses a Taq polymerase to expand short stretches of oligonucleotides, primers, which bind to specific sequences of DNA as designed. Because of the different temperature cycles employed, which include a denaturation cycle at 95^{o}C to separate double stranded

DNA, the enzyme could extend a piece of DNA multiple times, resulting in an amplified fragment.

Primers, short stretches of oligonucleotides, were required for PCR because Taq polymerase can only add new nucleotides to an existing strand of oligonucleotide. A forward primer reads from 5' to 3' from the sense strand and a reverse primer reads the anti-sense strand from the vector DNA. Forward primers were designed so that they were complementary to the beginning of the DNA fragment and reverse primers were complementary to the c-terminal of the fragment. Primers could also be designed so that specific sequences of restriction sites could be introduced to the DNA fragment amplified. Hence, when primers anneal to complementary DNA, the DNA sequence amplified will include the added restriction sites. This allows for introduction of specific restriction sites that are compatible with the restriction sites available in the multiple cloning site of the vector DNA. Compatible restriction sites allow for ligation between two pieces of DNA that are digested by the same enzyme (**Figure 6-5**). Primers were bought from VHBio or Invitrogen and Taq polymerase from Promega. The sequences of primers used to amplify DNA fragments for subcloning of each construct are listed in **Table 6-3**.

6.2.3 Separation and purification of DNA fragments by electrophoresis and gel extraction

The amplified DNA fragment was transferred directly from PCR to a 1% (w/v) agarose gel (appendix I) supplemented with SYBR Safe™ gel stain (10000 X) for visualisation. A DNA ladder (1kb plus ladder, Invitrogen) was loaded alongside sample DNA and the fragments were separated by electrophoresis at 100 – 140 mV for 30 min to 45 min in TBE buffer (Appendix I). DNA fragments were visualised under UV light and were excised from the agarose gel and purified with the Qiaquick Gel Extraction Kit (Qiagen) or the PureLink Quick Gel Extraction System (Invitrogen) following the suppliers' instructions. DNA was eluted from the silicon membrane with 30 µl of ddH_2O.

6.2.4 Ligation of vector DNA and insert

Purified DNA fragments and their respective vectors were digested with restriction enzymes to create compatible ends for ligation. Conditions for a typical restriction digest are shown in **Table 6-4**. Reactions were typically incubated at 37°C overnight. Products of overnight digestions were loaded on 1% (w/v) agarose gel in TBE buffer for electrophoresis. DNA fragments of the correct sizes were then excised from the agarose gel and purified by gel extraction (section **6.2.3**). Restriction enzymes were from NEB, Promega, or Fermentas.

Four ligation reactions and two control ligations were usually performed. Vector and insert DNA were used at different ratios to optimise the success in DNA ligation. If

100 ng of vector DNA was used each time, the amount of insert DNA required for each ligation was calculated using the following formula:

$$\frac{\textbf{ng of vector} \times \textbf{kb size of insert}}{\textbf{kb size of vector}} \times \frac{\textbf{molar ratio of insert}}{\textbf{molar ratio of vector}} = \textbf{ng of insert}$$

So if the vector:insert ratio to be used is 3:1, then the amount of insert DNA required for a 3.3 kb fragment is:

$$\frac{100\text{ng} \times 0.466\text{kb}}{3.3\text{kb}} \times \frac{1}{3} = 4.7\text{ng}$$

The vector: insert ratios typically used for ligation are 3:1, 1:1, 1:3 and 1:10. Two control ligations were carried out: vector + ligase (Promega) without insert, and vector without ligase or insert. The typical reaction conditions for ligation reactions are shown in **Table 6-5**. The first control ligation was performed in the absence of the insert to find out the amount of self-ligated vectors. In the second control ligation, the insert and T4 DNA ligase (Promega) were omitted to determine the amount of vector not digested by either enzyme. Reaction mixtures were incubated at room temperature for 15 min and then at 4^{o}C for at least 3 hr.

6.2.5 Amplification of plasmid DNA by *E. coli*

Constructs with ligated DNA were amplified by bacterial cell culture. *E. coli* can be chemically treated so that the bacteria are competent to acquire DNA that is introduced to them (Chen & Dubnau 2004). *E. coli* that has been treated is known as competent cells and the process by which they take up DNA introduced to them is known as transformation (described below). Vector DNA used for subcloning

contain antibiotic resistant genes and hence, *E. coli* that has been transformed by the DNA constructs introduced can be grown on agar dishes containing selective antibiotics. *E. coli* that has not acquired constructs with antibiotic resistance does not grow. Single colonies of *E. coli* were selected to grow in culture. Every *E. coli* in the culture now contains the desired construct and hence, the construct is amplified. The detailed protocols for preparation and transformation of competent cells are described below.

6.2.5.1 Preparation of competent cells

Scrapings of frozen XL-10 Gold cells (Stratagene) were incubated in 3ml LB medium (recipe: Appendix I) overnight at 37^{o}C, with shaking. The 3 ml culture was used to inoculate 250ml LB medium containing 20mM sterile $MgSO_4$ the following day. Cells were grown until the optical density of the cell suspension was between 0.4 – 0.6, measured at 600 nm. The bacterial culture was then pelleted at 4500 x g for 5 min at 4^{o}C and re-suspended in ice cold 100 ml TFB1 (recipe in appendix I). The suspension was subsequently incubated on ice for 5 min and pelleted at 4500 x g for 5 min (4^{o}C). The cell pellet was re-suspended in 10ml TFB2 (recipe Appendix I) and incubated on ice for 30 min. Cells were then aliquoted into 1.5ml pre-chilled eppendorf tubes (200 µl/tube) and snap frozen in a dry ice – isopropanol bath and stored at -70^{o}C. Each batch of competent cells was transformed with 0.1 ng of DNA to determine the transformation efficiency (the transformation protocol is found in the next section). The number of single colonies resulting from this transformation was counted and the transformation efficiency was calculated as the number of

colonies transformed per µg of DNA. Only cells which had a transformation efficiency of 10^6 colony forming unit/µg of DNA were used.

6.2.5.2 Transformation of competent cells

Frozen competent cells were brought up from -70°C on ice and allowed to thaw for 5 min. 100 µl of competent cells were then aliquoted to pre-chilled polypropylene tubes (100 µl competent cells per transformation). 10 µl of ligation reaction product was added to each tube of competent cells, including control reactions. Cells were then returned to ice and incubated for 30 min. After the 30 min incubation, cells were heat-shocked at 42°C for 90 sec. Cells were immediately returned to ice for 2 min after heat shock. 900 µl of pre-chilled LB was added to each 100 µl of cells and incubated at 37°C for 1 hr, shaking. After the 1 hr incubation, cells were pelleted at 4000 x g for 5 min and re-suspended in 100 µl of LB. The whole suspension was then plated on 1.5% (w/v) Agar plates (recipe Appendix I) containing the respective antibiotics and cultured overnight at 37°C. As mentioned above, vector DNA contains antibiotic resistance genes (see **Figure 6-4** for antibiotic resistance markers present in each plasmid), usually kanamycin or ampicillin, so that by culturing bacteria in the presence of selective antibiotics, only colonies that express the antibiotic resistance gene, and hence the gene of interest, could be selected.

Single colonies were counted for each ligation ratio the following day and the plate with the most colonies was selected. Well-separated single colonies were picked for culturing in 5ml LB at 37°C overnight, with shaking. DNA grown in these 5 ml

cultures can be extracted by miniprep plasmid DNA purification (section 6.2.6) and confirmation of the desired constructs was carried out before they were amplified any further.

6.2.6 Miniprep plasmid DNA purification protocol

Plasmid DNA purification was either performed by the Qiaprep Miniprep (Qiagen) or PureLink™ Quick Plasmid Miniprep Kit (Invitrogen) following the suppliers' instructions. All centrifugation steps were carried out on a microcentrifuge at 14000 x rpm. Briefly, bacterial cells containing the desired DNA were cultured in 5 ml LB medium overnight. Cells were then pelleted, lysed in an alkaline buffer and bacteria chromosomal DNA, proteins and cellular debris were precipitated, leaving plasmid DNA dissolved in a high concentrated salt solution. This solution is then passed through a silica membrane which absorbs plasmid DNA at high salt concentration and elutes at low salt concentration. 30 µl of either water or TE buffer, supplied with the miniprep kit, was added directly onto the silica membrane and incubated at room temperature for 1 min before centrifuging for 1 min to elute the DNA from the membrane. The DNA obtained was either stored at -20^{o}C or used immediately for restriction digest analysis to confirm the presence of the desired DNA construct. Digestion with unique restriction sites gives specific bands of known length and hence, helps identify the DNA fragments in the constructs.

6.2.7 Sequence confirmation

Purified plasmid DNA was sent to Cogenics, UK for sequence analysis. A pair of primers (forward and reverse) was designed to read from the vector into the insert through the two subcloning sites. A forward and a reverse primer were designed to read DNA sequences in an opposite direction of each other, the extended sequence crosses path and hence, the DNA sequence to be confirmed was read twice. To sequence longer fragments, several forward and reverse primers were designed so that all reading frames were overlapped. Sequencing results were aligned to the predicted DNA sequence using Vector NTI from Invitrogen. Only DNA sequences that had been confirmed and which contain the correct sequences would be used for further subcloning or transfection studies.

6.2.8 Maxiprep plasmid amplification protocol

After the plasmid sequence had been confirmed, a maxi-preparation of the plasmid was made. Single colonies from competent cells transformed with the miniprep DNA that had been sequenced were picked for 5 ml culture in LB medium containing the selective antibiotic for 8 hours and then transferred to a 250 ml LB culture overnight with selective antibiotics. Subsequently, a maxi preparation was carried out with either the PureLink HiPure Maxi Plasmid Prep (Invitrogen) or the HiSpeed Plasmid Maxi Kit (Qiagen). All procedures were carried out according to the manufacturers' instructions. The DNA concentration obtained from the maxi preparation was checked with a spectrophotometer reading at 260 nm. The concentration of DNA was calculated based on the fact that 50 µg of DNA has an absorbance of 1 when measured at 260 nm. Hence, the optical density measured

multiplied by 50 and the dilution factor of the diluted DNA will give the concentration of the DNA measured. Restriction digests were carried out to further confirm the presence of the desired constructs.

6.2.9 N2a and PC12 cell culture and transfection of recombinant constructs

Neuroblastoma 2a cells, also called N2a cells, were established by R.J. Klebe and F.H. Ruddle. N2a cells are tumour cells and are originated from a strain A albino mouse. N2a cells are endocrine cells which had been found to produce a range of peptides, vasopressin being one of them (Bamberger *et al.* 1995). Moreover, N2a cells release peptides via the regulated secretory pathway (Noel *et al.* 1989) and hence, these cells were used to test recombinant DNA constructs to study expression of fluorescent proteins in LDCVs. The pheochromocytoma cell line, PC12 cells (Greene & Tischler 1976), derived from the rat adrenal medulla is a popular neuroendocrine cell line used to study peptide vesicle release. PC12 cells used in this study were a gift from Dr Colin Rickman and were cultured on coverslips at 70% confluency, ready for transfection (**section 6.2.9.4**).

6.2.9.1 N2a culture

N2a cells were stored in cell freezing media (appendix I) at -196^{o}C (liquid nitrogen). Cells were brought up from liquid nitrogen storage and thawed quickly in a 37^{o}C water bath. DMSO in the freezing medium was washed away by pre-warmed N2a culture medium (appendix I) and cells were pelleted at 250 x g for 5 min. Cells were

then grown in fresh culture medium at 37°C, 5.5% CO_2. The N2a culture was then expanded by splitting cells at 80 – 90% confluency.

6.2.9.2 Expanding N2a culture

The growth medium was removed and the N2a cells which were adherent to the tissue culture flask were rinsed in HBSS (Gibco) to remove traces of serum, Mg^{2+} and Ca^{2+} which inhibit the trypsin reaction. Trypsin-EDTA (Sigma) was used to detach adherent cells from the culture flask. Cells were incubated in trypsin-EDTA for 1 to 2 min until sheets of cells were visibly detaching when the flask was agitated. To detach all the cells from the culture flask, the flask was rapped sharply several times on the side. To quench the activity of the trypsin, culture medium containing 10% (v/v) foetal calf serum was added and then cells were split into different tissue culture flasks in a suitable volume.

6.2.9.3 Cell freezing

Expanded N2a cells were frozen for storage for future use. Adherent cells were removed as described in section 2.6.1.2 and diluted in N2a culture medium containing 10% (v/v) foetal calf serum. Cells were then pelleted at 250 x g for 10 min and suspended in cell freezing medium (appendix I) at a density of 10^6 to 10^7 cells/ml and aliquoted into freezing vials. To freeze cells, the aliquots were held on ice for 5 min, and then stored in an isopropanol bath at -70°C overnight. The next day, cells were transferred to liquid nitrogen for long term storage.

6.2.9.4 Transfection of single cells

Lipofectamine™ 2000 (Invitrogen), was used to introduce plasmid DNA into N2a or PC12 cell culture to test the expression of ppANF-tagged constructs. N2a cells originally cultured in tissue culture flasks were transferred onto cover glasses of thickness #1 and were transfected at a confluency of 80 – 90%. PC12 cells were grown on coverslips ready for transfection at a confluency of ~70%. Before transfection, the DNA of interest was diluted in 100 µl of DMEM (Gibco) without serum. The DNA:Lipofectamine™ 2000 ratio was 1 µg:3 µl. For cultures grown in a 12-well culture dish, 4 µl of Lipofectamine™ 2000 was diluted in 100 µl of DMEM (Gibco) without serum or antibiotics. The mixture was incubated at room temperature for 5 min. After the 5 min incubation, the DNA mixture and the Lipofectamine™ 2000 mixture was combined and incubated at room temperature for 20 min. 200 µl of the transfection mixture was then added to each well containing the cells and 1 ml of culture medium which was then mixed gently by rocking the culture dish back and forth. The cells were then incubated at 37^{o}C, 5.5% CO_2 for at least 16 hr after transfection before fixing in 4% (w/v) PFA for immunofluorescence labelling.

2.6.9.5 Double immunofluorescence labelling for adhering single cell cultures

Immunocytochemistry for N2a cells and PC12 cells is similar to that carried out for free floating sections described in section Chapter 2. All steps carried out were at

room temperature on a gently rocking platform unless otherwise stated. First, the culture medium was removed and cells were washed for 10 min twice with 0.1 M PBS. Cells were then fixed with 4% (w/v) PFA for 30 min. The PFA was then washed by rinsing with 0.1M PBS for 10 min twice. 50 mM NH_4Cl was used to quench background fluorescence and free aldehyde groups by incubating cells in NH_4Cl-PBS for 10 min. NH_4Cl was then removed and the cells were washed twice for 10 min with 0.1 M PBS. The cell membranes were then permeabilised with 0.5% (v/v) Triton X100 in 0.1 M PBS for 15 min. The triton solution was then removed and the cells were washed with 0.1M PBS for 10 min twice. Non-specific binding was blocked by incubating cells in a block solution of 10% (v/v) pre-immune animal serum, 0.2% (v/v) Tween-20 (Sigma) in 0.1 M PBS for 30 min. The block solution was then removed and cells were incubated in a 1^{o}Ab cocktail made up in block solution overnight at 4^{o}C. After incubation in the 1^{o}Ab, cells were washed in a wash solution containing 0.2% (v/v) Tween-20 in 0.1 M PBS three times for 45 min. A 2^{o}Ab cocktail was made up in the block solution described above and cells were incubated in the 2^{o}Ab solution of 2 hr. After incubation in 2^{o}Ab, cells were washed three times for 45 min with wash solution after which, cells were rinsed with 0.1 M PBS for 10 min twice. Cells were then mounted onto glass microscope slides in Mowiol (Appendix I) and the mountant was left to cure in darkness before imaging.

6.2.10 Construction of recombinant adenoviral vectors

Constructs confirmed to have the correct sequences were subcloned into either the Adeno-X System 1 viral DNA (Clontech) to create the Tet-on expression system or

the LP-Adeno-X-TRE System 2 viral DNA (Clontech) to create the Tet-off expression system. All procedures for subcloning were carried out as described in **section 6.2.1** unless otherwise stated. Plasmid maps of pAdeno-X and pLP-Adeno-X-TRE can be found in **Figure 6-6A and 6-6B.**

6.2.10.1 Construction of recombinant adenoviral DNA for Tet-on expression system

Recombinant pTRE-shuttle2 vectors were digested by the endonucleases PI-SceI and I-CeuI. Adeno-X System 1 viral (pAdeno-X) DNA was pre-linearised with PI-SceI and I-CeuI so that once the recombinant pTRE-shuttle2 vectors were digested, it was ready for ligation. The gene of interest is subcloned into a shuttle vector and the recombinant shuttle vector is inserted into the viral vector via PI-SceI and I-Ceu sites (Mizuguchi & Kay 1998). All digestion and purification steps were carried out according to the Adeno-X^{TM} Tet-Off® & Tet-On® Expression System 1 User Manual (Clontech). Briefly, a double digest of 3 hr at 37^{o}C using PI-SceI and I-CeuI was carried out on recombinant pTRE-shuttle2 vectors. 3 – 5 µl of the reaction product was analysed on a 1% (w/v) agarose gel as described in section **6.2.3** except that DNA fragments were not excised from the agarose gel. After confirmation that the reaction product gave the right band sizes, the rest of the reaction product was purified using the Qiaquick Gel Extraction Kit (Qiagen) following the manufacturer's instruction. In this case, the reaction product was not incubated at 42^{o}C to dissolve the agarose gel since the reaction product was dissolved in solution. After purification of the linearised recombinant pTRE-shuttle2 vectors, ligation with the pre-linearised pAdeno-X DNA was carried out using T4 ligase as described in

section **6.2.4**. The ligation product was purified by adding 1 x TE Buffer (pH 8.0) to a final volume of 100 µl and 100 µl of phenol:chloroform:isoamyl alcohol (25:24:1) (Sigma Aldrich) to the ligation reaction to remove salts in the ligation buffer and proteins including the T4 ligase. The solutions were mixed and then separated by centrifugation at 14000 rpm for 5 min at 4^{o}C. The top aqueous layer which contains the DNA was removed and transferred to a clear eppendorf tube. To this tube, 400 µl of 95% (v/v) ethanol and 1/10 volume 3 M NaOAc was added to precipitate the DNA. This solution was transferred to a -20^{o}C freezer for an incubation of 10 min to help visualisation of the final purified DNA. The solution was then centrifuged at 14000 rpm for 5 min at 4^{o}C to pellet the DNA. The supernatant was removed and discarded and the DNA pellet was washed with 300 µl of 70% (v/v) ethanol. This was then spun again at 14000 rpm for 2 min. The ethanol was removed and the DNA pellet was left to dry at room temperature for 15 min. The DNA was then dissolved in 15 µl of sterile H_2O. The purified ligation product was then digested with SwaI, a restriction site found between the I-CeuI and PI-SceI sites in the pAdeno-X DNA (**Figure 6-6A**), to linearise non-recombinant, self-ligated pAdeno-X DNA. The restriction digest product was then purified using the phenol:chloroform:isoamyl alcohol method described above. After the DNA pellet was dried, it was dissolved in 10 µl of sterile H_2O which was then used to transform competent *E. coli* bacterial cells as described in section **6.2.5.2**. Bacterial cells were cultured in the presence of 100 µg/µl ampicillin, since the pAdeno-X vector contains the ampicillin resistance gene. Single colonies were used to inoculate a 5 ml culture, which were then grown for <24 hr at 37^{o}C, shaking. Cultures were then purified to obtain a mini-scale DNA preparation following the instructions in the Adeno-X^{TM}

Tet-Off® & Tet-On® Expression System 1 User Manual (Clontech). The purified recombinant pAdeno-X DNA was then analysed by PCR using a set of primers provided by Clontech (Adeno-X Forward and Reverse PCR Primers). These primers were designed to confirm the presence of recombinant pTRE-shuttle2 DNA in the recombinant pAdeno-X DNA. The forward primer binds to a sequence upstream of the I-CeuI site in the pAdeno-X DNA, whilst the reverse primer binds to a sequence downstream of the I-CeuI site of the recombinant pTRE-shuttle2 DNA. This is explained in **Figure 6-7**. The presence of inserted recombinant pTRE-shuttle2 DNA in the recombinant pAdeno-X DNA would produce a band of 287 bp which was analysed on a 1% (w/v) agarose gel after PCR. The PCR reaction mix used was as shown in **Table 6-1** and the reaction conditions are found in **Table 6-6**. PI-SceI and I-CeuI restriction digests were also carried out to verify the presence of insert DNA in the recombinant pAdeno-X vector.

6.2.10.2 Construction of recombinant adenoviral DNA for Tet-off expression system

Inserts subcloned into the pDNR-CMV vector were used to generate the Tet-off expression system. The pDNR-CMV vector contains two loxP sites used for Cre-loxP recombination. Cre recombinase is an enzyme which mediates recombination of DNA sequences at loxP sites. The pLP-Adeno-X-TRE contains one loxP site and act as the acceptor vector. The reaction was carried out according to the Clontech Adeno-X^{TM} Expression Systems 2 user manual where 1 µl of 200 ng recombinant pDNR-CMV vector and 1 µl of Cre recombinase (supplied with the Adeno-X

Expression Systems 2 kit) were added to 18 µl of Adeno-X LP TRE reaction mix containing Cre reaction buffer and BSA. Briefly, the reaction was incubated at room temperature for 15 min and then Cre recombinase was inactivated at 70°C for 5 min. Transformation of *E. coli* was carried out to amplify the recombinant viral DNA. Electrocompetent cells were used for transformation instead of the chemically competent cells described in section **6.2.5** for efficient transformation (transformation efficiency for XL10 Gold is $\geq 5 \times 10^9$ cfu/µg pUC18 control DNA (Stratagene)). Electrocompetent cells were purchased from Clontech (EZ10 ElectroCompetent cells; transformation efficiency = 10^{10} cfu/µg pUC19 control DNA) and each transformation was carried out with 40 µl of cells, 1.5 µl of Adeno-X LP TRE reaction mix at a voltage of 1.75 kV, 25 µF capacitance in a 0.1 cm cuvette (according to manufacturer's protocol) using the Biorad Gene Pulser II to deliver the pulse. Electroporated cells were then transferred to 960 µl of SOC medium (Appendix I) for 1 hr incubation at 37°C, shaking at 200 rpm. Cells were then pelleted and resuspended in 100 µl of SOC medium. The cell suspension was then plated out on sterile LB agar containing 7% (w/v) sucrose and 30 µg/ml chloramphenicol dissolved in 100% ethanol. pDNR-CMV vectors contain chloramphenicol resistance gene in the expression cassette between the loxP sites and the sucrase gene downstream the two loxP sites for negative selection (expression of the sucrase gene leads to inability of cells to grow in sucrose). Hence, chloramphenicol selected for recombinant pLP-Adeno-X-TRE constructs and sucrose selected against recombinant pDNR-CMV constructs that did not form recombinants with pLP-Adeno-X-TRE. Cultures on LB agar were grown for 30 hr at 37°C. When colonies were grown, they were used to inoculate 20 µl of sterile H_2O

each where 10 µl were then used to inoculate 5 ml of LB medium with 100 µg/ml ampicillin (ampicillin resistant gene found in pLP-Adeno-X-TRE) and 30 µg/µl chloramphenicol. The rest of the 10 µl was used to carry out colony PCR screening. The PCR reaction mix used was as shown in **Table 6-1** except that DNA was replaced with 10 µl of bacterial cell suspension. The forward and reverse primers used were supplied by Clontech (Adeno-X LP CMV Primer Mix) and the reaction conditions are found in **Table 6-6**. The PCR reaction products were then separated on a 1% (w/v) agarose gel and a 660 bp band was expected. XhoI digests were also carried out as suggested by Adeno-X^{TM} Expression Systems 2 user manual to verify the presence of insert DNA in the recombinant pLP-Adeno-X-TRE vector.

6.2.10.3 Miniscale preparation of recombinant Adeno-X DNA

Since the plasmid size of recombinant Adeno-X DNA is >10kb, miniscale preparation of DNA could not be carried out using either the Qiaprep Miniprep (Qiagen) or PureLink™ Quick Plasmid Miniprep Kit (Invitrogen). Miniscale preparations of recombinant pAdeno-X DNA and pLP-Adeno-X were performed by resuspension of pelleted bacterial cell cultures (2ml) in 150 µl of resuspension buffer P1 (see appendix I). 150 µl of lysis buffer P2 and neutralisation buffer N3 were then added to the mixture. After addition of buffer N3, the DNA sample was incubated on ice for 5 min. The DNA sample was then centrifuged at 4^{o}C at 14000 rpm for 5 min. DNA was purified using phenol:chloroform:isoamyl alcohol as described in section 6.2.10.1 and dissolved in 15µl of buffer TE.

6.2.11 HEK 293 cell culture

The Human Adenovirus 5-transformed Human Embryonic Kidney (HEK) 293 cell line stably expresses the Ad5 Early Regions 1 (E1) genes that are essential for the replication and transcription of Adeno-X viral DNA. This is because the E1 region of wild-type adenovirus has been deleted from the Ad5 genome in the Adeno-X viral DNA to restrict the cytopathic activity of the adenovirus. Hence, HEK 293 cells were used to package and propagate the recombinant adenoviral vectors. The cell culture protocol for HEK 293 cells is as described in section 2.6 for N2a cells. However, instead of DMEM with 10% (v/v) foetal calf serum, HEK 293 cells (Invitrogen) were first cultured in CD 293 medium (Invitrogen) without serum for up to 3 passages and then switched to DMEM with 10% (v/v) foetal calf serum according to the cell culture guidelines provided by invitrogen. The thawing, expansion and freezing of HEK 293 cells were exactly the same as those described for N2a cells in section 6.2.9.

6.2.11.1 Transfecting HEK 293 cells with recombinant Adeno-X DNA

After confirmation of the presence of the insert of interest in the Adeno-X vector by PCR, the recombinant Adeno-X DNA was digested with PacI at 37^{o}C for 2 hr to linearise the recombinant plasmid. After PacI restriction digestion, the recombinant pAdeno-X DNA was purified by phenol:chloroform:isoamyl alcohol purification as described in section 6.2.10.1. PacI linearised DNA was dissolved in 10 µl of sterile water and stored at -20^{o}C until used for HEK 293 cells transfection.

HEK 293 cells were plated in a 25 cm^2 tissue culture flask the day before the transfection to allow the cells to reach 50-70% confluency. Each 25 cm^2 flask of HEK 293 cells was transfected with 10 µl of PacI digested Adeno-X recombinant DNA using Lipofectamine^{TM} 2000 (Invitrogen) as described in section 6.2.9. When HEK 293 cells expressed recombinant Adeno-X DNA, cells become cytopathic. This cytopathic effect, where cells round up and detach from the tissue culture flask, takes place one to two weeks after transfection. Cells were then detached from the tissue culture flask by mechanical disruption without using trypsin and transferred to a 15 ml conical tube. The suspension was centrifuged at 1500 x g for 5 min at room temperature and the pellet was then resuspended in 500 µl sterile PBS. The cells were lysed with three consecutive freeze-thaw cycles where the cells were frozen in a dry ice/isopropanol bath and then thawed in a 37^oC water bath. Care was taken to not let the cells reach 37^oC. The cells were vortexed after each thaw. After the third cycle, the cell debris was pelleted by a brief centrifugation and the supernatant, which now contained the viral particles, was stored at -20^oC.

A fresh 25 cm^2 flask of HEK 293 cells was infected by the viral particles produced in the previous step by adding the lysate directly to the culture medium. If cytopathic effects were not evident within a week, the cells were detached from the 25cm^2 flask by mechanical disruption, and the cells were lysed to infect a fresh culture of HEK 293 cells. When more than 50% of cells had detached from the flask, cells were lysed using the method described above. This is the primary amplification stock and

the presence of the recombinant pAdeno-X DNA was verified by PCR as described in sections 6.2.10.1 and 6.2.10.2.

6.2.11.2 Amplifying recombinant adenovirus

To prepare high-titre stocks of the recombinant adenovirus, HEK 293 cells were plated in 75 cm^2 flasks and grown to 50 – 70% confluency and infected with primary amplification stock at a multiplicity of 1 – 5 pfu/cell suspended in 5 ml growth media. Cells were incubated at 37^oC for 90 min before 10 ml of fresh growth medium was added. Cells were cultured at normal growth conditions until cytopathic effects were evident. Cells were then lysed according to the protocol described in section 6.2.11.1.

6.2.11.3 Determining viral titre with end-point dilution assay

HEK 293 cells were grown in a 96-well plate the day before the assay. Each well contained approximately 10^4 cells in 100 µl of growth medium. The next day, a 1:100 dilution of the amplified viral particles was made and using this as a stock, eight serial dilutions of the viral particles were made giving a range of 10^{-3} – 10^{-10}. 100 µl of diluted virus were added to each well. This is summarised in **Figure 6-8**.

Cells were grown under normal growth conditions, without changing the culture medium, for 10 days. After which, cytopathic effects were evaluated from each well and the viral titre was calculated by counting the number of cytopathic effects

positive wells for each dilution divided by 10. The sum of the fractions of cytopathic effects positive wells, *x*, was used in the following formula to calculate the viral titre

Titre (pfu/ml) = $10^{(x+0.8)}$;

6.3 Results

6.3.1 Exogenous fluorescent protein expression in LDCVs

ppANF fusion protein is known to be expressed in LDCVs (Burke *et al.* 1997). To verify whether the ppANF-eGFP construct, used as a template for the amplification of the ppANF fragment for subcloning of other constructs, was indeed able to target eGFP expression to LDCVs, PC12 cells were transfected using Lipofectamine 2000 (Invitrogen). Cells were incubated at 37^{o}C overnight after transfection and fixed in 4% (w/v) PFA for immunostaining. PC12 cells were stained for chromogranin A (goat anti-chromogranin A antibody, 1:250 dilution, Santa Cruz Biotechnology, inc), a peptide found in LDCVs (Curry *et al.* 1991; Mahata *et al.* 1992).The secondary antibodies used were AlexaFluor donkey anti-goat 568 (1:500; Invitrogen) as described in previous chapters. ppANF-eGFP expression was excited with the 488 nm laser line and chromogranin A labelling excited with 568 nm laser. Images were acquired on the Zeiss Axiovert LSM510 laser scanning confocal microscope as described in previous chapters.

Figure 6-9 shows a PC12 cell transfected with the ppANF-eGFP construct and stained for chromogranin A. Colocalisation analysis was carried out by the Colocalisation Threshold plugin in ImageJ where the threshold for each channel was set automatically according to Costes' method (Costes *et al.* 2004). Comparing the Pearson's correlation coefficient for the two channels, ppANF-eGFP and chromogranin A staining, there is a significant difference ($p<0.006$, n=10/group) between control, where cells did not express ppANF-eGFP, and ppANF-eGFP-expressing cells. Colocalisation of ppANF-eGFP expression and chromogranin A staining shows that ppANF-eGFP was indeed targeted for expression in LDCVs. However, only partial colocalisation of ppANF-eGFP was observed with chromogranin A staining. This reflects the fact that chromogranin A staining did not label all dense core vesicles and that ppANF-eGFP was expressed in vesicles where chromogranin A failed to label.

6.3.2 Expression of ppANF-Timer and pTRE-ppANF-Timer

The ppANF-Timer construct was chosen to study the segregation of newly synthesised and aged vesicles since the Timer fluorophore matures and changes colour over 16 hr. The ppANF-Timer was generated by subcloning an amplified fragment of ppANF DNA, using ppANF-eGFP as a template, by PCR. **Figure 6-10B** shows the PCR amplification product of between 400 and 500 bp, which is expected of ppANF amplification (486 bp). Through PCR amplification, a HindIII restriction site and a AgeI restriction site were introduced to the 5' and 3' end of the ppANF fragment respectively and subcloned into unique HindIII and AgeI sites

found in the pTimer vector. The product of ppANF and pTimer ligation was amplified by maxi preparation of the plasmid and the product was digested by HindIII and AgeI to confirm the presence of ppANF in the construct. **Figure 6-10C** shows two DNA fragments of 3.27 kb and 461 bp as a result of HindIII and AgeI double digest, confirming the presence of the pTimer vector and ppANF insert. The ppANF-Timer construct was further analysed by sequence analysis (Cogenic), confirming that no base pair mutations were introduced through the subcloning process.

ppANF-Timer was then used to generate the inducible pTRE-ppANF-Timer construct by subcloning ppANF-Timer into the pTRE-shuttle2 vector (Clontech) where the Timer protein production can be switched on at selected time points to assure a controlled period time for expression. **Figure 6-10D** shows a 1.21 kb DNA fragment of ppANF-Timer amplified by PCR. The ppANF-Timer DNA amplified consists of a NheI site at the 5' end of the fragment and a EagI site at the 3' end. These sites were used to insert ppANF-Timer into the pTRE-shuttle2 vector. **Figure 6-10E** shows restriction digests of pTRE-ppANF-Timer after amplification of ligation products of pTRE-shuttle2 and ppANF-Timer. NheI and EagI double digest produced 4.4 kb and 1.16 kb fragments which were the band sizes expected for the digested vector and the ppANF-Timer insert. Single digests using NheI and EagI were also carried out and produced bands of DNA of 5.5 kb. An undigested supercoiled DNA sample was ran alongside digests as control to ensure that the

restriction enzymes used were effective. Sequence analysis was carried out for the pTRE-ppANF-Timer construct confirming the correct sequence of DNA present.

A double transfection with pTRE-ppANF-Timer and pTet-on containing the reverse tetracycline repressor protein (**Figure 6-1**), using 1 µg/ml doxycycline to induce expression, was then carried out on N2a cells. **Figure 6-11** shows an N2a cell expressing the pTRE-ppANF-Timer. Since ppANF targets fluorescent protein expression to LDCVs, a punctate expression of green and red fluorescence was expected, similar to eGFP expression in **Figure 6-9**. However, Timer protein expression was concentrated in "clumps" and was not seen throughout the cell. This aggregation of Timer protein is similar to the previously identified aggregation of DsRed in the ER (Lauf *et al.* 2001). **Figure 6-10F** shows the amplification of pTimer by PCR and **Figure 6-10G** shows pTRE-Timer restriction digests by NheI and EagI after the ligation of amplified pTimer to pTRE-shuttle2 vector. DNA fragments of 680 bp from the PCR amplification of pTimer was observed and NheI and EagI double digest produced DNA fragments of 4.4 kb and 680 bp, confirming the presence of the Timer insert in pTRE-shuttle2. **Figure 6-12** shows an N2a cell transfected with pTRE-Timer and pTet-on. Expression of pTRE-Timer was induced by 1 µg/ml doxycycline. As seen in **Figure 6-12**, Timer protein not tagged to ppANF was expressed throughout the cell cytoplasm and emitted in both green and red, as expected over >16 hr of maturation. It has been reported previously that untagged DsRed protein, like untagged eGFP, did not show aggregation in cellular compartments (Lauf *et al.* 2001). Hence, expression of Timer with the ppANF tag

hampered the correct cellular localisation of the fluorophore. Since this study wanted to look at the segregation of vesicle pools by age, the unability to express the Timer protein in LDCVs made it unfeasible to continue the use of this fluorophore further.

6.3.3 Expression of pTRE-ppANF-eGFP and pTRE-ppANF-tdTomato

ppANF-eGFP was amplified by PCR and inserted into the pTRE-shuttle2 vector via the NheI and EagI sites. tdTomato, as mentioned above, is 160% as bright as the conventional DsRed and matures within 1 hr, leaving no traces of green fluorescence. More importantly, the dimeric tdTomato does not form aggregates in cellular compartments. tdTomato was amplified using PCR to introduce a NheI and an EagI site to the 5' and 3' ends of the tdTomato DNA fragment. The amplified tdTomato was then inserted to the pTRE-ppANF-eGFP construct via the NheI and EagI sites to produce pTRE-ppANF-tdTomato. **Figure 6-13** shows the PCR amplification products of ppANF-eGFP (1.2 kb) and tdTomato (1.4 kb), and restriction digests using NheI and EagI of the pTRE-shuttle2 and ppANF-eGFP ligation product, and the pTRE-ppANF- and tdTomato ligation product. NheI and EagI double digest of pTRE-ppANF-eGFP produced DNA fragments of 4.4 kb and 1.2 kb, confirming the presence of ppANF-eGFP in the pTRE-shuttle2 vector. NheI and EagI double digest of pTRE-ppANF-tdTomato produced DNA fragments of 4.4 kb and 1.9 kb, confirming that tdTomato was inserted into the pTRE-ppANF- vector.

pTRE-ppANF-eGFP and pTRE-ppANF-tdTomato were expressed in PC12 cells via double transfections of the recombinant constructs and pTet-on, using 1 µg/ml doxycycline for induction of expression. **Figure 6-14A** shows PC12 cells expressing the pTRE-ppANF-eGFP and the pTRE-ppANF-tdTomato plasmids. PC12 cells were immunolabelled with Chromogranin A and a Golgi apparatus marker (mouse anti-GM130, BD laboratories, described in **Chapter 3**) was used to label the Golgi apparatus. Expression of both plasmids produced punctate expression of fluorescent proteins, as expected for ppANF targeting to LDCVs. Moreover, colocalisation analysis showed that like ppANF-eGFP expression (**Figure 6-9)**, expression of ppANF-tdTomato colocalised with the expression of the dense core vesicle marker, chromogranin A (**Figure 6-14B**; $p<0.001$) (Curry *et al.* 1991; Mahata *et al.* 1992), indicating that expression of both ppANF-tagged constructs were targeted to LDCVs. In this study, negative controls were carried out where transfected cells were not incubated in doxycycline. No expression of either constructs was observed.

An analysis of pTRE-ppANF-tdTomato expression at different time points was carried out on transfected PC12 cells to visualise segregation of vesicle pools at different time points. PC12 cells were double transfected with pTRE-ppANF-tdTomato and pTet-on with 1 µg/ml doxycycline at time 0. pTRE-ppANF-tdTomato expression was observed as early as 4 hr post-transfection. Cells were then fixed 8 hr, 16 hr and 24 hr after doxycycline was added to the medium and immunolabelled with GM130. Image stacks were acquired of PC12 cells expressing the pTRE-ppANF-tdTomato protein using the same imaging parameters as described (Chapter

3) and the sum fluorescent intensity (Chapter 2, section 2.2.5) of pTRE-ppANF-tdTomato expression in deconvolved images was obtained. pTRE-ppANF-tdTomato expression was measured in the GA, cell centre and cell periphery (the outer 1 µm of the cells). The areas measured were cut out so that expression of pTRE-ppANF-tdTomato in the GA, for example, was not taken into measurement of the other cell areas. **Figure 6-15** shows analysis of pTRE-ppANF-tdTomato expression in different cell areas at different time points normalised to the pTRE-ppANF-tdTomato expression in the GA. There was significantly higher expression in the GA compared to the rest of the cells at all time points ($p<0.05$, two-way ANOVA, post-hoc Student's t-test). There were no differences between pTRE-ppANF-tdTomato expression between the cell centre and cell periphery at any time points and no difference at expression at the cell centre and the cell periphery between any time points. There is a significant increase in pTRE-ppANF-tdTomato expression in the cell centre at 24 hr compared to 8 hr. Since cells were not stimulated for vesicle release, this indicates that non-released LDCVs accumulate after 24 hr and reside in the cell centre. This study showed that aged vesicles reside in the centre of PC12 cells, in accordance to the finding that aged, non-released vesicles were found in the centre of bovine adrenal chromaffin cells (Duncan *et al.* 2003). Moreover, this study shows that pulse-labelling of inducible ppANF-tagged fluorescent protein expression can be used to study vesicle pool segregation according to age.

6.3.4 Generation of pAdeno-X constructs

Mini-scale preparation of recombinant pAdeno-X constructs were analysed using the Adeno-X Forward and Reverse PCR Primers and I-CeuI/PI-SceI double restriction digest to confirm the presence of recombinant pTRE- inserts. PCR analysis (**Figure 6-7**) showed that both recombinant pAdeno-X constructs produced an amplified fragment of 287 bp, as would be expected (**Figure 6-16A**). Further PCR analysis using the Adeno-X Forward PCR Primer which binds upstream to the I-CeuI site of pAdeno-X viral DNA, and a reverse primer which binds to the insert ppANF-eGFP or ppANF-tdTomato DNA, respectively, also produced amplified DNA fragments of the expected band sizes (**Figures 6-16B** and **C**). HEK 293 cells were then transfected with pAdeno-X viral DNA to produce viral particles. Cells infected with recombinant pAdeno-X constructs were lysed and their lysates collected for PCR analysis. Despite the positive PCR analysis of recombinant viral DNA (**Figure 6-16A – C**), PCR analysis of viral stock using the Adeno-X Forward and Reverse PCR Primers did not show the presence of the expected 287 bp fragment. Further restriction analysis by double digestion with I-CeuI and PI-SceI did not produce DNA fragments of the expected sizes (2.8 kb and 32.67 kb for pAdeno-X-TRE-ppANF-eGFP and 3.5 kb and 32.67 kb for pAdeno-X-TRE-ppANF-tdTomato). Single digests with either enzyme produced DNA bands similar to undigested DNA in the case of pAdeno-X-TRE-ppANF-eGFP, indicating that either the restriction enzymes were compromised, or the I-CeuI and PI-SceI restriction sites were compromised (**Figure 6-16D**). Double digestion of pAdeno-X-TRE-ppANF-tdTomato revealed that the construct was cut by I-CeuI whilst PI-SceI was unsuccessful (**Figure 6-16D**).

I-CeuI and PI-SceI double digests were carried out on pTRE-ppANF-eGFP and pTRE-ppANF-tdTomato to find out whether the I-CeuI and PI-SceI restriction sites were compromised and whether both enzymes were efficient in the conditions used. **Figure 6-17A** shows that both I-CeuI and PI-SceI cut pTRE-ppANF-eGFP and pTRE-ppANF-tdTomato into bands of 2.8 kb and 2.8 kb, and 2.8 kb and 3.5 kb respectively, indicating that both enzymes were efficient in restriction digest under the conditions used. Further restriction analysis of pAdeno-X-TRE-ppANF-eGFP and pAdeno-X-TRE-ppANF-tdTomato using NheI and EagI showed that the 1.2 kb and 1.9 kb inserts were present in the pAdeno-X construct respectively (**Figure 6-17B**). However, the full length of the pAdeno-X DNA did not appear to be present. Adding up the band sizes of the NheI/EagI double digest of pAdeno-X-TRE-ppANF-eGFP found the plasmid size to be approximately 7 to 8 kb, which was a lot less than the 35.46 kb expected. The two constructs were subsequently sent away for sequence analysis and it was confirmed that although the I-CeuI sites were intact in both constructs, the PI-SceI sites were missing, as well as a large portion of the pAdeno-X viral DNA. Care was taken during the transformation of *E. coli* with recombinant Adeno-X DNA to amplify the recombinant constructs to prevent damage and recombination of Adeno-X constructs. XL-10 Gold cells (Stratagene) are recombination deficient, and colonies expressing the recombinant pAdeno-X constructs were picked <24 hr after transformation for miniprep cultures which were used the same day to inoculate maxiprep cultures. Maxiprep cultures were grown overnight for <24 hr hours before maxi DNA preparation was carried out. Cultures

expressing recombinant pAdeno-X constructs were always used fresh and never stored at room temperature or at 4^{o}C, minimising damage to Adeno-X DNA. Hence, it was concluded that the pAdeno-X DNA was originally damaged and Clontech had since replaced our pAdeno-X Tet-on expression system with the pLP-Adeno-X-TRE Tet-off expression system.

6.3.5 Expression of pDNR-ppANF-eGFP and pDNR-ppANF-tdTomato

pDNR-CMV donor vector (Clontech) was used to subclone ppANF-eGFP and ppANF-tdTomato into the inducible pLP-Adeno-X-TRE construct. Firstly, ppANF-eGFP was inserted into pDNR-CMV via the unique HindIII and XbaI restriction sites present in both ppANF-eGFP and pDNR-CMV vectors. HindIII and XbaI sites were also introduced to ppANF-tdTomato via PCR amplification (**Figure 6-18A**). After ligation of the pDNR-CMV vector with the insert DNA, mini-preparations of the constructs were carried out. HindIII and XbaI restriction digests on the mini-preps confirmed the presence of ppANF-eGFP (1.2 kb) and ppANF-tdTomato (1.9 kb) in the constructs (**Figures 6-18B and C**). These positive constructs were then sent for sequence analysis which confirmed the presence of insert DNA between the HindIII and XbaI sites (Cogenics).

N2a cells were transfected with pDNR-ppANF-eGFP and pDNR-ppANF-tdTomato to test for fluorescent protein expressions in these constructs. **Figures 6-19A and B** show the expression of pDNR-ppANF-eGFP in green and pDNR-ppANF-tdTomato

in red respectively, confirming that these constructs could be used for further pLP-Adeno-X-TRE subcloning.

6.3.6 Generation of pLP-Adeno-X-TRE constructs

pLP-Adeno-X-TRE DNA was ligated to pDNR-ppANF-eGFP and pDNR-ppANF-tdTomato via Cre recombination. The recombinant DNA was then used to transform electrocompetent cells using the procedures described in section **6.2.10.1** above. The transformed cells were then cultured for 1 hr at 37^{o}C and then used to inoculate sucrose/chloramphenicol agar, which was further cultured for 24 hr at 37^{o}C. Colony PCR was performed on selected colonies picked from the agar plates using Adeno-X LP CMV Primer Mix (section **6.2.10.1**). **Figures 6-20A** and **B** show the results of PCR analysis of pLP-Adeno-X-TRE-ppANF-eGFP and pLP-Adeno-X-TRE-ppANF-tdTomato respectively. Both analyses generated a band of 660 bp, which is consistent with the presence of the pDNR insert in the pLP-Adeno-X-TRE vector. Further analysis using the XhoI restriction enzyme showed that pLP-Adeno-X-TRE-ppANF-eGFP had a missing band at the expected 5.0 kb, which was where the insert DNA should be (**Figure 6-20C**). XhoI restriction analysis of pLP-Adeno-X-TRE-ppANF-tdTomato generated all the expected bands (14.5, 8.0, 5.8, 3.6, 2.5, and 1.4 kb; **Figure 6-20D**).

6.4 Discussion

Targeting of fluorescence to LDCVs allows direct visualisation of peptide release and vesicle pool segregation. ppANF, a peptide of 152 amino acids, had been shown to target fluorescent protein expression to LDCVs in PC12, bovine adrenal chromaffin cells and pituitary lactotrophs (Han *et al.* 1999; Ng *et al.* 2002; Stenovec *et al.* 2004; Duncan *et al.* 2003). Results from ppANF-eGFP transfection of PC12 cells had shown that eGFP expression was colocalised with chromogranin A staining (**Figure 6-9**), indicating that ppANF successfully targeted fluorescent protein expression to LDCVs. In this study, a fluorescent time stamp was tagged to ppANF for LDCV targeting. The fluorescent time stamp had been successfully used as an indication of vesicle age since the Timer fluorescent protein changes emission from green to red as it matures over time (Terskikh *et al.* 2000). Hence, over a time course, vesicles older than 16 hr emit in the red spectrum and newly synthesised vesicles emit in the green. However, the fluorescent time stamp also has complicated folding properties as it matures. The Timer protein matures and oligomerises into a tetramer for fluorescent emission, similar to the maturation process in DsRed (Wall *et al.* 2000). Previous studies have reported that untagged DsRed expressed in the cytoplasm and did not aggregate (Lauf *et al.* 2001). In this study, targeting of Timer to LDCVs was shown to have the same effect. As the results in section 6.3.2 have shown, tagging of the fluorescent Timer to ppANF resulted in aggregation of the fluorophore in perinuclear compartments, likely to be the ER (**Figure 6-11**). Similar to untagged DsRed expression untagged fluorescent Timer expression, was observed throughout the cytoplasm of N2a cells (**Figure 6-12**). This demonstrates that oligomerisation of the ppANF-Timer protein had resulted in aggregation of the fluorophore (**Figure 6-11**). Since ppANF tagged to eGFP or tdTomato, both form

dimers, resulted in correct targeting of the fluorophores to LDCVs, Timer expression had hampered ppANF targeting. Nevertheless, the fluorescent Timer had been shown previously to be successfully targeted to LDCVs in bovine adrenal chromaffin cells (Duncan *et al.* 2003) by tagging to ppANF. Hence, further experiments to tag the Timer protein to ppANF with differing lengths of linking bases which provide more flexibility for the oligomerisation of the Timer protein (Wall *et al.* 2000) might to crucial to expression of Timer protein in LDCVs. A study analysing the different mutants of the DsRed protein had found that mutants with different "free space", based on crystal structure analysis, around the fluorophore resulted in different maturing properties of the protein (Terskikh *et al.* 2002). It was hypothesised that aggregation of the Timer protein is due to electrostatic attraction between the negatively charged surface of the protein and the positively charged N-terminal. Mutation at the N-terminal of the Timer protein resulted in a non-aggregating form of the protein (Yanushevich *et al.* 2002). Therefore, it is crucial in future experiments to alter the linking region of ppANF and Timer and also to mutate the N-terminus of the Timer protein for efficient expression of the fluorescent protein.

Meanwhile, the inducible ppANF-tdTomato construct generated was shown to be efficient in pulse-chase labelling of newly synthesised and mature LDCVs. The Tet-on expression system involved subcloning fluorescent proteins into a vector with a tetracycline response element which upon binding of the tetracycline to the rtTA, activates transcription of the fluorescent proteins. Two fluorescent reporter proteins were chosen – eGFP which emits green and tdTomato which emits red. **Figure 6-14**

showed expression of the pTRE-ppANF-eGFP and pTRE-ppANF-tdTomato constructs in PC12 cells and colocalisation of fluorescent protein expression with chromogranin A staining. This shows that both fluorescent proteins were targeted to LDCVs and both inducible constructs are suitable for studying the dynamics of LDCVs. "Pulse-chase" expression of pTRE-ppANF-tdTomato had shown that there was a significant difference between mean fluorescent intensity in the GA compared to other cell areas at all time points measured, indicating that transfected cells were actively synthesising ppANF-tdTomato at all time points. Moreover, there was a significant increase in mean fluorescent intensity in the cell centre at 24 hr after induction of pTRE-ppANF-tdTomato expression compared to 8 hr. Since no stimulant was used in the culture medium, vesicles not released as a result of basal activity were retained in the cells, making up the reserve pool of vesicles. A significantly higher mean fluorescent intensity in the cell centre at 24 hr suggested that non-released aged vesicles join the reserve pool in the cell centre, in agreement to the vesicle pool arrangement found in bovine adrenal chromaffin cells (Duncan *et al.* 2003).

To express these constructs in magnocellular neurons, these constructs had to be inserted into the Adeno-X viral genome for transduction. The Tet-on expression system involved subcloning the recombinant pTRE-shuttle vector into pre-linearised Adeno-X DNA. However, **Figures 6-16D** and **E** and **6-17** showed that the PI-SceI sites of both pAdeno-X-TRE-ppANF-eGFP and pAdeno-X-TRE-ppANF-tdTomato were compromised. Further sequence analysis confirmed that the PI-SceI site was

absent. The pAdeno-X is a large plasmid, >32 kb, making it vulnerable to damage and recombination. The vulnerability to damage of the pAdeno-X plasmid was taken into consideration and hence, each incubation step from transformation of recombinant deficient *E. coli* to the growth of bacterial cultures was carried out in < 24 hr succession to the previous step. Taking all the precautions taken into account, one explanation of the absence of portions of Adeno-X DNA and the PI-SceI site was that the Adeno-X DNA was damaged prior to subcloning and transformation. Clontech technical support had also agreed that the Adeno-X DNA was damaged and the company has replaced our Adeno-X™ Tet-On® Expression Systems 1 with the Adeno-X™ Expression Systems 2 containing pLP-Adeno-X-TRE vector.

The reporter genes chosen for the Adeno-X™ Expression Systems 2 were ppANF-eGFP and ppANF-tdTomato. Subcloning of the two reporter constructs into the pDNR-CMV donor vector was shown to be successful in **Figure 6-18B** and **C**. Transfection of pDNR-ppANF-eGFP and pDNR-ppANF-tdTomato in N2a cells had also shown expression of the two constructs (**Figure 6-19**). Cre-loxP-mediated recombination was carried out to insert the gene of interest from the pDNR-constructs to the pLP-Adeno-X vector. Restriction digests with XhoI restriction enzyme had confirmed that the presence of the insert and pLP-Adeno-X-TRE vector in the pLP-Adeno-X-TRE-ppANF-tdTomato construct. Further sequence analysis also confirmed that the loxP sites used for recombination were intact, making this construct a strong candidate for inducible expression of ppANF-tdTomato protein in magnocellular neurons. Transduction of magnocellular neurons with adenovirus is

known to be an efficient means of exogenous protein expression. Adenovirus has low cytotoxicity, an important factor to consider in samples to be used in live cell imaging experiments. In addition, the tet-on and tet-off systems offer the opportunity to label newly synthesised and mature LDCVs by the addition of doxycycline, hence eliminating the use of the complicated Timer protein, and also ensuring that fluorescent protein expression ceases at the same time within each sample studied. Generation of viral particles containing the pLP-Adeno-X-TRE-ppANF constructs will inevitably be a big step forward in targeting fluorescent protein expression in LDCVs of magnocellular neurons and controlling fluorescent expression will allow pulse chase study of vesicle release in magnocellular dendrites.

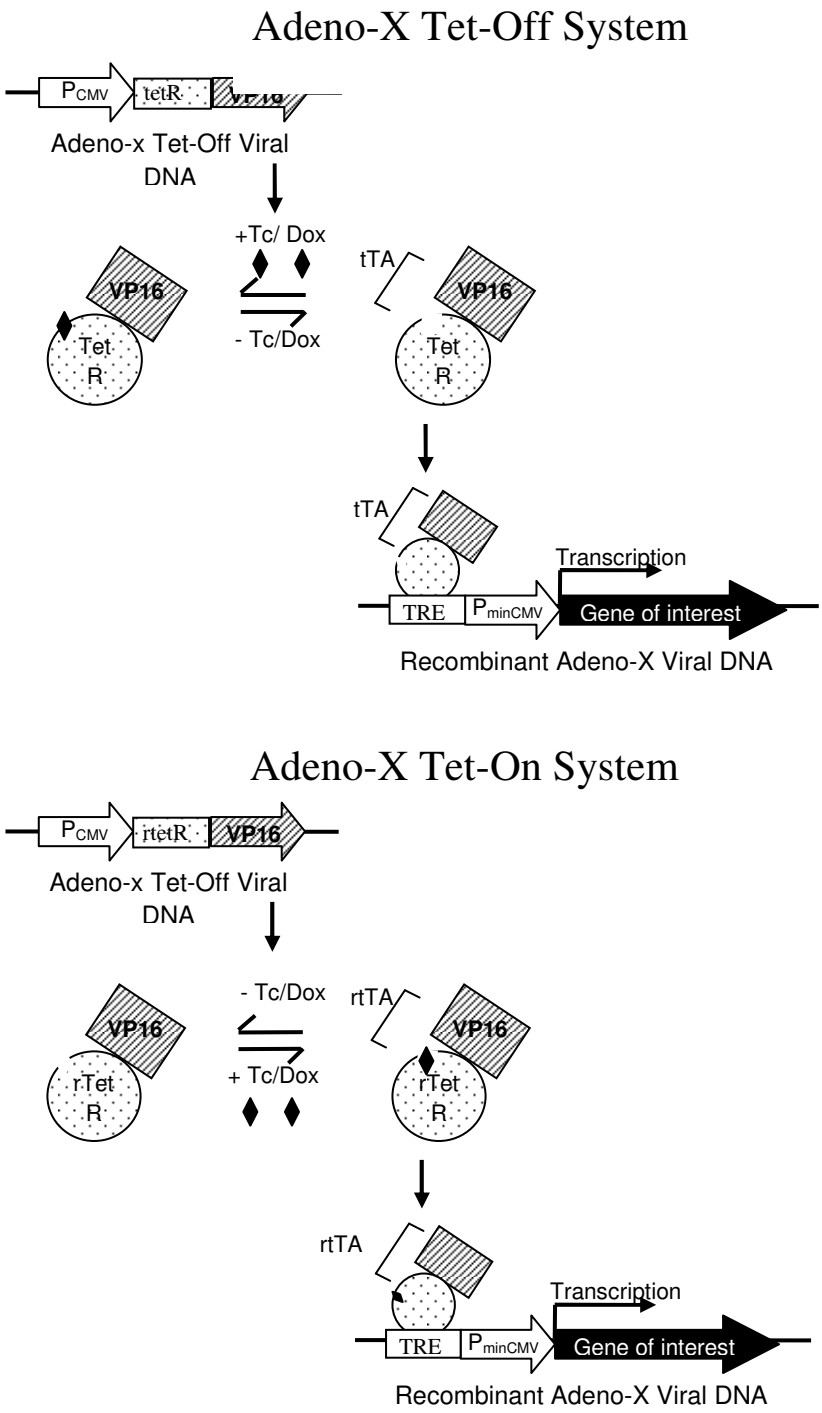

Figure 6-1. Adeno-x Tet-Off and Tet-on system. Transcription is turned off/on by the addition of doxycycline. P_{CMV} = cytomegalovirus promoter; (r)tetR = (reverse) tetracycline repressor protein; VP16 = c-terminal activation domain of Herpes simplex virus; (r)tTA = (reverse) tetracycline-controlled transactivator; TRE = tetracycline response element; P_{minCMV} = minimal immediate early promoter of cytomegalovirus; Tc = tetracycline; Dox = doxycycline. Diagram adapted from Adeno-X^{TM} Tet-Off® & Tet-On® Expression System 1 User Manual.

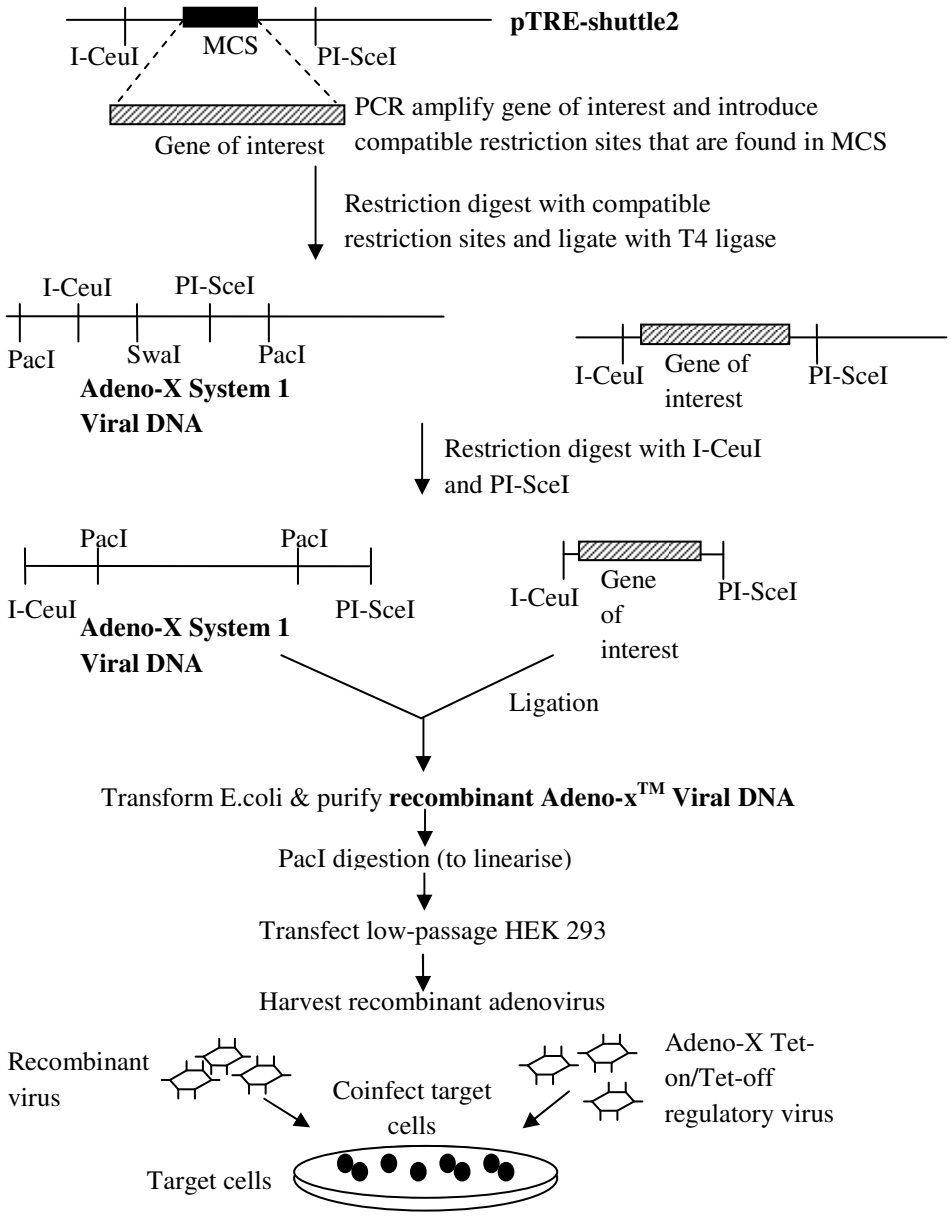

Figure 6-2. Overview of recombinant adenovirus construction and infection. The gene of interest was subcloned into the pTRE-shuttle2 vector via the multiple cloning site (MCS). Insert DNA, bearing the restriction sites compatible with restriction sites in the MCS, and pTRE-shuttle2 vector were digested creating compatible restriction sites for ligation to create recombinant pTRE-shuttle2 vectors. pTRE-shuttle2 vectors contain PI-SceI and I-CeuI restriction sites compatible with those found in the pAdeno-X viral vector and can be subcloned via these sites by T4 ligation. Recombinant pAdeno-X vectors were then amplified via transformation and culture of bacterial cells. Amplified viral DNA was linearised by PacI digestion and HEK 293 cells were infected with viral DNA to add packaging of viral particles. Recombinant viral particles can then be used to infect target magnocellular cells along with Tet-on regulatory virus for inducible expression of the gene of interest. Figure adapted from Adeno-X™ Tet-Off® & Tet-On® Expression System 1 User Manual.

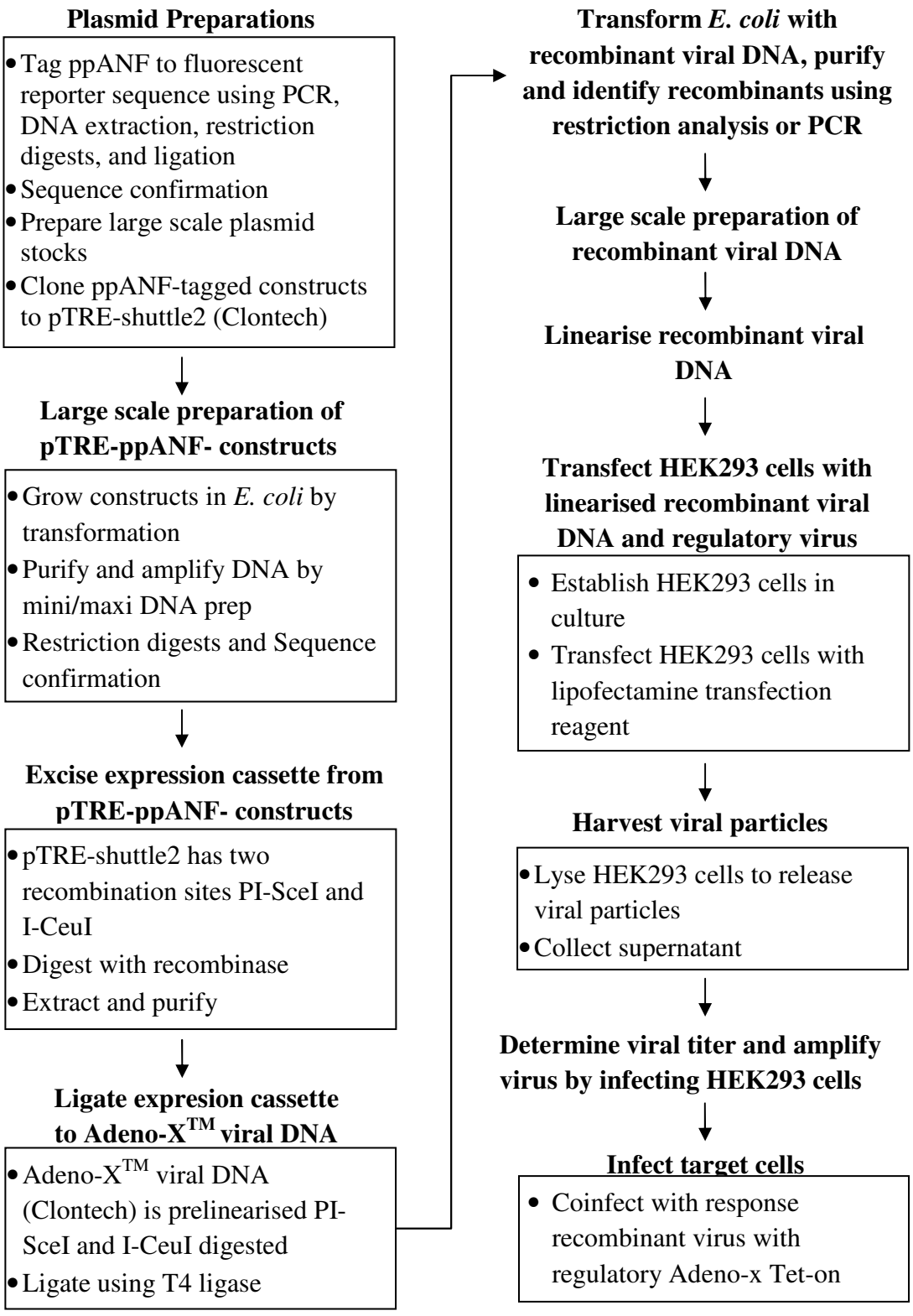

Figure 6-3. Overview of the generation of inducible ppANF-tagged constructs to the generation of viral particles using the Adeno-X™ Expression System 1 (Clontech).

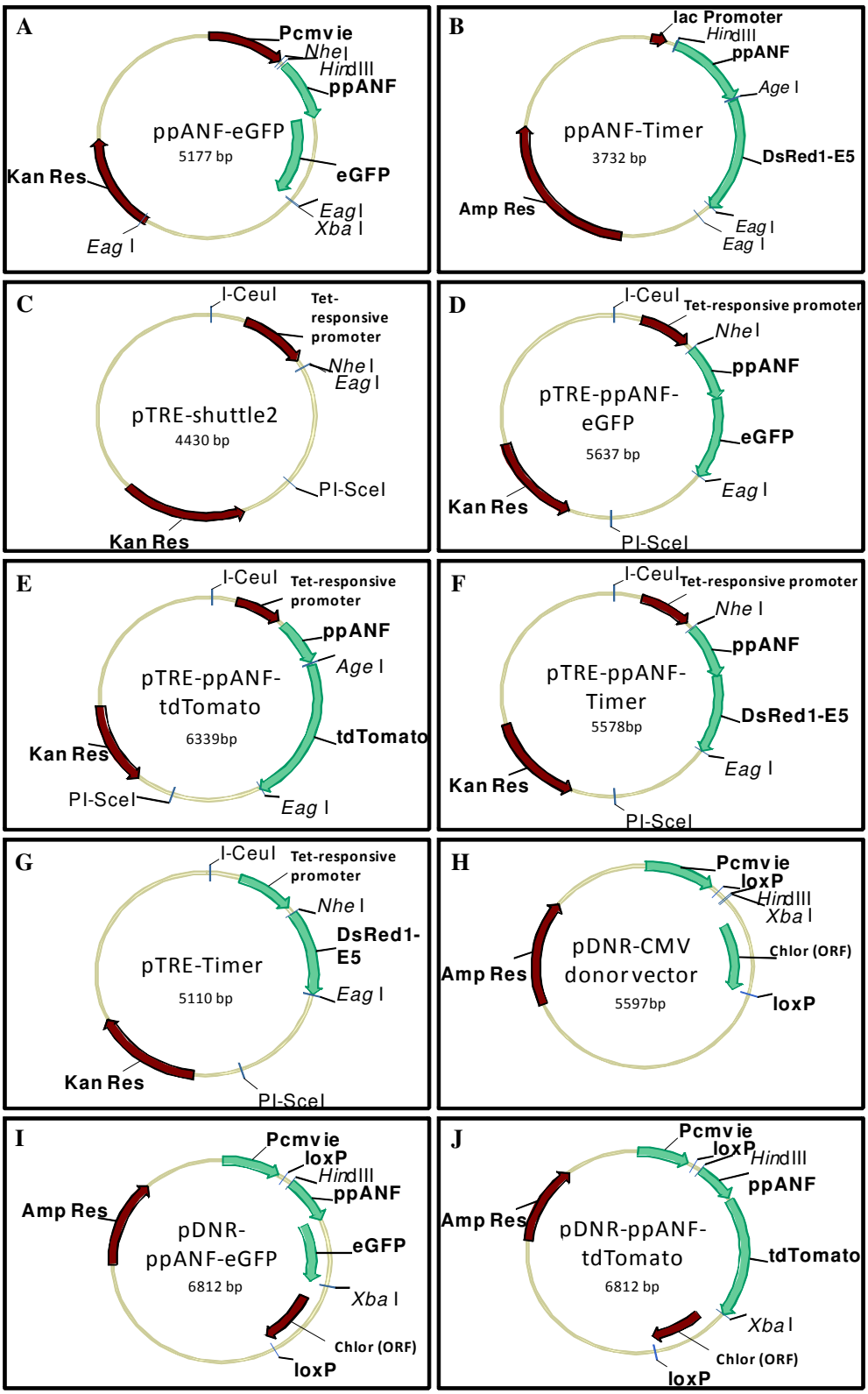

Figure6-4. Plasmid maps of ppANF tagged fluorescent constructs and inducible constructs showing the promoters, proteins expressed, restriction sites used for subcloning, antibiotic resistant markers, and the sizes of the constructs. Vector maps generated with Vector NTI (Invitrogen).

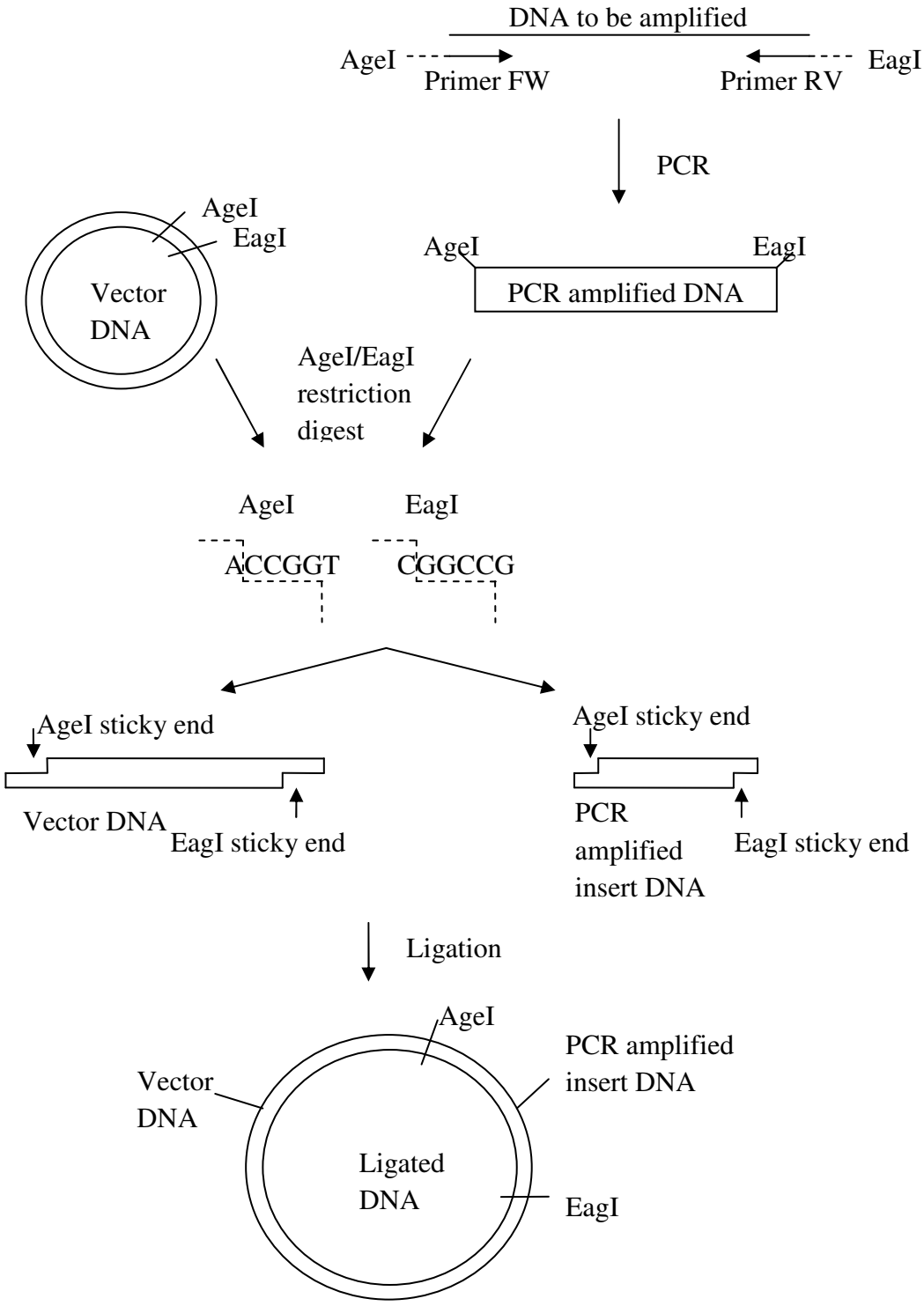

Figure 6-5. PCR amplification and introduction of restriction sites. Compatible sites with the vector DNA, where the amplified DNA would be subcloned into, were chosen, in this example, AgeI and EagI. Restriction digests result in non-paired oligonucleotides producing sticky ends for ligation. Ligation involves the use of T4 ligase, where sticky ends from the same restriction digests are joined together. Primer FW = forward primer; Primer RV = reverse primer.

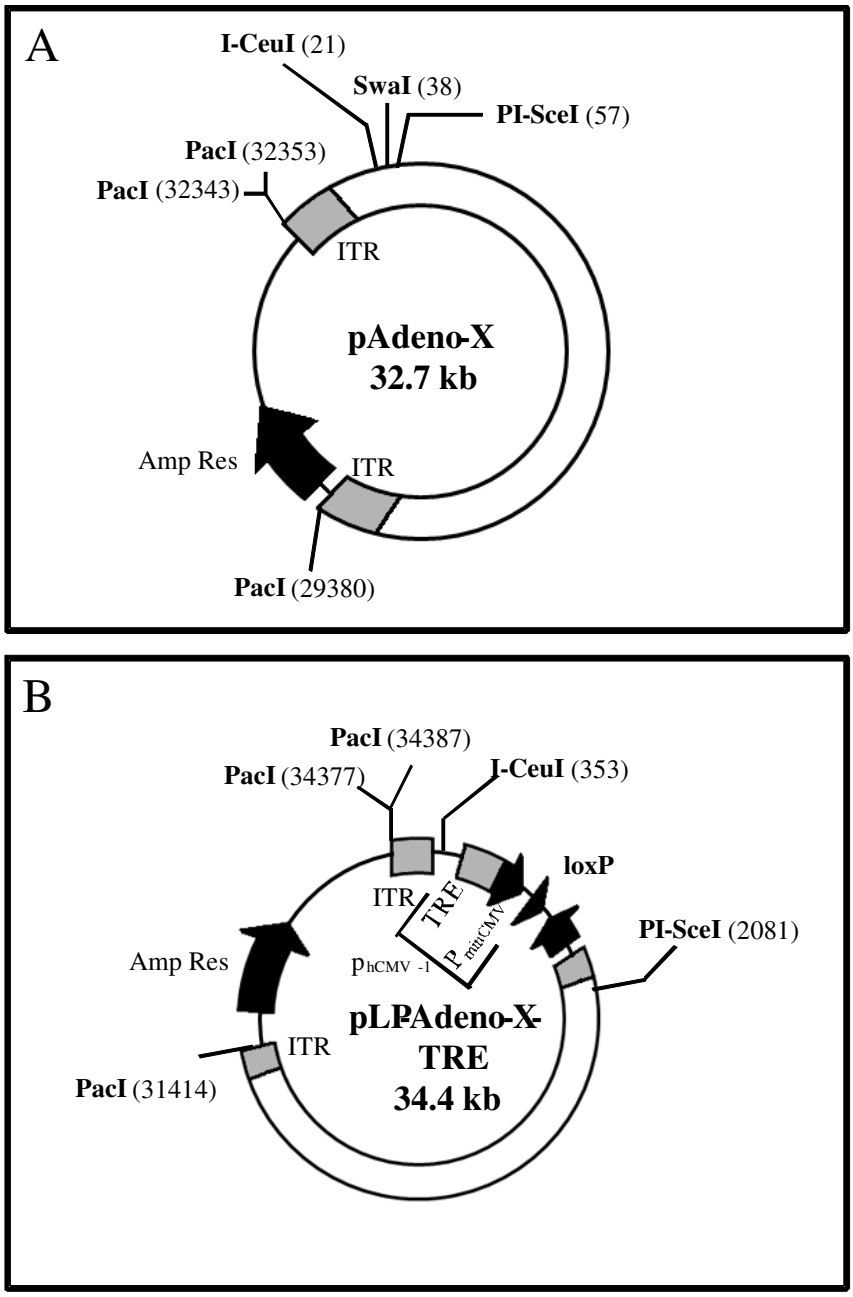

Figure 6-6. **A**) Plasmid map of pAdeno-x containing two inverted terminal repeats, the ampicillin resistance gene, PacI sites for linearization of viral vector, and the PI-SceI and I-CeuI sites for subcloning of recombinant pTRE-shuttle2 vectors. **B**) Plasmid map of pLP-Adeno-X-TRE containing similar features as (**A**) plus the TRE located upstream of the minimal cytomegalovirus promoter (P_{minCMV}). Together, the TRE and P_{minCMV} makes up the $P_{hCMV\ -1}$ which is silent when the tTA is activated in the presence of tetracycline. pLP-Adeno-X-TRE also contains a loxP site for Cre-loxP recombination with recombinant pDNR-CMV vectors. Both plasmid maps show positions of restriction sites and the size of the Adeno-X vectors. Figures adapted from Adeno-X^{TM} Expression System 1 and Adeno-X^{TM} Expression Systems 2 user manuals (Clontech).

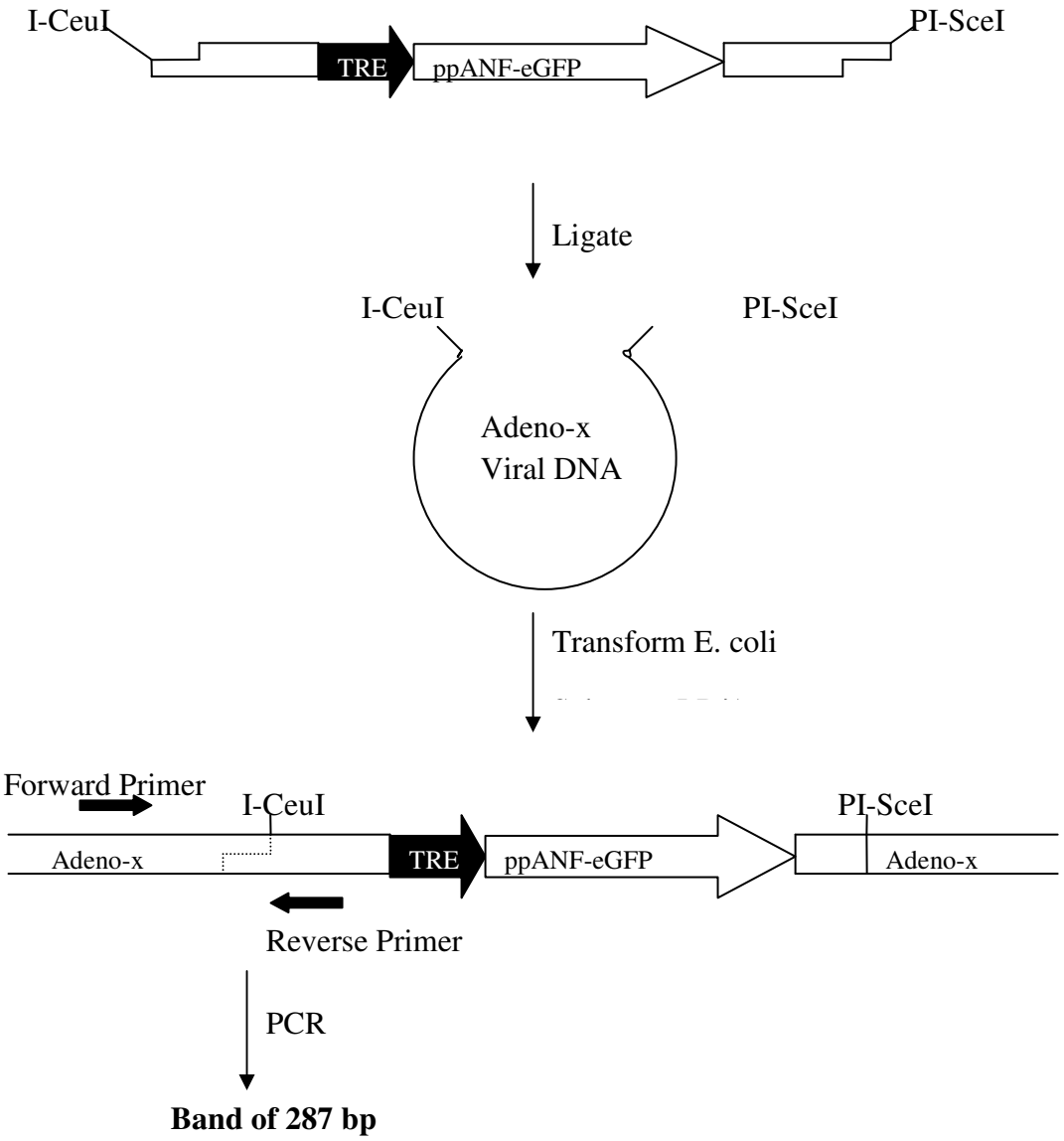

Figure 6-7. Confirmation of recombinant pAdeno-x-ppANF-DsRed1-E5 ligation and transformation by PCR screening. Figure adapted from Adeno-X^{TM} PCR Screening Primer Set protocol.

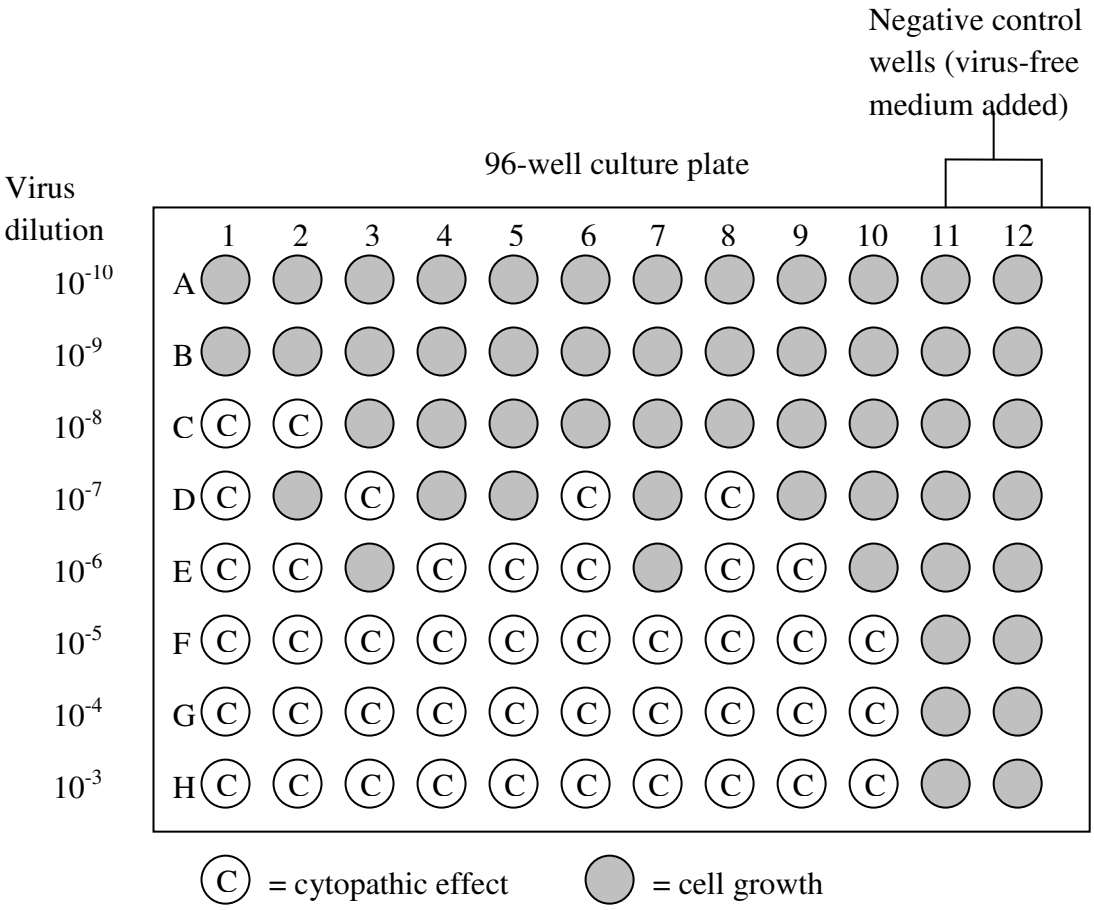

Figure 6-8. Determining viral titre with the end-point dilution assay. HEK 293 cells were plated in a 96-well plate for 10 days. The recombinant virus was diluted from a 10 µl virus stock and serial dilutions were carried out to dilutions of 10^{-3} to 10^{-10}. 100 µl of diluted virus was added to each well containing HEK 293 cells. Negative controls were carried out by adding virus-free media to cells. Shaded circles represent cell growth and circles marked with C represent cytopathic effect of cells seen in each well. The number of wells containing cells with cytopathic effect was noted for each dilution used. Figure adapted from Adeno-X™ Tet-Off® & Tet-On® Expression System 1 User Manual.

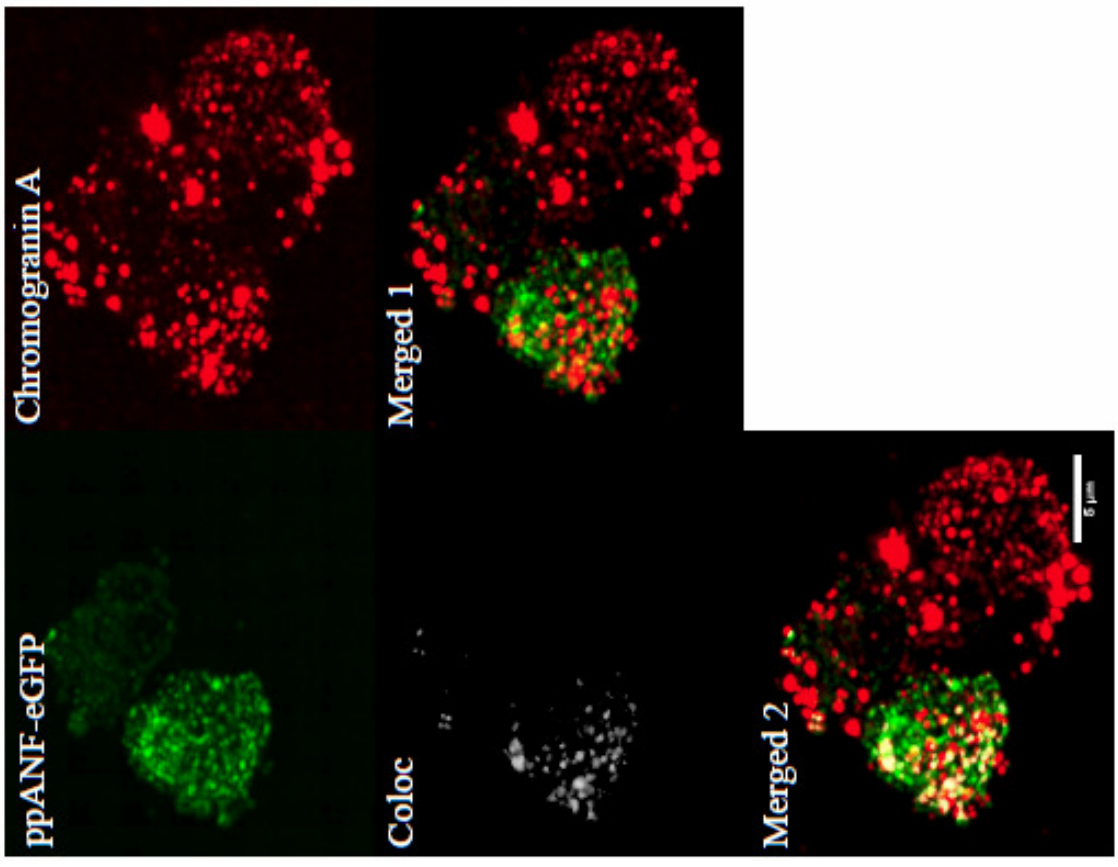

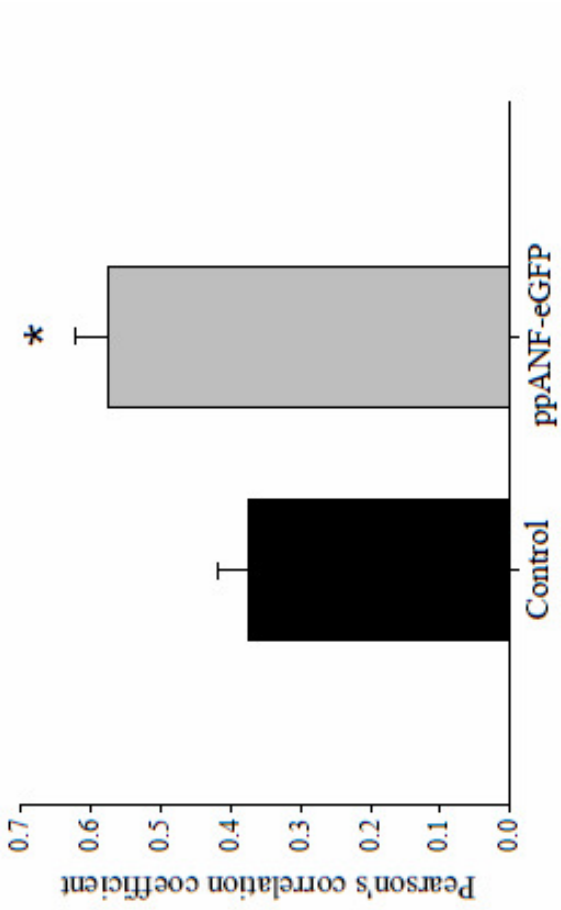

Figure 6-9. ppANF-eGFP transfection of PC12 cells. Images show ppANF-eGFP expression in green and staining of chromogranin A in red Colocalisation analysis (Coloc) is represented in white showing colocalisation of chromogranin A and ppANF-eGFP, indicating that ppANF-eGFP was targeted to LDCVs. Merged 1 is a merged image of all channels excluding the coloc channel. Merged 2 is a merged image of all channels. Scale bars = 5 µm. Mean Pearson's correlation coefficients shown. Student's t-test showed a significant difference between control and ppANF-eGFP colocalisation with chromogranin A ; $p<0.006$, n=10.

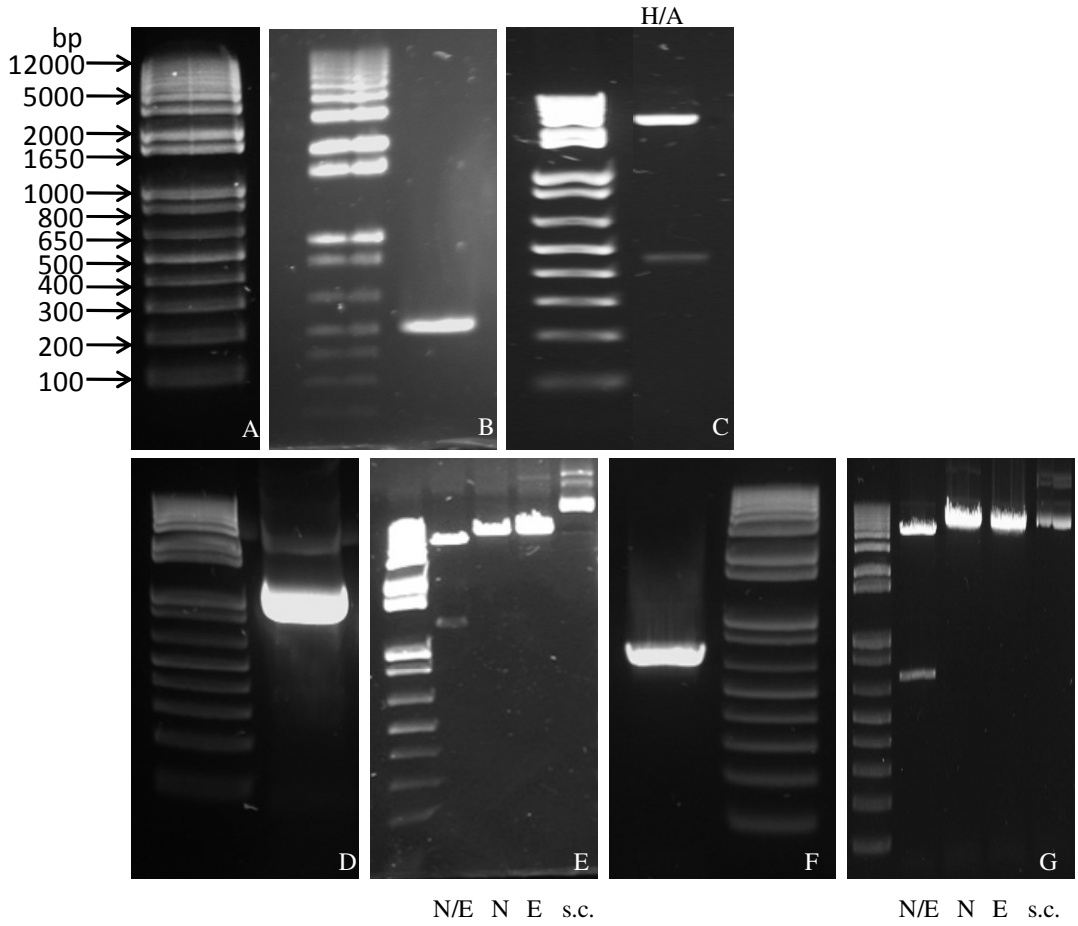

Figure 6-10. Gel images from electrophoresis of PCR amplification products of ppANF, ppANF-Timer and pTimer and restriction digest of ppANF-Timer, pTRE-ppANF-Timer and pTRE-Timer. **A**) DNA ladder (Invitrogen) labelled with band sizes in bp. **B**) PCR amplification of ppANF (486 bp). **C**) Restriction digest of ppANF-Timer using HindIII (H) and AgeI (A); sizes of DNA fragments shown are 3.27 kb and 461 bp; confirming the presence of ppANF in the pTimer vector. **D**) PCR amplification of ppANF-Timer (1.21 kb). **E**) Restriction digests of pTRE-ppANF-Timer – N/E = NheI/EagI double digest, N = NheI single digest, E = EagI single digest, s.c. = supercoiled undigested DNA. Single digests show band sizes of 5.58 kb and double digest shows band sizes of 4.4 kb and 1.16 kb, confirming the presence of ppANF-Timer in the pTRE-shuttle2 vector. **F**) PCR amplification of pTimer (680 bp). **G**) Restriction digests of pTRE-Timer using NheI and EagI. Single digests show band sizes of 5.1 kb and double digest shows band sizes of 4.4 kb and 680 bp, confirming the presence of pTimer in the pTRE-shuttle2 vector.

Figure 6-11. Transfection of N2a cells with pTRE-ppANF-Timer. A transmitted light image of a N2a cell is shown on the top left. N2a cells were excited with an argon laser and a HeNe 1 laser (excitation wavelengths are 488 nm and 568 nm respectively). pTRE-ppANF-Timer expression is shown in both green and red channels. The merged image shows merging of the green and the red channels. Scale bar = 5 µm.

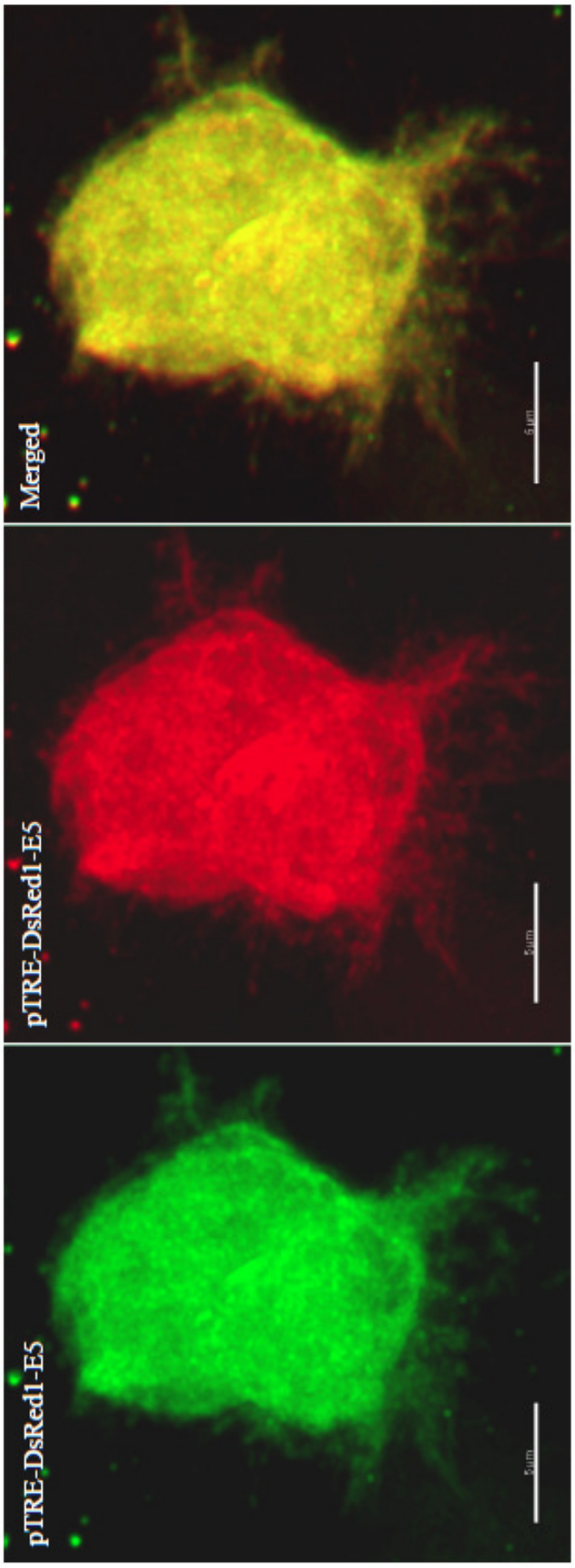

Figure 6-12. pTRE-Timer transfection of a N2a cell. The timer protein changes it's fluorescent emission from green to red over ~16 hours. The merged image shows merging of the green and the red channel. Expression of Timer which was not tagged to ppANF demonstrated that the ppANF tag hindered expression of the timer fluorescent protein, since direct subcloning of Timer into the pTRE-shuttle2 vector resulted in fluorescent expression in both green and red, as shown in the above images. Scale bars = 5 μm.

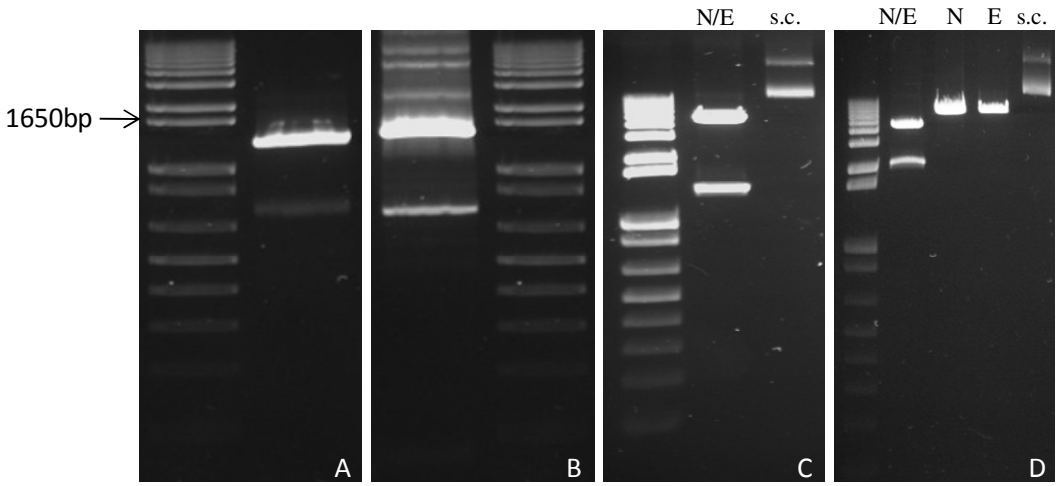

Figure 6-13. Gel images from electrophoresis of PCR amplification products of ppANF-eGFP and tdTomato and restriction digest of pTRE-ppANF-eGFP, pTRE-ppANF-tdTomato. **A**) PCR amplification of ppANF-eGFP (1.2 kb). **B**) PCR amplification of tdTomato (1.4 kb). **C** and **D**) Restriction digest of pTRE-ppANF-eGFP and pTRE-ppANF-tdTomato using NheI (N) and EagI (E); sizes of DNA fragments shown are 4.4 kb and 1.2 kb for pTRE-ppANF-eGFP; and 4.4 kb and 1.9 kb for pTRE-ppANF-tdTomato confirming the presence of both ppANF-eGFP and ppANF-tdTomato inserts in the pTRE-shuttle2 vector. N/E = NheI/EagI double digest, N = NheI single digest, E = EagI single digest, s.c. = supercoiled undigested DNA.

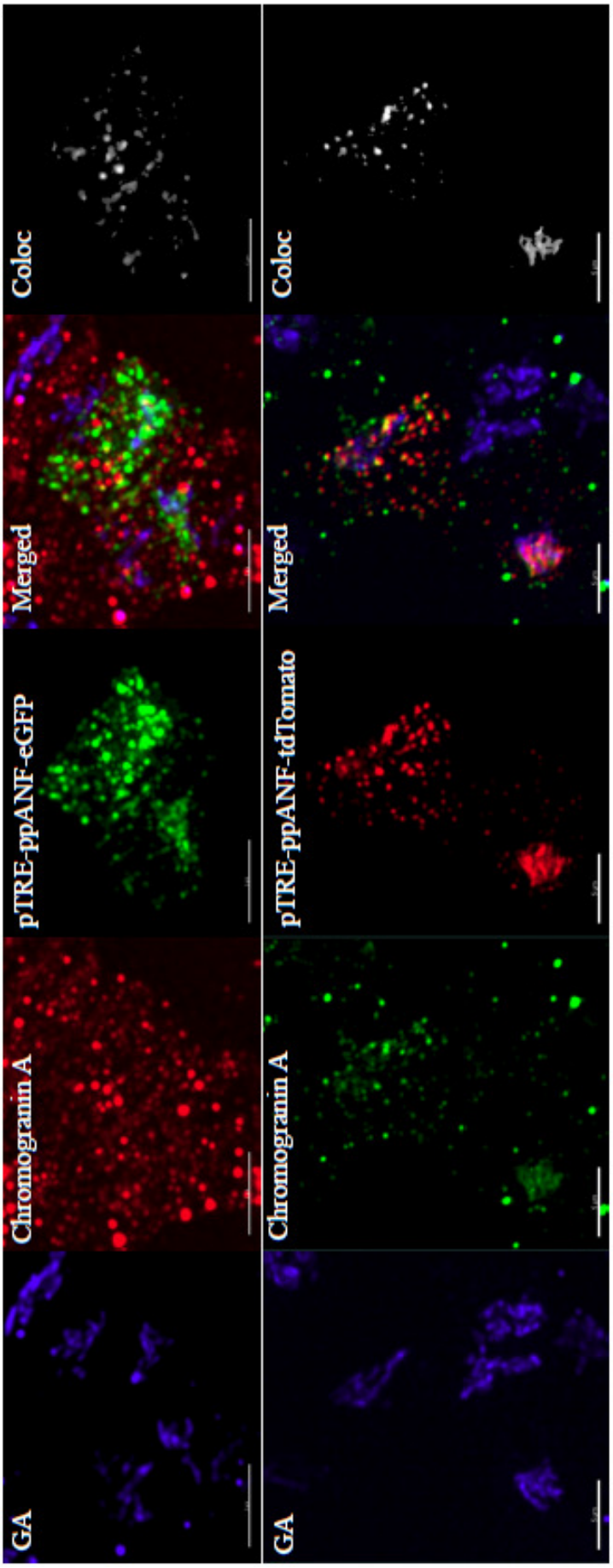

Figure 6-14A. Transfection of PC12 cells with pTRE-ppANF-eGFP and pTRE-ppANF-tdTomato. Top panel: immunofluorescence labelling of GA (blue), choromogranin A (red) and expression of pTRE-ppANF-eGFP (green). Bottom panel: immunofluorescence labelling of GA (blue), chromogranin A (green) amd expression of pTRE-ppANF-tdTomato (red). Coloc (white) represents colocalisation of chromogranin A and either pTRE-ppANF-eGFP or pTRE-ppANF-tdTomato, showing that both ppANF-tagged constructs were targeted to LDCVs. Merged images excludes coloc channels. Scale bar = 5 μm.

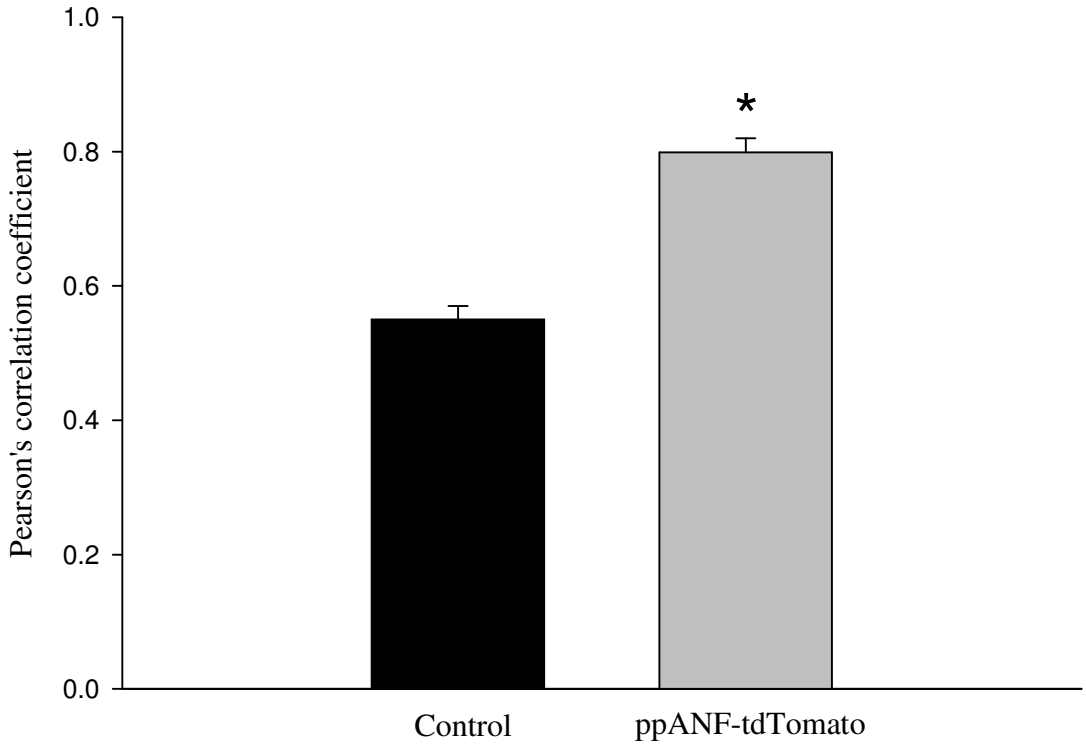

Figure 6-14B. Colocalisation between ppANF-tdTomato and chromogranin A. Mean Pearson's correlation coefficients of control (non-transfected cells) and pTRE-ppANF-tdTomato transfection. Student's t-test showed a significant difference between control and ppANF-tdTomato colocalisation with chromogranin A ; $p<0.001$, $n=10$.

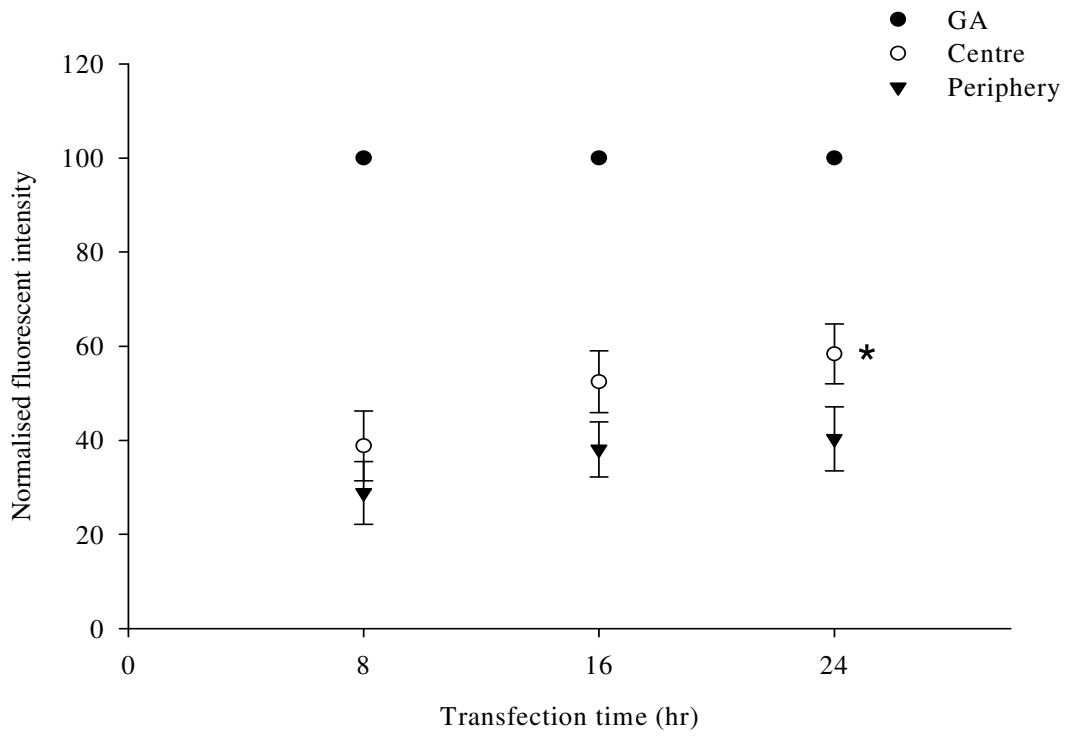

Figure 6-15. pTRE-ppANF-tdTomato expression in the GA, cell centre and cell periphery in transfected PC12 cells. Cells were transfected for 8 (n = 7), 16 (n=10) and 24 hr (n=8). There are significant differences in pTRE-ppANF-tdTomato expression between the GA of all time points compared to the cell centre and the cell periphery. pTRE-ppANF-tdTomato expression in the cell centre at 24 hr was significantly higher than expression at 8 hr ($p<0.05$, two-way ANOVA, post-hoc Student's t-test). There were no significant differences in other cell areas at the different time points.

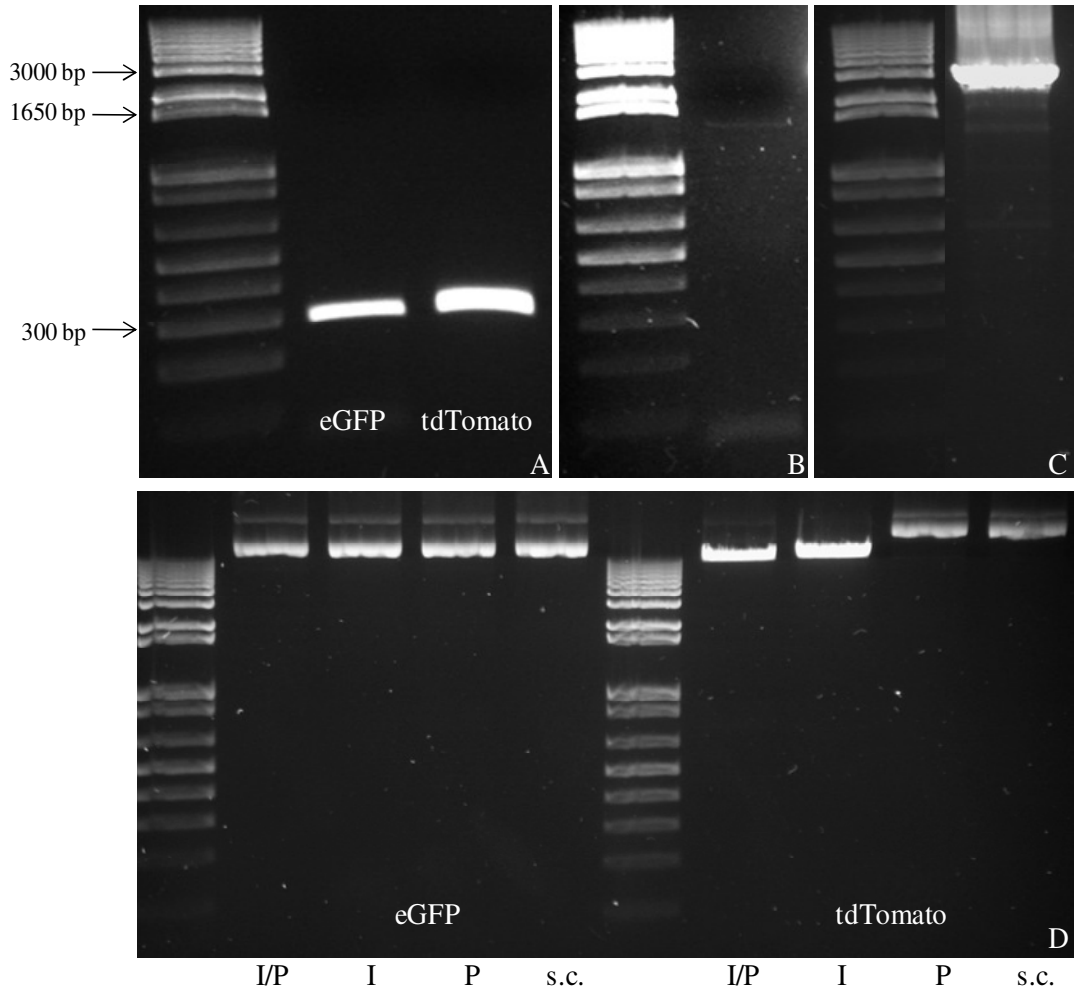

Figure 6-16. Analysis of pAdeno-X-TRE-ppANF-eGFP and pAdeno-X-TRE-ppANF-tdTomato. **A)** PCR analysis of pAdeno-X-TRE-ppANF-eGFP and pAdeno-X-TRE-ppANF-tdTomato using pAdeno-X Forward and Reverse PCR Primers, DNA fragment amplified – 287 bp. **B** and **C**) PCR analysis of pAdeno-X-TRE-ppANF-eGFP and pAdeno-X-TRE-ppANF-tdTomato using pAdeno-X PCR forward primer and a reverse primer binding directly to the insert DNA. **B**) Reverse primer binding to the c-terminal of the ppANF fragment in pAdeno-X-TRE-ppANF-eGFP, DNA fragment amplified – 1.2 kb. **C**) Reverse primer binding to the c-terminal of the tdTomato fragment in pAdeno-X-TRE-ppANF-tdTomato, DNA fragment amplified – 2.7 kb. **D**) P/I = PI-SceI/I-CeuI double digest, P = PI-SceI single digest and I = I-CeuI single digest, s.c. = undigested supercoiled DNA. P/I double digest should generate two DNA fragments for each plasmid: 2.8 kb and 32.67 kb for pAdeno-X-TRE-ppANF-eGFP and 3.5 kb and 32.67 kb for pAdeno-X-TRE-ppANF-tdTomato. Single digests showed that I-CeuI restriction enzyme worked on pAdeno-X-TRE-ppANF-tdTomato pAdeno-X-TRE-ppANF-eGFP and PI-SceI did not digest either construct since DNA fragments observed were similar to undigested supercoiled DNA.

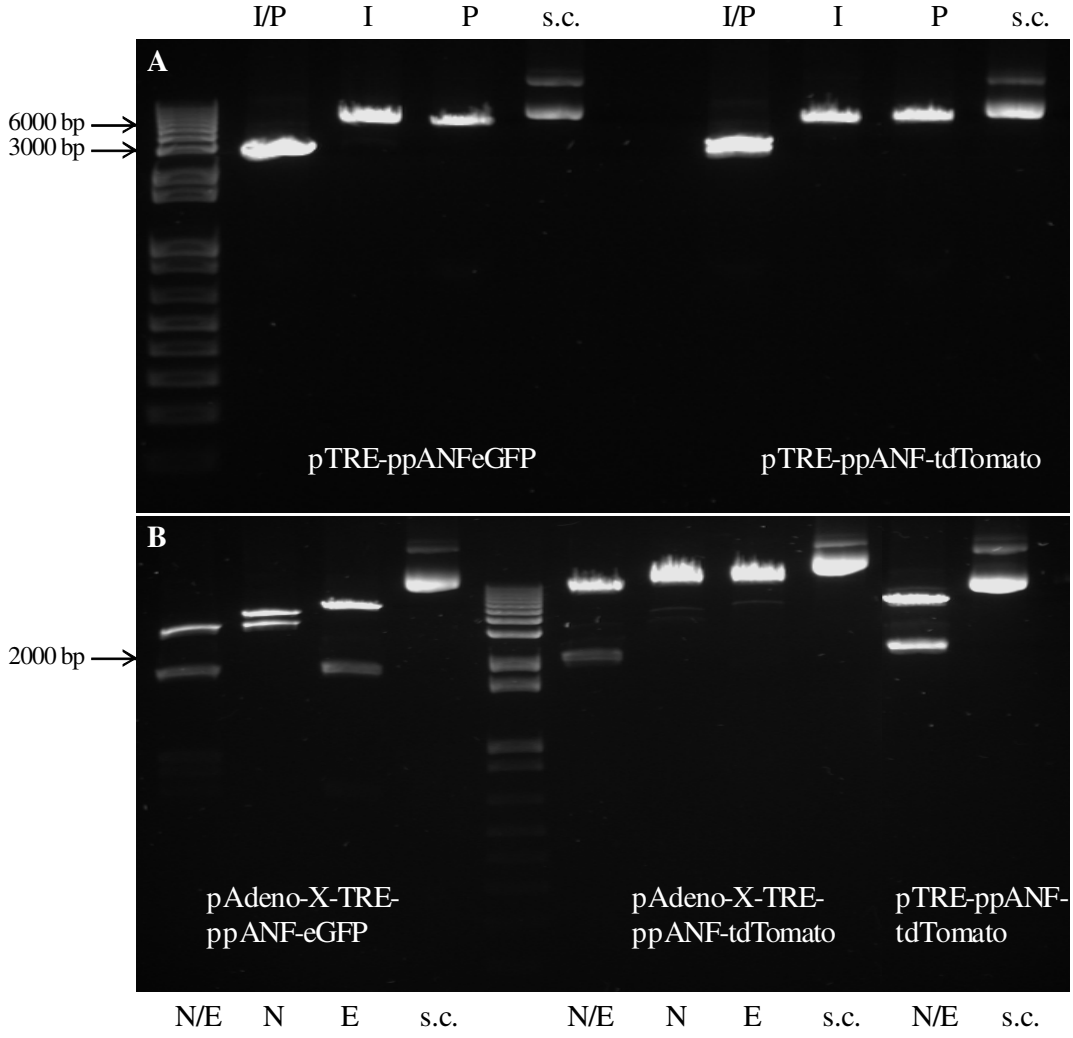

Figure 6-17. **A**) Restriction analysis of pTRE-ppANF-eGFP and pTRE-ppANF-tdTomato with I-CeuI and PI-SceI. I/P = I-CeuI and PI-SceI double digest, I = I-CeuI single digest, P = PI-SceI single digest and s.c. = undigested supercoiled DNA. Double digest of pTRE-ppANF-eGFP produced two bands at 2.79 kb and 2.85 kb, and single digests produced bands at 5.6 kb. Double digest of pTRE-ppANF-tdTomato produced two bands, one at 2.8 kb and one at 3.5 kb. These band sizes confirmed the presence of ppANF-eGFP and ppANF-tdTomato within the I-CeuI and PI-SceI sites of pTRE-shuttle2 vector, both restriction enzymes were successful at digest, and both restriction sites were intact in the recombinant pTRE-shuttle vectors. **B**) Restriction analysis of pAdeno-X-TRE-ppANF-eGFP and pAdeno-X-TRE-ppANF-tdTomato with NheI and EagI. N/E = NheI and EagI double digest, N = NheI single digest and E = EagI single digest. pTRE-ppANF-tdTomato NheI/EagI double digest was included as a positive control of the double restriction digest. NheI and EagI digests of pAdeno-X-TRE-ppANF-eGFP revealed the total size of the recombinant pAdeno-X DNA to be between 7 and 8 kb. Meanwhile, a ~ 2 kb and a band higher than 12 kb were seen in NheI and EagI digests of pAdeno-X-TRE-ppANF-tdTomato.

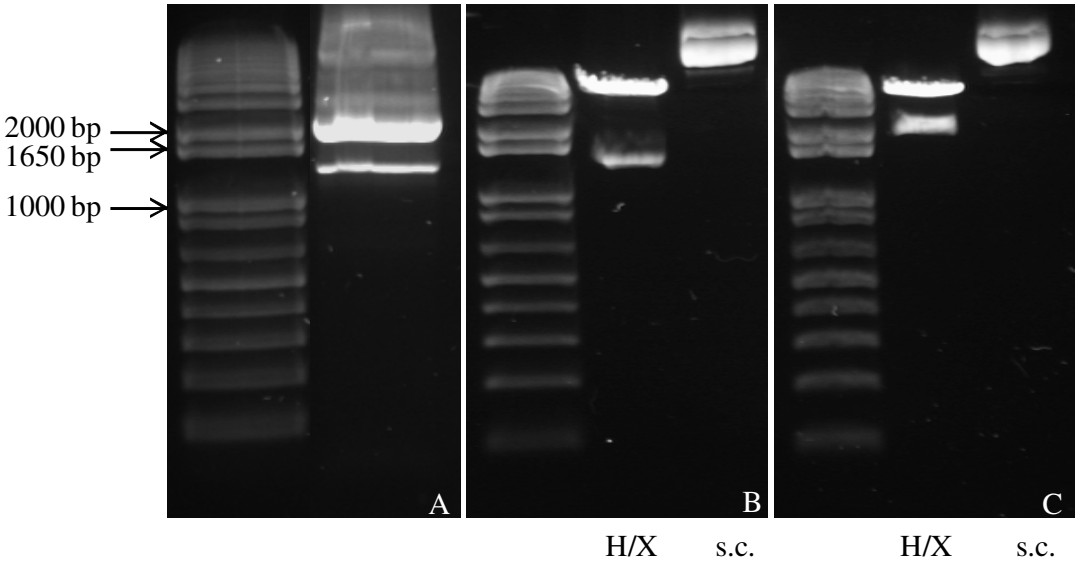

Figure 6-18. Analysis of pDNR-ppANF-eGFP and pDNR-ppANF-tdTomato. **A)** PCR amplification of ppANF-tdTomato, DNA fragment amplified – 1.9 kb. **B**) HindIII (H) and XbaI (X) double digest of pDNR-ppANF-eGFP showing band sizes of 1.2 kb and 5.6 kb. **C**) H/X double digest of pDNR-ppANF-tdTomato showing band sizes of 1.9 kb and 5.6 kb. S.c. = undigested supercoiled DNA.

Figure 6-19. Transfection of N2a cells with pDNR-ppANF-eGFP and pDNR-ppANF-tdTomato showing the expression of the reporter genes in these two constructs respectively. Images were acquired using the Leica DMR widefield microscope (Leica DFC 490 camera) fitted with Fitc 488 nm and Texas Red 568 nm excitation filters coupled with 516 -556 nm and 604 - 644 nm emission filters.

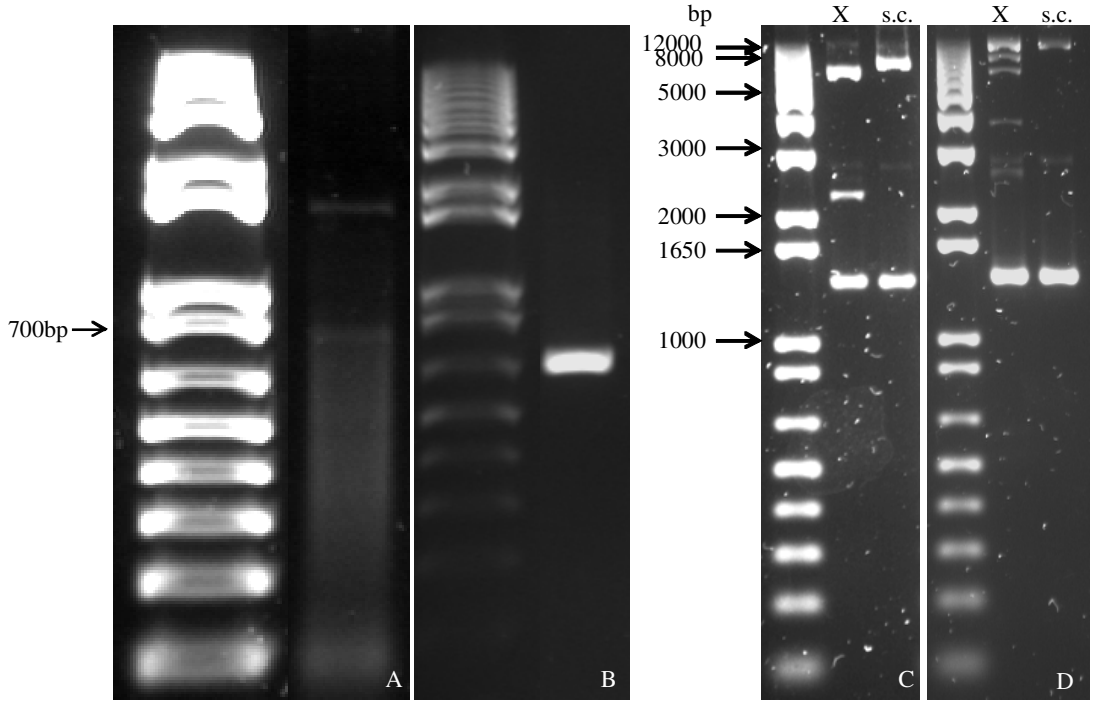

Figure 6-20. Analysis of pLP-Adeno-X-TRE-ppANF-eGFP and pAdeno-X-LPTRE-ppANF-tdTomato. **A** and **B**) Colony PCR analysis of pLP-Adeno-X-TRE-ppANF-eGFP (**A**) and pAdeno-X-LPTRE-ppANF-tdTomato (**B**) using Adeno-X LP CMV Primer Mix. DNA fragments amplified – 660 bp. **C** and **D)** XhoI restriction digests (X) of pAdeno-X-LPTRE-ppANF-eGFP (**C**) and pAdeno-X-LPTRE-ppANF-tdTomato (**D**). DNA fragments expected (kb) – pAdeno-X-LPTRE-ppANF-eGFP: 14.5, 8.0, 5.0, 3.6, 2.5, 1.4, 0.6; pAdeno-X-LPTRE-ppANF-tdTomato – 14.5, 8.0, 5.8, 3.6, 2.5, 1.4, and 0.6. s.c. = undigested, supercoiled DNA.

PCR Mix	Sample (µl)	Negative Control (µl)	Final Concentration
PCR Buffer	10	10	1x
d'NTPs	1	1	0.2mM @
$MgCl_2$	4	4	2mM
Forward Primer (µM)	5	5	0.2 – 0.3 µM
Reverse Primer (µM)	5	5	0.2 – 0.3 µM
DNA (1ng/µl)	1	-	1ng/50µl
Taq Polymerase	0.25	0.25	1.25u
H_2O	23.75	24.75	-
Total Volume	50µl		

Table 6-1. Typical reaction mix for PCR.

PCR cycles	Temperature	Duration	No. of Cycles
Denaturation	95°C	2 min	1
Denaturation	95°C	1 min	32
Annealing	64°C	30 sec	
Elongation	72°C	1 min 30 sec	
Elongation	72°C	5 min	1
Hold	4°C	Indefinite	-

Table 6-2. PCR Cycles for the amplification of DNA fragment.

DNA fragment amplified	Forward primers	Reverse primers
ppANF	GCTCAAGCTTATGGGCTCCTTCTCCATCACCAAG	ACTGACCGGTCGTCGGTACCGGAAGCTGTTGCAG
ppANF-eGFP	TCACGCTAGCCAGATGGGCTCCTTCTCCATCAC	TATGGCTGATTATGATCTAGAGTCG
tdTomato	TCACACCGGTCCACGCACAAGCCACCATGGTGAGCAAGGG	CAGACGGCCGCTTTACTTGTACAGCTCGTCCATG
ppANF-Timer	TCACGCTAGCATGGGCTCCTTCTCCATCACCAA	CCAGACAAGTTGGTAATGGTAGCG
Timer	TCAGGCTAGCATGGTGCGCTCCTCCAAGAACGT	CCAGACAAGTTGGTAATGGTAGCG
ppANF-tdTomato	GCTCAAGCTTATGGGCTCCTTCTCCATCACCAAG	CAGATCTAGATTACTTGTACAGCTCGTCCATG

Table 6-3. Primers used in PCR amplification of DNA fragments for subcloning. Forward and reverse primers listed in 5' to 3' for each DNA fragment amplified.

	Insert DNA (µl)	Vector DNA (µl)			
DNA (1 µg/µl)	30	5	1	1	1
Enzyme 1	1	1	1	-	-
Enzyme 2	1	1	-	1	-
10x Digestion Buffer	4	2	2	2	2
H_2O	4	11	16	16	17
Total Volume	40	20			

Table 6-4. Conditions for a typical restriction digest.

	3:1 (µl)	1:1 (µl)	1:5 (µl)	1:10 (µl)	Control 1 (µl)	Control 2 (µl)
Vector DNA (100ng/µl)	1	1	1	1	1	1
Insert DNA (1.4 kb, 33ng/µl)	0.3	1	4.5	8.9	-	-
T4 ligase	1	1	1	1	1	-
2x Ligation Buffer	5	5	6.5	10.9	5	5
H_2O	2.7	2	-	-	3	4
Total Volume	10	10	13	21.8	10	10

Table 6-5. Conditions for a typical ligation reaction.

PCR cycles	Temperature	Duration	No. of Cycles
Denaturation	94°C	2 min	1
Denaturation	94°C	1 min	32
Annealing	64°C	30 sec	
Elongation	68°C	1 min 30 sec	
Elongation	68°C	5 min	1
Hold	4°C	Indefinite	-

Table 6-6. PCR Cycles for the screening of recombinant pAdeno-X and pLP-Adeno-X.

Chapter 7
Discussion

7. DISCUSSION

It is known that dendritic peptide release is temporally and functionally different from axonal terminal release (Ludwig *et al.* 2002). However, the mechanism regulating this difference in peptide release is not fully understood. The present study investigated the mechanism of dendritic peptide release by studying the regulation of vesicle pools in dendrites. Intracellular mobilisation of calcium is known to recruit vasopressin-containing vesicles to the periphery of the plasma membrane (Tobin *et al.* 2004), suggesting the recruitment of a reserve vesicle pool for release. In peptide-releasing bovine adrenal chromaffin cells, newly synthesised vesicles were found to be preferentially recruited to the readily releasable pool whilst aged vesicles made up the reserve pool (Duncan *et al.* 2003; Wiegand *et al.* 2003), suggesting vesicular age is an important factor for vesicle pool regulation. It is not known whether magnocellular dendrites contain vesicle pools functionally different depending on age, and it is not known if there are specific mechanisms governing the routing of vesicles to dendrites.

7.1 Vesicle pools and routing

The segregation of different LDCV vesicle pools in axonal terminals and in endocrine cell lines are well documented. These vesicle pools were found to be functionally different from each other where depolarisation of the cell membrane

initially triggers the release of the RRP and prolonged depolarisation triggers release of the RP (Horrigan & Bookman 1994; Voets *et al.* 1999). Previous morphological studies found that lysosomes are present in magnocellular dendrites (Morris & Dyball 1974), which suggests the existence of the machinery for degradation of aged organelles, including unreleased LDCVs in these parts of the neurons. The present study found that lysosomes in magnocellular dendrites are significantly correlated with high vasopressin density, suggesting that lysosomes in magnocellular dendrites have important functions in the degradation of vasopressin LDCVs. Lysosomes were found to be located in the centre of dendrites, suggesting that they are ideally positioned to handle aged, non-released LDCVs. Although lysosomes were found in magnocellular dendrites and were found to be correlated with high vasopressin density, it was not known whether dendrites are important compartments for degradation like the Herring bodies found in neuronal terminals (Heap *et al.* 1975; Krsulovic *et al.* 2005). If dendrites were compartments of degradation; i.e. a compartment filled with aged vesicles ready to be degraded, then aged vesicles may be specifically routed to dendrites. However, using low temperature to block vesicle exit from the GA revealed that newly synthesised vesicles do translocate to dendrites indicating that dendrites contain a mixture of newly synthesised vesicles and aged vesicles and that vesicle routing to magnocellular dendrites is not dependant on vesicle age. Since dendrites are structures of ~200 µm in length, it is interesting to find out whether newly synthesised vesicles translocate to specific parts of dendrites. If newly synthesised vesicles were specifically translocated to any portion of the dendritic profile, this might suggest that different portions of a dendrite have different release properties. Tracking of newly packaged vesicles from the GA along

the profile of dendrites suggested that there was no difference in the distribution of newly assembled vesicles from the GA. This suggests that release properties are similar in all parts of a dendrite. Although dendrites measured in this study only represent the proximal to middle portion of the full lengths of dendrites, this result agreed with the finding that all parts of the dendritic membranes were capable of exocytosis (Pow & Morris 1989) and no active zones for release were found. Hence, if newly synthesised vesicles were preferentially recruited for readily releasable pool secretion, there is no difference in preferential release throughout the length of dendrites.

In bovine adrenal chromaffin cells, the divalent cation barium was found to preferentially release vesicles from the reserve vesicle pool and possibly the non-releasable pool (Seward *et al.* 1996; Duncan *et al.* 2003) indicating that barium was able to activate a distinct release pathway specific to vesicles in the reserve pool. Reserve pool vesicles in magnocellular dendrites are known to potentiate stimulus-dependent release (Ludwig *et al.* 2002); however, whether vesicles from the reserve pool can also be preferentially released from magnocellular dendrites and hence has differential functions to RRP vesicles is unknown. In contrast, Ba^{2+} was found to be unable to stimulate reserve vesicle pool or non-releasable pool release from neurohypophysial terminals (Seward *et al.* 1996). The model proposed by Heap *et al.* 1975 and later extended by Krsulovic *et al.* 2005 suggested that in the neural lobe, the RRP vesicles are found in endings and RP vesicles are segregated in specialised swellings and Herring bodies where there is a lower chance for re-recruitment for

release. Since dendrites do not contain the specialised compartmentalisation found in the neural lobe, it would be interesting to find out whether RP vesicles have distinct release mechanisms as found in chromaffin cells. Meanwhile, LDCVs found in the Herring bodies represent aged vesicles which cannot be recruited for release (Krsulovic *et al.* 2005). Aged LDCVs in the neural lobe are known to undergo continuous proteolysis (Nordmann & Labouesse 1981) and contain less hormones than newly synthesised vesicles either due to continual proteolysis or leakage through vesicular membrane (Nordmann & Morris 1984). It is not known whether dendrites also contain a non-releasable pool of vesicles. If aged vesicles with different peptide content can be recruited for release, will there be functional differences between release of newly synthesised and aged vesicles? Nevertheless, presence of newly synthesised vesicles and lysosomes in dendrites ensures plasticity in response to change in demands for dendritic peptide release.

7.2 New tools for studying dendritic peptide release

Organotypic slice cultures are known for their advantages in the preservation of differentiated neurons where synaptic connections are maintained in the process of culture. Moreover, they allow for pharmacological and gene transfer experimentations. In the present study, live cell imaging of dendritic peptide release was successfully carried out using organotypic slice cultures of the hypothalamus of neonatal VP-eGFP rats. Although vasopressin is known to be present in the

hypothalamus before birth (Sinding *et al.* 1980b), systemic activation of the SON in neonatal rats has not been shown. The activation of the SON after systemic osmotic challenge found in this study proves the physiological significance in using neonatal rats for further studies.

Several problems were encountered using brain slices for live cells imaging. Firstly, instability and movements in both the microscope and the tissue are the major problems. A 1^{o}C change in temperature of the microscope set up could account for a 1 µm movement in the lateral or axial direction (Kasparov *et al.* 2002). Therefore, it was important to minimise these movements by the use of environmental chambers, heated microscope stage, heated solutions and by taking a stack of images in the Z direction to make sure that the whole cell is accounted for. An environmental chamber had been used to keep the temperature on the microscope stage stable. Solution flow rate and change of solution can also affect displacement of the tissue. Hence, two outflow tubes had been attached to the perfusion chamber to ensure steady flow of solutions. Aside from the inherent problems encountered from the microscope set up, scattering of light and difference in light absorbance throughout the thickness of the section affect the resulting image quality. These affect organotypic slice cultures to a lesser extent since cultures are made from neonatal animals which are optically optimal; and slice explants flatten to a few cell layers. Nevertheless, to image whole neuronal cell bodies along with their dendritic projections may require imaging depths of tens of micrometers. This depth of image is in itself a problem since fluorescence from the top of the image has less distance to

travel compared to fluorescence from within the tissue; i.e. fluorescent intensity is stronger at the top of the image. This has to be taken into consideration when quantifying fluorescent intensity and hence, 10 optical slices (~1.67 µm in total) in the centre of the stack were selected for image analysis. Lastly, photobleaching and phototoxicity are the most important factors of concern in live cell imaging. The fluorescence used in the live cell imaging experiments is eGFP, which is a mutated (S65T) version of wild-type green fluorescent protein, GFP. Photobleaching in eGFP had been reported to be relatively low (Swaminathan *et al.* 1997; Tsien 1998) making it suitable as a reporter protein in live cell imaging experiments. Live cell imaging of VP-eGFP in organotypic slice cultures revealed significant loss of VP-eGFP within dendrites after depolarisation by 50 mM K^+ and further potentiated release by depolarisation after thapsigargin pre-treatment. This is in accordance with findings in *in vitro* experiments where isolated SON was stimulated and release measured by radioimmunoassays (Ludwig *et al.* 2002; Ludwig *et al.* 2005). The live cell imaging protocol established further confirmed the findings that thapsigargin was able to potentiate dendritic vasopressin release subsequent to high K^+ stimulation. Since the amount of VP-eGFP loss found in the live cell imaging experiments was comparable to the percentage of vasopressin release found in *in vitro* experiments (please refer to Chapter 4), live cell imaging using organotypic slice explants proves to be a robust model to study dendritic peptide release.

The experimental models established allow for targeted gene transfer to be carried out in conjunction with live cell imaging to study the segregation of vesicle pools in magnocellular dendrites. Non-dividing cells, such as neurons, are known to be

difficult to transfect using standard transfection techniques. The biolistic technique had been shown to be successful in transfecting magnocellular neurons (Thomas *et al.* 1998). The present study also showed that biolistic transfection is an effective method to transfect magnocellular neurons. Although the number of neurons transfected using this technique is relatively low, compared to the total number of cells transfected, it is possible to target gene expression to neurons by driving gene expression with neuronal specific promoters (Thomas *et al.* 1998), hence reducing the total number of transfected cells and allowing better identification of transfected neuronal cells. However, the major problem encountered with biolistic transfection in this study is the light reflection caused by scattered gold particles used as "bullets" for transfection. Since gold particles are scattered throughout the tissue, and the amount of reflected light varies (personal observation), it is difficult to judge the actual size of the particles. This study focuses on the dynamics and segregation of vesicle pools in magnocellular dendrites and hence, gold particle reflection which resembles fluorescently labelled LDCVs, made this technique unsuitable for further optimisation and use for further studies.

Therefore, to express exogenous fluorescent reporter proteins in LDCVs to study the release of different vesicle pools, the adenoviral transduction system was used. The adenoviral system chosen was an inducible system whereby expression of exogenous reporter proteins can be switched on/off by addition of doxycycline. To confirm that ppANF-tagged reporter proteins were expressed in LDCVs, N2a cells were transfected and then immunolabelled for chromogranin A expression. Colocalisation

analysis showed that ppANF-tagged reporter proteins were expressed in LDCVs. The fluorescent time-stamp pTimer had also been tested for expression in LDCVs. However, the fluorescent Timer did not produce desirable expression when tagged to ppANF. This had further been analysed by subcloning the non-ppANF tagged pTimer DNA into the inducible pTRE-shuttle vector for expression. N2a cells transfected with pTRE-Timer expressed red and green fluorescence as expected. Since pTimer tagged to ppANF did not result in expression in LDCVs, two other fluorophores were chosen for expression: ppANF-eGFP and ppANF-tdTomato. Expression of these two constructs, subcloned into the inducible pTRE-shuttle vector when co-transfected with pTet-on, resulted in fluorescent expression in LDCVs. Studies on vesicle segregation using double transfected PC12 cells (pTRE-ppANF-tdTomato and pTet-on) showed that pulse labelling experiments were able to label different vesicle pools after 24 hr, proving that pulse-labelling was efficient in identifying vesicle pools. Although this study started out with using the pAdeno-X coupled to the tet-on system, the pAdeno-X DNA was found to be damaged (**Figures 6-16 and 6-17**); hence, the viral system was replaced with the pLP-Adeno-X-TRE tet-off system. Adenovirus-induced transduction coupled with the tTA had been previously shown in cultured hippocampal neurons (Harding *et al.* 1997; Ralph *et al.* 2000) and since expression of exogenous proteins can be switched off simply by adding doxycycline to the culture medium, the LP-Adeno-X-TRE virus is an ideal candidate to be used for pulse chase labelling experiments in magnocellular dendrites. Subcloning of ppANF-eGFP and ppANF-tdTomato into a donor vector, pDNR-CMV vector, ensured the correct insertion of ppANF-eGFP and ppANF-tdTomato into the pLP-Adeno-X-TRE vector. The use of ppANF-eGFP as a reporter

gene allows for pulse-chase labelling where magnocellular neurons can be identified by immunolabelling. In addition, the use of ppANF-tdTomato as a reporter gene allows for pulse-chase labelling experiments to be carried out in conjunction with live cell imaging of magnocellular dendrites from VP-eGFP rats. Furthermore, the inducible adenoviral constructs can be used in *in vivo* transduction of magnocellular neurons where expression of reporter proteins have been demonstrated by injection of adenoviral constructs directly into the SON or via retrograde uptake of the adenovirus by injection of the neural lobe (Vasquez *et al.* 1998; Vasquez *et al.* 2001). *In vivo* transduction allows pulse-chase labelling to be carried out in intact infected animals where visualisation of vesicle pool segregation in magnocellular dendrites can be carried out on perfusion fixed brain sections. Live cell imaging of magnocellular dendrites can also be achieved by culturing sections of the hypothalamus of VP-eGFP rats infected with inducible ppANF-tdTomato. The induction of viral constructs containing the TRE-coupled promoter *in vivo* has been achieved by simply adding doxycycline to drinking water (Lee *et al.* 2005). Hence, the successful production of the pLP-Adeno-X-TRE-ppANF-tdTomato construct brought us one step closer to the visualisation of vesicle pool segregation in magnocellular dendrites.

7.3 Future directions

With the successful production of adenoviruses containing the pLP-Adeno-X-TRE-ppANF-tdTomato construct, LDCVs in magnocellular neurons can be labelled. Preferential release by recruitment of specific pools, for example barium recruitment

of the reserve/non-releasable pool (Seward *et al.* 1996; Duncan *et al.* 2003) can also be studied to investigate the functional difference of vesicle pools. *In vivo* injection of the inducible viral constructs can be combined with physiological assays or visualisation techniques to study release mechanisms of different vesicle pools. Infection of magnocellular vasopressin neurons prior to salt loading, whilst terminating reporter protein expression at different time points, will provide an understanding to the functional significance of different vesicle pools in magnocellular dendrites.

On the molecular level, although there is evidence that SNARE-associated proteins are involved in dendritic peptide release in magnocellular neurons: synaptotagmin, SNAP-25 and syntaxin (Schwab *et al.* 2001), VAMP/synaptobrevin (de Kock *et al.* 2003), and α-SNAP (Morris *et al.* 2000); immunolabelling revealed that VAMP2, the major VAMP isoform found in magnocellular nerve terminals (Jurgutis *et al.* 1996), was absent in magnocellular dendrites (Ludwig *et al.* 2006). Hence, magnocellular dendrites use a different isoform of VAMP compared to axon terminals to regulate exocytosis. In dopaminergic neurons, botulinum toxin B, which cleaves VAMP, inhibited exocytosis from dopaminergic nerve terminals but not from the somato-dendritic compartment, leading to speculation that different VAMP isoforms can be present in terminals and in the soma/dendrites. A possible VAMP isoform, VAMP4, has been found to be upregulated in the SON after a hypoosomolar challenge (Mutsuga *et al.* 2005), indicating that VAMP4 may have important functions in dendritic peptide release. Identification of specific VAMP isoforms found in

magnocellular dendrites will allow specific targeting of dendritic peptide release via expression of dominant negative genes or siRNA. Expression of a dominant negative form of VAMP had been shown in chromaffin cells to result in reduced exocytotic events (Sorensen *et al.* 2002). Meanwhile, targeting of siRNA to magnocellular neurons has also been achieved *in vivo* (Jensen *et al.* 2008). Identification of other SNARE-associated proteins is also important in decoding the molecular mechanisms of dendritic peptide release. Munc18, which binds syntaxin at its closed conformation to prevent SNARE complex formation (Nicholson *et al.* 1998; Han *et al.* 2009; Rickman & Duncan 2010), and Ca^{2+}-dependent activator protein (CAPS 1) which plays an important role in exocytosis downstream of vesicle docking (Fujita *et al.* 2007), have both been reported in magnocellular dendrites (Ludwig *et al.* 2006).

Furthermore, membrane capacitance measurements showed evidence that endocytosis occurs in the somata/dendrites of magnocellular neurons (Soldo *et al.* 2004; de Kock *et al.* 2003). The endocytotic machinery in magnocellular soma/dendrites has not been investigated in detail. The development of a fixable membrane dye, FM1-43FX (green) and FM4-64FX (red) (Invitrogen), provides a means to study endocytosis and vesicle recycling in magnocellular dendrites in slice preparation where the cytoarchitecture of dendrites is retained. In hippocampal neurons, LDCV recycling and kiss-and-run exocytosis of peptide-vesicles had been demonstrated in soma and dendrites (Xia *et al.* 2009). Kiss-and-run exocytosis has also been demonstrated in LDCVs in nerve terminals in posterior pituitary

preparations (Klyachko & Jackson 2002). In pancreatic β cells, kiss-and run exocytosis of LDCVs was shown to release small molecules such as ATP that is co-packaged with insulin (MacDonald *et al.* 2006). It is not known whether vesicle recycling and kiss-and-run exocytosis occurs in magnocellular dendrites. Uptake of the FM dye in dendrites will demonstrate endocytosis, whereas, subsequent stimulation protocol to look at release of the membrane dye will suggest whether magnocellular dendrites contain recycling vesicles. In addition, neurons containing VP-eGFP can be employed to study kiss-and-run exocytosis in dendrites where uptake of membrane dyes colocalised with eGFP would suggest partial release of vesicle content.

7.4 Conclusion

Dendritic peptide release from magnocellular neurons serves as an important source of peptides in the brain. Dendritic release of vasopressin and oxytocin has been shown to be important in autoregulation and paracrine control of neuronal activity. Peptides found in the CSF are believed to be released from dendrites and hence, dendritic peptide release has been implicated in the regulation of behaviour (Ludwig & Leng 2006). The temporal and functional difference between dendritic and axon terminal peptide release in magnocellular neurons indicate differences in the mechanisms regulating release in these two compartments. The finding that newly synthesised LDCVs translocate to dendrites suggests that dendritic peptide release can be up- or down-regulated independent of axon terminal release. Moreover, dendrites also contain their own resources for degradation, indicating that dendrites

are self-sufficient compartments for the destruction of aged organelles. The live cell imaging technique established will be invaluable in studying the regulation LDCV release in a system where homologous cell lines are unavailable. Furthermore, inducible reporter proteins targeted to LDCVs are essential to label different vesicle pools. *In vivo* or *in vitro* viral transduction with targeted proteins for expression in LDCVs can hence further our understanding in vesicle pool segregation in magnocellular dendrites.

Reference List

Aguilera G & Rabadan-Diehl C 2000 Vasopressinergic regulation of the hypothalamic-pituitary-adrenal axis: implications for stress adaptation. *Regul.Pept.* **96** 23-29.

Aisenbrey GA, Handelman WA, Arnold P, Manning M & Schrier RW 1981 Vascular effects of arginine vasopressin during fluid deprivation in the rat. *J.Clin.Invest* **67** 961-968.

Aitken PG, Breese GR, Dudek FF, Edwards F, Espanol MT, Larkman PM, Lipton P, Newman GC, Nowak TS, Jr., Panizzon KL & . 1995 Preparative methods for brain slices: a discussion. *J.Neurosci.Methods* **59** 139-149.

Aiyer MS, Chiappa SA & Fink G 1974 A priming effect of luteinizing hormone releasing factor on the anterior pituitary gland in the female rat. *J.Endocrinol.* **62** 573-588.

Alberts B, Bray D, Lewis J, Raff M, Roberts K & Watson JD 1994 Vesicular Traffic in the Secretory and Endocytic Pathways. In *Molecular Biology of the Cell*, edn Third, pp 599-651. Ed Miranda Robertson. Garland Publishing Inc.

Alonso G & Assenmacher I 1981 Radioautographic studies on the neurohypophysial projections of the supraoptic and paraventricular nuclei in the rat. *Cell Tissue Res.* **219** 525-534.

Alonso G & Assenmacher I 1983 Retrograde axoplasmic transport of neurosecretory material. An immunocytochemical and electron-microscopic study of transected axons in normal and colchicine-treated rats. *Cell Tissue Res.* **233** 183-196.

Altman J & Bayer SA 1986 The development of the rat hypothalamus. *Adv.Anat.Embryol.Cell Biol.* **100** 1-178.

Andrejewski N, Punnonen EL, Guhde G, Tanaka Y, Lullmann-Rauch R, Hartmann D, von Figura K & Saftig P 1999 Normal lysosomal morphology and function in LAMP-1-deficient mice. *J Biol.Chem.* **274** 12692-12701.

Andrews ZB 2005 Neuroendocrine regulation of prolactin secretion during late pregnancy: easing the transition into lactation. *J.Neuroendocrinol.* **17** 466-473.

Antoni FA 1993 Vasopressinergic control of pituitary adrenocorticotropin secretion comes of age. *Front Neuroendocrinol.* **14** 76-122.

Aravanis AM, Pyle JL & Tsien RW 2003 Single synaptic vesicles fusing transiently and successively without loss of identity. *Nature* **423** 643-647.

Armstrong WE 1995 Morphological and electrophysiological classification of hypothalamic supraoptic neurons. *Prog.Neurobiol.* **47** 291-339.

Armstrong WE, Scholer J & McNeill TH 1982 Immunocytochemical, Golgi and electron microscopic characterization of putative dendrites in the ventral glial lamina of the rat supraoptic nucleus. *Neuroscience* **7** 679-694.

Armstrong WE, Warach S, Hatton GI & McNeill TH 1980 Subnuclei in the rat hypothalamic paraventricular nucleus: a cytoarchitectural, horseradish peroxidase and immunocytochemical analysis. *Neuroscience* **5** 1931-1958.

Arnold D, Feng L, Kim J & Heintz N 1994 A strategy for the analysis of gene expression during neural development. *Proc.Natl.Acad.Sci.U.S.A* **91** 9970-9974.

Arnold DB & Clapham DE 1999 Molecular determinants for subcellular localization of PSD-95 with an interacting K+ channel. *Neuron* **23** 149-157.

Bamberger AM, Pu LP, Cool DR & Loh YP 1995 The Neuro-2a neuroblastoma cell line expresses [Met]-enkephalin and vasopressin mRNA and peptide. *Mol.Cell Endocrinol.* **113** 155-163.

Bankir L 2001 Antidiuretic action of vasopressin: quantitative aspects and interaction between V1a and V2 receptor-mediated effects. *Cardiovasc.Res.* **51** 372-390.

Barberis C, Mouillac B & Durroux T 1998 Structural bases of vasopressin/oxytocin receptor function. *J.Endocrinol.* **156** 223-229.

Bay AEP, Ibañez LI & Marengo FD 2007 Rapid recovery of releasable vesicles and formation of nonreleasable endosomes follow intense exocytosis in chromaffin cells. *Am J Physiol Cell Physiol* **293** C1509-C1522.

Beagley GH & Hatton GI 1992 Rapid morphological changes in supraoptic nucleus and posterior pituitary induced by a single hypertonic saline injection. *Brain Res.Bull.* **28** 613-618.

Ben Barak Y, Russell JT, Whitnall MH, Ozato K & Gainer H 1985 Neurophysin in the hypothalamo-neurohypophysial system. I. Production and characterization of monoclonal antibodies. *J.Neurosci.* **5** 81-97.

Benda P, De Vitry F, Picart R & Tixier-Vidal A 1975 Dissociated cell cultures from fetal mouse hypothalamus. Patterns of organization and ultrastructural features. *Exp.Brain Res.* **23** 29-47.

Berciano MT, Villagra NT, Pena E, Navascues J, Casafont I & Lafarga M 2002 Structural and functional compartmentalization of the cell nucleus in supraoptic neurons. *Microsc.Res.Tech.* **56** 132-142.

Bicknell RJ & Leng G 1981 Relative efficiency of neural firing patterns for vasopressin release in vitro. *Neuroendocrinology* **33** 295-299.

Blume A, Bosch OJ, Miklos S, Torner L, Wales L, Waldherr M & Neumann ID 2008 Oxytocin reduces anxiety via ERK1/2 activation: local effect within the rat hypothalamic paraventricular nucleus. *Eur.J.Neurosci.* **27** 1947-1956.

Boland B, Kumar A, Lee S, Platt FM, Wegiel J, Yu WH & Nixon RA 2008 Autophagy induction and autophagosome clearance in neurons: relationship to autophagic pathology in Alzheimer's disease. *J.Neurosci.* **28** 6926-6937.

Boland B & Nixon RA 2006 Neuronal macroautophagy: from development to degeneration. *Mol.Aspects Med.* **27** 503-519.

Bosch OJ, Meddle SL, Beiderbeck DI, Douglas AJ & Neumann ID 2005 Brain oxytocin correlates with maternal aggression: link to anxiety. *J.Neurosci.* **25** 6807-6815.

Bourque CW 1998 Osmoregulation of vasopressin neurons: a synergy of intrinsic and synaptic processes. *Prog.Brain Res.* **119** 59-76.

Bright NA, Gratian MJ & Luzio JP 2005 Endocytic delivery to lysosomes mediated by concurrent fusion and kissing events in living cells. *Curr.Biol.* **15** 360-365.

Brimble MJ, Dyball RE & Forsling ML 1978 Oxytocin release following osmotic activation of oxytocin neurones in the paraventricular and supraoptic nuclei. *J.Physiol* **278** 69-78.

Broadwell RD, Oliver C & Brightman MW 1980 Neuronal transport of acid hydrolases and peroxidase within the lysosomal system or organelles: involvement of agranular reticulum-like cisterns. *J.Comp Neurol.* **190** 519-532.

Brownstein MJ 1983 Biosynthesis of vasopressin and oxytocin. *Annu.Rev.Physiol* **45** 129-135.

Brunton PJ & Russell JA 2008 The expectant brain: adapting for motherhood. *Nat.Rev.Neurosci.* **9** 11-25.

Buijs RM, Geffard M, Pool CW & Hoorneman EM 1984 The dopaminergic innervation of the supraoptic and paraventricular nucleus. A light and electron microscopical study. *Brain Res.* **323** 65-72.

Buijs RM & Swaab DF 1979 Immuno-electron microscopical demonstration of vasopressin and oxytocin synapses in the limbic system of the rat. *Cell Tissue Res.* **204** 355-365.

Buijs RM, van Eden CG, Goncharuk VD & Kalsbeek A 2003 The biological clock tunes the organs of the body: timing by hormones and the autonomic nervous system. *J.Endocrinol.* **177** 17-26.

Buma P, Roubos EW & Buijs RM 1984 Ultrastructural demonstration of exocytosis of neural, neuroendocrine and endocrine secretions with an in vitro tannic acid (TARI-) method. *Histochemistry* **80** 247-256.

Burbach JP, Luckman SM, Murphy D & Gainer H 2001 Gene regulation in the magnocellular hypothalamo-neurohypophysial system. *Physiol Rev.* **81** 1197-1267.

Burke NV, Han W, Li D, Takimoto K, Watkins SC & Levitan ES 1997 Neuronal peptide release is limited by secretory granule mobility. *Neuron* **19** 1095-1102.

Bush PG, Wokosin DL & Hall AC 2007 Two-versus one photon excitation laser scanning microscopy: critical importance of excitation wavelength. *Front Biosci.* **12** 2646-2657.

Cajal RS 1891 Significacion fisologica de las expansiones protoplasmatica y nerviosas de las celulas de la substancia gris. *Rev Cie Med Barcelona* **22** 23.

Caldwell HK, Lee HJ, Macbeth AH & Young WS, III 2008a Vasopressin: behavioral roles of an "original" neuropeptide. *Prog.Neurobiol.* **84** 1-24.

Caldwell HK, Wersinger SR & Young WS, III 2008b The role of the vasopressin 1b receptor in aggression and other social behaviours. *Prog.Brain Res.* **170** 65-72.

Caldwell JD & Moe BD 1999 Conjugated estradiol increases female sexual receptivity in response to oxytocin infused into the medial preoptic area and medial basal hypothalamus. *Horm.Behav.* **35** 38-46.

Callahan MF, Ludwig M, Tsai KP, Sim LJ & Morris M 1997 Baroreceptor input regulates osmotic control of central vasopressin secretion. *Neuroendocrinology* **65** 238-245.

Campbell RE, Tour O, Palmer AE, Steinbach PA, Baird GS, Zacharias DA & Tsien RY 2002 A monomeric red fluorescent protein. *Proc.Natl.Acad.Sci.U.S.A* **99** 7877-7882.

Castino R, Davies J, Beaucourt S, Isidoro C & Murphy D 2005a Autophagy is a prosurvival mechanism in cells expressing an autosomal dominant familial neurohypophyseal diabetes insipidus mutant vasopressin transgene. *FASEB J* **19** 1021-1023.

Castino R, Isidoro C & Murphy D 2005b Autophagy-dependent cell survival and cell death in an autosomal dominant familial neurohypophyseal diabetes insipidus in vitro model. *FASEB J* **19** 1024-1026.

Catheline G, Touquet B, Lombard MC, Poulain DA & Theodosis DT 2006 A study of the role of neuro-glial remodeling in the oxytocin system at lactation. *Neuroscience* **137** 309-316.

Chapman DB, Theodosis DT, Montagnese C, Poulain DA & Morris JF 1986 Osmotic stimulation causes structural plasticity of neurone-glia relationships of the oxytocin but not vasopressin secreting neurones in the hypothalamic supraoptic nucleus. *Neuroscience* **17** 679-686.

Chen I & Dubnau D 2004 DNA uptake during bacterial transformation. *Nature Rev.Microbiol.* **2** 241-249.

Chen TS, Zeng SQ, Luo QM, Zhang ZH & Zhou W 2002 High-order photobleaching of green fluorescent protein inside live cells in two-photon excitation microscopy. *Biochem.Biophys.Res.Commun.* **291** 1272-1275.

Cheramy A, Leviel V & Glowinski J 1981 Dendritic release of dopamine in the substantia nigra. *Nature* **289** 537-542.

Chevaleyre V, Dayanithi G, Moos FC & Desarmenien MG 2000 Developmental regulation of a local positive autocontrol of supraoptic neurons. *J.Neurosci.* **20** 5813-5819.

Chevaleyre V, Moos FC & Desarmenien MG 2001 Correlation between electrophysiological and morphological characteristics during maturation of rat supraoptic neurons. *Eur.J.Neurosci.* **13** 1136-1146.

Cho ES, Lee SY, Park JY, Hong SG & Ryu PD 2007 Organotypic slice culture of the hypothalamic paraventricular nucleus of rat. *J.Vet.Sci.* **8** 15-20.

Cho MM, DeVries AC, Williams JR & Carter CS 1999 The effects of oxytocin and vasopressin on partner preferences in male and female prairie voles (Microtus ochrogaster). *Behav.Neurosci.* **113** 1071-1079.

Coltman BW & Ide CF 1996 Temporal characterization of microglia, IL-1 beta-like immunoreactivity and astrocytes in the dentate gyrus of hippocampal organotypic slice cultures. *Int.J Dev.Neurosci.* **14** 707-719.

Conde H 1992 Organization and physiology of the substantia nigra. *Exp.Brain Res.* **88** 233-248.

Costes SV, Daelemans D, Cho EH, Dobbin Z, Pavlakis G & Lockett S 2004 Automatic and quantitative measurement of protein-protein colocalization in live cells. *Biophys.J* **86** 3993-4003.

Crowley RS & Amico JA 1993 Gonadal steroid modulation of oxytocin and vasopressin gene expression in the hypothalamus of the osmotically stimulated rat. *Endocrinology* **133** 2711-2718.

Cuervo AM, Stefanis L, Fredenburg R, Lansbury PT & Sulzer D 2004 Impaired degradation of mutant alpha-synuclein by chaperone-mediated autophagy. *Science* **305** 1292-1295.

Curry WJ, Johnston CF, Hutton JC, Arden SD, Rutherford NG, Shaw C & Buchanan KD 1991 The tissue distribution of rat chromogranin A-derived peptides: evidence for differential tissue processing from sequence specific antisera. *Histochemistry* **96** 531-538.

Czapiga M & Colton CA 1999 Function of microglia in organotypic slice cultures. *J Neurosci.Res.* **56** 644-651.

Davies J & Murphy D 2002 Autophagy in hypothalamic neurones of rats expressing a familial neurohypophysial diabetes insipidus transgene. *J.Neuroendocrinol.* **14** 629-637.

Dayanithi G, Sabatier N & Widmer H 2000 Intracellular calcium signalling in magnocellular neurones of the rat supraoptic nucleus: understanding the autoregulatory mechanisms. *Exp.Physiol* **85 Spec No** 75S-84S.

de Bree FM, Van Der Kleij AA, Nijenhuis M, Zalm R, Murphy D & Burbach JP 2003 The Hormone Domain of the Vasopressin Prohormone is Required for the Correct Prohormone Trafficking Through the Secretory Pathway. *J.Neuroendocrinol.* **15** 1156-1163.

de Kock CP, Wierda KD, Bosman LW, Min R, Koksma JJ, Mansvelder HD, Verhage M & Brussaard AB 2003 Somatodendritic secretion in oxytocin neurons is upregulated during the female reproductive cycle. *J.Neurosci.* **23** 2726-2734.

Dellmann HD & Rodriguez EM 1970 Herring bodies; an electron microscopic study of local degeneration and regeneration of neurosecretory axons. *Z.Zellforsch.Mikrosk.Anat.* **111** 293-315.

DeVries AC, Young WS, III & Nelson RJ 1997 Reduced aggressive behaviour in mice with targeted disruption of the oxytocin gene. *J.Neuroendocrinol.* **9** 363-368.

Di S, Boudaba C, Popescu IR, Weng FJ, Harris C, Marcheselli VL, Bazan NG & Tasker JG 2005 Activity-dependent release and actions of endocannabinoids in the rat hypothalamic supraoptic nucleus. *J.Physiol* **569** 751-760.

Doussau F & Augustine GJ 2000 The actin cytoskeleton and neurotransmitter release: an overview. *Biochimie* **82** 353-363.

Drake CT, Terman GW, Simmons ML, Milner TA, Kunkel DD, Schwartzkroin PA & Chavkin C 1994 Dynorphin opioids present in dentate granule cells may function as retrograde inhibitory neurotransmitters. *J.Neurosci.* **14** 3736-3750.

Duncan RR, Greaves J, Wiegand UK, Matskevich I, Bodammer G, Apps DK, Shipston MJ & Chow RH 2003 Functional and spatial segregation of secretory vesicle pools according to vesicle age. *Nature* **422** 176-180.

Dyball RE & Garten LL 1988 Stimulus-related changes in the dendrites of magnocellular neurones. *Brain Res.Bull.* **20** 675-680.

Dyball RE & Kemplay SK 1982 Dendritic trees of neurones in the rat supraoptic nucleus. *Neuroscience* **7** 223-230.

Ehrengruber MU, Hennou S, Bueler H, Naim HY, Deglon N & Lundstrom K 2001 Gene transfer into neurons from hippocampal slices: comparison of recombinant Semliki Forest Virus, adenovirus, adeno-associated virus, lentivirus, and measles virus. *Mol.Cell Neurosci.* **17** 855-871.

Ehrhart-Bornstein M, Thorn NA & Treiman M 1990 Chronic osmotic stimulation reduces vasopressin but not synaptophysin content in rat neurohypophysis. *Neurosci.Lett.* **119** 122-124.

Engelmann M, Ebner K, Landgraf R, Holsboer F & Wotjak1 CT 1999 Emotional stress triggers intrahypothalamic but not peripheral release of oxytocin in male rats. *J.Neuroendocrinol.* **11** 867-872.

Ermisch A, Brust P, Kretzschmar R & Ruhle HJ 1993 Peptides and blood-brain barrier transport. *Physiol Rev.* **73** 489-527.

Eskelinen EL 2006 Roles of LAMP-1 and LAMP-2 in lysosome biogenesis and autophagy. *Mol.Aspects Med* **27** 495-502.

Eskelinen EL, Schmidt CK, Neu S, Willenborg M, Fuertes G, Salvador N, Tanaka Y, Lullmann-Rauch R, Hartmann D, Heeren J, von Figura K, Knecht E & Saftig P 2004 Disturbed cholesterol traffic but normal proteolytic function in LAMP-1/LAMP-2 double-deficient fibroblasts. *Mol.Biol.Cell* **15** 3132-3145.

Fahrbach SE, Morrell JI & Pfaff DW 1985 Possible role for endogenous oxytocin in estrogen-facilitated maternal behavior in rats. *Neuroendocrinology* **40** 526-532.

Felgner PL, Gadek TR, Holm M, Roman R, Chan HW, Wenz M, Northrop JP, Ringold GM & Danielsen M 1987 Lipofection: a highly efficient, lipid-mediated DNA-transfection procedure. *Proc.Natl.Acad.Sci.U.S.A* **84** 7413-7417.

Fields RL, House SB & Gainer H 2003 Regulatory domains in the intergenic region of the oxytocin and vasopressin genes that control their hypothalamus-specific expression in vitro. *J.Neurosci.* **23** 7801-7809.

Fisher AW, Price PG, Burford GD & Lederis K 1979 A 3-dimensional reconstruction of the hypothalamo-neurohypophysial system of the rat. The neurons projecting to the neuro/intermediate lobe and those containing vasopressin and somatostatin. *Cell Tissue Res.* **204** 343-354.

Fisher TE & Bourque CW 1995 Distinct omega-agatoxin-sensitive calcium currents in somata and axon terminals of rat supraoptic neurones. *J.Physiol* **489 (Pt 2)** 383-388.

Fisher TE & Bourque CW 1996 Calcium-channel subtypes in the somata and axon terminals of magnocellular neurosecretory cells. *Trends Neurosci.* **19** 440-444.

Freund-Mercier MJ, Moos F, Poulain DA, Richard P, Rodriguez F, Theodosis DT & Vincent JD 1988 Role of central oxytocin in the control of the milk ejection reflex. *Brain Res.Bull.* **20** 737-741.

Freund-Mercier MJ & Richard P 1981 Excitatory effects of intraventricular injections of oxytocin on the milk ejection reflex in the rat. *Neurosci.Lett.* **23** 193-198.

Freund-Mercier MJ, Stoeckel ME & Klein MJ 1994 Oxytocin receptors on oxytocin neurones: histoautoradiographic detection in the lactating rat. *J.Physiol* **480 (Pt 1)** 155-161.

Fujita Y, Xu A, Xie L, Arunachalam L, Chou TC, Jiang T, Chiew SK, Kourtesis J, Wang L, Gaisano HY & Sugita S 2007 Ca2+-dependent activator protein for secretion 1 is critical for constitutive and regulated exocytosis but not for loading of transmitters into dense core vesicles. *J Biol.Chem.* **282** 21392-21403.

Gahwiler BH, Capogna M, Debanne D, McKinney RA & Thompson SM 1997 Organotypic slice cultures: a technique has come of age. *Trends Neurosci.* **20** 471-477.

Gainer H, Fields RL & House SB 2001 Vasopressin gene expression: experimental models and strategies. *Exp.Neurol.* **171** 190-199.

Gerardo RP, Rosalinda MR, Guadalupe ML & Miguel CL 2010 Oxytocin, but not vassopressin, modulates nociceptive responses in dorsal horn neurons. *Neurosci.Lett.* **476** 32-35.

Gillard ER, Coburn CG, de Leon A, Snissarenko EP, Bauce LG, Pittman QJ, Hou B & Curras-Collazo MC 2007 Vasopressin autoreceptors and nitric oxide-dependent glutamate release are required for somatodendritic vasopressin release from rat magnocellular neuroendocrine cells responding to osmotic stimuli. *Endocrinology* **148** 479-489.

Gimpl G & Fahrenholz F 2001 The oxytocin receptor system: structure, function, and regulation. *Physiol Rev.* **81** 629-683.

Gimpl G, Reitz J, Brauer S & Trossen C 2008 Oxytocin receptors: ligand binding, signalling and cholesterol dependence. *Prog.Brain Res.* **170** 193-204.

Giovannelli L, Shiromani PJ, Jirikowski GF & Bloom FE 1992 Expression of c-fos protein by immunohistochemically identified oxytocin neurons in the rat hypothalamus upon osmotic stimulation. *Brain Res.* **588** 41-48.

Goedert M, Crowther RA & Garner CC 1991 Molecular characterization of microtubule-associated proteins tau and MAP2. *Trends Neurosci.* **14** 193-199.

Gorman AM 2008 Neuronal cell death in neurodegenerative diseases: recurring themes around protein handling. *J.Cell Mol.Med.* **12** 2263-2280.

Gossen M & Bujard H 1992 Tight control of gene expression in mammalian cells by tetracycline-responsive promoters. *Proc.Natl.Acad.Sci.U.S.A* **89** 5547-5551.

Gossen M & Bujard H 1995 Efficacy of tetracycline-controlled gene expression is influenced by cell type: commentary. *Biotechniques* **19** 213-216.

Gouzenes L, Desarmenien MG, Hussy N, Richard P & Moos FC 1998 Vasopressin regularizes the phasic firing pattern of rat hypothalamic magnocellular vasopressin neurons. *J.Neurosci.* **18** 1879-1885.

Graham FL & van der Eb AJ 1973 A new technique for the assay of infectivity of human adenovirus 5 DNA. *Virology* **52** 456-467.

Greber UF, Willetts M, Webster P & Helenius A 1993 Stepwise dismantling of adenovirus 2 during entry into cells. *Cell* **75** 477-486.

Greene LA & Tischler AS 1976 Establishment of a noradrenergic clonal line of rat adreanl pheochromocytoma cells which respond to nerve growth factor. *Proc.Natl.Acad.Sci.U.S.A* **73** 2424-2428.

Griffiths G, Pfeiffer S, Simons K & Matlin K 1985 Exit of newly synthesized membrane proteins from the trans cisterna of the Golgi complex to the plasma membrane. *J.Cell Biol.* **101** 949-964.

Griffiths G & Simons K 1986 The trans Golgi network: sorting at the exit site of the Golgi complex. *Science* **234** 438-443.

Grindstaff RR & Cunningham JT 2001 Cardiovascular regulation of vasopressin neurons in the supraoptic nucleus. *Exp.Neurol.* **171** 219-226.

Gu F & Gruenberg J 1999 Biogenesis of transport intermediates in the endocytic pathway. *FEBS Lett.* **452** 61-66.

Han L, Jiang T, Han GA, Malintan NT, Xie L, Wang L, Tse FW, Gaisano HY, Collins BM, Meunier FA & Sugita S 2009 Rescue of Munc18-1 and -2 double knockdown reveals the essential functions of interaction between Munc18 and closed syntaxin in PC12 cells. *Mol.Biol.Cell* **20** 4962-4975.

Han W, Ng YK, Axelrod D & Levitan ES 1999 Neuropeptide release by efficient recruitment of diffusing cytoplasmic secretory vesicles. *Proc.Natl.Acad.Sci.U.S.A* **96** 14577-14582.

Harata N, Pyle JL, Aravanis AM, Mozhayeva M, Kavalali ET & Tsien RW 2001 Limited numbers of recycling vesicles in small CNS nerve terminals: implications for neural signaling and vesicular cycling. *Trends Neurosci.* **24** 637-643.

Harding TC, Geddes BJ, Noel JD, Murphy D & Uney JB 1997 Tetracycline-regulated transgene expression in hippocampal neurones following transfection with adenoviral vectors. *J Neurochem.* **69** 2620-2623.

Hatton GI 1990 Emerging concepts of structure-function dynamics in adult brain: the hypothalamo-neurohypophysial system. *Prog.Neurobiol.* **34** 437-504.

Heap PF, Jones CW, Morris JF & Pickering BT 1975 Movement of neurosecretory product through the anatomical compartments of the neural lobe of the pituitary gland. An electron microscopic autoradiographic study. *Cell Tissue Res.* **156** 483-497.

Herbison AE, Voisin DL, Douglas AJ & Chapman C 1997 Profile of monoamine and excitatory amino acid release in rat supraoptic nucleus over parturition. *Endocrinology* **138** 33-40.

Hermes ML, Ruijter JM, Klop A, Buijs RM & Renaud LP 2000 Vasopressin increases GABAergic inhibition of rat hypothalamic paraventricular nucleus neurons in vitro. *J.Neurophysiol.* **83** 705-711.

Hernando F, Schoots O, Lolait SJ & Burbach JP 2001 Immunohistochemical localization of the vasopressin V1b receptor in the rat brain and pituitary gland: anatomical support for its involvement in the central effects of vasopressin. *Endocrinology* **142** 1659-1668.

Heuser JE, Reese TS, Dennis MJ, Jan Y, Jan L & Evans L 1979 Synaptic vesicle exocytosis captured by quick freezing and correlated with quantal transmitter release. *J Cell Biol.* **81** 275-300.

Hirasawa M, Schwab Y, Natah S, Hillard CJ, Mackie K, Sharkey KA & Pittman QJ 2004 Dendritically released transmitters cooperate via autocrine and retrograde actions to inhibit afferent excitation in rat brain. *J.Physiol* **559** 611-624.

Hirokawa N, Sobue K, Kanda K, Harada A & Yorifuji H 1989 The cytoskeletal architecture of the presynaptic terminal and molecular structure of synapsin 1. *J.Cell Biol.* **108** 111-126.

Hoffman GE, Smith MS & Verbalis JG 1993 c-Fos and related immediate early gene products as markers of activity in neuroendocrine systems. *Front Neuroendocrinol.* **14** 173-213.

Hokfelt T, Ceccatelli S, Gustafsson L, Hulting AL, Verge V, Villar M, Xu XJ, Xu ZQ, Wiesenfeld-Hallin Z & Zhang X 1994 Plasticity of NO synthase expression in the nervous and endocrine systems. *Neuropharmacology* **33** 1221-1227.

Horch HW, Kruttgen A, Portbury SD & Katz LC 1999 Destabilization of cortical dendrites and spines by BDNF. *Neuron* **23** 353-364.

Horrigan FT & Bookman RJ 1994 Releasable pools and the kinetics of exocytosis in adrenal chromaffin cells. *Neuron* **13** 1119-1129.

Hosoi N, Sakaba T & Neher E 2007 Quantitative analysis of calcium-dependent vesicle recruitment and its functional role at the calyx of Held synapse. *J Neurosci.* **27** 14286-14298.

House SB, Thomas A, Kusano K & Gainer H 1998 Stationary organotypic cultures of oxytocin and vasopressin magnocellular neurones from rat and mouse hypothalamus. *Journal of Neuroendocrinology* **10** 849-861.

Hsu SF & Jackson MB 1996 Rapid exocytosis and endocytosis in nerve terminals of the rat posterior pituitary. *J.Physiol* **494 (Pt 2)** 539-553.

Hurbin A, Boissin-Agasse L, Orcel H, Rabie A, Joux N, Desarmenien MG, Richard P & Moos FC 1998 The V1a and V1b, but not V2, vasopressin receptor genes are expressed in the supraoptic nucleus of the rat hypothalamus, and the transcripts are essentially colocalized in the vasopressinergic magnocellular neurons. *Endocrinology* **139** 4701-4707.

Hurbin A, Orcel H, Alonso G, Moos F & Rabie A 2002 The vasopressin receptors colocalize with vasopressin in the magnocellular neurons of the rat supraoptic nucleus and are modulated by water balance. *Endocrinology* **143** 456-466.

Huttner WB, Ohashi M, Kehlenbach RH, Barr FA, Bauerfeind R, Braunling O, Corbeil D, Hannah M, Pasolli HA, Schmidt A & . 1995 Biogenesis of neurosecretory vesicles. *Cold Spring Harb.Symp.Quant.Biol.* **60** 315-327.

Ignarro LJ 1990 Nitric oxide. A novel signal transduction mechanism for transcellular communication. *Hypertension* **16** 477-483.

Inoue T, Nonoguchi H & Tomita K 2001 Physiological effects of vasopressin and atrial natriuretic peptide in the collecting duct. *Cardiovasc.Res.* **51** 470-480.

Insel TR & Hulihan TJ 1995 A gender-specific mechanism for pair bonding: oxytocin and partner preference formation in monogamous voles. *Behav.Neurosci.* **109** 782-789.

Insel TR, Wang ZX & Ferris CF 1994 Patterns of brain vasopressin receptor distribution associated with social organization in microtine rodents. *J.Neurosci.* **14** 5381-5392.

Jahraus A, Tjelle TE, Berg T, Habermann A, Storrie B, Ullrich O & Griffiths G 1998 In vitro fusion of phagosomes with different endocytic organelles from J774 macrophages. *J.Biol.Chem.* **273** 30379-30390.

Jard S, Barberis C, Audigier S & Tribollet E 1987 Neurohypophyseal hormone receptor systems in brain and periphery. *Prog.Brain Res.* **72** 173-187.

Jellinger KA & Stadelmann C 2000 Mechanisms of cell death in neurodegenerative disorders. *J.Neural Transm.Suppl* **59** 95-114.

Jensen D, Zhang Z & Flynn FW 2008 Trafficking of tachykinin neurokinin 3 receptor to nuclei of neurons in the paraventricular nucleus of the hypothalamus following osmotic challenge. *Neuroscience* **155** 308-316.

Jiao S, Cheng L, Wolff JA & Yang NS 1993 Particle bombardment-mediated gene transfer and expression in rat brain tissues. *Biotechnology (N.Y.)* **11** 497-502.

Jirikowski G, Reisert I & Pilgrim C 1981 Neuropeptides in dissociated cultures of hypothalamus and septum: quantitation of immunoreactive neurons. *Neuroscience* **6** 1953-1960.

Jurgutis P, Shuang R, Fletcher A & Stuenkel EL 1996 Characterization and distribution of SNARE proteins at neuroendocrine nerve endings. *Neuroendocrinology* **64** 379-392.

Kalsbeek A, Buijs RM, Engelmann M, Wotjak CT & Landgraf R 1995 In vivo measurement of a diurnal variation in vasopressin release in the rat suprachiasmatic nucleus. *Brain Res.* **682** 75-82.

Kalsbeek A, Teclemariam-Mesbah R & Pevet P 1993 Efferent projections of the suprachiasmatic nucleus in the golden hamster (Mesocricetus auratus). *J.Comp Neurol.* **332** 293-314.

Kasparov S, Teschemacher AG & Paton JF 2002 Dynamic confocal imaging in acute brain slices and organotypic slice cultures using a spectral confocal microscope with single photon excitation. *Exp.Physiol* **87** 715-724.

Kawasaki M, Yamaguchi K, Saito J, Ozaki Y, Mera T, Hashimoto H, Fujihara H, Okimoto N, Ohnishi H, Nakamura T & Ueta Y 2005 Expression of immediate early genes and vasopressin heteronuclear RNA in the paraventricular and supraoptic nuclei of rats after acute osmotic stimulus. *J.Neuroendocrinol.* **17** 227-237.

Keir SD, House SB, Li J, Xiao X & Gainer H 1999 Gene transfer into hypothalamic organotypic cultures using an adeno-associated virus vector. *Exp.Neurol.* **160** 313-316.

Kelly RB 1985 Pathways of protein secretion in eukaryotes. *Science* **230** 25-32.

Kita I, Yoshida Y & Nishino S 2006 An activation of parvocellular oxytocinergic neurons in the paraventricular nucleus in oxytocin-induced yawning and penile erection. *Neurosci.Res.* **54** 269-275.

Klionsky DJ 2005 The molecular machinery of autophagy: unanswered questions. *J Cell Sci.* **118** 7-18.

Klyachko VA & Jackson MB 2002 Capacitance steps and fusion pores of small and large-dense-core vesicles in nerve terminals. *Nature* **418** 89-92.

Kobayashi H, Oota Y & Hirano T 1962 Acid phosphatase activity of the hypothalamo-hypophyseal system of dehydrated rats and pigeons in relation to neurosecretion. *Gen Comp Endocrinol* **2** 495-498.

Koike M, Shibata M, Waguri S, Yoshimura K, Tanida I, Kominami E, Gotow T, Peters C, von Figura K, Mizushima N, Saftig P & Uchiyama Y 2005 Participation of autophagy in storage of lysosomes in neurons from mouse models of neuronal ceroid-lipofuscinoses (Batten disease). *Am J Pathol.* **167** 1713-1728.

Kombian SB, Mouginot D, Hirasawa M & Pittman QJ 2000 Vasopressin preferentially depresses excitatory over inhibitory synaptic transmission in the rat supraoptic nucleus in vitro. *J.Neuroendocrinol.* **12** 361-367.

Krsulovic J, Peruzzo B, Alvial G, Yulis CR & Rodriguez EM 2005 The destination of the aged, nonreleasable neurohypophyseal peptides stored in the neural lobe is associated to the remodeling of the neurosecretory axon. *Microsc.Res.Tech.* **68** 347-359.

Kuromi H & Kidokoro Y 1998 Two distinct pools of synaptic vesicles in single presynaptic boutons in a temperature-sensitive Drosophila mutant, shibire. *Neuron* **20** 917-925.

Kuromi H & Kidokoro Y 2003 Two synaptic vesicle pools, vesicle recruitment and replenishment of pools at the Drosophila neuromuscular junction. *J.Neurocytol.* **32** 551-565.

Ladinsky MS, Wu CC, McIntosh S, McIntosh JR & Howell KE 2002 Structure of the Golgi and distribution of reporter molecules at 20 degrees C reveals the complexity of the exit compartments. *Mol.Biol.Cell* **13** 2810-2825.

Lambert RC, Dayanithi G, Moos FC & Richard P 1994 A rise in the intracellular Ca2+ concentration of isolated rat supraoptic cells in response to oxytocin. *J.Physiol* **478 (Pt 2)** 275-287.

Lambert RC, Moos FC & Richard P 1993 Action of endogenous oxytocin within the paraventricular or supraoptic nuclei: a powerful link in the regulation of the bursting pattern of oxytocin neurons during the milk-ejection reflex in rats. *Neuroscience* **57** 1027-1038.

Landgraf R & Ludwig M 1991 Vasopressin release within the supraoptic and paraventricular nuclei of the rat brain: osmotic stimulation via microdialysis. *Brain Res.* **558** 191-196.

Landgraf R & Neumann ID 2004 Vasopressin and oxytocin release within the brain: a dynamic concept of multiple and variable modes of neuropeptide communication. *Front Neuroendocrinol.* **25** 150-176.

Landry M, Vila-Porcile E, Hokfelt T & Calas A 2003 Differential routing of coexisting neuropeptides in vasopressin neurons. *Eur.J.Neurosci.* **17** 579-589.

Landry M, Xu ZQD, Calas A & Hokfelt T 2005 Galanin, A New Candidate for Somato-Dendritic Release. In *Dendritic Neurotransmitter Release*, pp 239-256. Ed M Ludwig. Springer.

Langle SL, Poulain DA & Theodosis DT 2003 Induction of rapid, activity-dependent neuronal-glial remodelling in the adult rat hypothalamus in vitro. *Eur.J.Neurosci.* **18** 206-214.

Lauf U, Lopez P & Falk MM 2001 Expression of fluorescently tagged connexins: a novel approach to rescue function of oligomeric DsRed-tagged proteins. *FEBS Lett.* **498** 11-15.

Lee HJ, Caldwell HK, Macbeth AH, Tolu SG & Young WS, III 2008 A conditional knockout mouse line of the oxytocin receptor. *Endocrinology* **149** 3256-3263.

Lee YB, Glover CP, Cosgrave AS, Bienemann A & Uney JB 2005 Optimizing regulatable gene expression using adenoviral vectors. *Exp.Physiol* **90** 33-37.

Leng G, Bicknell RJ, Brown D, Bowden C, Chapman C & Russell JA 1994 Stimulus-induced depletion of pro-enkephalins, oxytocin and vasopressin and pro-enkephalin interaction with posterior pituitary hormone release in vitro. *Neuroendocrinology* **60** 559-566.

Leng G, Brown CH & Russell JA 1999 Physiological pathways regulating the activity of magnocellular neurosecretory cells. *Prog.Neurobiol.* **57** 625-655.

Leng G & Ludwig M 2008 Neurotransmitters and peptides: whispered secrets and public announcements. *J.Physiol* **586** 5625-5632.

Levine B & Klionsky DJ 2004 Development by self-digestion: molecular mechanisms and biological functions of autophagy. *Dev.Cell* **6** 463-477.

Levitan ES 1998 Studying neuronal peptide release and secretory granule dynamics with green fluorescent protein. *Methods* **16** 182-187.

Lewis CE, Morris JF & Fink G 1985 The role of microfilaments in the priming effect of LH-releasing hormone: an ultrastructural study using cytochalasin B. *J.Endocrinol.* **106** 211-218.

Lo DC, McAllister AK & Katz LC 1994 Neuronal transfection in brain slices using particle-mediated gene transfer. *Neuron* **13** 1263-1268.

Loh YP 1987 Peptide precursor processing enzymes within secretory vesicles. *Ann.N.Y.Acad.Sci.* **493** 292-307.

Lonberg-Holm K & Philipson L 1969 Early events of virus-cell interaction in an adenovirus system. *J.Virol.* **4** 323-338.

Luckman SM, Antonijevic I, Leng G, Dye S, Douglas AJ, Russell JA & Bicknell RJ 1993 The maintenance of normal parturition in the rat requires neurohypophysial oxytocin. *J.Neuroendocrinol.* **5** 7-12.

Luckman SM, Dyball RE & Leng G 1994 Induction of c-fos expression in hypothalamic magnocellular neurons requires synaptic activation and not simply increased spike activity. *J.Neurosci.* **14** 4825-4830.

Ludwig M 1998 Dendritic release of vasopressin and oxytocin. *J.Neuroendocrinol.* **10** 881-895.

Ludwig M, Bull PM, Tobin VA, Sabatier N, Landgraf R, Dayanithi G & Leng G 2005 Regulation of activity-dependent dendritic vasopressin release from rat supraoptic neurones. *J.Physiol* **564** 515-522.

Ludwig M, Callahan MF, Landgraf R, Johnson AK & Morris M 1996a Neural input modulates osmotically stimulated release of vasopressin into the supraoptic nucleus. *Am.J.Physiol* **270** E787-E792.

Ludwig M, Callahan MF & Morris M 1995 Effects of tetrodotoxin on osmotically stimulated central and peripheral vasopressin and oxytocin release. *Neuroendocrinology* **62** 619-627.

Ludwig M, Callahan MF, Neumann I, Landgraf R & Morris M 1994a Systemic osmotic stimulation increases vasopressin and oxytocin release within the supraoptic nucleus. *J.Neuroendocrinol.* **6** 369-373.

Ludwig M, Horn T, Callahan MF, Grosche A, Morris M & Landgraf R 1994b Osmotic stimulation of the supraoptic nucleus: central and peripheral vasopressin release and blood pressure. *Am.J.Physiol* **266** E351-E356.

Ludwig M & Landgraf R 1992 Does the release of vasopressin within the supraoptic nucleus of the rat brain depend upon changes in osmolality and Ca2+/K+? *Brain Res.* **576** 231-234.

Ludwig M, Lelos N, Onaka T, Nakata M & Tobin V 2006 Expression and location of exocytosis proteins in magnocellular neurons. *Front Neuroendocrinol.* **27** 125.

Ludwig M & Leng G 1997 Autoinhibition of supraoptic nucleus vasopressin neurons in vivo: a combined retrodialysis/electrophysiological study in rats. *Eur.J.Neurosci.* **9** 2532-2540.

Ludwig M & Leng G 2006 Dendritic peptide release and peptide-dependent behaviours. *Nature Reviews Neuroscience* **7** 126-136.

Ludwig M, Sabatier N, Bull PM, Landgraf R, Dayanithi G & Leng G 2002 Intracellular calcium stores regulate activity-dependent neuropeptide release from dendrites. *Nature* **418** 85-89.

Ludwig M, Williams K, Callahan MF & Morris M 1996b Salt loading abolishes osmotically stimulated vasopressin release within the supraoptic nucleus. *Neurosci.Lett.* **215** 1-4.

Luzio JP, Pryor PR & Bright NA 2007 Lysosomes: fusion and function. *Nat.Rev.Mol.Cell Biol.* **8** 622-632.

Lytton J, Westlin M & Hanley MR 1991 Thapsigargin inhibits the sarcoplasmic or endoplasmic reticulum Ca-ATPase family of calcium pumps. *J.Biol.Chem.* **266** 17067-17071.

Ma D & Morris JF 2002 Protein synthetic machinery in the dendrites of the magnocellular neurosecretory neurons of wild-type Long-Evans and homozygous Brattleboro rats. *J.Chem.Neuroanat.* **23** 171-186.

MacDonald PE, Braun M, Galvanovskis J & Rorsman P 2006 Release of small transmitters through kiss-and-run fusion pores in rat pancreatic beta cells. *Cell Metab* **4** 283-290.

Mahata SK, Mahata M, Steiner HJ, Fischer-Colbrie R & Winkler H 1992 In situ hybridization: mRNA levels of secretogranin II, neuropeptides and carboxypeptidase H in brains of salt-loaded and Brattleboro rats. *Neuroscience* **48** 669-680.

Marsh BJ, Soden C, Alarcon C, Wicksteed BL, Yaekura K, Costin AJ, Morgan GP & Rhodes CJ 2007 Regulated autophagy controls hormone content in secretory-deficient pancreatic endocrine beta-cells. *Mol.Endocrinol.* **21** 2255-2269.

Mason WT, Hatton GI, Ho YW, Chapman C & Robinson IC 1986 Central release of oxytocin, vasopressin and neurophysin by magnocellular neurone depolarization: evidence in slices of guinea pig and rat hypothalamus. *Neuroendocrinology* **42** 311-322.

Matsunaga W, Miyata S, Hashimoto Y, Lin SH, Nakashima T, Kiyohara T & Matsumoto T 1999 Microtubule-associated protein-2 in the hypothalamo-neurohypophysial system: low-molecular-weight microtubule-associated protein-2 in pituitary astrocytes. *Neuroscience* **88** 1289-1297.

Matter K, Dreyer F & Aktories K 1989 Actin involvement in exocytosis from PC12 cells: studies on the influence of botulinum C2 toxin on stimulated noradrenaline release. *J.Neurochem.* **52** 370-376.

Maxfield FR & McGraw TE 2004 Endocytic recycling. *Nat.Rev.Mol.Cell Biol.* **5** 121-132.

McKinley MJ, Allen AM, May CN, McAllen RM, Oldfield BJ, Sly D & Mendelsohn FA 2001 Neural pathways from the lamina terminalis influencing cardiovascular and body fluid homeostasis. *Clin.Exp.Pharmacol.Physiol* **28** 990-992.

Meier O & Greber UF 2003 Adenovirus endocytosis. *J Gene Med* **5** 451-462.

Melander T, Hokfelt T, Rokaeus A, Cuello AC, Oertel WH, Verhofstad A & Goldstein M 1986 Coexistence of galanin-like immunoreactivity with catecholamines, 5-hydroxytryptamine, GABA and neuropeptides in the rat CNS. *J.Neurosci.* **6** 3640-3654.

Melis MR, Melis T, Cocco C, Succu S, Sanna F, Pillolla G, Boi A, Ferri GL & Argiolas A 2007 Oxytocin injected into the ventral tegmental area induces penile erection and increases extracellular dopamine in the nucleus accumbens and paraventricular nucleus of the hypothalamus of male rats. *Eur.J.Neurosci.* **26** 1026-1035.

Mens WB, Witter A & Wimersma Greidanus TB 1983 Penetration of neurohypophyseal hormones from plasma into cerebrospinal fluid (CSF): half-times of disappearance of these neuropeptides from CSF. *Brain Res.* **262** 143-149.

Merrifield CJ, Feldman ME, Wan L & Almers W 2002 Imaging actin and dynamin recruitment during invagination of single clathrin-coated pits. *Nat.Cell Biol.* **4** 691-698.

Michell RH, Kirk CJ & Billah MM 1979 Hormonal stimulation of phosphatidylinositol breakdown with particular reference to the hepatic effects of vasopressin. *Biochem.Soc.Trans.* **7** 861-865.

Mizuguchi H & Kay MA 1998 Efficient construction of a recombinant adenovirus vector by an improved in vitro ligation method. *Hum.Gene Ther.* **9** 2577-2583.

Mohr E, Morris JF & Richter D 1995 Differential subcellular mRNA targeting: deletion of a single nucleotide prevents the transport to axons but not to dendrites of rat hypothalamic magnocellular neurons. *Proc.Natl.Acad.Sci.U.S.A* **92** 4377-4381.

Molnar M & Hertelendy F 1990 Regulation of intracellular free calcium in human myometrial cells by prostaglandin F2 alpha: comparison with oxytocin. *J.Clin.Endocrinol.Metab* **71** 1243-1250.

Montagnese C, Poulain DA & Theodosis DT 1990 Influence of ovarian steroids on the ultrastructural plasticity of the adult rat supraoptic nucleus induced by central administration of oxytocin. *J.Neuroendocrinol.* **2** 225-231.

Moos F, Freundmercier MJ, Guerne Y, Guerne JM, Stoeckel ME & Richard P 1984 Release of Oxytocin and Vasopressin by Magnocellular Nuclei Invitro - Specific Facilitatory Effect of Oxytocin on Its Own Release. *Journal of Endocrinology* **102** 63-&.

Moos F, Poulain DA, Rodriguez F, Guerne Y, Vincent JD & Richard P 1989 Release of oxytocin within the supraoptic nucleus during the milk ejection reflex in rats. *Exp.Brain Res.* **76** 593-602.

Moos F & Richard P 1989 Paraventricular and supraoptic bursting oxytocin cells in rat are locally regulated by oxytocin and functionally related. *J.Physiol* **408** 1-18.

Moriguchi A, Ferrario CM, Brosnihan KB, Ganten D & Morris M 1994 Differential regulation of central vasopressin in transgenic rats harboring the mouse Ren-2 gene. *Am.J.Physiol* **267** R786-R791.

Morris JF 2005 Morphological Studies of Dendrites and Dendritic Secretion. In *Dendritic Neurotransmitter Release*, pp 15-33. Ed M Ludwig. New York, USA: Springer.

Morris JF, Christian H, Ma D & Wang H 2000 Dendritic secretion of peptides from hypothalamic magnocellular neurosecretory neurones: a local dynamic control system and its functions. *Exp.Physiol* **85 Spec No** 131S-138S.

Morris JF & Dyball RE 1974 A quantitative study of the ultrastructural changes in the hypothalamo-neurohypophysial system during and after experimentally induced hypersecretion. *Cell Tissue Res.* **149** 525-535.

Morris JF & Ludwig M 2004 Magnocellular dendrites: Prototypic receiver/transmitters. *Journal of Neuroendocrinology* **16** 403-408.

Morris JF & Pow DV 1988 Capturing and Quantifying the Exocytotic Event. *Journal of Experimental Biology* **139** 81-103.

Morris JF & Pow DV 1991 Widespread release of peptides in the central nervous system: quantitation of tannic acid-captured exocytoses. *Anat.Rec.* **231** 437-445.

Morris, J. F., Pow, D. V., Sokol, H. W., and Ward, A. Dendritic release of peptides from magnocellular neurons in normal rats, Brattleboro rats and mice with hereditary nephrogenic diabetes insipidus. P.Gross, D.Richter, and G.L.Robertson. 171-182. 1993. Paris, John Libbey Eurotext. In: Vasopressin.
Ref Type: Conference Proceeding

Morris M & Alexander N 1989 Baroreceptor influences on oxytocin and vasopressin secretion. *Hypertension* **13** 110-114.

Morris SA & Schmid SL 1995 Synaptic vesicle recycling. The Ferrari of endocytosis? *Curr.Biol.* **5** 113-115.

Mundigl O, Matteoli M, Daniell L, Thomas-Reetz A, Metcalf A, Jahn R & De Camilli P 1993 Synaptic vesicle proteins and early endosomes in cultured hippocampal neurons: differential effects of Brefeldin A in axon and dendrites. *J.Cell Biol.* **122** 1207-1221.

Murai I & Ben Jonathan N 1987 Posterior pituitary lobectomy abolishes the suckling-induced rise in prolactin (PRL): evidence for a PRL-releasing factor in the posterior pituitary. *Endocrinology* **121** 205-211.

Murphy RC & Messer A 2001 Gene transfer methods for CNS organotypic cultures: a comparison of three nonviral methods. *Mol.Ther.* **3** 113-121.

Murphy RF 1991 Maturation models for endosome and lysosome biogenesis. *Trends Cell Biol.* **1** 77-82.

Murthy VN & De Camilli P 2003 Cell biology of the presynaptic terminal. *Annu.Rev.Neurosci.* **26** 701-728.

Mutsuga N, Shahar T, Verbalis JG, Xiang CC, Brownstein MJ & Gainer H 2005 Regulation of gene expression in magnocellular neurons in rat supraoptic nucleus during sustained hypoosmolality. *Endocrinology* **146** 1254-1267.

Neher E 1998 Vesicle pools and Ca2+ microdomains: new tools for understanding their roles in neurotransmitter release. *Neuron* **20** 389-399.

Nephew BC & Bridges RS 2008 Central actions of arginine vasopressin and a V1a receptor antagonist on maternal aggression, maternal behavior, and grooming in lactating rats. *Pharmacol.Biochem.Behav.* **91** 77-83.

Neumann I, Douglas AJ, Pittman QJ, Russell JA & Landgraf R 1996 Oxytocin released within the supraoptic nucleus of the rat brain by positive feedback action is involved in parturition-related events. *J.Neuroendocrinol.* **8** 227-233.

Neumann I, Ludwig M, Engelmann M, Pittman QJ & Landgraf R 1993a Simultaneous microdialysis in blood and brain: oxytocin and vasopressin release in response to central and peripheral osmotic stimulation and suckling in the rat. *Neuroendocrinology* **58** 637-645.

Neumann I, Russell JA & Landgraf R 1993b Oxytocin and vasopressin release within the supraoptic and paraventricular nuclei of pregnant, parturient and lactating rats: a microdialysis study. *Neuroscience* **53** 65-75.

Neumann ID 2007 Stimuli and consequences of dendritic release of oxytocin within the brain. *Biochem.Soc.Trans.* **35** 1252-1257.

Neumann ID, Torner L & Wigger A 2000 Brain oxytocin: differential inhibition of neuroendocrine stress responses and anxiety-related behaviour in virgin, pregnant and lactating rats. *Neuroscience* **95** 567-575.

Ng YK, Lu X & Levitan ES 2002 Physical mobilization of secretory vesicles facilitates neuropeptide release by nerve growth factor-differentiated PC12 cells. *J.Physiol* **542** 395-402.

Nicholson KL, Munson M, Miller RB, Filip TJ, Fairman R & Hughson FM 1998 Regulation of SNARE complex assembly by an N-terminal domain of the t-SNARE Sso1p. *Nat Struct.Biol.* **5** 793-802.

Noel G, Zollinger L, Laliberte F, Rassart E, Crine P & Boileau G 1989 Targeting and processing of pro-opiomelanocortin in neuronal cell lines. *J Neurochem.* **52** 1050-1057.

Nofal S, Becherer U, Hof D, Matti U & Rettig J 2007 Primed vesicles can be distinguished from docked vesicles by analyzing their mobility. *J.Neurosci.* **27** 1386-1395.

Nordmann JJ & Labouesse J 1981 Neurosecretory granules: evidence from an aging process within the neurohypophysis. *Science* **211** 595-597.

Nordmann JJ & Morris JF 1984 Method for quantitating the molecular content of a subcellular organelle: hormone and neurophysin content of newly formed and aged neurosecretory granules. *Proc.Natl.Acad.Sci.U.S.A* **81** 180-184.

O'Brien JA, Holt M, Whiteside G, Lummis SC & Hastings MH 2001 Modifications to the hand-held Gene Gun: improvements for in vitro biolistic transfection of organotypic neuronal tissue. *J.Neurosci.Methods* **112** 57-64.

Okuya S, Inenaga K, Kaneko T & Yamashita H 1987 Angiotensin II sensitive neurons in the supraoptic nucleus, subfornical organ and anteroventral third ventricle of rats in vitro. *Brain Res.* **402** 58-67.

Park JJ, Koshimizu H & Loh YP 2009 Biogenesis and transport of secretory granules to release site in neuroendocrine cells. *J.Mol.Neurosci.* **37** 151-159.

Park YS, Jun DJ, Hur EM, Lee SK, Suh BS & Kim KT 2006 Activity-dependent potentiation of large dense-core vesicle release modulated by mitogen-activated protein kinase/extracellularly regulated kinase signaling. *Endocrinology* **147** 1349-1356.

Parton RG, Simons K & Dotti CG 1992 Axonal and dendritic endocytic pathways in cultured neurons. *J.Cell Biol.* **119** 123-137.

Patterson GH, Knobel SM, Sharif WD, Kain SR & Piston DW 1997 Use of the green fluorescent protein and its mutants in quantitative fluorescence microscopy. *Biophys.J.* **73** 2782-2790.

Pedersen CA & Prange AJ, Jr. 1979 Induction of maternal behavior in virgin rats after intracerebroventricular administration of oxytocin. *Proc.Natl.Acad.Sci.U.S.A* **76** 6661-6665.

Penny ML, Bruno SB, Cornelius J, Higgs KA & Cunningham JT 2005 The effects of osmotic stimulation and water availability on c-Fos and FosB staining in the supraoptic and paraventricular nuclei of the hypothalamus. *Exp.Neurol.* **194** 191-202.

Perlmutter LS, Tweedle CD & Hatton GI 1985 Neuronal/glial plasticity in the supraoptic dendritic zone in response to acute and chronic dehydration. *Brain Res.* **361** 225-232.

Phillips MI 1987 Functions of angiotensin in the central nervous system. *Annu.Rev Physiol* **49** 413-435.

Pillay CS, Elliott E & Dennison C 2002 Endolysosomal proteolysis and its regulation. *Biochem.J.* **363** 417-429.

Pow DV & Morris JF 1989 Dendrites of hypothalamic magnocellular neurons release neurohypophysial peptides by exocytosis. *Neuroscience* **32** 435-439.

Pow DV, Morris JF & Toescu EC 1990 Dendrosomes - A New Preparation of Isolated Neurosecretory Dendrites. *Journal of Neuroendocrinology* **2** 103-106.

Pucak ML & Grace AA 1994 Regulation of substantia nigra dopamine neurons. *Crit Rev.Neurobiol.* **9** 67-89.

Raju PA, McSloy N, Truong NK & Kendall MA 2006 Assessment of epidermal cell viability by near infrared multi-photon microscopy following ballistic delivery of gold micro-particles. *Vaccine* **24** 4644-4647.

Ralph GS, Bienemann A, Harding TC, Hopton M, Henley J & Uney JB 2000 Targeting of tetracycline-regulatable transgene expression specifically to neuronal and glial cell populations using adenoviral vectors. *Neuroreport* **11** 2051-2055.

Randle JC, Bourque CW & Renaud LP 1984 Alpha-adrenergic activation of rat hypothalamic supraoptic neurons maintained in vitro. *Brain Res.* **307** 374-378.

Richard P, Moos F & Freund-Mercier MJ 1991 Central effects of oxytocin. *Physiol Rev.* **71** 331-370.

Richards DA, Guatimosim C, Rizzoli SO & Betz WJ 2003 Synaptic vesicle pools at the frog neuromuscular junction. *Neuron* **39** 529-541.

Rickman C & Duncan RR 2010 Munc18/Syntaxin interaction kinetics control secretory vesicle dynamics. *J Biol.Chem.* **285** 3965-3972.

Ridoux V, Robert J, Perricaudet M, Mallet J & Le Gal LS 1995 Adenovirus mediated gene transfer in organotypic brain slices. *Neurobiol.Dis.* **2** 49-54.

Rimmele U, Hediger K, Heinrichs M & Klaver P 2009 Oxytocin makes a face in memory familiar. *J.Neurosci.* **29** 38-42.

Ring RH, Malberg JE, Potestio L, Ping J, Boikess S, Luo B, Schechter LE, Rizzo S, Rahman Z & Rosenzweig-Lipson S 2006 Anxiolytic-like activity of oxytocin in male mice: behavioral and autonomic evidence, therapeutic implications. *Psychopharmacology (Berl)* **185** 218-225.

Rizzoli SO & Betz WJ 2005 Synaptic vesicle pools. *Nat.Rev.Neurosci.* **6** 57-69.

Rowland NE, Li BH, Rozelle AK, Fregly MJ, Garcia M & Smith GC 1994a Localization of changes in immediate early genes in brain in relation to hydromineral balance: intravenous angiotensin II. *Brain Res.Bull.* **33** 427-436.

Rowland NE, Li BH, Rozelle AK & Smith GC 1994b Comparison of fos-like immunoreactivity induced in rat brain by central injection of angiotensin II and carbachol. *Am J Physiol* **267** R792-R798.

Rusnak M, House SB & Gainer H 2003 Long-term effects of ciliary neurotrophic factor on the survival of vasopressin magnocellular neurones in the rat supraoptic nucleus in vitro. *J.Neuroendocrinol.* **15** 933-939.

Russell JA, Leng G & Douglas AJ 2003 The magnocellular oxytocin system, the fount of maternity: adaptations in pregnancy. *Front Neuroendocrinol.* **24** 27-61.

Sabatier N, Caquineau C, Dayanithi G, Bull P, Douglas AJ, Guan XM, Jiang M, Van der PL & Leng G 2003 Alpha-melanocyte-stimulating hormone stimulates oxytocin release from the dendrites of hypothalamic neurons while inhibiting oxytocin release from their terminals in the neurohypophysis. *J.Neurosci.* **23** 10351-10358.

Sabatier N, Richard P & Dayanithi G 1998 Activation of multiple intracellular transduction signals by vasopressin in vasopressin-sensitive neurones of the rat supraoptic nucleus. *J.Physiol* **513 (Pt 3)** 699-710.

Sabatier N, Shibuya I & Dayanithi G 2004 Intracellular calcium increase and somatodendritic vasopressin release by vasopressin receptor agonists in the rat supraoptic nucleus: involvement of multiple intracellular transduction signals. *J.Neuroendocrinol.* **16** 221-236.

Saraste J, Palade GE & Farquhar MG 1986 Temperature-sensitive steps in the transport of secretory proteins through the Golgi complex in exocrine pancreatic cells. *Proc.Natl.Acad.Sci.U.S.A* **83** 6425-6429.

Scala-Guenot D, Strosser MT & Richard P 1987 Electrical stimulations of perifused magnocellular nuclei in vitro elicit Ca2+-dependent, tetrodotoxin-insensitive release of oxytocin and vasopressin. *Neurosci.Lett.* **76** 209-214.

Schneggenburger R, Meyer AC & Neher E 1999 Released fraction and total size of a pool of immediately available transmitter quanta at a calyx synapse. *Neuron* **23** 399-409.

Schwab Y, Mouton J, Chasserot-Golaz S, Marty I, Maulet Y & Jover E 2001 Calcium-dependent translocation of synaptotagmin to the plasma membrane in the dendrites of developing neurones. *Brain Res.Mol.Brain Res.* **96** 1-13.

Seidman CE, Duby AD, Choi E, Graham RM, Haber E, Homcy C, Smith JA & Seidman JG 1984 The structure of rat preproatrial natriuretic factor as defined by a complementary DNA clone. *Science* **225** 324-326.

Seward EP, Chernevskaya NI & Nowycky MC 1996 Ba2+ ions evoke two kinetically distinct patterns of exocytosis in chromaffin cells, but not in neurohypophysial nerve terminals. *J Neurosci.* **16** 1370-1379.

Shahar T, House SB & Gainer H 2004 Neural activity protects hypothalamic magnocellular neurons against axotomy-induced programmed cell death. *J Neurosci.* **24** 6553-6562.

Shaner NC, Campbell RE, Steinbach PA, Giepmans BN, Palmer AE & Tsien RY 2004 Improved monomeric red, orange and yellow fluorescent proteins derived from Discosoma sp. red fluorescent protein. *Nat Biotechnol.* **22** 1567-1572.

Sharp FR, Sagar SM, Hicks K, Lowenstein D & Hisanaga K 1991 c-fos mRNA, Fos, and Fos-related antigen induction by hypertonic saline and stress. *J.Neurosci.* **11** 2321-2331.

Shaw PJ & Rawlins DJ 1991 The point spread function of a confocal microscope: its measurement and use in deconvolution . *J Microsc* **163** 151-165.

Shields PP, Sprenkle AB, Taylor EW & Glembotski CC 1990 Rat pro-atrial natriuretic factor expression and post-translational processing in mouse corticotropic pituitary tumor cells. *J.Biol.Chem.* **265** 10905-10911.

Shigekawa K & Dower WJ 1988 Electroporation of eukaryotes and prokaryotes: a general approach to the introduction of macromolecules into cells. *Biotechniques* **6** 742-751.

Shuster SJ, Riedl M, Li X, Vulchanova L & Elde R 1999 Stimulus-dependent translocation of kappa opioid receptors to the plasma membrane. *J.Neurosci.* **19** 2658-2664.

Sinding C, Robinson AG & Seif SM 1980a Levels of neurohypophyseal peptides in the rat during the first month of life. II. Response to physiological stimuli. *Endocrinology* **107** 755-760.

Sinding C, Robinson AG, Seif SM & Schmid PG 1980b Neurohypophyseal peptides in the developing rat fetus. *Brain Res.* **195** 177-186.

Slack RS & Miller FD 1996 Viral vectors for modulating gene expression in neurons. *Curr.Opin.Neurobiol.* **6** 576-583.

Smith RE & Farquhar MG 1966 Lysosome Function in Regulation of Secretory Process in Cells of Anterior Pituitary Gland. *Journal of Cell Biology* **31** 319-&.

Sofroniew MV & Glasmann W 1981 Golgi-Like Immunoperoxidase Staining of Hypothalamic Magnocellular Neurons That Contain Vasopressin, Oxytocin Or Neurophysin in the Rat. *Neuroscience* **6** 619-643.

Soldo BL, Giovannucci DR, Stuenkel EL & Moises HC 2004 Ca(2+) and frequency dependence of exocytosis in isolated somata of magnocellular supraoptic neurones of the rat hypothalamus. *J Physiol* **555** 699-711.

Sorensen JB, Matti U, Wei SH, Nehring RB, Voets T, Ashery U, Binz T, Neher E & Rettig J 2002 The SNARE protein SNAP-25 is linked to fast calcium triggering of exocytosis. *Proc.Natl.Acad.Sci.U.S.A* **99** 1627-1632.

Stenovec M, Kreft M, Poberaj I, Betz WJ & Zorec R 2004 Slow spontaneous secretion from single large dens-core vesicles monitored in neuroendocrine cells. *FASEB* 1270-1272.

Stern JE & Zhang W 2005 Cellular sources, targets and actions of constitutive nitric oxide in the magnocellular neurosecretory system of the rat. *J Physiol* **562** 725-744.

Steyer JA, Horstmann H & Almers W 1997 Transport, docking and exocytosis of single secretory granules in live chromaffin cells. *Nature* **388** 474-478.

Stoppini L, Buchs PA & Muller D 1991 A Simple Method for Organotypic Cultures of Nervous-Tissue. *Journal of Neuroscience Methods* **37** 173-182.

Storrie B & Desjardins M 1996 The biogenesis of lysosomes: is it a kiss and run, continuous fusion and fission process? *Bioessays* **18** 895-903.

Straub M, Lodemann P, Holroyd P, Jahn R & Hell SW 2000 Live cell imaging by multifocal multiphoton microscopy. *Eur.J.Cell Biol.* **79** 726-734.

Stuart G, Schiller J & Sakmann B 1997 Action potential initiation and propagation in rat neocortical pyramidal neurons. *J.Physiol* **505 (Pt 3)** 617-632.

Swaminathan R, Hoang CP & Verkman AS 1997 Photobleaching recovery and anisotropy decay of green fluorescent protein GFP-S65T in solution and cells: cytoplasmic viscosity probed by green fluorescent protein translational and rotational diffusion. *Biophys.J.* **72** 1900-1907.

Swanson LW & Sawchenko PE 1983 Hypothalamic Integration - Organization of the Paraventricular and Supraoptic Nuclei. *Annual Review of Neuroscience* **6** 269-324.

Tao X, Finkbeiner S, Arnold DB, Shaywitz AJ & Greenberg ME 1998 Ca2+ influx regulates BDNF transcription by a CREB family transcription factor-dependent mechanism. *Neuron* **20** 709-726.

Taupenot L 2007 Analysis of regulated secretion using PC12 cells. *Curr.Protoc.Cell Biol.* **Chapter 15** Unit.

Terskikh A, Fradkov A, Ermakova G, Zaraisky A, Tan P, Kajava AV, Zhao X, Lukyanov S, Matz M, Kim S, Weissman I & Siebert P 2000 "Fluorescent timer": protein that changes color with time. *Science* **290** 1585-1588.

Terskikh AV, Fradkov AF, Zaraisky AG, Kajava AV & Angres B 2002 Analysis of DsRed Mutants. Space around the fluorophore accelerates fluorescence development. *J.Biol.Chem.* **277** 7633-7636.

Theodosis DT 1982 Secretion-related accumulation of horseradish peroxidase in magnocellular cell bodies of the rat supraoptic nucleus. *Brain Res.* **233** 3-16.

Theodosis DT 2002 Oxytocin-secreting neurons: A physiological model of morphological neuronal and glial plasticity in the adult hypothalamus. *Front Neuroendocrinol.* **23** 101-135.

Theodosis DT, El Majdoubi M, Pierre K & Poulain DA 1998 Factors governing activity-dependent structural plasticity of the hypothalamoneurohypophysial system. *Cell Mol.Neurobiol.* **18** 285-298.

Theodosis DT & Poulain DA 1992 Neuronal-glial and synaptic plasticity of the adult oxytocinergic system. Factors and consequences. *Ann.N.Y.Acad.Sci.* **652** 303-325.

Theodosis DT & Poulain DA 2001 Maternity leads to morphological synaptic plasticity in the oxytocin system. *Prog.Brain Res.* **133** 49-58.

Theodosis DT, Poulain DA & Oliet SH 2008 Activity-dependent structural and functional plasticity of astrocyte-neuron interactions. *Physiol Rev.* **88** 983-1008.

Thevenaz P, Ruttimann UE & Unser M 1998 A pyramid approach to subpixel registration based on intensity. *IEEE Trans.Image Process* **7** 27-41.

Thomas A, Kim DS, Fields RL, Chin H & Gainer H 1998 Quantitative analysis of gene expression in organotypic slice-explant cultures by particle-mediated gene transfer. *J.Neurosci.Methods* **84** 181-191.

Thurmond DC, Gonelle-Gispert C, Furukawa M, Halban PA & Pessin JE 2003 Glucose-stimulated insulin secretion is coupled to the interaction of actin with the t-SNARE (target membrane soluble N-ethylmaleimide-sensitive factor attachment protein receptor protein) complex. *Mol.Endocrinol.* **17** 732-742.

Toba K, Ouchi Y, Liang J, Akishita M & Orimo H 1994 Role of central vasopressin in cardiovascular regulation: effect of dehydration and sex. *Gerontology* **40 Suppl 2** 16-22.

Tobin VA, Hurst G, Norrie L, Dal Rio FP, Bull PM & Ludwig M 2004 Thapsigargin-induced mobilization of dendritic dense-cored vesicles in rat supraoptic neurons. *Eur.J.Neurosci.* **19** 2909-2912.

Tobin VA & Ludwig M 2007a The actin filament and dendritic peptide release. *Biochem.Soc.Trans.* **35** 1243-1246.

Tobin VA & Ludwig M 2007b The role of the actin cytoskeleton in oxytocin and vasopressin release from rat supraoptic nucleus neurons. *J.Physiol* **582** 1337-1348.

Trembleau A, Morales M & Bloom FE 1994 Aggregation of vasopressin mRNA in a subset of axonal swellings of the median eminence and posterior pituitary: light and electron microscopic evidence. *J.Neurosci.* **14** 39-53.

Triezenberg SJ, Kingsbury RC & McKnight SL 1988 Functional dissection of VP16, the trans-activator of herpes simplex virus immediate early gene expression. *Genes Dev.* **2** 718-729.

Trifaro J, Rose SD, Lejen T & Elzagallaai A 2000 Two pathways control chromaffin cell cortical F-actin dynamics during exocytosis. *Biochimie* **82** 339-352.

Tsien RY 1998 The green fluorescent protein. *Annu.Rev.Biochem.* **67** 509-544.

Tweedle CD & Hatton GI 1984 Synapse formation and disappearance in adult rat supraoptic nucleus during different hydration states. *Brain Res.* **309** 373-376.

Tyzio R, Represa A, Jorquera I, Ben Ari Y, Gozlan H & Aniksztejn L 1999 The establishment of GABAergic and glutamatergic synapses on CA1 pyramidal neurons is sequential and correlates with the development of the apical dendrite. *J.Neurosci.* **19** 10372-10382.

Ueta Y, Fujihara H, Serino R, Dayanithi G, Ozawa H, Matsuda K, Kawata M, Yamada J, Ueno S, Fukuda A & Murphy D 2005 Transgenic expression of enhanced green fluorescent protein enables direct visualization for physiological studies of vasopressin neurons and isolated nerve terminals of the rat. *Endocrinology* **146** 406-413.

Ueta Y, Levy A, Chowdrey HS & Lightman SL 1995 Water deprivation in the rat induces nitric oxide synthase (NOS) gene expression in the hypothalamic paraventricular and supraoptic nuclei. *Neurosci.Res.* **23** 317-319.

Ueta Y, Levy A & Lightman SL 2002 Gene expression in the supraoptic nucleus. *Microsc.Res.Tech.* **56** 158-163.

Vaccari C, Lolait SJ & Ostrowski NL 1998 Comparative distribution of vasopressin V1b and oxytocin receptor messenger ribonucleic acids in brain. *Endocrinology* **139** 5015-5033.

Vacher CM, Fretier P, Creminon C, Calas A & Hardin-Pouzet H 2002 Activation by serotonin and noradrenaline of vasopressin and oxytocin expression in the mouse paraventricular and supraoptic nuclei. *J Neurosci.* **22** 1513-1522.

Vandesande F, Dierickx K & De Mey J 1977 The origin of the vasopressinergic and oxytocinergic fibres of the external region of the median eminence of the rat hypophysis. *Cell Tissue Res.* **180** 443-452.

Vasquez EC, Beltz TG, Haskell RE, Johnson RF, Meyrelles SS, Davidson BL & Johnson AK 2001 Adenovirus-mediated gene delivery to cells of the magnocellular hypothalamo-neurohypophyseal system. *Exp.Neurol.* **167** 260-271.

Vasquez EC, Johnson RF, Beltz TG, Haskell RE, Davidson BL & Johnson AK 1998 Replication-deficient adenovirus vector transfer of gfp reporter gene into supraoptic nucleus and subfornical organ neurons. *Exp.Neurol.* **154** 353-365.

Verbalis JG & Dohanics J 1991 Vasopressin and oxytocin secretion in chronically hyposmolar rats. *Am J Physiol* **261** R1028-R1038.

Villar MJ, Ceccatelli S, Ronnqvist M & Hokfelt T 1994 Nitric oxide synthase increases in hypothalamic magnocellular neurons after salt loading in the rat. An immunohistochemical and in situ hybridization study. *Brain Res.* **644** 273-281.

Vitale ML, Seward EP & Trifaro JM 1995 Chromaffin cell cortical actin network dynamics control the size of the release-ready vesicle pool and the initial rate of exocytosis. *Neuron* **14** 353-363.

Voets T, Neher E & Moser T 1999 Mechanisms underlying phasic and sustained secretion in chromaffin cells from mouse adrenal slices. *Neuron* **23** 607-615.

Volpi S, Rabadan-Diehl C & Aguilera G 2004 Regulation of vasopressin V1b receptors and stress adaptation. *Ann.N.Y.Acad.Sci.* **1018** 293-301.

Wall MA, Socolich M & Ranganathan R 2000 The structural basis for red fluorescence in the tetrameric GFP homolog DsRed. *Nature Structural Biology* **7** 1133-1138.

Wang BC, Share L & Crofton JT 1982 Central infusion of vasopressin decreased plasma vasopressin concentration in dogs. *Am.J.Physiol* **243** E365-E369.

Wang H, Ward AR & Morris JF 1995 Oestradiol acutely stimulates exocytosis of oxytocin and vasopressin from dendrites and somata of hypothalamic magnocellular neurons. *Neuroscience* **68** 1179-1188.

Wang LY & Kaczmarek LK 1998 High-frequency firing helps replenish the readily releasable pool of synaptic vesicles. *Nature* **394** 384-388.

Washbourne P & McAllister AK 2002 Techniques for gene transfer into neurons. *Curr.Opin.Neurobiol.* **12** 566-573.

Watson SJ, Akil H, Fischli W, Goldstein A, Zimmerman E, Nilaver G & wimersma Griedanus TB 1982 Dynorphin and vasopressin: common localization in magnocellular neurons. *Science* **216** 85-87.

Wellmann H, Kaltschmidt B & Kaltschmidt C 1999 Optimized protocol for biolistic transfection of brain slices and dissociated cultured neurons with a hand-held gene gun. *J.Neurosci.Methods* **92** 55-64.

Whitaker S & LaBella FS 1972 Ultrastructural localization of acid phosphatase in the posterior pituitary of the dehydrated rat. *Z.Zellforsch.Mikrosk.Anat.* **125** 1-15.

Wiegand UK, Duncan RR, Greaves J, Chow RH, Shipston MJ & Apps DK 2003 Red, yellow, green go!--A novel tool for microscopic segregation of secretory vesicle pools according to their age. *Biochem.Soc.Trans.* **31** 851-856.

Williams RS, Johnston SA, Riedy M, Devit MJ, Mcelligott SG & Sanford JC 1991 Introduction of Foreign Genes Into Tissues of Living Mice by Dna-Coated Microprojectiles. *Proceedings of the National Academy of Sciences of the United States of America* **88** 2726-2730.

Wilson JR, Ludowyke RI & Biden TJ 2001 A redistribution of actin and myosin IIA accompanies Ca(2+)-dependent insulin secretion. *FEBS Lett.* **492** 101-106.

Windle RJ, Shanks N, Lightman SL & Ingram CD 1997 Central oxytocin administration reduces stress-induced corticosterone release and anxiety behavior in rats. *Endocrinology* **138** 2829-2834.

Winslow JT, Hearn EF, Ferguson J, Young LJ, Matzuk MM & Insel TR 2000 Infant vocalization, adult aggression, and fear behavior of an oxytocin null mutant mouse. *Horm.Behav.* **37** 145-155.

Wotjak CT, Ganster J, Kohl G, Holsboer F, Landgraf R & Engelmann M 1998 Dissociated central and peripheral release of vasopressin, but not oxytocin, in response to repeated swim stress: new insights into the secretory capacities of peptidergic neurons. *Neuroscience* **85** 1209-1222.

Wotjak CT, Ludwig M & Landgraf R 1994 Vasopressin facilitates its own release within the rat supraoptic nucleus in vivo. *Neuroreport* **5** 1181-1184.

Xia X, Lessmann V & Martin TF 2009 Imaging of evoked dense-core-vesicle exocytosis in hippocampal neurons reveals long latencies and kiss-and-run fusion events. *J.Cell Sci.* **122** 75-82.

Xiang Z, Hrabetova S, Moskowitz SI, Casaccia-Bonnefil P, Young SR, Nimmrich VC, Tiedge H, Einheber S, Karnup S, Bianchi R & Bergold PJ 2000 Long-term maintenance of mature hippocampal slices in vitro. *J.Neurosci.Methods* **98** 145-154.

Yamagishi S, Fujikawa N, Kohara K, Tominaga-Yoshino K & Ogura A 2000 Increased exocytotic capability of rat cerebellar granule neurons cultured under depolarizing conditions. *Neuroscience* **95** 473-479.

Yanushevich YG, Staroverov DB, Savitsky AP, Fradkov AF, Gurskaya NG, Bulina ME, Lukyanov KA & Lukyanov SA 2002 A strategy for the generation of non-aggregating mutants of *Anthozoa* fluorescent proteins. *FEBS* **511** 11-14.

Ye GN, Daniell H & Sanford JC 1990 Optimization of delivery of foreign DNA into higher-plant chloroplasts. *Plant Mol.Biol.* **15** 809-819.

Young WS, III, Iacangelo A, Luo XZ, King C, Duncan K & Ginns EI 1999 Transgenic expression of green fluorescent protein in mouse oxytocin neurones. *J.Neuroendocrinol.* **11** 935-939.

Young WS, III, Shepard E, Amico J, Hennighausen L, Wagner KU, LaMarca ME, McKinney C & Ginns EI 1996 Deficiency in mouse oxytocin prevents milk ejection, but not fertility or parturition. *J.Neuroendocrinol.* **8** 847-853.

Zhang BJ, Kusano K, Zerfas P, Iacangelo A, Young WS, III & Gainer H 2002 Targeting of green fluorescent protein to secretory granules in oxytocin magnocellular neurons and its secretion from neurohypophysial nerve terminals in transgenic mice. *Endocrinology* **143** 1036-1046.

Zhang BJ, Yamashita M, Fields R, Kusano K & Gainer H 2005 EGFP-tagged vasopressin precursor protein sorting into large dense core vesicles and secretion from PC12 cells. *Cell Mol.Neurobiol.* **25** 581-605.

Zingg HH 1996 Vasopressin and oxytocin receptors. *Baillieres Clin.Endocrinol.Metab* **10** 75-96.

Appendix I – Recipes

aCSF-sucrose-KOH solution

- 220 mM sucrose
- 1.2 mM KCl, 10 mM HEPES
- 10 mM glucose
- 1.2 mM KH_2PO_4
- 2 mM $MgCl_2$
- 2.5 mM $CaCl_2$
- pH to 7.4 with 1M KOH
- Check osmolarity = 300 mOsm/L

Agarose, 1% (w/v)

- 50 ml TBE buffer (see below for recipe)
- 0.5 g agarose
- Microwave till agarose dissolves
- Cool solution under cold water
- Add 5 ul of Sybrsafe (Invitrogen) for DNA visualization under UV light

Buffer N3

- 5 M KOAc
- Autoclave and store at 4^oC

Buffer P1

- 25 mM Tris-HCl (pH 8.0)
- 10 mM EDTA

- 50 mM glucose
- Autoclave and store at 4^{o}C

Buffer P2

- 0.2 M NaOH
- 1% (v/v) SDS

Buffer TE

- 10 mM Tris-HCl (pH 8.0)
- 1 mM EDTA

Cell freezing media

- DMEM (Gibco)
- 10% (v/v) Foetal calf serum (Harlan)
- 5% (v/v) DMSO (Sigma)

Cryoprotectant solution

- 20% (v/v) glycerol
- 30% (v/v) ethylene glocol
- 0.2 M PBS
- Titrate to pH 5.5

Gelatine solution for subbing slides

- Heat up distilled H_2O
- 5 g/L gelatine
- Let solution cool

- Add 0.5 g/L chromic potassium sulphate
- Filter solution before use

Hep-Saline solution (Heparinised saline)

- 9 g/L NaCl
- 0.129 g/L Heparin

LB; Luria-Bertani, medium

- 10 g tryptone
- 5 g yeast extract
- 5 g NaCl
- 1 L water
- pH 7.5
- Autoclave

LB Agar

- 1 L of LB medium (pH 7.5)
- 15 g agar
- Autoclave

Mowiol

- 4.76 ml glycerol (density 1.26 g/L)
- 2.4 g Mowiol 4-88 (Calbiochem)
- 12 ml distilled water
- 12 ml 0.2M Tris pH 8.5
- Warm up to 50^{o}C for 2 hours
- Aliquot into 50 ml centrifuge tubes

- Centrifuge at 2000 rpm for 15 min, save supernatant
- Add 0.72 g DABCO (1,4 diazabicyclo [2,2,2]-octane)
- Aliquot into 10 ml in 15 ml conical tubes
- Store at -20^{o}C

N2a culture medium

- DMEM (with L-Glutamine, 4500 mg/L D-Glucose, 110 mg/L Sodium Pyruvate, Gibco)
- 10% (v/v) Foetal cal serum (Harlan)
- 1:50 Pen/Strep/Neo (Sigma)

Nickel II sulphate solution for Fos immunohistochemistry

- 100ml of 0.2M sodium acetate buffer
- 5g nickel II sulphate
- 0.8g glucose
- 0.16g ammonium chloride
- 50mg DAB is added to 98ml dH_20
- 0.006g glucose oxidase type VII-s (Sigma G7016) was added immediately prior to use

4% (w/v) PFA in 0.1 M PB(S)

- 4 % (w/v) Paraformaldehyde
- 0.2 M PB or PBS
- distilled H_2O
- Heat up distilled H_2O
- Add paraformaldehyde
- Dissolve paraformaldehyde with 10 M NaOH
- Add equal volume of 0.2 M PB(S)

- Titrate to pH 7.4 when cooled

Phosphate buffer (PB) 0.1M

- 11.5 g/L Na_2HPO_4
- 2.964 g/L $NaH_2PO_4.2H_2O$
- Make up in distilled H_2O
- Titrate to pH 7.4

Phosphate buffered saline (PBS) 0.1M

- 11.5 g/L Na_2HPO_4
- 2.964 g/L $NaH_2PO_4.2H_2O$
- 8.5 g/L NaCl
- Make up in distilled H_2O
- Titrate to pH 7.4

Serum-containing medium

- 50% (v/v) Eagles basal medium (BME, Sigma-Aldrich, UK)
- 25% (v/v) heat-inactivated horse serum (Harlan, UK)
- 25% (v/v) Hanks balanced salt solution (Gibco)
- 0.5% (w/v) glucose (Sigma-Aldrich, UK)
- 2 mM glutamine (Sigma-Aldrich, UK)
- 25 µg/ml penicillin/streptomycin (Sigma-Aldrich, UK)
- 20 ng/ml ciliary neurotrophic factor (CNTF) (Sigma-Aldrich, UK)
- The osmolarity of the medium was 320-325 mOsm/L

SOC medium

- 0.5% (w/v) yeast extract

- 2% (w/v) Tryptone
- 10 mM NaCl
- 2.5 mM KCl
- 10 mM $MgCl_2$
- 10 mM $MgSO_4$
- 20 mM Glucose

TBE buffer (1M Tris, 1M Boric Acid, 20mM EDTA)

- 24.22 g Tris
- 12.366 g boric acid
- 1.489 g EDTA
- Adjust pH to 8.3. QS to 2 liters. Autoclave.

TFB1

- 30 mM potassium acetate
- 10 mM $CaCl_2$
- 50 mM $MnCl_2$
- 100 mM $RbCl_2$
- 15% (v/v) glycerol
- Adjust pH to 5.8 with 1 M acetic acid
- Filter sterilise with Millipore vacuum filter (0.22 um pore size)

TFB2

- 10 mM MOPs
- 75 mM $CaCl_2$
- 10 mM $RbCl_2$
- 15% (v/v) glycerol
- Adjust pH to 6.5 with 1 M KOH

- Filter sterilise with Millipore vacuum filter (0.22 um pore size)

Tyrode solutions

Control tyrode solution

- 121 mM NaCl
- 5 mM KCl
- 1.2 mM $NaH_2PO_4 \cdot 2H_2O$
- 2.4 mM $CaCl_2 \cdot 2H_2O$
- 1.3 mM $MgCl_2 \cdot 6H_2O$
- 10 mM D-glucose
- 5 mM HEPES
- 26 mM $NaHCO_3$

50mM KCl solution

- 76 mM NaCl
- 50 mM KCl
- 1.2 mM $NaH_2PO_4 \cdot 2H_2O$
- 2.4 mM $CaCl_2 \cdot 2H_2O$
- 1.3 mM $MgCl_2 \cdot 6H_2O$
- 10 mM D-glucose
- 5 mM HEPES
- 26 mM $NaHCO_3$

Table 1. Excitation and emission maxima of secondary antibodies used for indirect immunofluorescence labelling.

	Excitation Maximum (nm)	Emission Maximum (nm)
Alexa Fluor 488	495	519
Alexa Fluor 568	578	603
Alexa Fluor 633	632	647

Figure 1. Fluorescence spectra of fluorophores used (Alexa Fluor 488, 568 and 633 antibody conjugates and green fluorescent protein). Spectra graphs generated with Fluorescence SpectraViewer, Invitrogen (http://www.invitrogen.com/site/us/en/home/support/Research-Tools/Fluorescence-SpectraViewer.html).

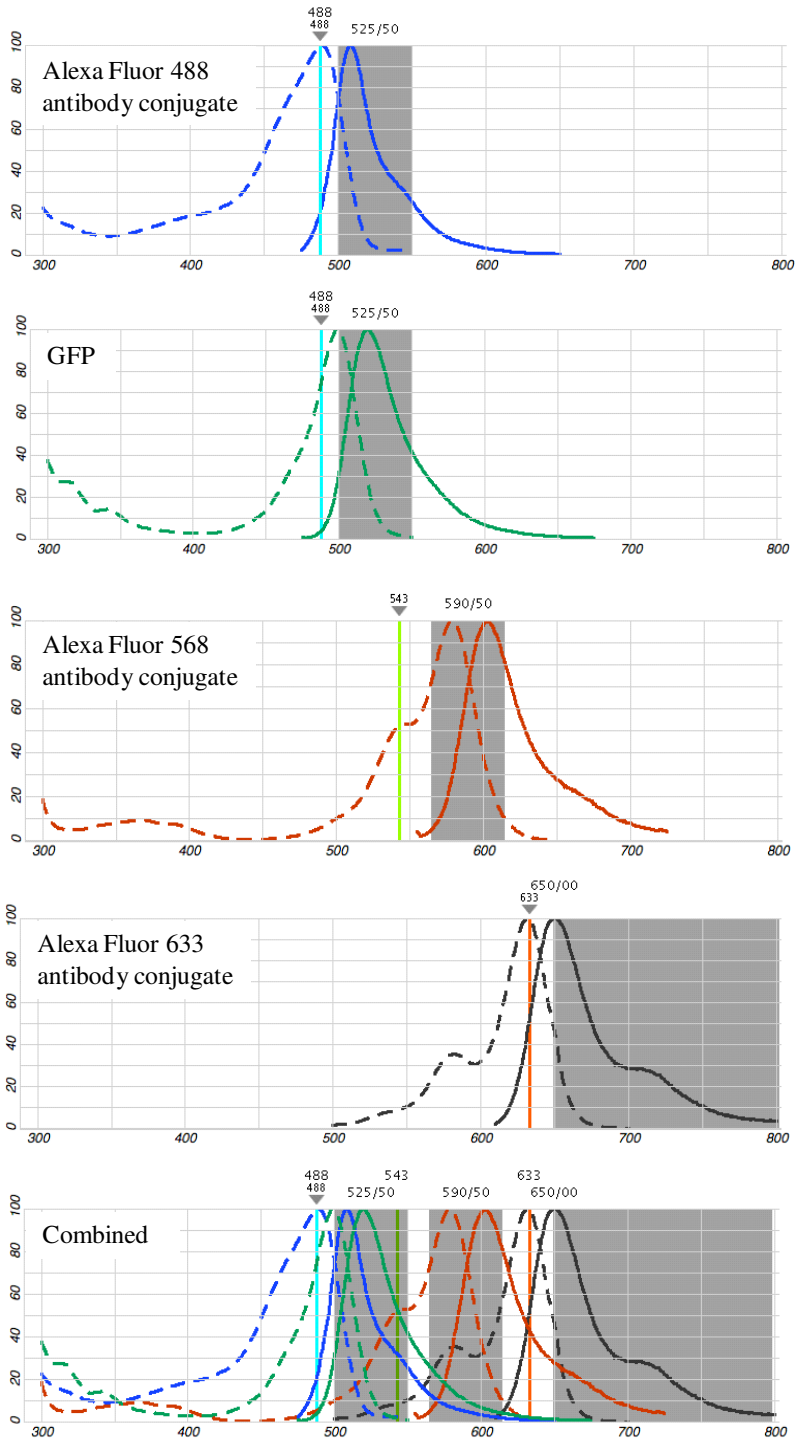

Appendix II – Hot spots for degradation in dendrites of magnocellular neurones

Hot spots for degradation in dendrites of magnocellular neurones

Centre for Integrative Physiology, School of Biomedical Sciences, University of Edinburgh, Edinburgh, EH8 9XD, UK.

Short title: Degradation sites in dendrites of magnocellular neurones

Correspondence to:

Email:

Telephone:

Key words: dendrites, magnocellular neurones, lysosomes, degradation, vasopressin-eGFP

Supported by the BBSRC and Society for Endocrinology

Abstract

The magnocellular neurones of the supraoptic nucleus (SON) and paraventricular nucleus (PVN) are capable of neuropeptide release from their axon terminals and dendrites. In magnocellular axon terminals, swellings known as Herring bodies are responsible for the degradation of aged, unreleased peptide vesicles. Peptide vesicles that have entered Herring bodies cannot be re-recruited for release and degradation in Herring bodies is carried out by the large amounts of lysosomes found in them. Interestingly, Herring bodies were found to be extremely dynamic and plastic structures which increase in number during dehydration and decreases during rehydration. Dendrites of the magnocellular neurones contain a large proportion of the neuronal peptide content. Swellings similar to Herring bodies found in axon terminals have not been reported in dendrites. In the present study, immunofluorescent labelling of lysosomes in dendrites expressing vasopressin (VP) endogenously tagged to eGFP (VP-eGFP) showed that there are "hot spots" for degradation in magnocellular dendrites. Lysosomes were found to be preferentially located where there was a high density of VP-eGFP expression. Further analysis found that lysosomes were mostly found in the centre of dendrites. Previous studies in endocrine cell lines reported that aged, unreleased vesicles reside in the centre of cells. The central localisation of lysosomes in dendrites indicates a role for degradation of aged, unreleased vesicles in dendrites.

Introduction

The magnocellular neurones of the SON and PVN have been widely used as a model system to study neuroendocrine peptide release due to the fact that these neurones exclusively release large amounts of two peptide hormones VP and oxytocin (OT). VP and OT are released into the circulation via the pituitary gland in the neural lobe where VP and OT exert their peripheral functions. Magnocellular neurones also release peptides from their dendrites and this release is different to that from the pituitary in that peptides largely remain in the CSF and act on the brain. However, the major difference found between peptide release from axon terminals in the pituitary and peptide release from dendrites in the brain is that release from axon terminals and dendrites can be differentially stimulated and occurs via different mechanisms (1,2). This led to the acknowledgement that axon terminals and dendrites of the magnocellular neurones are different compartments where release of neuroactive substances can be differentially regulated. To better understand the mechanisms governing the difference in peptide release between axon terminals and dendrites of magnocellular neurones, it is essential to investigate differences in peptide handling between these two compartments.

The neurosecretory axons in the neural lobe is made up of different compartments consisting of undilated segments, endings and swellings (3). Peptide vesicles were proposed to arrive at the endings through the undilated segments, and become stored in the swellings if they were not released (3,4). A specialised compartment, known as the Herring body, was found to be filled with lysosomes (5) and was found to be the site of degradation for aged, non-released peptide vesicles

(4). Neurosecretory vesicles that have entered the Herring body cannot be re-recruited for release, suggesting that Herring bodies are specialised compartments for degradation of cellular organelles. A dehydration regime showed large amounts of peptide vesicles residing in Herring bodies and a dehydration-rehydration protocol showed reduced amounts of Herring bodies associated with axon terminals indicating that Herring bodies are also dynamic and plastic. In comparison, dendrites are morphologically different to axon terminals and no specialised bodies had been reported in association with dendrites (6).

A large amount of peptides is stored within the dendritic compartment. In the case of VP, 95% of the VP content in VP-ergic neurones is contained within the dendrites (7,8), indicating that dendrites are important compartments for peptide storage and release. High potassium depolarisation applied to the SON, which exclusively contains cell bodies and dendrites, for 10 -15 min released ~2.5% of oxytocin vesicles (1), and 30 min microdialysis in the SON of suckling rats released ~10% of oxytocin vesicles from the somato-dendritic compartment (9,10). Hence, a large amount of peptide vesicles in dendrites are not released. Non-released vesicles age and will eventually be degraded. In hippocampal neurones, degradation was found to occur only in cell bodies. Endocytosis had been shown to occur throughout the length of hippocampal dendrites but evidence of lysosomes were only found in cell bodies (11). In contrast, evidence of lysosome staining had been seen in magnocellular dendrites (6). There is also evidence of both endocytosis (12) and autophagy (13) in magnocellular dendrites, indicating that magnocellular dendrites are actively involved in membrane recycling and the disposal of aged/damaged

organelles. Moreover, since magnocellular dendrites act as a major storage compartment of peptide vesicles, they may also be important sites for degradation.

Since special swellings/bodies for degradation were not found in magnocellular dendrites, the organisation of degradation sites in the dendritic compartment is not known. Recently, a transgenic rat line was established where endogenous VP was tagged with eGFP fluorescent protein (VP-eGFP) (14) which enables visualisation of endogenous VP without prior staining. Staining of lysosomes in brain sections containing VP-eGFP hence enabled correlation analysis of lysosomal localisations with endogenous VP. The aims of this study were to investigate the physiological significance of lysosomes in magnocellular dendrites and the organisation of these degradation sites in magnocellular dendrites.

Materials and Methods

Indirect Immunofluorescence Labelling for Free-floating Sections

Four adult male transgenic VP-eGFP rats (200 – 300 g), were anaesthetised with sodium pentobarbitone and transcardially perfused with heparin-containing saline and then 4% paraformaldehyde. Rats were then decapitated and their brains removed and stored in post-fix solutions (15% sucrose w/v in 4% paraformaldehyde). Sections were stored in cryoprotective solution (30% sucrose w/v in 0.1 M PB). Immunofluorescence labelling was performed on cryostat cut 52 µm sections containing the SON. Briefly, sections were washed three times for 10 min in 0.1 M PBS on an orbital rotation and then incubated in 50 mM NH_4Cl for 10 min. Sections were washed again three times in 0.1 M PBS. Non-specific antibody

binding was prevented by incubating brain sections in a blocking solution which contains 0.1 M PBS, 0.3% (v/v) Triton X100, and 10% (v/v) pre-immune goat serum for 30 min at room temperature. The primary antibody used to label lysosomes is the mouse monoclonal IgG raised against lysosomal associated membrane protein 1 (LAMP-1, LY1C6, Santa Cruz Biotechnology, Inc.). Primary anti-LAMP1 antibody was added to the blocking solution at 1:50 dilution (4 µg/ml) and sections were incubated in the primary antibody cocktail at 4^{o}C overnight. Negative controls were carried out by replacing primary antibody incubation with pre-immune serum incubation. The next day, the primary antibody was washed off three times in 0.1 M PBS for 10 min before incubation in secondary antibody solution containing AlexaFluor 568 (1:500 dilution, Invitrogen) made up in blocking solution at 4^{o}C overnight. Sections were washed three times 10 min and mounted onto gelatinised slides, air dried and embedded with mowiol (Calbiochem) mounting medium and coverslipped. The mounting medium was left to cure overnight protected from light and sections were imaged once the medium was dry.

Microscopic Image Acquisition

The Zeiss LSM510 inverted microscope was used for all imaging. The 488 nm line of the Argon laser was used to excite eGFP that has an excitation maximum of 488 nm and an emission maximum of 509 nm. A dichroic beam splitter, HFT 488, was in place and the excitation laser passed through two mirrors before the emitted light was collected by a band pass 500 – 550 filter. The helium-neon 1 (HeNe1) laser line (excitation wavelength 543 nm) was used to excite the AlexaFluor 568 staining

(excitation maximum 578 nm, emission maximum 603 nm). The photomultiplier tube (PMT) settings and laser powers were kept exactly the same for all samples. Images were acquired by sequential scanning to avoid bleed through of emitted light from either channel. An x63 oil immersion objective (NA1.4) was used. Images were acquired close to double Nyquist sampling rate to avoid under sampling (Nyquist calculator available at www.svi.nl). 3-dimensional images were obtained by scanning the x, y –planes at 60 nm, achieved by line scanning 1024 x 1024 pixels with an optical zoom of 2.4, and intervals of 170 nm along the z-axis. 8 bit pixel depth, line averaging of 1 (no averaging) and maximum scan speed were chosen for image acquisition to avoid photobleaching.

Image Processing

The acquired stack of images was deconvolved to remove aberrations caused by the intrinsic physical properties of the microscope. Deconvolution of images was achieved by use of the Huygens Essential software (Scientific Volume Imaging, NL, www.svi.nl) available in the IMPACT imaging facility in our centre. The Huygens deconvolution software restores convolution in images taken by removing blurring caused by diffraction of light and noise introduced by the microscope photomultiplier tube. Image restoration is based on the iterative application of a maximum likelihood estimate algorithm where the point spread function – the smallest fluorescent single point object that can be resolved in 3 dimensions by the microscopic parameters used, is used to calculate and reassign out-of focus light signals to the point of origin (15).

The microscopic parameters used for deconvolution was set according to the parameters used for imaging: microscope type – confocal; numerical aperture – 1.4; lens immersion and medium refractive indices – 1.51 and 1.4; x and y sample sizes – 60 nm; z sample size – 170 nm; excitation wavelengths – 488 nm, 543 nm; emission wavelength – 509 nm, 603 nm; excitation photon count – 1; pinhole = 1 Airy unit. These parameters help the deconvolution software to calculate a theoretical point spread function used. A signal to noise ratio is used in the software to control the sharpness of the restoration result of the image and can be calculated as the square root of the brightest intensity in the image divided by the average intensity of a single photon hit caused by photon noise. Generally, the lowest signal to noise ratio, 3, was employed, assuming a very noisy image, so that no background noise would be enhanced by deconvolution. Because of the calculations involved in deconvolution, 8 bit unsigned images were converted to 32 bit float images.

Image Analysis

Dendrites were imaged according to the protocol described above. Images were selected where long profiles of dendrites with no overlapping could be seen clearly. Lysosomes were located by going through optical sections in the z direction to ensure that stained lysosomes analysed were not from presynaptic terminals but occurred within the dendrites. Images were separated into the green (eGFP signal) and red (LAMP-1 staining) channels using ImageJ (http://rsb.info.nih.gov/ij/). Correlation analysis, but not colocalisation analysis, was carried out because lytic activity in the lysosome could change eGFP excitation and/or emission or simply

deform the eGFP fluorophore. Emission of green fluorescent protein is also highly pH sensitive (16). Hence, the low pH, pH 4.5, found in lysosomes will greatly reduce the fluorescent intensity of eGFP. Moreover, correlation analysis will give an idea of whether lysosomes are located where there is a high density of vasopressin eGFP vesicles. After all the areas of interest were obtained, the red channel was switched off and the original 32-bit image of the green channel was used for a "SUM" projection of the image where pixel intensities were summed up in each column of pixels in the z-stack using ImageJ to take into account the whole dendrite in 3 dimension. The saved areas of interest were then superimposed onto the green channel Please refer to Figure 1 for a diagrammatic representation of the image analysis and an example of areas of interest drawn on a representative dendrite.

To find out whether lysosomes are located in the centre of dendrites, the width of dendrites where lysosomes were situated was measured. The midpoint of the dendrite was calculated and the locations of lysosomes were expressed as % displacement from midpoint.

Statistics

To compare whether lysosomal locations are preferentially situated where there is a high density of vasopressin-containing vesicles, the difference between the mean spots VP-eGFP fluorescent intensity and the whole dendrite VP-eGFP fluorescent intensity was obtained and compared using the Chi-square test (Sigma Stat) (all measurements are relative to whole dendrite VP-eGFP intensity).

The % displacement from midpoint was calculated for each lysosome measured. Bins of 5% displacements were obtained to analyse where lysosomes were preferentially located throughout the width of dendrites.

Results

Correlation of lysosomal localisations with VP-eGFP intensity in magnocellular dendrites

To compare whether lysosomal locations are preferentially situated where there is a high density of VP-containing vesicles, lysosomes were stained with the LAMP1 antibody as described above. LAMP1 is the lysosome associated membrane protein 1 and a specific marker for lysosomes. The signal intensity of eGFP endogenously tagged to VP was used as a measurement of VP vesicle density. An area of 1 µm in diameter was drawn around each stained lysosomes. Mean VP-eGFP intensity measurements (density/area) were calculated for each area (spot intensity). Areas of interest were also made for whole dendrites and mean VP-eGFP intensity measurements recorded. The difference between the mean spots VP-eGFP fluorescent intensity and the whole dendrite VP-eGFP fluorescent intensity was obtained and compared using the Chi-square test where positive intensity = location of lysosome correlated to high VP-eGFP density, zero = no difference and negative intensity = location of lysosome correlated to low VP-eGFP density (all measurements are relative to whole dendrite VP-eGFP intensity). Figure 2 shows the Chi-square plot (mean spot intensity – mean whole dendrite intensity for each

dendrite measured). Chi-square test showed that the spot intensities were significantly different from zero ($p<0.001$) suggesting a positive correlation of lysosome locations and areas with high VP vesicle density. This indicates that lysosomes are either targeted to areas of high concentration of VP vesicles to be degraded. Another possibility is that aged/spent vesicles aggregate preferentially around lysosomes. However, this study cannot conclude which of these mechanisms was taking place.

Localisation of lysosomes in magnocellular dendrites

Staining of lysosomes showed that lysosomes are mostly localised in the centre of dendrites. Figure 3 shows optical sections of representative lysosome staining in VP-eGFP-expressing dendrites. Figure 3A and B show that lysosomes are located in the centre of dendrites. However, lysosomes are not exclusively localised in the centre, as depicted in Figure 3C. % displacement from the midpoint of dendrites was calculated for each lysosome measured and these measurements were grouped into bins of 5% (Figure 3D). The positive skewness of this graph represents that most lysosomes were located near the centre of dendrites. Moreover, normality test showed that lysosomes were not normally distributed throughout the dendrite ($p<0.001$). The preferential localisation of lysosomes in the centre of dendrites also agree with a previous study showing that aged, non-released dense core vesicles are preferentially located at the centre of the cell (17), indicating that degradation of spent vesicles occur in the centre of the dendrites. Meanwhile, clustering of

lysosomes in one specific segment of the dendrite was not seen (Figure 3A-C), indicating that dendrites do not contain specialised compartments for degradation.

Discussion

The Herring bodies in magnocellular terminals are filled with lysosomes and are the final destination for aged vesicles (4) providing a local capacity for degradation where aged vesicles do not need to be transported back to the cell body. It was not known whether dendrites, like neuhypophyseal terminals contain specialised compartments for degradation. Magnocellular dendrites have been shown to contain lysosomes (6), however, their functional significance in dendrites was not known. In hippocampal neurones, lysosomes were found only in cell bodies and very proximal segments of dendrites, and endocytosed materials were found to be retrogradely transported to cell bodies, where lysosomes were found (11). This study indicated that local degradation occurs in the dendritic compartment of magnocellular neurones. Since magnocellular dendrites contain a large reserve of vesicles, it is possible that "centres" for degradation occur in the dendritic compartment. In the present study, it was found that instead of clustering of lysosomes found in one special part of the dendrite, lysosomes were found to be located at areas where there was high density of vasopressin vesicles. These hot spots for degradation were found throughout the dendrites. Since magnocellular dendrites were not found to contain accumulations of lysosome clusters, it is unlikely that dendrites are the destination of all aged and non-released vesicles. However, lysosomes were found where vasopressin-eGFP vesicles cluster suggesting that non-

released vesicles gather as a pool around these lysosomes or lysosomes were preferentially transported to these non-released pools of vesicles. Dendritic lysosomal content is known to be variable where the number of lysosomes increases during high cellular activity, e.g. dehydration, and decreases during low activity, e.g. rehydration (6). Similarly, in axon terminals, lysosomes-containing Herring bodies were found to be abolished during rehydration (4) suggesting that Herring bodies are plastic structures that disappeared when old vesicles were spent and newly synthesised vesicles do not enter the lysosomal pathway. Hence, it is likely that lysosomes are targeted to loci where there is a high demand for degradation; i.e. where pools of non-released secretory vesicles reside. In the magnocellular neuronal terminal, the smooth endoplasmic reticulum (SER) was found to contribute to the formation of lysosomes (18). Elements of the rough endoplasmic reticulum (RER) had been shown in magnocellular dendrites (19), however, elements of the SER had not been studied. Hence, there could be two ways in which lysosomes are targeted to dendrites: 1) translocation from the soma to sites of aged, non-released vesicle pools in dendrites; and/or 2) local synthesis of lysosomes in dendrites. However, the capability of dendrites to synthesise lysosomes require further studies. Nevertheless, there is evidence of transport of lysosomes between the soma and dendrites of magnocellular neurones (20,21).

In many different cell types, lysosomal degradation is a plastic process which increases in activity according to the demand of the cell. Early studies in rat anterior pituitary cells showed that lysosomes have important functions in the regulation of prolactin secretion (22). When suckling pups were separated from lactating mothers, production of prolactin continued until there was an increase in the number of

lysosomes and lysosomal enzyme activity. In secretion deficient β-pancreatic islet cells, increased autophagic activity was shown to control hormone content in the cells under stimulation for insulin production (23). Crinophagy and autophagy both occur in this cell type. Crinophagy is the process where β-granules fuse with a pre-existing lysosome-related body, and autophagy is where β-granules form autophagosomes, a pre-lysosomal body, which subsequently forms the lysosome either through maturation and acquisition of lysosomal proteins or by fusion to pre-existing mature lysosomes (24). There is no evidence of crinophagy in magnocellular neurones. Intracellular degradation is believed to be via autophagy and aged/spent organelles, including unreleased peptides, form autophagosomes before being degraded by mature lysosomes (13). Previous studies where truncated VP peptides were expressed showed an increase in the number of lysosomes in magnocellular neurones (13) and this increase in lysosomal activity was found to be important in the survival of these neurones (25), indicating that autophagy has a role in regulating the content of peptides in magnocellular neurones as well as having pro-survival effects. The results from the present study suggest that autophagy is an important mechanism for regulation of intracellular peptide content in magnocellular dendrites where evidence of lysosomes were found to be preferentially situated at areas of high VP-vesicle density. It should be noted that not every lysosome stained was correlated to high VP-eGFP density. The magnocellular VP neurone produces and releases other neuroactive substances in addition to VP (26-29). Hence, lysosomes can also be situated where there is a segregation of other neuropeptides than VP in the dendrite.

In the present study, it was also found that lysosomes are located in the centre of dendrites (Figure 3). In bovine adrenal chromaffin cells (17,30) and PC12 (31) cells newly synthesised vesicles are preferentially targeted to the cell membrane and aged vesicles reside in the centre of the cell. Since aged vesicles were shown to be associated with lysosomal degradation (4), this suggests that aged, non-released vesicles reside in the centre of dendrites allowing newly synthesised vesicles to be primed close to the plasma membrane in accordance with the findings in bovine adrenal chromaffin cells. However, as discussed so far, whether aged, non-released vesicles actively aggregate to lysosomal localisations, or whether lysosomes are targeted to areas of high density of aged organelles is unknown. Figure 3C and D shows that lysosomes are not exclusively located at the centre of the dendrite, indicating lysosomes have other roles in addition to degradation of aged, unreleased peptide vesicles. A dehydration protocol, using different time periods of dehydration, can be employed to increase exocytosis and hence, membrane retrieval from endocytosis. Labelling endocytosed membranes or membrane cargoes with extracellular markers will enable localisation of endocytosed materials. Hence, it will be possible to identify whether more lysosomes and endosomes were targeted to dendrites after prolonged dehydration and whether these lysosomes are colocalised with endocytosed markers, indicating that lysosomes may be targeted to areas of high density of organelles to be degraded or recycled.

References

1. Ludwig M, Sabatier N, Bull PM, Landgraf R, Dayanithi G, Leng G. Intracellular calcium stores regulate activity-dependent neuropeptide release from dendrites *Nature* 2002; **418:** 85-89.

2. Ludwig M, Leng G. Dendritic peptide release and peptide-dependent behaviours *Nat Rev Neurosci* 2006; **7:** 126-136.

3. Heap PF, Jones CW, Morris JF, Pickering BT. Movement of neurosecretory product through the anatomical compartments of the neural lobe of the pituitary gland. An electron microscopic autoradiographic study *Cell Tissue Res* 1975; **156:** 483-497.

4. Krsulovic J, Peruzzo B, Alvial G, Yulis CR, Rodriguez EM. The destination of the aged, nonreleasable neurohypophyseal peptides stored in the neural lobe is associated to the remodeling of the neurosecretory axon *Microsc Res Tech* 2005; **68:** 347-359.

5. Dellmann HD, Rodriguez EM. Herring bodies; an electron microscopic study of local degeneration and regeneration of neurosecretory axons *Z Zellforsch Mikrosk Anat* 1970; **111:** 293-315.

6. Morris JF, Dyball RE. A quantitative study of the ultrastructural changes in the hypothalamo-neurohypophysial system during and after experimentally induced hypersecretion *Cell Tissue Res* 1974; **149:** 525-535.

7. Pow DV, Morris JF. Dendrites of hypothalamic magnocellular neurons release neurohypophysial peptides by exocytosis *Neuroscience* 1989; **32:** 435-439.

8. Leng G, Ludwig M. Neurotransmitters and peptides: whispered secrets and public announcements *J Physiol* 2008; **586:** 5625-5632.

9. Neumann I, Russell JA, Landgraf R. Oxytocin and vasopressin release within the supraoptic and paraventricular nuclei of pregnant, parturient and lactating rats: a microdialysis study *Neuroscience* 1993; **53:** 65-75.

10. Neumann I, Ludwig M, Engelmann M, Pittman QJ, Landgraf R. Simultaneous microdialysis in blood and brain: oxytocin and vasopressin release in response to central and peripheral osmotic stimulation and suckling in the rat *Neuroendocrinology* 1993; **58:** 637-645.

11. Parton RG, Simons K, Dotti CG. Axonal and dendritic endocytic pathways in cultured neurons *J Cell Biol* 1992; **119:** 123-137.

12. de Kock CP, Wierda KD, Bosman LW, Min R, Koksma JJ, Mansvelder HD, Verhage M, Brussaard AB. Somatodendritic secretion in oxytocin neurons is

upregulated during the female reproductive cycle *J Neurosci* 2003; **23:** 2726-2734.

13. Davies J, Murphy D. Autophagy in hypothalamic neurones of rats expressing a familial neurohypophysial diabetes insipidus transgene *J Neuroendocrinol* 2002; **14:** 629-637.

14. Ueta Y, Fujihara H, Serino R, Dayanithi G, Ozawa H, Matsuda K, Kawata M, Yamada J, Ueno S, Fukuda A, Murphy D. Transgenic expression of enhanced green fluorescent protein enables direct visualization for physiological studies of vasopressin neurons and isolated nerve terminals of the rat *Endocrinology* 2005; **146:** 406-413.

15. Shaw PJ, Rawlins DJ. The point spread function of a confocal microscope: its measurement and use in deconvolution *J Microsc* 1991; **163:** 151-165.

16. Tsien RY. The green fluorescent protein *Annu Rev Biochem* 1998; **67:** 509-544.

17. Duncan RR, Greaves J, Wiegand UK, Matskevich I, Bodammer G, Apps DK, Shipston MJ, Chow RH. Functional and spatial segregation of secretory vesicle pools according to vesicle age *Nature* 2003; **422:** 176-180.

18. Whitaker S, LaBella FS. Ultrastructural localization of acid phosphatase in the posterior pituitary of the dehydrated rat *Z Zellforsch Mikrosk Anat* 1972; **125:** 1-15.

19. Ma D, Morris JF. Protein synthetic machinery in the dendrites of the magnocellular neurosecretory neurons of wild-type Long-Evans and homozygous Brattleboro rats *J Chem Neuroanat* 2002; **23:** 171-186.

20. Gorenstein C, Bundman MC, Lew PJ, Olds JL, Ribak CE. Dendritic transport. I. Colchicine stimulates the transport of lysosomal enzymes from cell bodies to dendrites *J Neurosci* 1985; **5:** 2009-2017.

21. Gorenstein C, Ribak CE. Dendritic transport. II. Somatofugal movement of neuronal lysosomes induced by colchicine: evidence for a novel transport system in dendrites *J Neurosci* 1985; **5:** 2018-2027.

22. Smith RE, Farquhar MG. Lysosome Function in Regulation of Secretory Process in Cells of Anterior Pituitary Gland *Journal of Cell Biology* 1966; **31:** 319-&.

23. Marsh BJ, Soden C, Alarcon C, Wicksteed BL, Yaekura K, Costin AJ, Morgan GP, Rhodes CJ. Regulated autophagy controls hormone content in secretory-deficient pancreatic endocrine beta-cells *Mol Endocrinol* 2007; **21:** 2255-2269.

24. Luzio JP, Pryor PR, Bright NA. Lysosomes: fusion and function *Nat Rev Mol Cell Biol* 2007; **8:** 622-632.

25. Castino R, Davies J, Beaucourt S, Isidoro C, Murphy D. Autophagy is a prosurvival mechanism in cells expressing an autosomal dominant familial neurohypophyseal diabetes insipidus mutant vasopressin transgene *FASEB J* 2005; **19:** 1021-1023.

26. Brailoiu GC, Dun SL, Yang J, Ohsawa M, Chang JK, Dun NJ. Apelin-immunoreactivity in the rat hypothalamus and pituitary *Neurosci Lett* 2002; **327:** 193-197.

27. Landry M, Roche D, Angelova E, Calas A. Expression of galanin in hypothalamic magnocellular neurones of lactating rats: co-existence with vasopressin and oxytocin *J Endocrinol* 1997; **155:** 467-481.

28. Reaux A, Gallatz K, Palkovits M, Llorens-Cortes C. Distribution of apelin-synthesizing neurons in the adult rat brain *Neuroscience* 2002; **113:** 653-662.

29. Shuster SJ, Riedl M, Li X, Vulchanova L, Elde R. The kappa opioid receptor and dynorphin co-localize in vasopressin magnocellular neurosecretory neurons in guinea-pig hypothalamus *Neuroscience* 2000; **96:** 373-383.

30. Wiegand UK, Duncan RR, Greaves J, Chow RH, Shipston MJ, Apps DK. Red, yellow, green go!--A novel tool for microscopic segregation of secretory vesicle pools according to their age *Biochem Soc Trans* 2003; **31:** 851-856.

31. Tsuboi T, Kitaguchi T, Karasawa S, Fukuda M, Miyawaki A. Age-dependent Preferential Dense-core Vesicle Exocytosis in Neuroendocrine Cells Revealed by Newly Developed Monomeric Fluorescent Timer Protein *Mol Biol Cell* 2009.

Figure 1. Measurement of VP-eGFP intensity relative to locations of LAMP1 immunofluorescence. (A) Schematic diagram of VP-eGFP intensity measurement. Red circles in the top panel = LAMP1 labelling of lysosomes; green circles in bottom panel = VP-eGFP. Masks of 1 μm diameter (bold circles) were drawn on images with the green VP-eGFP channel switched off to identify locations of LAMP1 labelling. These masks were then imported onto the green channel of the same image and the intensity of VP-eGFP at these locations was measured as spots (mean intensity/area). The whole dendrite in 3-dimension was taken into account by taking a sum of the image stack. The intensity of the whole dendrite was then measured for comparison (B) Determination of areas of interest as discussed above; one optical section is shown. (C) 3-D image stack converted to 2-D by the sum slices function in ImageJ where the sum of the pixels from the stack of images were displayed from 32-bit optical slices. Areas of interest described in (A) were then imported onto this image to measure VP-eGFP intensiy. (D) VP-eGFP intensity of the whole dendrite was then obtained by measuring sum slices image of the whole dendrite. Scale bar = 3 μm.

Figure 2. Correlation of LAMP1 labelling with VP-eGFP intensity in the dendrite. Full circles represent mean spot intensity – mean dendrite intensity for dendrites measured. Filled box represent the mean of all the data points (error bar = ±SEM). Chi-squared test showed that there is a significant difference between the mean intensity of spots and the mean intensity of whole dendrites ($p<0.001$; $n = 26$). This suggests that lysosomes were predominantly located in areas with high density of vasopressin vesicles.

Figure 3. A-C) LAMP1 immunofluorescence labelling (red) in VP-eGFP dendrite. Scale bar = 5 μm. D) Localisations of lysosomes in dendrites measured as % displacement. 391 lysosomes were measured in 18 dendrites. A and B) Representative images of lysosome localisation in the centre of dendrites (arrows). C) Lysosomes are not exclusively located in the centre of dendrites. D) % displacement of lysosome localisations from the midpoint of dendrites grouped in 5% bins. Normality test showed that lysosomes are not normally distributed throughout the width of dendrites ($p<0.001$). The positive skew indicates that lysosomes are preferentially located near the midpoint of dendrites.

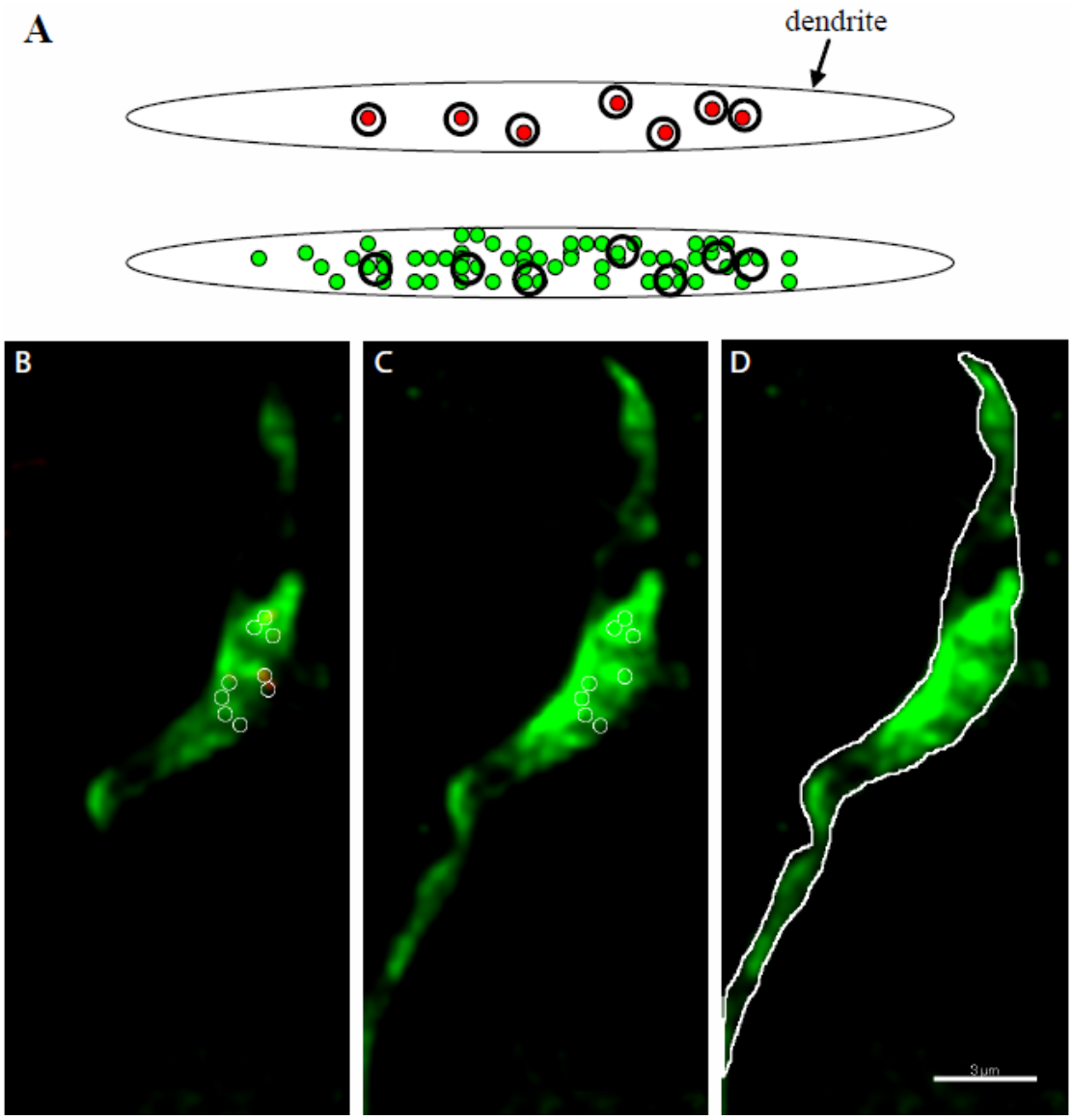

Figure 1

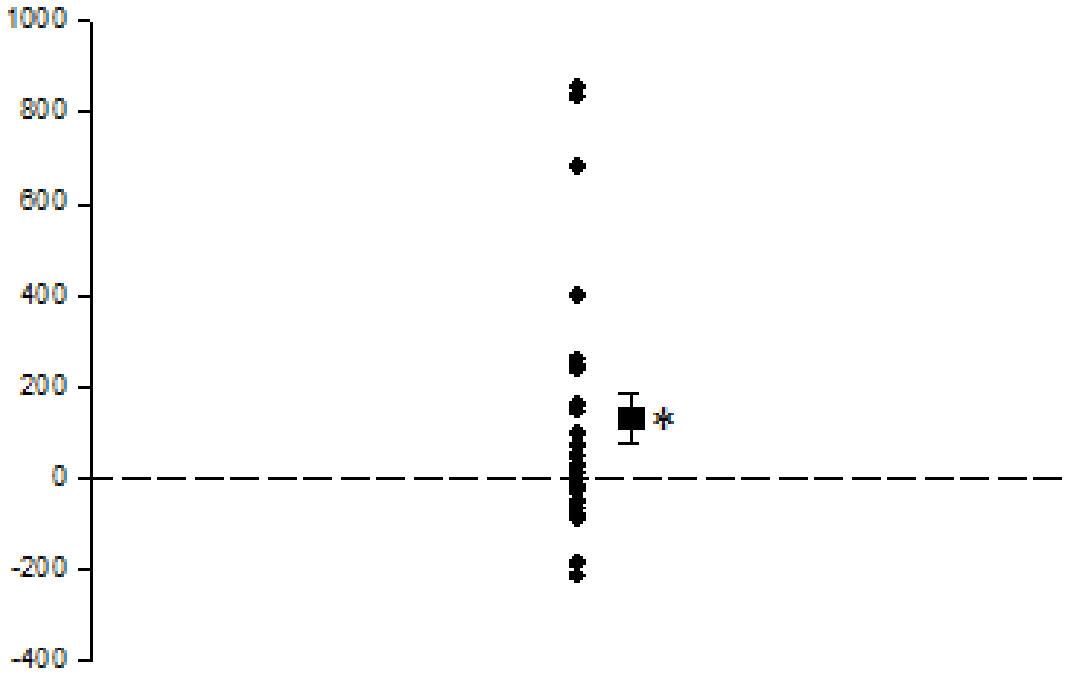

Figure 2

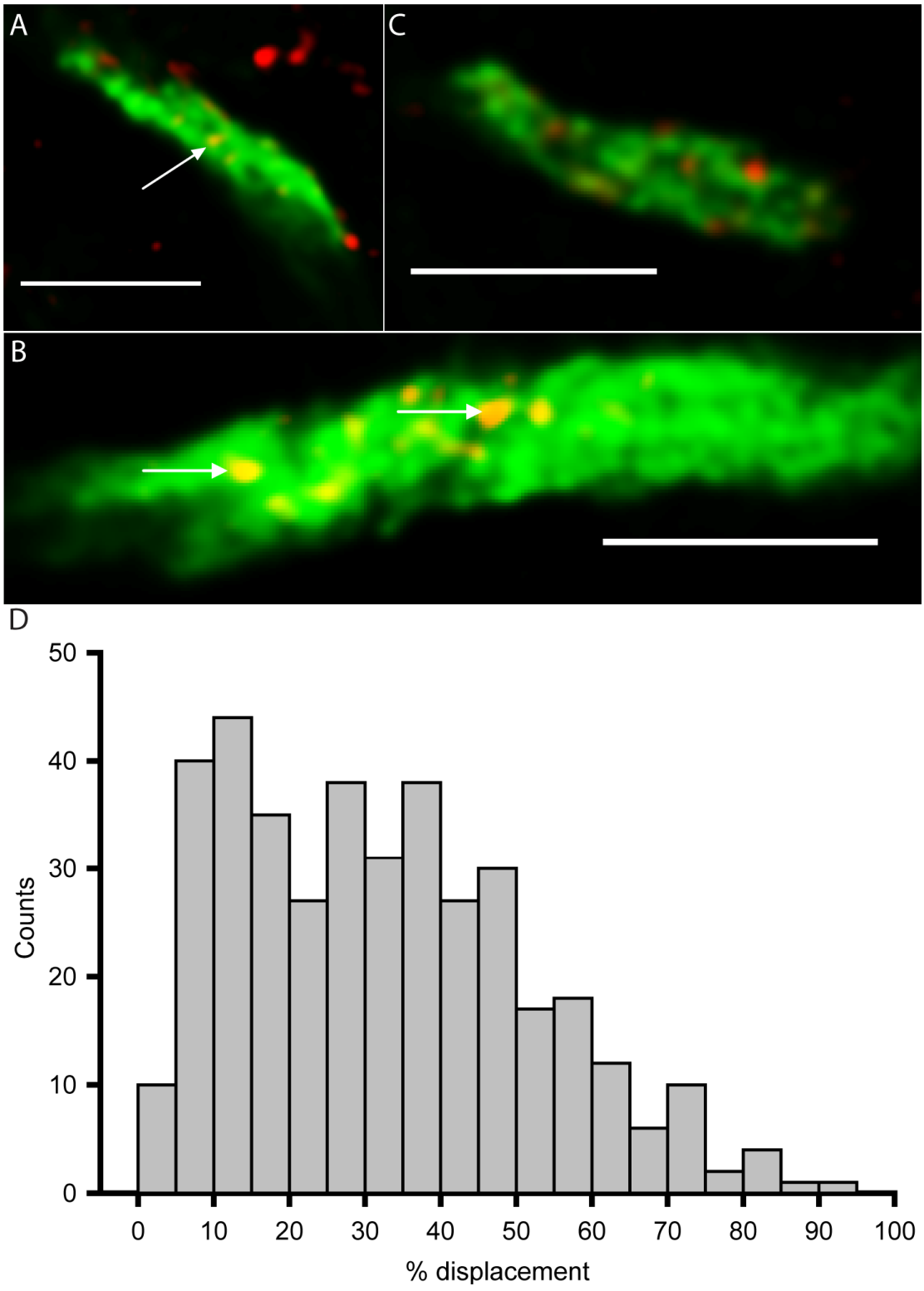

Figure 3